School of Electrical Engineering, Computing and
Mathematical Sciences

Transceiver Designs for MIMO Relay Communication Systems

Justin Lee Bing
0000-0002-5907-3410

This thesis is presented for the Degree of
Doctor of Philosophy
of
Curtin University

January 2021

Declaration

To the best of my knowledge and belief this thesis contains no material previously published by any other person except where due acknowledgement has been made.

This thesis contains no material which has been accepted for the award of any other degree or diploma in any university.

Signature: .....

Date: .....

Acknowledgements

First and foremost, I would like to express my sincere appreciation to my thesis supervisors Associate Prof. Lenin Gopal, Prof. Yue Rong, and Dr. Raymond Chiong Choo Wee, for their constant support and encouragement during the entire period of my PhD studies. Their inspiration, motivation, and immense knowledge had directed me to reach the goal. They were always patient and caring in their instructive and research support, which guided me to pursue the right path.

Besides my supervisors, I would like to express my gratitude to Associate Prof. Zhuquan Zang, Chairperson of my thesis committee for his necessary administrative guidance and help at all levels of this research work.

Most importantly, I would like to thank the Curtin Malaysia Graduate School, which offered me the Curtin Malaysia Postgraduate Research Scholarship (CMPRS), which covers my tuition fees and living allowance for my study duration. I would also like to thank Curtin University for giving me the opportunity to complete my postgraduate studies of Doctor of Philosophy.

Most of all, I am indebted to my unconditionally loving parents, whose moral support in my research endeavours has made this dissertation possible.

Lastly, I would like to thank the anonymous reviewers for their time and efforts in providing helpful comments to improve my thesis's quality.

Abstract

In recent years, the application of simultaneous wireless information and power transfer (SWIPT) in the energy-limited wireless system has attracted much attention from researchers around the world. This is due to the SWIPT technology's capability to prolong the limited lifetime of wireless sensor networks (WSNs) by harvesting energy from radio frequency (RF) signals while receiving information from the transmitter. A relay node plays a vital role in a wireless communication system when the transmitter and receiver cannot communicate due to long transmission distance. Relay node helps to extend the network coverage of the wireless communication system. Moreover, the multiple-input multiple-output (MIMO) technique, which can be easily implemented by installing multiple antennas at the system nodes, is a promising technique to enhance the system performance of a wireless communication network. In this thesis, the investigation concerning the application of SWIPT in the MIMO relay system is investigated with the consideration of practical aspects of the wireless channel, e.g., channel estimation errors.

The impact of channel state information (CSI) mismatch between the exact CSI and estimated CSI is investigated for the MIMO relay system with a general system model setup. The precoding matrices for the source nodes, relay nodes, and destination nodes are optimized to minimize the system's weighted mean square error (WMSE). The complex optimization problem is decomposed into several subproblems with low computational complexity by deriving the optimal structure for the relay precoding matrices. The subproblems are tackled using optimization techniques such as Karush-Kuhn-Tucker (KKT) conditions and the semi-definite programming (SDP) technique. The proposed transceiver design is equipped with robustness to counter the degradation caused by the CSI mismatch.

Next, the hybridized power-time splitting-based relaying (HPTSR) protocol is introduced to the SWIPT amplified-and-forward (AF) MIMO relay system. The HPTSR

protocol is an innovative SWIPT relaying protocol that combines the time-switching relaying (TSR) protocol with the power-splitting relaying (PSR) protocol. By combining the two well-known SWIPT relaying protocols, the system is equipped with a higher degree of freedom in optimizing the system's performance. The optimal structures for the source and relay precoding matrices are proposed to simplify the complicated optimization problem, which maximizes the system mutual information (MI) between the source and destination node. The lower bound and the upper bound of the system MI are exploited in solving the optimization problem. With the convexity theorem, the optimization problems are shown to be convex and solved by using CVXtoolbox. The system MI provided by the HPTSR protocol is shown to be better than the existing SWIPT relaying protocols.

Then, the source and relay precoding matrices for a TSR decode-and-forward (DF) MIMO relay system are jointly optimized to maximize the system MI with the consideration of CSI mismatch. The system performance is investigated for the fixed power transmission scheme and the flexible power transmission scheme. In the fixed power transmission scheme, the optimization problem can be solved by using the KKT conditions. In the flexible power transmission scheme, the primal decomposition method is used to decouple the coupled constraint. Moreover, the practical peak power limits are introduced to the flexible power transmission scheme. With the consideration of CSI mismatch, the proposed algorithms with robustness show better system performance than the existing non-robust algorithm.

Lastly, the transceiver design is investigated for an AF MIMO relay system with an energy harvesting (EH) relay node. The relay node forwards the received information data by using the energy harvested based on the RF signal transmitted by the source node using the TSR protocol. The CSI mismatch is considered in the proposed transceiver design, and it is modeled based on the Gaussian Kronecker model. The source and relay precoding matrices are jointly optimized to maximize the system MI. The optimization problem is solved using several optimization techniques, such as the primal decomposition method, the KKT conditions, Lagrangian multiplier method, and water-filling algorithms. Through numerical simulations, it is shown that the proposed algorithm is equipped with robustness to reduce the degradation caused by the CSI mismatch.

Publications arising from the Thesis

Parts of this thesis and concepts from it is submitted to the following journal which will be published in the near future.

Journal Papers

[1] J. L. Bing, Y. Rong, L. Gopal, and C. W. R. Chiong,"Transceiver Design for SWIPT MIMO Relay Systems with Hybridized Power-Time Splitting-Based Relaying Protocol", *IEEE Access*, vol. 8, pp. 190922-190933, Oct. 2020.

[2] J. L. Bing, L. Gopal, Y. Rong, C. W. R. Chiong, and Z. Zang,"Robust Transceiver Design for Multihop AF MIMO Relay Multicasting from Multiple Sources", *IEEE Trans. Veh. Technol.*, accepted, Dec. 2020.

[3] J. L. Bing, Y. Rong, L. Gopal, and C. W. R. Chiong, "Robust Transceiver Design for SWIPT DF MIMO Relay System with Time Switching Protocol", *IEEE Trans. Commun.*, submitted, Dec. 2020.

[4] J. L. Bing, Y. Rong, L. Gopal, and C. W. R. Chiong, "Joint Transceiver Design for AF MIMO Relay System with Time-Switching Relaying Protocol and Imperfect Channel State Information", *IEEE Transactions on Green Communications and Networking*, submitted, Dec. 2020.

Contents

List of Figures

List of Acronyms

1D	One-Dimensional
2D	Two-Dimensional
5G	Fifth-Generation
AF	Amplify-and-Forward
AWGN	Additive White Gaussian Noise
BER	Bit-Error-Rate
CCI	Co-Channel Interference
CSI	Channel State Information
DF	Decode-and-Forward
EH	Energy Harvesting
EVD	Eigenvalue Decomposition
i.i.d.	Independe and Identically Distributed
ID	Information Decoding
KKT	Karush-Kuhn-Tucker
LMMSE	Linear Minimum Mean-Squared Error
MI	Mutual Information
MIMO	Multiple-Input Multiple-Output
NMSE	Normalized Mean-Squared Error

NOMA	Non-Orthogonal Multi-Access
NP	Non-deterministic Polynomial
OFDM	Orthogonal Frequency-Division Multiplexing
OSTBC	Orthogonal Space-Time Block-Code
PS	Power-Splitting
PSD	Positive Semi-Definite
PSR	Power-Splitting-based Relaying
QoS	Quality of Services
QPSK	Quadrature Phase Shift Keying
R-E	Rate-Energy
RF	Radio Frequency
SDP	Semi-Definite Programming
SISO	Single-Input Single-Output
SNR	Signal-to-Noise Ratio
SQP	Sequential Quadratic Programming
STC	Space-time Coding
SWIPT	Simultaneous Wireless Information and Power Transfer
TS	Time-Switching
TSR	Time-Switching-based Relaying
WIT	Wireless Information Transfer
WMMSE	Weighted Minimum Mean-Squared Error
WMSE	Weighted Mean-Square Error
WPT	Wireless Power Transer
WSN	Wireless Sensor Network

Chapter 1

Introduction

Over the years, energy harvesting (EH) has been a popular research topic that attracted attention from researchers around the world. This is because EH provides the capability to extend the lifetime of energy-constraint wireless communication devices and break the limitation for replenishing energy-depleted wireless devices physically and/or economically. The innovative EH method, which harvests energy from radio frequency (RF) signals, has been widely investigated in recent years. Besides being recognized as a potential alternative source of wireless power transfer (WPT) , RF signals are commonly used for wireless information transfer (WIT) . Thus, the EH method, which exploits the usage of RF signals in both WPT and WIT simultaneously, is known as simultaneous wireless information and power transfer (SWIPT). In this introductory chapter, the study's necessary background about the SWIPT multiple-input multiple-output (MIMO) relay system is briefly presented. Moreover, the aim and objectives of the research are discussed. An overview of the thesis and its contributions are described in the following section.

1.1 Background of the Study

In Section 1.1, the background of the research study is presented. The history and the existing research works regarding the SWIPT are discussed in Subsection 1.1.1. Then, the knowledge of SWIPT is extended to the relay communication system with the relay node being considered energy constricted wireless device will be presented in Subsection 1.1.2. Next, the well-known MIMO technology, which is installing multiple antennas at the communication nodes, is introduced in Subsection 1.1.3. Lastly, the application of

SWIPT in the MIMO relay communication system with the relay node being considered an energy-constricted wireless device is discussed in Subsection 1.1.4.

1.1.1 Simultaneous Wireless Information and Power Transfer

Over the years, the amount of wireless communication devices is significantly increased. However, the performance of wireless communication devices is limited due to its confined lifetime. Even though the mentioned limitation of energy constricted wireless communication device can be solved by replacing its battery, it will sometimes be associated with some physical and/or economic constraints, which will result in high cost and high difficulties to perform the battery replacement for those devices. As an illustration, some wireless devices are installed inside living bodies to collect essential data [1]. As an alternative solution to extend the limited lifetime of the wireless communication devices, the EH technique, which is capable of harvesting energy from the environment, is adapted. Traditional EH techniques such as harvesting energy from solar, wind, and vibrations are heavily relying on natural resources. Hence, it limits the application of the traditional EH techniques in wireless communication devices due to the unreliability in providing necessary energy in a critical scenario, e.g. a solar-powered sensor unable to function when it is out of battery at night or during the day's time without solar power available. As the traditional EH techniques are not convenient to provide a reliable energy source to wireless communication devices, an alternative EH technique is introduced in [2] and adapted to the wireless communication devices. This EH technique, which is by harvesting energy based on the RF signal transmitted from the transmitter, is introduced based on the WPT concept introduced by Nikola Tesla in the 1980s. The alternative EH technique is a promising solution as it is capable of providing stable and controllable wireless energy supply to the energy-constraint wireless communication devices [3]. Besides WPT, RF signals are often used for WIT. The concept which exploits the usage of RF signals in both WPT and WIT at the same time is known as SWIPT.

In the early day, the proposed SWIPT system [2, 4] is assumed to be able to perform information decoding (ID) and EH from the same received RF signal simultaneously, This type of SWIPT system is known as the ideal SWIPT receiver architecture. However, the circuits applied for EH in the practical scenario cannot perform ID directly from the information-bearing signal [1]. Besides, the WIT and WPT are operated at different sensitivity in practice. Hence the conventional ID receiver may not provide

optimal performances for the SWIPT system [5]. Thus, the ideal SWIPT receiver faced difficulties when it comes to practical realization. In [6], the practical SWIPT receiver architectures are proposed to overcome the practical limitation for SWIPT system implementation in practice, namely, separated SWIPT receiver and co-located SWIPT receiver.

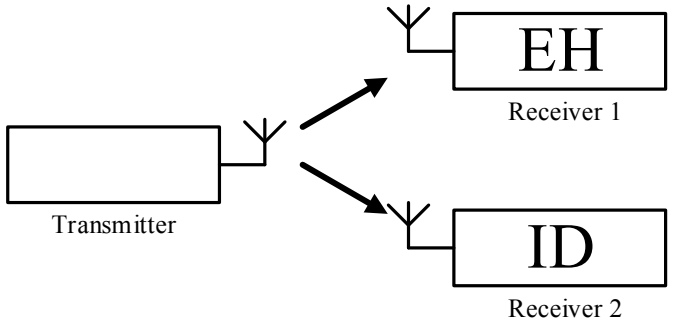

Figure 1.1: Practical implementation for SWIPT system with separated receiver architecture.

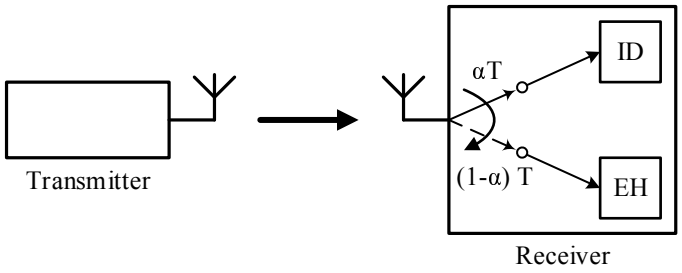

Figure 1.2: Practical implementation for SWIPT system with a co-located receiver under TS receiver architecture.

The separated receiver architecture for the SWIPT system is illustrated in Fig. 1.1. It can be noticed that the EH functioning block and the ID functioning block are implemented as two independent receivers with the RF signals transmitted by a common transmitter. The implementation of this SWIPT architecture is easy as both the EH and ID receivers can be obtained from commercialized products. For co-located receiver architectures, the receiver is installed with both EH and ID functioning blocks. There are two types of co-located receivers, namely, time-switching (TS) receiver and power-splitting (PS) receiver. The TS receiver architecture is illustrated in Fig. 1.2 while the PS receiver architecture is shown in Fig. 1.3. In TS receiver architecture, a time switch is implemented at the receiver antenna to systematically switch between EH and ID

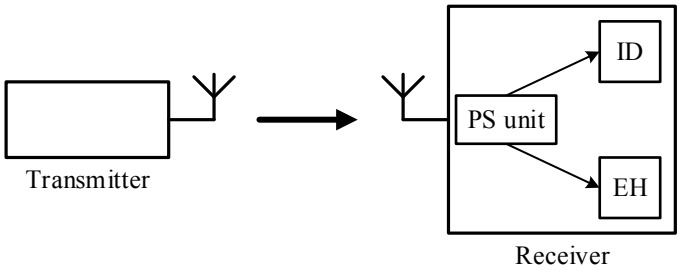

Figure 1.3: Practical implementation for SWIPT system with a co-located receiver under PS receiver architecture.

function blocks based on the designed TS sequences [6]. By denoting $\alpha \in [0, 1]$ as the TS factor, the received RF signal at the receiver during α portions of time in a single communication cycle will be used for EH while the remaining time will be used for ID. In PS receiver architecture, the received RF signal is divided into two separated signal streams by the PS unit installed at the receiver antenna. Then, these signal streams will be forwarded to the corresponding EH and ID functioning block to perform EH and ID [6, 7].

In the next subsection, understanding of a relay-assisted communication system with the application of SWIPT in the relay node is briefly described.

1.1.2 Energy Constricted Relay Communication System

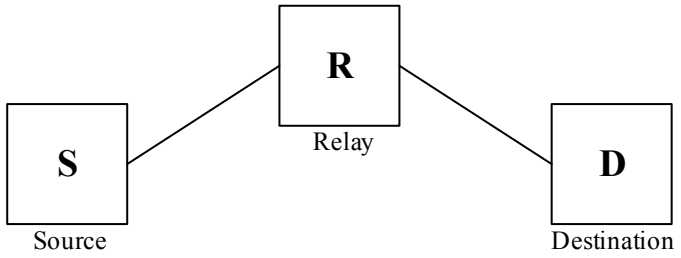

Figure 1.4: The simplest relay system with three communication nodes.

One of the wireless communication system's limitations is that the transmitter and receiver's placement are too far apart, and this results in the transmitter and receiving failing to communicate with each other. Generally, relay technology is applied as a promising strategy to solve the limitation. Relay nodes can help to expand the network coverage of wireless communication [8]. The primary relay system is illustrated in Fig. 1.4, where it consists of three communication nodes in the system, which are the

source, relay, and destination nodes. A relay node can be applied to a half-duplex system and/or full-duplex system. A half-duplex relay is required to function in two separated channels, while a full-duplex relay is operated at the same channel [9]. There are two types of relay schemes on how the relay operates to transmit the received signals to the consecutive communication node [8], namely, regenerative scheme and non-regenerative scheme. In the regenerative scheme, the relay node will first decode the received RF signals; it will then re-encode the decoded information signals before transmitting the re-encoded signals to the next communication node. The relay that adapted the regenerative scheme is also known as decode-and-forward (DF) relay. In the non-regenerative scheme, the relay node will not decode the received RF signals but boost the received signals and transmit the amplified signals to the next node. The relay that adapted the non-regenerative scheme is also known as the amplify-and-forward (AF) relay. In [10], the performance-complexity tradeoffs for the AF relay and DF relay are investigated. The DF relay provides better performance compared to the AF relay as it does not amplify the noise which is induced at the relay node. However, it required higher complexity with associated decoding delay and great processing power. On the other hand, the AF relay provides low complexity and zero-decoding delay with low processing power compared to the DF relay. It is believed by many that the AF relay offers a better tradeoff between the performance and the implementation costs [8].

In recent years, the knowledge of SWIPT is extended to relay communication systems considering the relay is an energy-constricted wireless communication device. In [11], the TS and PS SWIPT receiver architectures are implemented to the relay node. The relaying protocol where the relay node adapts the TS receiver structure is known as the TS-based relaying (TSR) protocol. The relaying protocol where the relay node adapts the PS receiver structure is known as the PS-based relaying (PSR) protocol. The energy harvested at the relay node through the TSR and/or PSR protocol will be fully used to process and forward the received signals to the destination node. In the past few years, several research works were carried out to investigate the relay communication systems with SWIPT relay nodes [11–19], which adapted the TSR protocol and/or PSR protocol. In [12, 13], the authors investigate the influence of different power allocation strategies adapted at the relay node with regard to the harvested energy to the system performance for a cooperative communication system, in which multiple pair of transceivers communicate with the corresponding partner. In [14], the power allocation problem for SWIPT in interference relay communication networks is tackled by the

authors using the game-theory mathematical model. In [15], the authors study the system performance for the harvest-use and the harvest-use-store models in a full-duplex EH relay communication system with PSR protocol. In [16], the authors investigate the effects of co-channel interference (CCI) to the SWIPT relay communication system with full-duplex relay under PSR protocol. The authors view the CCI as an additional energy source that could be harvested using the in-built EH circuit. However, with the increase in the power of CCI signals, the system performance can be heavily influenced. In [17], the achievable capacity of the system is investigated for the SWIPT relay communication system with TSR protocol for the regenerative and non-regenerative relay. In [18], the system performance for the SWIPT DF relay system with PSR protocol is studied considering the decoding cost introduced at the relay and the destination node to perform ID. In [19], the authors demonstrate that the EH relays capable of achieving the same diversity gain as self-powered relays for the SWIPT system with randomly placed DF relays.

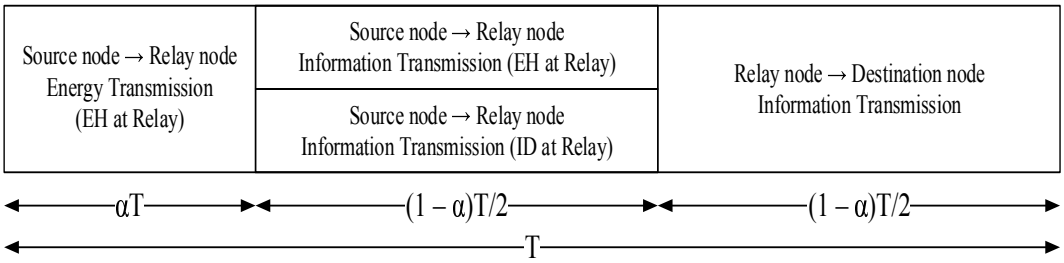

Figure 1.5: HPTSR framework with a full communication cycle split into three time intervals.

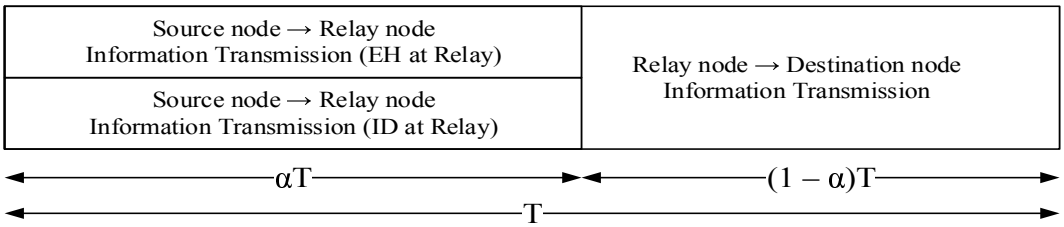

Figure 1.6: HPTSR framework with a full communication cycle split into two time intervals.

An innovative EH relaying protocol, known as hybridized power-time splitting-based relaying protocol (HPTSR), is introduced to improve the system performance by increasing the amount of energy harvested at the relay node. There are two distinct

frameworks for the mentioned HPTSR protocol as illustrated in Fig.1.5 and Fig. 1.6. As illustrated in Fig. 1.5, a full communication cycle is divided into three time intervals. For the first time interval, the relay node harvests RF signals transmitted from the source node. For the second time interval, the relay node splits the received RF signals with one portion of the received RF signal used for EH, while the remaining portion of the received RF signal is used for ID. In the last time interval, the relay node forwards the processed information signals to the destination node. This HPTSR framework can be viewed as the conventional TSR protocol with the inclusion of PSR protocol during the second time interval. Throughout the years, the existing studies with regard to the SWIPT relay communication system with the relay adapting the HPTSR framework illustrated in Fig. 1.5 are carried out in [20–23]. In [20], the authors investigated the system performance of the SWIPT AF relay system with HPTSR protocol. It is demonstrated that the TSR and PSR protocol will have a throughput crossover point while the HPTSR protocol outperforms the TSR and PSR protocol at the point. In [21], the system throughput for the SWIPT relay communication system with the HPTSR protocol is investigated, and it is shown that the HPTSR protocol provides better system performance compared to the TSR and PSR protocol. The authors also provide a unified system and analytical model for regenerative and non-regenerative EH relay with the HTPSR, TSR, and PSR protocols. In [22], the authors investigated the system performance for the proposed improved-HPTSR protocol with the consideration of direct communication between the transceiver. The improved-HPTSR protocol exploits the direct link between the transceiver where the receiver decodes the RF signals transmitted by the transmitter during the relay energy harvesting phase. In [23], the authors investigated the system performance for the HPTSR protocol adapted to the non-orthogonal multi-access (NOMA) relay system.

As illustrated in Fig. 1.6, a full communication cycle is divided into two time intervals. In the first time interval, the relay node splits the received RF signal into two individual streams and forwards the split streams to the EH circuit and ID circuit. In the next time interval, the relay node forwards the processed information signals to the destination node. With the introduction of the TS ratio, this HPTSR framework can adjust the time allocated for the relay node to perform EH and ID. This HPTSR framework can be viewed as the PSR protocol adapting the TSR protocol to provide the optimal amount of time for EH and ID at the relay node. The existing studies with regard to the SWIPT relay communication system with the relay adapting the HPTSR

framework illustrated in Fig. 1.6 are carried out in [24–26]. In [24], it is demonstrated that the secrecy performance of the EH relay system using the HPTSR protocol provides better performances compared to the conventional relay system at high signal-to-noise ratios (SNRs) . In [25], the system performance of the SWIPT relay system with HPTSR protocol is investigated with the existence of a direct link. In [26], the system throughputs for the regenerative and non-regenerative relay system are investigated with the relay node adapting the HPTSR protocol. The system performance of the HPTSR protocol is compared to the TSR protocol and the PSR protocol, and it is shown that the HPTSR protocol provides a significant gain in terms of system throughput at high SNRs.

In the next subsection, the studies concern that the single-antenna wireless communication system is replaced with a multi-antenna wireless communication system.

1.1.3 MIMO Wireless Communication System

MIMO is a well-known technique in enhancing the system performance for the conventional communication system with a single antenna installed at the communication nodes. It can be easily implemented by installing multiple antennas at the communication nodes. Compared to the single-input single-output (SISO) system, the MIMO system can provide a higher data rate at the same power and bandwidth. With the MIMO technology, the improvement on the system performances is due to the array gain, diversity gain, spatial multiplexing gain, and interference mitigation provided by the MIMO configuration[27, 28].

- Array gain can be achieved through processing at the transmitter and the receiver. Besides, the average receive SNR of the system is significantly increased due to the coherent combining effect of the received RF signals. The array gain is relying on the number of antennas at the transmitter and receiver. Besides, the channel knowledge of the transmitter and receiver are required.

- In the wireless communication system, the signal power fades. Diversity is a promising method to reduce the fading effects of wireless communication system. The diversity method depends on the signal transmission over a different independently fading path in time, frequency, or space. Compared to the time and frequency diversity, spatial diversity is usually preferred as it does not subject to the transmission time and bandwidth. Moreover, the spatial diversity gain

is obtainable without the channel knowledge of the transmitter and receiver by using suitably designed transmit signals where this type of method is known as space-time coding [29–32].

- Increments in channel capacity without extra cost in power and bandwidth can be achieved by MIMO technology through spatial multiplexing gain [33]. Spatial multiplexing gain is actualized by the independent transmission of RF signals from individual antennas. As the receiver can distinguish the different streams under conducive channel condition, the channel capacity is linearly increased.

- In the wireless communication system, frequency reuse often results in CCI. The MIMO system can mitigate the interference by exploiting the differentiation between the expected signal and co-channel signals through the spatial pattern. Interference mitigation is also applicable to the transmitter to minimize the interference energy transmitted to the co-channel users. With frequency mitigation, the limitation of frequency reuse is mitigated while the multicell capacity is increased.

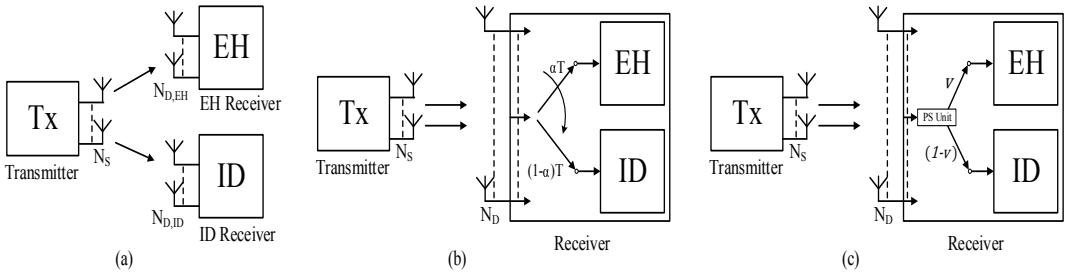

Figure 1.7: Practical SWIPT receiver structures in the MIMO system.

As the MIMO technique can improve the spectral and energy efficiency of the communication system [34, 35], WPT in the MIMO system is more efficient than the SISO system. The practical SWIPT receiver in the MIMO system is illustrated in Fig. 1.7 [36]. As illustrated in Fig. 1.7 (a), separated SWIPT receiver protocol consists of EH and ID functioning blocks, which are implemented as two independent receivers with individual sets of receiving antennas. For PS receiver architecture as illustrated in Fig. 1.7 (b), a PS unit is implemented at each antenna to perform PS on the receiving RF signals. In TS receiver protocol as illustrated in Fig. 1.7 (c), a time-switch is installed at each antenna to rhythmically switch between the EH and ID functioning blocks according to the designed TS-sequences. Existing works with regard to the application of

SWIPT in the MIMO system have been carried out in [6, 37–41]. In [6], the rate-energy (R-E) region for a MIMO system with the application of SWIPT using the separated receiver, TS receiver, and PS receiver is studied. In [37], the joint optimization of stasis PS ratio and transmitter precoding matrix for the MIMO system with PS receiver is investigated with the objective is to maximize the energy harvested under system capacity constraint. In [38], the RE regions for the SWIPT MIMO system with the separated receiver, TS receiver, and PS receiver under the non-linear EH model are investigated. The tradeoffs between the maximal energy transfer and information rate are identified. In [39], the transmitter precoding matrix and PS ratios are jointly optimized for SWIPT multiuser MIMO system using the PS protocol at the receivers with the objective is to minimize the transmit power under mean-square error (MSE) and provided EH constraints. In [40], the authors studied the energy efficiency optimization problem with the consideration of transmit power and EH constraints for the multiuser MIMO system with receivers using TS protocol. In [41], a two-dimensional (2D) search method is proposed to jointly optimize the transmitter precoding matrix and stasis PS ratio, which maximizes the energy harvested at the receiver for the SWIPT MIMO system.

In the next subsection, the literature reviews with regard to the existing studies are presented for the application of SWIPT in the MIMO relay system where the relay is an energy-constricted wireless device.

1.1.4 SWIPT in MIMO Relay Communication System

MIMO relay system is a relay system with the system nodes are installed with more than one antenna. The application of SWIPT in MIMO relay systems with energy-constrained relay node have been investigated in recent years [1, 42–56]. In [1], the authors investigate the joint optimization problem in maximizing the achievable rate for AF MIMO relay system with TSR and PSR protocol by obtaining the optimal source and relay precoding matrices. In [42], the energy efficiency optimization problem for a two way AF MIMO relay system with an EH relay using the PSR protocol is investigated. In [43], the authors investigated the MSE optimization problem for an AF MIMO relay network with a relay node adopting the PSR protocol to harvest energy. Two approaches are proposed to tackle the optimization problem presented in [43], namely, alternating optimization scheme and diagonalization scheme. In [44], the maximization of system capacity for a DF MIMO relay system with the TSR and PSR protocol is studied with finite-alphabet input instead of having Gaussian distribution entries as the

input signals of the system. In [45], the authors investigate the AF massive MIMO relay system with the TSR and PSR protocol implemented at the relay node. Besides, the authors derived asymptotic harvested energy, SNR, and sum-rate expressions when there are infinite relay antennas in the system. In [46], energy-flow assisted relaying protocol for a multi-antenna relay system with single antenna transceiver nodes is proposed, and the system performance is investigated. Dissimilar to the non-energy-flow assisted relaying protocol, energy-flow assisted relaying protocol performs EH by processing the superposition of the energy flow from the destination and the source information signals. In [47], the authors extend the work in [46] from a single antenna transceiver system to a multi-antennas transceiver system. It is shown that the energy flow is beneficial to the energy-flow assisted relaying protocol in improving the system performance when the relay is located closer to the destination node. In [48], the maximization of the system capacity for the SWIPT AF MIMO relay system is investigated under power constraint. The authors proposed to tackle the maximization problem by using an iterative scheme. In [49], the authors investigate SWIPT in the MIMO AF relay system by obtaining the optimal source and relay precoding matrices to characterize the R-E region introduced by the system capacity and stored energy at the relay node for the PSR and TSR protocol. In [50], the work performed in [49] is extended to a similar system with DF relay instead of AF relay. In [51], the capacity optimization problem for a half-duplex AF MIMO relay system with an energy-constrained relay node using PSR protocol with non-uniform PS ratio is investigated and tackled by using the primal-dual algorithm. In [52], the work carried out in [51] is extended to a full-duplex DF relay. In [52], the self-interference signals at the relay node are exploited as an additional form of energy to be harvested by the energy-constrained relay node. In [53], the joint optimization problem for source and relay precoding matrices and TS ratio is studied for AF MIMO relay system with TSR protocol under the consideration of where the source and destination node are able to communicate with each other directly. In [54], the authors extend the work in [53] to the case where the direct link between the source and destination node is absent. It is also shown in [54] that the optimal TS ratio can be obtained via a one-dimensional (1D) search. In [55], the MIMO relay communication system with the EH relay adapting the PSR protocol is investigated with the PS ratio implemented at each relay antenna is not uniformed. The optimization problem arose in [55] is tackled by three proposed algorithms, namely, sequential quadratic programming (SQP) algorithm, upper boundary algorithm, and lower boundary algorithm. In [56],

the existing work carried out in [54] and [55] is extended to an energy-constrained DF relay system.

It can be observed that the channel state information (CSI) of the source-relay and relay-destination link in the existing research [1, 42–48, 51–56] are assumed to be fully known at the receiving nodes, which is impractical in practice. In the practical scenario, the receiving nodes do not have the channel knowledge, and the CSI between the transmitting node and receiving node is estimated. Hence, channel mismatch between the exact CSI and the estimated CSI will arise. The channel mismatch is produced due to the channel noise, quantization errors, channel estimation error, and feedback delay error. When the MIMO relay system with energy-constrained relay is optimized based on estimated CSI, the quality of services (QoS) of the existing proposed transceiver design will experience degradation. In other words, the expected QoS of the proposed system with regard to the system mutual information (MI) between the transceiver, system capacity, and MSE is not achieved due to the degradation caused by the CSI mismatch. Thus, a more realistic assumption is that the true channel matrices have their entries selected based on the independent and identically distributed Gaussian distribution. Its mean value considered as the estimated channel matrices, and the channel estimation errors are modeled based on the well-known Gaussian-Kronecker model [57]. With the consideration concerning the channel estimation error, the QoS of the proposed transceiver design will be provided with robustness to counter the degradation caused by the CSI mismatch.

1.2 Thesis Objectives

The aim of this research is to investigate and propose transceiver design schemes for the SWIPT MIMO relay communication systems with the consideration of imperfect CSI between the source-relay link and the relay-destination link based on the QoS performance, such as, the system MI and the MSE. Furthermore, the EH and the harvested energy consumption are jointly investigated in this research.

In particular, the objectives for the research are to:

- investigate the existing popular transceiver design approaches to optimize the QoS of the SWIPT MIMO relay communication systems for further improvement.

- design new and inventive transceiver design schemes for the SWIPT MIMO relay systems, which are robust against the CSI mismatch with theoretical justifications using computationally efficient optimization algorithms.
- justify and validate the performance of the proposed design schemes with numerical analysis and computer simulations.

In order to achieve the objectives of the research, several optimization techniques are applied, such as the Karush-Kuhn-Tucker (KKT) conditions and the semi-definite programming (SDP) technique to solve the formulated optimization problems.

1.3 Thesis Overview

According to [58], the next-generation wireless communication system is shifting towards a "greener" communication system to reduce the carbon footprint by minimizing the power consumption in a wireless communication system. The next-generation wireless communication system is also required to meet the demands of improved system capacity, communication data rate, and enhanced QoS. Based on [19], it is noted that the EH relay is capable of providing almost identical performance as the self-powered relay node. Hence, the application of SWIPT in relay-assisted communication networks plays a vital role in providing a "greener" communication system for the next-generation wireless communication system. Moreover, MIMO technology can boost the spectral and energy efficiency of the communication system, enhancing the WPT and WIT in the communication system.

In recent decades, the application of SWIPT in the MIMO relay communication system have attracted many research interests from researchers worldwide. However, in the existing research [1, 42–48, 51–56], the CSI is assumed to be known at receiving nodes, which is impractical in practice. In the practical scenario, the receiving nodes do not have the channel knowledge, and the CSI between the transmitting node and receiving node is estimated. Hence, channel mismatch between the exact CSI and the estimated CSI will arise. The channel mismatch is produced due to channel noise, quantization errors, channel estimation error, and feedback delay error. When the MIMO relay system with energy-constrained relay is optimized based on estimated CSI, the performances of the existing proposed transceiver design will experience degradation. Thus, the true channel matrices considered in this thesis is have their entries selected

based on the independent and identically distributed Gaussian distribution, the mean value is considered the estimated channel matrices. The channel estimation errors are modeled based on the well-known Gaussian-Kronecker model [57]. With the consideration with regard to the channel estimation error, the algorithms are proposed to optimize the system performance for the MIMO relay system with an energy-constrained relay.

In Chapter 2, the optimization problem of transceiver design to minimize MSE of the received signal waveform estimation at the destination nodes for a multi-hop AF MIMO relay system with self-powered relay is investigated with the consideration of channel mismatch. The system considered in the chapter consists of multiple sources node transmit individual information signals to multiple destination nodes via relays node arranged in series. In Chapter 3, the maximization of MI between transceiver for the MIMO relay system consisting of one source node, one EH relay node, and one destination node is studied. An innovative EH relaying scheme inspired by the works of [20–23] is proposed for the MIMO relay system. The system performance of the proposed EH relaying scheme is investigated and compared to the existing EH relaying schemes. The study is carried out in the assumption of full CSI is available at the receiving nodes. In Chapter 4, the optimization problem for the MIMO DF relay system with EH relay adapting the TSR protocol is investigated with the consideration of channel mismatch. The system performance is optimized for fixed power schemes and flexible power schemes with and/or without peak power limits. The joint optimization problem of source and relay precoding matrices and TS ratio to maximize the MI between the source and destination node is solved by the proposed algorithms. In Chapter 5, a robust transceiver design is presented to maximize the MI between the transceiver of the considered system, which consists of one transmitter, one EH relay node, and one receiver. Each node is equipped with multiple antennas. The proposed robust algorithm is investigated by comparing its performance to the existing algorithm. In Chapter 6, thesis's conclusions are drawn with the future works which can be carried out in the research field are highlighted.

1.4 Thesis Contributions

Chapter 2: Robust Transceiver Design for Multihop AF MIMO Relay Multicasting from Multiple Sources is based on the following journal submission:

- J. L. Bing, L. Gopal, Y. Rong, C. W. R. Chiong, and Z. Zang, "Robust transceiver design for multi-hop AF MIMO relay multicasting from multiple sources", *IEEE Trans. Veh. Technol.*, accepted, Dec. 2020.

The investigation regarding the transceiver design optimization problem for a multi-hop multicasting AF MIMO relay system is carried out. In the considered approach, numerous transmitters transmit independent information signals to a group of receivers with a series of relay nodes. All the system nodes are equipped with multiple antennas. The CSI mismatch between the exact CSI and estimated CSI, which is modeled based on the Gaussian-Kronecker model, is considered in developing the transceiver design. The transceivers design with robustness is proposed to minimize the maximal weighted mean-square error (WMSE) of the received message at all destination nodes. The WMSE is made statistically robust against the CSI mismatch by average through the exact CSI distributions. A low computational complexity algorithm is developed by decomposing the WMSE optimization problem into multiple optimization subproblems. Through numerical simulations, the proposed transceiver design with robustness outperforms the existing non-robust transceiver design.

Chapter 3: Transceiver Design for SWIPT MIMO Relay Systems with Hybridized Power-Time Splitting-Based Relaying Protocol is based on the following journal publication:

- J. L. Bing, Y. Rong, L. Gopal, and C. W. R. Chiong, "Transceiver Design for SWIPT MIMO Relay Systems with Hybridized Power-Time Splitting-Based Relaying Protocol", *IEEE Access*, vol. 8, pp. 190922-190933, Oct. 2020.

A dual-hop SWIPT AF MIMO relay communication system with an energy-constraint relay node is investigated. In the considered system, the relay node harvests energy from the RF signals transmitted by the source node through the proposed EH relaying scheme, which is called the HPTSR protocol. The relay node fully uses the harvested energy to forward information signal to the destination node. The joint optimization of the TS ratio, source and relay precoding matrices, and the PS ratio vector is proposed to maximize the MI between the source and destination nodes. The optimal structure for the source and relay precoding matrices are derived to simplify the transceiver optimization problem. The upper-bound and lower bound of the objective function are

exploited to solve the optimization problem efficiently with low computational complexity. Through numerical examples, the performance of the proposed algorithms is demonstrated, and it shows that the proposed HPTSR scheme provides better system performance compared to the TSR scheme and the PSR scheme.

Chapter 4: Robust Transceiver Design for SWIPT DF MIMO Relay System with Time Switching Relaying Protocol is based on the following journal submission:

- J. L. Bing, Y. Rong, L. Gopal, and C. W. R. Chiong, "Robust Transceiver Design for SWIPT DF MIMO Relay System with Time Switching Protocol", *IEEE Trans. Commun.*, submitted, Dec. 2020.

A two hop SWIPT DF MIMO relay communication system is studied with the consideration of channel estimation error. In the considered system, the relay node is an energy-constrained device and required to harvest energy based on the RF signal transmitted from the source node through the TS protocol. The harvested energy is used to decode and forward the re-encoded information to the destination node. Joint optimization of the TS factor, source and relay precoding matrices is proposed with robustness against the CSI mismatch to maximize the MI between the source and destination node. Under fixed and flexible power constraints, the optimal structure for the source and relay precoding matrices are derived to simplify the transceiver optimization problem. It is shown through numerical examples that the proposed algorithm with robustness provides better MI performance than existing non-robust algorithms.

Chapter 5: Joint Optimization Precoder Design for SWIPT AF MIMO Relay System with Time-Switching Protocol and Imperfect Channel State Information is based on the following journal submission:

- J. L. Bing, Y. Rong, L. Gopal, and C. W. R. Chiong, "Joint Transceiver Design for AF MIMO Relay System with Time-Switching Relaying Protocol and Imperfect Channel State Information", *IEEE Transactions on Green Communications and Networking*, submitted, Dec. 2020.

A dual-hop AF MIMO relay communication system with an EH relay node is investigated with channel mismatch. The relay node harvests energy based on the RF

signal transmitted by the source node through the TS protocol, and the harvested energy is used to precode the received signal and forward it to the destination node. The TS factor, source and relay precoding matrices are jointly optimized to maximize the system MI. The optimization problem is simplified to a power allocation problem by introducing the optimal structure for the source and relay precoding matrices. The proposed algorithm with robustness is shown through numerical examples to provide better system MI than the non-robust algorithm.

1.5 Notations

In this thesis, the notations used are as follows: Boldface lower case letters such as $\mathbf{x}$ and $\boldsymbol{\lambda}$ are used to denote vectors. Boldface upper case letters such as $\mathbf{A}$ and $\boldsymbol{\Lambda}$ are used to represent matrices. Non-bold lower and upper case letters such as α, k, N, and Υ are used to denote scalars. Identity matrix of size N is denoted as $\mathbf{I}_N$. Note that the scope of any variable in each chapter is limited to that particular chapter.

Chapter 2

Robust Transceiver Design for Multihop AF MIMO Relay Multicasting from Multiple Sources

In this chapter, the transceiver design optimization problem is investigated for multihop multicasting AF MIMO relay systems, where multiple source nodes broadcast their message to multiple destination nodes via multiple relay nodes. Multiple antennas are installed at the sources, relays, and destination nodes. In the transceiver design, the CSI mismatch between the true and the estimated CSI is considered. The CSI mismatch is modeled based on the Gaussian-Kronecker model. In the proposed transceiver design, a robust transceiver design algorithm is developed to jointly optimize the matrices of source, relay, and destination nodes to minimize the maximal WMSE of the received message at all destination nodes. In particular, the WMSE is made statistically robust against the CSI mismatch by averaging the exact CSI distributions. Moreover, the WMSE decomposition is exploited to decrease the computational complexity of the transceiver optimization. Numerical simulations show a better performance of the proposed transceiver design with robustness against the channel mismatch.

In Section 2.1, an overview of existing techniques provided in the literature is presented. The system model of a multihop multicasting relay system with multiple trans-

mitters is presented in Section 2.2. In Section 2.3, the optimal structures for the transceiver designs are proposed with derivation. In Section 2.4, simulation results are presented to demonstrate the performance of the proposed designs. Lastly, the chapter is summarized in Section 2.5.

2.1 Overview of Existing Techniques

With the recent booming of wireless applications such as streaming media and geographic information services, wireless multicasting systems have attracted significant research interest as they enable common information to be concurrently transmitted to multiple recipients. This significantly enhances the bandwidth efficiency and reduces the power consumption at the source node side [59]. The wireless channel is undoubtedly the choice for multicasting applications due to its broadcasting nature. Wireless multicasting technology has been included in communication standards such as WiMAX 802.16m and evolved multimedia broadcast/multicast service standards defined by the Third Generation Partnership Project for LTE-advanced networks [60].

Generally, the design of the optimal beamforming vectors for multicasting is complicated due to its non-convex nature. In [61], the transmit beamforming vector for the multicasting problem has been investigated, considering the perfect CSI is known at the source node. In [61], two design criteria are formulated based on the minimum transmission power and the max-min received power, respectively, and both optimization problems are shown to be non-deterministic polynomial (NP) hard. In [62], the channel capacity for a multi-antenna broadcasting system is investigated. The influence of correlated fading channels on the system capacity for a multi-antenna broadcasting system has been investigated in [63]. Two broadcasting schemes have been proposed in [32], namely the stochastic beamforming and the Alamouti-assisted rank-two beamforming, where the latter technique is a combination of source beamforming and the Alamouti space-time coding. Precoder design for multi-group multicasting with a common message has been addressed in [64].

The works in [32, 61–64] focused on multicasting systems with single-antenna destination nodes, and these works have been extended to multi-antenna destination nodes to improve the system performance. A generalized block diagonalization is developed in [65] to distinguish different multicasting groups. In [66], the design of linear precoders based on the maximization of the achievable rate and minimization of the weighted sum

delay problem has been proposed for multicasting systems with multi-antenna transmitter and receivers.

While the works discussed in [32, 61–66] considered single-hop multicasting systems, it becomes necessary to deploy relay nodes when the source-destination transmission distance is long, or the wireless channel is strongly shadowed [67]. The relay node helps to mitigate the wireless channel pathloss and the shadowing effect of wireless links due to obstacles such as tall buildings and hills. In [68], a distributed beamforming algorithm has been proposed for single antenna communication with multi-group multicasting relay networks to minimize the power consumption of the relays. In [69], jointly optimization problem of source and relay precoder design is investigated for a dual-hop multicasting MIMO relay system, where all nodes are installed with multiple antennas.

A more general multicasting relay network is studied in [70] and [71]. In particular, transceiver design for dual-hop multicasting MIMO relay system with multiple transmitters has been investigated in [70]. In [71], the transceiver design for communication system proposed in [70] is extended to a multihop MIMO relay system with multiple transmitters and receivers. A multihop relay system is necessary when dual-hop multicasting relay systems cannot provide a reliable link between transmitters and receivers. The transceiver designs in [69–71] were developed with the assumption that the full CSI is provided at the source node. However, the full CSI is unavailable in the practical wireless system, and there is always a mismatch between the exact and estimated CSI. Such CSI mismatch degrades the performance of the proposed algorithms in [69–71], and thus, a more robust transceiver design is needed. The works in [69] and [70] have been extended in [72–74] to consider the channel mismatch between the waveform of the exact and estimated signal in the transceiver optimization. This improves the performance of the transceiver optimization against the channel mismatch. However, the transceiver design algorithms in [72–75] are for systems with only one source node and one relay node.

In [76], a robust transceiver optimization problem for AF multihop MIMO relay networks has been developed based on various design criteria, and a general design algorithm was proposed based on the majorization theory and properties of matrix-monotone functions. This work has been further extended in [77] and [78], where the covariance shaping constraints and per-antenna power constraints have been considered in the transceiver design of multihop AF MIMO relay networks. However, the

transceiver design algorithms developed in [76–78] are for systems with only one source node and one destination node.

The CSI mismatch is explicitly considered to develop a transceiver design with robustness for a multihop AF MIMO relay multicasting system. In the system, multiple source nodes multicast their information to a group of destination nodes through a line of relay nodes. All the system nodes are installed with multiple antennas. Different from [71], the impact of the channel estimation error is examined using the Gaussian-Kronecker model. Then, the transceiver optimization problem is formulated to minimize the maximal WMSE of the estimated signals at all destination nodes, where the WMSE is made statistically robust against the CSI mismatch by averaging through the distributions of the true CSI. Hence, various robust transceiver design problems such as the WMSE minimization and the system capacity maximization can be solved via transferring into a weighted minimum mean-squared error (WMMSE) problem.

The contributions and challenges faced in this chapter are summarized below:

- The impact of channel estimation error modeled by the Gaussian-Kronecker model towards the system performance of multihop multicasting AF MIMO relay systems is examined.

- The transceiver design proposed can provide robustness to combat against the unavoidable channel mismatch between the exact and the estimated CSI in the practical scenario, which improved the system performance of existing transceiver design under the similar system model [71].

- The works carried out in this chapter is extended from the existing works carried out in [72–75] in which the system model only considers a single source node and a relay node to multiple source nodes with multiple relay nodes arranged in series. In other words, the system model investigated can support a very long-distance communication system with more transmitters for multicasting the signal information simultaneously through multiple relay nodes to the multiple destination nodes.

- The works carried out in this chapter is extended from the existing works carried out in [76–78] in which the system model only considers a single pair of source-destination node to the system model with multiple source nodes and multiple destination nodes. In other words, the system model considered in this chapter is more general in which there are multiple transmitters transmit information signals

simultaneously to multiple destination nodes by exploiting the broadcasting nature of the RF signal.

- Compare to the existing works [72–78], more relay nodes are considered, which significantly increase the challenge in solving the optimization problem.
- A robust transceiver design with low computation complexity is proposed, which reduces the computation time required to achieve the optimum result.
- The optimization problem for transceiver design with the WMSE objective function is more challenging to solve than those in [71–75], particularly when the weight matrix is not an identity matrix.

The optimal structure of the multihop relay matrices is derived to simplify the transceiver optimization problem, enabling the objective function to be decomposed into the sum of L WMSE terms, where L is the number of hops. It is shown that the original problem can be decomposed into L subproblems under high SNRs assumption. By exploiting upper-bounds of the objective functions, the precoding matrices for the first $L-2$ relay nodes are noted to have a closed-form water-filling solution. For non-identity weight matrices, the subproblems of optimizing the source matrices and the precoding matrix at the last relay node are non-convex. Hence, iterative algorithms are proposed in order to tackle these challenging subproblems. It is shown through numerical simulations that the developed transceiver design with robustness outperforms the transceiver design algorithm developed in [71].

2.2 Multihop Multicasting Relay System Model

In the proposed system as shown in Fig. 2.1, a multicasting MIMO relay system with L-hop ($L \geq 2$) is considered where K source nodes concurrently multicast their information to M destination nodes via $L-1$ AF relay nodes. $N_{s,k}$ and $N_{r,l}$ are the numbers of antennas installed at the kth source node and the lth relay node, respectively. For simplicity, each destination node is installed with N_D antennas. However, the algorithm proposed is easily extended to multicasting systems with various multi-antennas destination nodes. Direct links do not exist between the source nodes and destination nodes as well as those between any two non-consecutive relays due to severe pathloss/shadowing.

As the relay nodes are assumed to work in the half-duplex mode to avoid self-interference, the data communication between the source and destination nodes takes

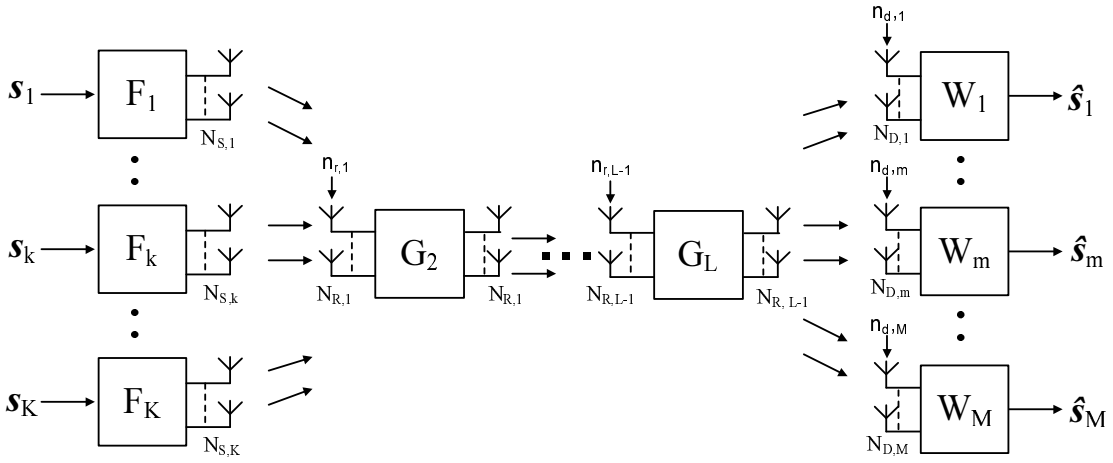

Figure 2.1: Block diagram of a multihop AF multicasting MIMO relay system with multiple sources.

place over L time slots. The kth source node precodes the modulated signal vector $\mathbf{s}_k \in \mathbb{C}^{N_{B,k}\times 1}$ by a linear precoding matrix $\mathbf{F}_k \in \mathbb{C}^{N_{S,k}\times N_{B,k}}$ and transmits the precoded vector $\mathbf{F}_k\mathbf{s}_k$ to the first relay node at the first time slot. The covariance matrix of $\mathbf{s}_k$ is given as $E\{\mathbf{s}_k\mathbf{s}_k^H\} = \mathbf{I}_{N_{B,k}}$ with $N_{B,k} \leq N_{S,k}$, where $E\{\cdot\}$ represents statistical expectation with respect to the signal and noise, $\mathbf{I}_n$ represents as identity matrix with order n, and $(\cdot)^H$ represents the matrix Hermitian transpose. Let introduce $N_B = \sum_{k=1}^{K} N_{B,k}$ as the total number of signals from all K users, which satisfies $N_B \leq \min(N_{R,1}, \cdots, N_{R,L-1}, N_D)$.

The received signal vector at the first relay node is expressed as

$$\mathbf{y}_1 = \sum_{k=1}^{K} \mathbf{H}_{1,k}\mathbf{F}_k\mathbf{s}_k + \mathbf{n}_{r,1} \triangleq \mathbf{H}_1\mathbf{G}_1\mathbf{s} + \mathbf{n}_{r,1} \triangleq \mathbf{H}_1\mathbf{x}_1 + \mathbf{n}_{r,1} \tag{2.1}$$

where $\mathbf{H}_{1,k} \in \mathbb{C}^{N_{R,1}\times N_{S,k}}$ is the MIMO channel matrix between the kth source node and the first relay node, $\mathbf{n}_{r,1} \in \mathbb{C}^{N_{R,1}\times 1}$ is the additive white Gaussian noise (AWGN) vector induced at the first relay node, $\mathbf{H}_1 = [\mathbf{H}_{1,1}, \mathbf{H}_{1,2}, \cdots, \mathbf{H}_{1,K}]$, $\mathbf{x}_1 = \mathbf{G}_1\mathbf{s}$, $\mathbf{G}_1 \triangleq \mathrm{bd}(\mathbf{F}_1, \mathbf{F}_2, \cdots, \mathbf{F}_K)$, and $\mathbf{s} \triangleq [\mathbf{s}_1^T, \mathbf{s}_2^T, \cdots, \mathbf{s}_K^T]^T$. Here $(\cdot)^T$ represent the transposition of a matrix and $\mathrm{bd}(\cdot)$ represent the block-diagonalization of matrices.

It is noted that the transmitted signal vector from the lth relay node is expressed as

$$\mathbf{x}_{l+1} = \mathbf{G}_{l+1}\mathbf{y}_l, \quad l = 1, \cdots, L-1 \tag{2.2}$$

where $\mathbf{G}_{l+1} \in \mathbb{C}^{N_{R,l}\times N_{R,l}}$ is the lth relay linear precoding matrix and $\mathbf{y}_l \in \mathbb{C}^{N_{R,l}\times 1}$ is

the received signal at the lth relay node which is expressed as

$$\mathbf{y}_l = \mathbf{H}_l \mathbf{x}_l + \mathbf{n}_{r,l}, \quad l = 1, \cdots, L-1. \tag{2.3}$$

where $\mathbf{H}_l \in \mathbb{C}^{N_{R,l} \times N_{R,l-1}}$ is the lth hop MIMO channel matrix ($N_{R,0} = \sum_{i=1}^{K} N_{S,k}$), and $\mathbf{n}_{r,l} \in \mathbb{C}^{N_{R,l} \times 1}$ is the AWGN vector induced at the lth relay node. In general scenario, i.e. $L \geq 3$, the received signal vector (2.3) at the lth relay node by applying (2.1) and (2.2) is equivalently expressed as

$$\mathbf{y}_l = \prod_{i=l}^{1} (\mathbf{H}_i \mathbf{G}_i)\, \mathbf{s} + \sum_{j=2}^{l} \left(\prod_{i=l}^{j} (\mathbf{H}_i \mathbf{G}_i)\, \mathbf{n}_{r,j-1} \right) + \mathbf{n}_{r,l} \quad l = 2, \cdots, L-1 \tag{2.4}$$

where $\prod_{i=l}^{k} \mathbf{X}_i$ represent multiplication over a series of $\mathbf{X}_i$ from the lth to the kth terms.

The received signal vector $\mathbf{x}_L$ at the last relay node is multicast to all M destination nodes. Based on (2.4), the received signal at the mth destination node can be expressed as

$$\begin{aligned} \mathbf{y}_{d,m} &= \mathbf{H}_{L,m} \mathbf{G}_L \prod_{l=L-1}^{1} (\mathbf{H}_l \mathbf{G}_l)\, \mathbf{s} + \mathbf{H}_{L,m} \mathbf{G}_L \left(\sum_{j=2}^{L-1} \left(\prod_{l=L-1}^{j} (\mathbf{H}_l \mathbf{G}_l)\, \mathbf{n}_{r,j-1} \right) + \mathbf{n}_{r,L-1} \right) \\ &\quad + \mathbf{n}_{d,m} \\ &\triangleq \bar{\mathbf{A}}_m \mathbf{s} + \mathbf{v}_m, \qquad m = 1, \cdots, M \end{aligned} \tag{2.5}$$

where $\mathbf{H}_{L,m} \in \mathbb{C}^{N_D \times N_{R,L-1}}$ is the MIMO channel matrix between the last relay node and the mth destination node, $\mathbf{n}_{d,m} \in \mathbb{C}^{N_D \times 1}$ is the AWGN vector induced at the mth destination node. For $m = 1, \cdots, M$, the equivalent MIMO channel matrix between source nodes and the mth destination node can be written as

$$\bar{\mathbf{A}}_m = \mathbf{H}_{L,m} \mathbf{G}_L \prod_{l=L-1}^{1} (\mathbf{H}_l \mathbf{G}_l) \tag{2.6}$$

and the equivalent noise vector received at the mth destination node is given by

$$\mathbf{v}_m = \mathbf{H}_{L,m} \mathbf{G}_L \left(\sum_{j=2}^{L-1} \left(\prod_{l=L-1}^{j} (\mathbf{H}_l \mathbf{G}_l) \mathbf{n}_{r,j-1} \right) + \mathbf{n}_{r,L-1} \right) + \mathbf{n}_{d,m}. \tag{2.7}$$

It is observed that although the system model (2.5) is developed for a narrow band system, for orthogonal frequency-division multiplexing (OFDM) based broadband multihop AF multicasting MIMO relay systems, the developed algorithm can be applied to each subcarrier of the OFDM system.

Usually, the perfect CSI is needed for the optimal precoder matrices design. However, the exact CSI is unavailable in practice due to channel estimation errors, which results in a mismatch between the true and estimated CSI. Thus, the true channel matrices $\mathbf{H}_{1,k}$, $\mathbf{H}_l$, and $\mathbf{H}_{L,m}$ can be modelled as [75, 76, 79, 80]

$$\mathbf{H}_{1,k} = \widehat{\mathbf{H}}_{1,k} + \mathbf{\Delta}_{1,k}, \qquad k = 1, \cdots, K \tag{2.8}$$
$$\mathbf{H}_l = \widehat{\mathbf{H}}_l + \mathbf{\Delta}_l, \qquad l = 2, \cdots, L-1, L \geq 3 \tag{2.9}$$
$$\mathbf{H}_{L,m} = \widehat{\mathbf{H}}_{L,m} + \mathbf{\Delta}_{L,m}, \ m = 1, \cdots, M \tag{2.10}$$

where $\widehat{\mathbf{H}}_{1,k}$, $\widehat{\mathbf{H}}_l$, and $\widehat{\mathbf{H}}_{L,m}$ are the estimated channel matrices between the kth source node and the first relay node, the $(l-1)$th relay node and the lth relay node, and the last relay node and the mth destination node, respectively, $\mathbf{\Delta}_{1,k}$, $\mathbf{\Delta}_l$, and $\mathbf{\Delta}_{L,m}$ are the corresponding CSI mismatch matrices. The CSI mismatch matrices are modelled based on the Gaussian-Kronecker model [75] which are given as

$$\mathbf{\Delta}_{1,k} \sim \mathcal{CN}(\mathbf{0}, \mathbf{\Sigma}_{1,k} \otimes \mathbf{\Psi}_{1,k}^T) \tag{2.11}$$
$$\mathbf{\Delta}_l \sim \mathcal{CN}(\mathbf{0}, \mathbf{\Sigma}_l \otimes \mathbf{\Psi}_l^T) \tag{2.12}$$
$$\mathbf{\Delta}_{L,m} \sim \mathcal{CN}(\mathbf{0}, \mathbf{\Sigma}_{L,m} \otimes \mathbf{\Psi}_{L,m}^T) \tag{2.13}$$

where $\otimes$ represents as the Kronecker product, $\mathbf{\Sigma}_{1,k}$, $\mathbf{\Sigma}_l$ and $\mathbf{\Sigma}_{L,m}$ are the row covariance matrices for $\mathbf{\Delta}_{1,k}$, $\mathbf{\Delta}_l$ and $\mathbf{\Delta}_{L,m}$ respectively, and $\mathbf{\Psi}_{1,k}$, $\mathbf{\Psi}_l$ and $\mathbf{\Psi}_{L,m}$ are the column covariance matrices for $\mathbf{\Delta}_{1,k}$, $\mathbf{\Delta}_l$ and $\mathbf{\Delta}_{L,m}$ respectively. These covariance matrices model the correlation among antennas at each node [75].

Based on (2.8)-(2.13), the true channel matrices $\mathbf{H}_{1,k}$, $\mathbf{H}_l$, and $\mathbf{H}_{L,m}$ is rewritten into [75]

$$\mathbf{H}_{1,k} = \widehat{\mathbf{H}}_{1,k} + \mathbf{\Sigma}_{1,k}^{\frac{1}{2}} \mathbf{H}_{\omega_{1,k}} \mathbf{\Psi}_{1,k}^{\frac{1}{2}}, \qquad k = 1, \cdots, K \tag{2.14}$$
$$\mathbf{H}_l = \widehat{\mathbf{H}}_l + \mathbf{\Sigma}_l^{\frac{1}{2}} \mathbf{H}_{\omega_l} \mathbf{\Psi}_l^{\frac{1}{2}}, \qquad l = 2, \cdots, L-1 \tag{2.15}$$
$$\mathbf{H}_{L,m} = \widehat{\mathbf{H}}_{L,m} + \mathbf{\Sigma}_{L,m}^{\frac{1}{2}} \mathbf{H}_{\omega_{L,m}} \mathbf{\Psi}_{L,m}^{\frac{1}{2}}, \ m = 1, \cdots, M \tag{2.16}$$

where $\mathbf{H}_{\omega_{1,k}}$, $\mathbf{H}_{\omega_l}$, and $\mathbf{H}_{\omega_{L,m}}$ elements drawn from independent and identically distributed (i.i.d.) complex Gaussian distribution with zero mean and unit variance.

Lemma 1: [75], [81] For $\mathbf{H} \sim \mathcal{CN}(\widehat{\mathbf{H}}, \mathbf{\Sigma} \otimes \mathbf{\Psi}^T)$ and any constant matrix $\mathbf{A}$, there is

$$E\{\mathbf{HAH}^H\} = \widehat{\mathbf{H}}\mathbf{A}\widehat{\mathbf{H}}^H + tr\{\mathbf{A\Psi}\}\mathbf{\Sigma} \tag{2.17}$$

where $tr\{\cdot\}$ stands for matrix trace.

Due to simplicity, a linear receiver with a weight matrix $\mathbf{W}_m$ is adapted at the mth destination node to recover the transmitted signal waveform. Thus, the estimated signal vector at the mth destination node is expressed as

$$\widehat{\mathbf{s}}_m = \mathbf{W}_m \mathbf{y}_{d,m}, \quad m = 1, \cdots, M. \tag{2.18}$$

It is shown in [76] that various performance metrics for transceiver design such as weighted MSE and system capacity are functions of the MSE matrix of the estimated signal waveform at the destination nodes. Moreover, considering that capacity maximization can be solved via transferring into a WMMSE problem [82], a Hermitian weight matrix $\mathbf{O}$ is introduced. Similar to [83], the weight matrix $\mathbf{O}$ is used to convert the capacity maximization problem to a weighted MSE minimization problem. When solving the capacity maximization problem, the weight matrix $\mathbf{O}$ can be updated iteratively following [82]. Thus, by applying (2.5) and (2.18), the WMSE of the estimated signal waveform at the destination nodes can be expressed as

$$\begin{aligned} E_m &= E\{tr\{\mathbf{O}(\widehat{\mathbf{s}}_m - \mathbf{s})(\widehat{\mathbf{s}}_m - \mathbf{s})^H\}\} \\ &= tr\big\{\mathbf{O}(\mathbf{W}_m E\{\mathbf{y}_{d,m}\mathbf{y}_{d,m}^H\}\mathbf{W}_m^H - \mathbf{W}_m\bar{\mathbf{A}}_m - \bar{\mathbf{A}}_m^H\mathbf{W}_m^H + \mathbf{I}_{N_B})\big\}, \quad m = 1, \cdots, M. \end{aligned} \tag{2.19}$$

The transmission power needed by the kth source node is $tr\{\mathbf{F}_k\mathbf{F}_k^H\}$, $k = 1, \cdots, K$. From (2.2), the transmission power required by the lth relay node can be derived as

$$\begin{aligned} P(\mathbf{G}_{l+1}) &= tr\big\{E\{\mathbf{x}_{l+1}\mathbf{x}_{l+1}^H\}\big\} \\ &= tr\{\mathbf{G}_{l+1}E\{\mathbf{y}_l\mathbf{y}_l^H\}\mathbf{G}_{l+1}^H\}, \quad l = 1, \cdots, L-1. \end{aligned} \tag{2.20}$$

2.3 Proposed Transceiver Design

From (2.19), it can be concluded that it is difficult to design $\mathbf{W}_m$ to optimize E_m without the perfect $\mathbf{H}_{1,k}$, $\mathbf{H}_l$ and $\mathbf{H}_{L,m}$. If designing $\mathbf{W}_m$, $\mathbf{G}_l$, and $\mathbf{F}_k$ is based on estimated channel matrices, the system performance may degrade significantly due to the channel estimation errors $\mathbf{\Delta}_{1,k}$, $\mathbf{\Delta}_l$, and $\mathbf{\Delta}_{L,m}$. Thus, instead of optimizing E_m, the transceiver precoding matrices is designed to minimize J_m which is given as

$$J_m \triangleq E_H\{E_m\} \tag{2.21}$$

where $E_H\{\cdot\}$ denotes the statistical expectation with respect to MIMO channel matrices with distributions in (2.8)-(2.13). Using *Lemma 1*, the WMSE function in (2.21) can

be written as

$$J_m = tr\{\mathbf{O}(\mathbf{I}_{N_B} + \mathbf{W}_m\mathbf{R}_{\mathbf{y}_{d,m}}\mathbf{W}_m^H - \mathbf{W}_m\widehat{\mathbf{A}}_m - \widehat{\mathbf{A}}_m^H\mathbf{W}_m^H)\}, \quad m = 1, \cdots, M. \tag{2.22}$$

The detailed derivations of (2.22) can be found in Appendix 2.6.1. For $m = 1, \cdots, M$, $\widehat{\mathbf{A}}_m$ is the estimated MIMO channel matrix from all source nodes to the mth destination node and $\mathbf{R}_{\mathbf{y}_{d,m}}$ is the expectation of the covariance matrix of $\mathbf{y}_{d,m}$ with respect to the distribution in (2.14) - (2.16). It is noted that $\mathbf{R}_{\mathbf{y}_l} = E_H\{E\{\mathbf{y}_l\mathbf{y}_l^H\}\}$ is the expectation of the covariance matrix of $\mathbf{y}_l$ with respect to the distribution in (2.15) and is calculated recursively by

$$\mathbf{R}_{\mathbf{y}_l} = \widehat{\mathbf{H}}_l\mathbf{G}_l\mathbf{R}_{\mathbf{y}_{l-1}}\mathbf{G}_l^H\widehat{\mathbf{H}}_l^H + tr\{\mathbf{G}_l\mathbf{R}_{\mathbf{y}_{l-1}}\mathbf{G}_l^H\mathbf{\Psi}_l\}\mathbf{\Sigma}_l + \mathbf{I}_{N_{R,l}}, \qquad l = 2, \cdots, L-1$$

and for $l = 1$

$$\mathbf{R}_{\mathbf{y}_1} = \widehat{\mathbf{H}}_1\mathbf{G}_1\mathbf{G}_1^H\widehat{\mathbf{H}}_1^H + \sum_{k=1}^{K} tr\{\mathbf{F}_k\mathbf{F}_k^H\mathbf{\Psi}_{1,k}\}\mathbf{\Sigma}_{1,k} + \mathbf{I}_{N_{R,1}}.$$

As the exact MIMO channel matrices are not available, the power constraints at the lth relay node (2.20) can be expressed as

$$E_H\{P(\mathbf{G}_{l+1})\} = tr\{\mathbf{G}_{l+1}\mathbf{R}_{\mathbf{y}_l}\mathbf{G}_{l+1}^H\}, \quad l = 1, \cdots, L-1. \tag{2.23}$$

The objective of the proposed robust transceiver design is to minimize the maximal of WMSE given in (2.22) across all destination nodes restricted by the power constraints at the source and relay nodes. Based on (2.22) and (2.23), the optimization problem can be rewritten as

$$\min_{\{\mathbf{F}_k\},\{\mathbf{G}_l\},\{\mathbf{W}_m\}} \max_m \quad J_m \tag{2.24a}$$

$$s.t.\ tr\{\mathbf{G}_l\mathbf{R}_{\mathbf{y}_{l-1}}\mathbf{G}_l^H\} \le P_{r,l},\ l = 2, \cdots, L \tag{2.24b}$$

$$tr\{\mathbf{F}_k\mathbf{F}_k^H\} \le P_{s,k}, \qquad k = 1, \cdots, K \tag{2.24c}$$

where $\{\mathbf{F}_k\} \triangleq \{\mathbf{F}_k, k = 1, \cdots, K\}$, $\{\mathbf{G}_l\} \triangleq \{\mathbf{G}_l, l = 2, \cdots, L\}$, and $\{\mathbf{W}_m\} \triangleq \{\mathbf{W}_m, m = 1, \cdots, M\}$, (2.24b) is the power constraint at the $(l-1)$th relay node with a power limit of $P_{r,l} > 0$ and (2.24c) is the transmission power constraint at the kth source node with the power budget $P_{s,k} > 0$. Due to the complicated objective function (2.24a), it is very challenging to determine the solution to the min-max problem (2.24) with a reasonable

computational complexity[1]. A low computational complexity approach is developed to solve the problem (2.24).

2.3.1 Optimization of $\mathbf{W}_m$ and $\mathbf{G}_l$

For any given $\{\mathbf{F}_k\}$ and $\{\mathbf{G}_l\}$, the optimal $\mathbf{W}_m$ which minimizes J_m in (2.22) is the linear minimum MSE (LMMSE) receiver expressed as [85]

$$\mathbf{W}_m = \widehat{\mathbf{A}}_m^H \mathbf{R}_{\mathbf{y}_{d,m}}^{-1}, \quad m = 1, \cdots, M \tag{2.25}$$

where $(\cdot)^{-1}$ represent the inverse matrix. By substituting (2.25) to (2.22), the WMSE function can be rewritten as

$$J_m = tr\big\{\mathbf{O}\big(\mathbf{I}_{N_B} - \widehat{\mathbf{A}}_m^H \mathbf{R}_{\mathbf{y}_{d,m}}^{-1} \widehat{\mathbf{A}}_m\big)\big\}. \tag{2.26}$$

With the input-output relationship (2.4), it can be shown that the optimal $\mathbf{G}_l$ has the optimal structure of [82, 86]

$$\mathbf{G}_l = \mathbf{T}_l \mathbf{D}_l, \qquad l = 2, \cdots, L \tag{2.27}$$

where $\mathbf{T}_l \in \mathbb{C}^{N_{R,l-1} \times N_B}$ is a linear filter which is viewed as the transmitting precoder matrix for the effective lth hop MIMO channel, and $\mathbf{D}_l = \mathbf{O}^{\frac{H}{2}} \mathbf{K}_{l-1}^H \mathbf{R}_{\mathbf{y}_{l-1}}^{-1} \in \mathbb{C}^{N_B \times N_{R,l-1}}$ is the LMMSE receiver weight matrix for the $(l-1)$th relay node received signal. Here $\mathbf{K}_l = \prod_{i=l}^{1} (\widehat{\mathbf{H}}_i \mathbf{G}_i)$, $l = 1, \cdots, L-1$. Using (2.27), (2.26) is equivalently expressed as the sum of L MSE functions as

$$\begin{aligned} J_m = & tr\big\{\mathbf{O}(\mathbf{I}_{N_B} + \mathbf{G}_1^H \widehat{\mathbf{H}}_1^H \mathbf{\Xi}_1^{-1} \widehat{\mathbf{H}}_1 \mathbf{G}_1)^{-1}\big\} \\ & + \sum_{l=2}^{L-1} tr\big\{(\mathbf{Z}_l^{-1} + \mathbf{T}_l^H \widehat{\mathbf{H}}_l^H \mathbf{\Xi}_l^{-1} \widehat{\mathbf{H}}_l \mathbf{T}_l)^{-1}\big\} \\ & + tr\big\{(\mathbf{Z}_L^{-1} + \mathbf{T}_L^H \widehat{\mathbf{H}}_{L,m}^H \mathbf{\Xi}_{L,m}^{-1} \widehat{\mathbf{H}}_{L,m} \mathbf{T}_L)^{-1}\big\} \end{aligned} \tag{2.28}$$

where

$$\mathbf{\Xi}_1 = \sum_{k=1}^{K} tr\{\mathbf{F}_k \mathbf{F}_k^H \mathbf{\Psi}_{1,k}\} \mathbf{\Sigma}_{1,k} + \mathbf{I}_{N_{R,1}} \tag{2.29}$$

$$\mathbf{Z}_l = \mathbf{O}^{\frac{H}{2}} \mathbf{K}_{l-1}^H \mathbf{R}_{\mathbf{y}_{l-1}}^{-1} \mathbf{K}_{l-1} \mathbf{O}^{\frac{1}{2}}, \qquad l = 2, \cdots, L \tag{2.30}$$

$$\mathbf{\Xi}_l = tr\{\mathbf{T}_l \mathbf{Z}_l \mathbf{T}_l^H \mathbf{\Psi}_l\} \mathbf{\Sigma}_l + \mathbf{I}_{N_{R,l}}, \quad l = 2, \cdots, L-1 \tag{2.31}$$

$$\mathbf{\Xi}_{L,m} = tr\{\mathbf{T}_L \mathbf{Z}_L \mathbf{T}_L^H \mathbf{\Psi}_{L,m}\} \mathbf{\Sigma}_{L,m} + \mathbf{I}_{N_D}, m = 1, \cdots, M. \tag{2.32}$$

[1]For systems with perfect CSI, the problem (2.24) can be solved by an iterative algorithm similar to [71] based on the conditional quadratic structure of J_m [84] with respect to the variables $\{\mathbf{F}_k\}, \{\mathbf{G}_l\}, \{\mathbf{W}_m\}$. However, when the CSI mismatch is considered, such structure does not hold in (2.24a) and (2.24b).

When the perfect CSI is available, it can be noted that $\mathbf{\Xi}_l = \mathbf{I}_{N_{R,l}}$, $l = 1, \cdots, L-1$, and $\mathbf{\Xi}_{L,m} = \mathbf{I}_{N_D}$, $m = 1, \cdots, M$. Then (2.28) can be viewed as the MSE decomposition based on multihop multicasting MIMO relay systems without channel estimation error, i.e., $\widehat{\mathbf{H}}_{1,k} = \mathbf{H}_{1,k}$, $\widehat{\mathbf{H}}_l = \mathbf{H}_l$, and $\widehat{\mathbf{H}}_{L,m} = \mathbf{H}_{L,m}$. Moreover, it can be noticed that the first term in (2.28) is actually the WMSE of the first-hop signal waveform estimation with the LMMSE receiver $\mathbf{\Gamma} = \mathbf{G}_1^H \widehat{\mathbf{H}}_1^H \mathbf{R}_{\mathbf{y}_1}^{-1}$ at the first relay node which is expressed as

$$\begin{aligned} J_s &= E_H\left\{E\{tr\{\mathbf{O}\big((\mathbf{\Gamma}\mathbf{y}_1 - \mathbf{s})(\mathbf{\Gamma}\mathbf{y}_1 - \mathbf{s})^H\big)\}\}\right\} \\ &= tr\{\mathbf{O}\big(\mathbf{\Gamma}\mathbf{R}_{\mathbf{y}_1}\mathbf{\Gamma}^H - \mathbf{\Gamma}\widehat{\mathbf{H}}_1\mathbf{G}_1 - \mathbf{G}_1^H\widehat{\mathbf{H}}_1^H\mathbf{\Gamma}^H + \mathbf{I}_{N_B})\} \\ &= tr\big\{\mathbf{O}\big(\mathbf{I}_{N_B} + \mathbf{G}_1^H\widehat{\mathbf{H}}_1^H\mathbf{\Xi}_1^{-1}\widehat{\mathbf{H}}_1\mathbf{G}_1)^{-1}\big\}. \end{aligned}$$

The subsequence terms in (2.28) can be considered as the increments of the MSE caused by the consecutive hops.

By adapting (2.27) and (2.30), the $(l-1)$th relay node required transmission power is expressed as

$$tr\{\mathbf{G}_l\mathbf{R}_{\mathbf{y}_{l-1}}\mathbf{G}_l^H\} = tr\{\mathbf{T}_l\mathbf{Z}_l\mathbf{T}_l^H\}, \quad l = 2, \cdots, L. \tag{2.33}$$

Substituting (2.33) into (2.24), the optimization problem (2.24) can be obtained as

$$\min_{\{\mathbf{F}_k\},\{\mathbf{T}_l\}} \max_m \; J_m \tag{2.34a}$$

$$s.t.\; tr\{\mathbf{T}_l\mathbf{Z}_l\mathbf{T}_l^H\} \le P_{r,l}, \qquad l = 2, \cdots, L \tag{2.34b}$$

$$tr\{\mathbf{F}_k\mathbf{F}_k^H\} \le P_{s,k}, \qquad k = 1, \cdots, K \tag{2.34c}$$

where $\{\mathbf{T}_l\} \triangleq \{\mathbf{T}_l, l = 2, \cdots, L\}$. Based on the matrix inversion lemma [87], (2.30) can be rewritten as

$$\begin{aligned} \mathbf{Z}_l &= \mathbf{O}^{\frac{H}{2}}\mathbf{K}_{l-1}^H(\mathbf{K}_{l-1}\mathbf{K}_{l-1}^H + \mathbf{\Omega}_{l-1})^{-1}\mathbf{K}_{l-1}\mathbf{O}^{\frac{1}{2}} \\ &= \mathbf{O}^{\frac{H}{2}}\mathbf{K}_{l-1}^H\mathbf{\Omega}_{l-1}^{-1}\mathbf{K}_{l-1}(\mathbf{K}_{l-1}^H\mathbf{\Omega}_{l-1}^{-1}\mathbf{K}_{l-1} + \mathbf{I}_{N_B})^{-1}\mathbf{O}^{\frac{1}{2}} \qquad l = 2, \cdots, L \end{aligned} \tag{2.35}$$

where

$$\begin{aligned} \mathbf{\Omega}_1 &= \mathbf{\Xi}_1 \\ \mathbf{\Omega}_l &= \sum_{j=2}^{l}\prod_{i=l}^{j}(\widehat{\mathbf{H}}_i\mathbf{G}_i)\mathbf{\Xi}_{j-1}\prod_{i=j}^{l}(\mathbf{G}_i^H\widehat{\mathbf{H}}_i^H) + \mathbf{\Xi}_l, l = 2, \cdots, L. \end{aligned}$$

It is noted that $\mathbf{Z}_l$ can be approximated as $\mathbf{O}$ with high SNRs i.e. $\mathbf{K}_{l-1}^H\mathbf{\Omega}_{l-1}^{-1}\mathbf{K}_{l-1} \gg \mathbf{I}_{N_B}$ Hence, the problem (2.34) is expressed into

$$\min_{\{\mathbf{F}_k\},\{\mathbf{T}_l\}} \max_m \; tr\big\{\mathbf{O}(\mathbf{I}_{N_B}+\mathbf{G}_1^H\widehat{\mathbf{H}}_1^H\boldsymbol{\Xi}_1^{-1}\widehat{\mathbf{H}}_1\mathbf{G}_1)^{-1}\big\} + \sum_{l=2}^{L-1} tr\big\{(\mathbf{O}^{-1}+\mathbf{T}_l^H\widehat{\mathbf{H}}_l^H\boldsymbol{\Upsilon}_l^{-1}\widehat{\mathbf{H}}_l\mathbf{T}_l)^{-1}\big\} + tr\big\{(\mathbf{O}^{-1}+\mathbf{T}_L^H\widehat{\mathbf{H}}_{L,m}^H\boldsymbol{\Upsilon}_{L,m}^{-1}\widehat{\mathbf{H}}_{L,m}\mathbf{T}_L)^{-1}\big\} \tag{2.36a}$$

$$s.t.\; tr\{\mathbf{T}_l\mathbf{O}\mathbf{T}_l^H\} \le P_{r,l}, \qquad l=2,\cdots,L \tag{2.36b}$$

$$tr\{\mathbf{F}_k\mathbf{F}_k^H\} \le P_{s,k}, \qquad k=1,\cdots,K \tag{2.36c}$$

where $\{\boldsymbol{\Upsilon}_l, l=2,\cdots,L-1\}$ and $\{\boldsymbol{\Upsilon}_{L,m}, m=1,\cdots,M\}$ are given as

$$\boldsymbol{\Upsilon}_l = tr\{\mathbf{T}_l\mathbf{O}\mathbf{T}_l^H\boldsymbol{\Psi}_l\}\boldsymbol{\Sigma}_l + \mathbf{I}_{N_{R,l}} \tag{2.37}$$

$$\boldsymbol{\Upsilon}_{L,m} = tr\{\mathbf{T}_L\mathbf{O}\mathbf{T}_L^H\boldsymbol{\Psi}_{L,m}\}\boldsymbol{\Sigma}_{L,m} + \mathbf{I}_{N_D}. \tag{2.38}$$

When the exact CSI is available, there are $\boldsymbol{\Xi}_1 = \mathbf{I}_{N_{R,1}}$, $\boldsymbol{\Upsilon}_l = \mathbf{I}_{N_{R,l}}$, $l=2,\cdots,L-1$, and $\boldsymbol{\Upsilon}_{L,m} = \mathbf{I}_{N_D}$, $m=1,\cdots,M$, and the problem (2.36) can be viewed as a non-robust transceiver design problem. In other words, the proposed transceiver design with robustness extends the non-robust transceiver design algorithm to the general practical multicasting MIMO system with CSI mismatch and WMSE objective function.

It can be observed that each trace term in (2.36a) can be optimized independently. Thus, the problem (2.36) can be decomposed into L subproblems. In particular, the problem of optimizing the source precoding matrices can be written as

$$\min_{\{\mathbf{F}_k\}} tr\big\{\mathbf{O}(\mathbf{I}_{N_B}+\mathbf{G}_1^H\widehat{\mathbf{H}}_1^H\boldsymbol{\Xi}_1^{-1}\widehat{\mathbf{H}}_1\mathbf{G}_1)^{-1}\big\} \tag{2.39a}$$

$$s.t.\; tr\{\mathbf{F}_k\mathbf{F}_k^H\} \le P_{s,k}, \qquad k=1,\cdots,K. \tag{2.39b}$$

For $L \ge 3$, the problem of optimizing the $(l-1)$th relay node precoding matrix, $l = 2,\cdots,L-1$, is given by

$$\min_{\mathbf{T}_l} tr\big\{(\mathbf{O}^{-1}+\mathbf{T}_l^H\widehat{\mathbf{H}}_l^H\boldsymbol{\Upsilon}_l^{-1}\widehat{\mathbf{H}}_l\mathbf{T}_l)^{-1}\big\} \tag{2.40a}$$

$$s.t.\; tr\{\mathbf{T}_l\mathbf{O}\mathbf{T}_l^H\} \le P_{r,l}. \tag{2.40b}$$

The precoding matrix at the last relay node is optimized by solving

$$\min_{\mathbf{T}_L} \max_m tr\big\{\mathbf{O}(\mathbf{I}_{N_B}+\tilde{\mathbf{T}}_L^H\widehat{\mathbf{H}}_{L,m}^H\boldsymbol{\Upsilon}_{L,m}^{-1}\widehat{\mathbf{H}}_{L,m}\tilde{\mathbf{T}}_L)^{-1}\big\} \tag{2.41a}$$

$$s.t.\; tr\{\tilde{\mathbf{T}}_L\tilde{\mathbf{T}}_L^H\} \le P_{r,L} \tag{2.41b}$$

where $\tilde{\mathbf{T}}_L = \mathbf{T}_L\mathbf{O}^{\frac{1}{2}}$.

2.3.2 Optimization of $\{\mathbf{F}_k\}$

When $\mathbf{O} = \mathbf{I}_{N_B}$, the problem (2.39) can be modified to a convex SDP problem. However in general case ($\mathbf{O} \neq \mathbf{I}_{N_B}$), the problem (2.39) is difficult to be formulated into a convex optimization problem. Thus, (2.39a) is reformulated as follows

$$tr\big\{\mathbf{O}(\mathbf{I}_{N_B} + \mathbf{G}_1^H \widehat{\mathbf{H}}_1^H \mathbf{\Xi}_1^{-1} \widehat{\mathbf{H}}_1 \mathbf{G}_1)^{-1}\big\} = \min_{\mathbf{L}} E_H\{tr(\mathbf{O}E\{(\mathbf{L}^H\mathbf{y}_1 - \mathbf{s})(\mathbf{L}^H\mathbf{y}_1 - \mathbf{s})^H\})\} \tag{2.42}$$

where $\mathbf{L}$ is the weight matrix of a linear receiver for the MIMO system in (2.1). Further, the proof of left-hand side of (2.42) is detailed in Appendix 2.6.2. By utilizing (2.42), the problem (2.39) can be solved through the following problem

$$\min_{\{\mathbf{F}_k\},\mathbf{L}} tr\Big\{(\mathbf{O}^{\frac{H}{2}}\mathbf{L}^H\widehat{\mathbf{H}}_1\mathbf{G}_1 - \mathbf{O}^{\frac{H}{2}})(\mathbf{O}^{\frac{H}{2}}\mathbf{L}^H\widehat{\mathbf{H}}_1\mathbf{G}_1 - \mathbf{O}^{\frac{H}{2}})^H + \mathbf{O}^{\frac{H}{2}}\mathbf{L}^H\mathbf{\Xi}_1\mathbf{L}\mathbf{O}^{\frac{1}{2}}\Big\} \tag{2.43a}$$

$$s.t.\ tr\{\mathbf{F}_k\mathbf{F}_k^H\} \leq P_{s,k}, \qquad k = 1, \cdots, K. \tag{2.43b}$$

In general cases of $\mathbf{\Psi}_{1,k} \neq \sigma_e^2\mathbf{I}_{N_{S,k}}$, the problem (2.43a) is difficult to solve as a result of $\mathbf{\Xi}_1$ being a function of $\{\mathbf{F}_k\}$. Thus, the following inequality [88] is applied to overcome the challenge

$$tr\{\mathbf{AB}\} \leq tr\{\mathbf{A}\}\,\lambda_m(\mathbf{B}) \tag{2.44}$$

where $\lambda_m(\cdot)$ is defined as the maximal eigenvalue of a matrix. By applying the inequality (2.44), an upper-bound of $\mathbf{\Xi_1}$ is given by

$$\mathbf{\Xi}_1 \leq \sum_{k=1}^{K} P_{s,k}\lambda_m(\mathbf{\Psi}_{1,k})\mathbf{\Sigma}_{1,k} + \mathbf{I}_{N_{R,1}} \triangleq \mathbf{\Phi}_1. \tag{2.45}$$

Using (2.45), the problem (2.43) can be written as

$$\min_{\{\mathbf{F}_k\},\mathbf{L}} tr\Big\{(\mathbf{O}^{\frac{H}{2}}\mathbf{L}^H\widehat{\mathbf{H}}_1\mathbf{G}_1 - \mathbf{O}^{\frac{H}{2}})(\mathbf{O}^{\frac{H}{2}}\mathbf{L}^H\widehat{\mathbf{H}}_1\mathbf{G}_1 - \mathbf{O}^{\frac{H}{2}})^H + \mathbf{O}^{\frac{H}{2}}\mathbf{L}^H\mathbf{\Phi}_1\mathbf{L}\mathbf{O}^{\frac{1}{2}}\Big\} \tag{2.46a}$$

$$s.t.\ tr\{\mathbf{F}_k\mathbf{F}_k^H\} \leq P_{s,k}, \qquad k = 1, \cdots, K. \tag{2.46b}$$

In the following, an iterative algorithm is proposed to solve the problem (2.46). In the proposed iterative algorithm, $\mathbf{L}$ is optimized by (2.66) based on $\{\mathbf{F}_k\}$ from the previous iteration. Then using the $\mathbf{L}$ obtained from the current iteration, $\{\mathbf{F}_k\}$ are optimized by solving the following problem,

$$\min_{\{\mathbf{F}_k\}} tr\Big\{(\mathbf{P}\mathbf{G}_1 - \mathbf{O}^{\frac{H}{2}})(\mathbf{P}\mathbf{G}_1 - \mathbf{O}^{\frac{H}{2}})^H\Big\} \tag{2.47a}$$

$$s.t.\ tr\{\mathbf{F}_k\mathbf{F}_k^H\} \leq P_{s,k}, \qquad k = 1, \cdots, K \tag{2.47b}$$

where $\mathbf{P} = \mathbf{O}^{\frac{H}{2}}\mathbf{L}^H\widehat{\mathbf{H}}_1$. The $\{\mathbf{F}_k\}$ and $\mathbf{L}$ are alternatively updated until convergence. By introducing $\mathbf{P}_k$ and $\mathbf{O}_k$, which contain the $\sum_{j=0}^{k-1} N_{S,j}+1$ to $\sum_{j=0}^{k} N_{S,j}$ columns of $\mathbf{P}$ and the $\sum_{j=0}^{k-1} N_{B,j}+1$ to $\sum_{j=0}^{k} N_{B,j}$ columns of $\mathbf{O}^{\frac{H}{2}}$ respectively, $k = 1, \cdots, K$, with $N_{S,0} = N_{B,0} = 0$, the objective function (2.47a) can be rewritten as

$$\sum_{k=1}^{K} tr\Big\{(\mathbf{P}_k\mathbf{F}_k - \mathbf{O}_k)(\mathbf{P}_k\mathbf{F}_k - \mathbf{O}_k)^H\Big\}. \tag{2.48}$$

It can be seen from (2.47b) and (2.48) that the problem (2.47) can be decomposed into K subproblems. By solving the following optimization problem, each $\mathbf{F}_k$ can be obtained.

$$\min_{\mathbf{F}_k} tr\Big\{(\mathbf{P}_k\mathbf{F}_k - \mathbf{O}_k)(\mathbf{P}_k\mathbf{F}_k - \mathbf{O}_k)^H\Big\} \tag{2.49a}$$

$$s.t.\ tr\{\mathbf{F}_k\mathbf{F}_k^H\} \leq P_{s,k}. \tag{2.49b}$$

The Lagrange multiplier method [89] can be used to solve the optimization problem (2.49) and solution to the optimization problem (2.49) is

$$\mathbf{F}_k = (\mathbf{P}_k^H\mathbf{P}_k + \lambda_k\mathbf{I}_{N_{S,k}})^{-1}\mathbf{P}_k^H\mathbf{O}_k \tag{2.50}$$

where $\lambda_k \geq 0$ is the Lagrangian multiplier, for $k = 1, \cdots, K$.

Based on (2.66) and (2.50), the computational complexity order of optimizing $\{\mathbf{F}_k\}$ at the first relay node can be estimated as $\mathcal{O}(c_1(KN_{S,k}^3 + N_{R,1}^3))$, where c_1 is the number of iterations till the convergence of $\{\mathbf{F}_k\}$.

2.3.3 Optimization of $\{\mathbf{T}_l\}$

In general cases of $\mathbf{\Psi}_l \neq \sigma_e^2\mathbf{I}_{N_{R,l}}$, the problem (2.40) is difficult to solve as $\mathbf{\Upsilon}_l$ is a function of $\mathbf{T}_l$. Thus, the inequality (2.44) is applied to overcome the challenge. By applying the inequality (2.44), an upper-bound of (2.37) is given by

$$\mathbf{\Upsilon}_l \leq P_{r,l}\lambda_m(\mathbf{\Psi}_l)\mathbf{\Sigma}_l + \mathbf{I}_{N_{R,l}} \triangleq \mathbf{\Phi}_l. \tag{2.51}$$

Using (2.51), an upper-bound of (2.40a) is given by

$$tr\{(\mathbf{O}^{-1} + \mathbf{T}_l^H\mathbf{B}_l\mathbf{T}_l)^{-1}\} \tag{2.52}$$

where $\mathbf{B}_l \triangleq \widehat{\mathbf{H}}_l^H\mathbf{\Phi}_l^{-1}\widehat{\mathbf{H}}_l$. From (2.52), the problem (2.40) can be written as

$$\min_{\mathbf{T}_l} tr\{(\mathbf{O}^{-1} + \mathbf{T}_l^H \mathbf{B}_l \mathbf{T}_l)^{-1}\} \tag{2.53a}$$

$$s.t.\ tr\{\mathbf{T}_l \mathbf{O} \mathbf{T}_l^H\} \leq P_{r,l}. \tag{2.53b}$$

The eigenvalue decomposition (EVD) of $\mathbf{O}$ and $\mathbf{B}_l$ is introduced as $\mathbf{O} = \mathbf{U}_O \mathbf{\Sigma}_O \mathbf{U}_O^H$ and $\mathbf{B}_l = \mathbf{V}_l \mathbf{\Lambda}_{\mathbf{B}_l} \mathbf{V}_l^H$ respectively, where the diagonal elements of $\mathbf{\Sigma}_O$ and $\mathbf{\Lambda}_{\mathbf{B}_l}$ are sorted in descending sequence. The optimization problem (2.53) can be solved by using the *Lemma 2* in [86]. Using the *Lemma 2* in [86], the linear filter matrix $\mathbf{T}_l$ can be written as

$$\mathbf{T}_l = \mathbf{V}_{l,1} \mathbf{\Lambda}_{\mathbf{T}_l}^{\frac{1}{2}} \mathbf{U}_O^H \tag{2.54}$$

where $\mathbf{V}_{l,1}$ contains the leftmost N_B columns of $\mathbf{V}_l$, and $\mathbf{\Lambda}_{\mathbf{T}_l}$ is a diagonal matrix with nonnegative diagonal entries. By applying (2.54), the problem (2.53) can be converted to the following problem with scalar variables

$$\min_{\{\lambda_{\mathbf{T}_l,i}\}} \sum_{i=1}^{N_B} \frac{1}{\sigma_{O,i}^{-1} + \lambda_{\mathbf{T}_l,i} \lambda_{\mathbf{B}_l,i}} \tag{2.55a}$$

$$s.t. \sum_{i=1}^{N_B} \lambda_{\mathbf{T}_l,i} \sigma_{O,i} \leq P_{r,l} \tag{2.55b}$$

$$\lambda_{\mathbf{T}_l,i} \geq 0, \qquad i = 1, \cdots, N_B \tag{2.55c}$$

where $\{\lambda_{\mathbf{T}_l,i}\} \triangleq \{\lambda_{\mathbf{T}_l,i}, i = 1, \cdots, N_B\}$, $\lambda_{\mathbf{T}_l,i}$, $\sigma_{O,i}$, and $\lambda_{\mathbf{B}_l,i}$ are the ith diagonal elements of $\mathbf{\Lambda}_{\mathbf{T}_l}$, $\mathbf{\Sigma}_O$, and $\mathbf{\Lambda}_{\mathbf{B}_l}$, respectively. By applying the Karush-Kuhn-Tucker (KKT) optimality conditions, the optimal solution for the problem (2.55) is obtained as

$$\lambda_{\mathbf{T}_l,i} = \frac{1}{\lambda_{\mathbf{B}_l,i}} \left(\sqrt{\frac{\lambda_{\mathbf{B}_l,i}}{\mu_l \sigma_{O,i}}} - \frac{1}{\sigma_{O,i}} \right)^+, \quad i = 1, \cdots, N_B \tag{2.56}$$

where $(x)^+ = \max(x, 0)$ and $\mu_l > 0$ is the solution to the non-linear equation of $\sum_{i=1}^{N_B} \frac{\sigma_{O,i}}{\lambda_{\mathbf{B}_l,i}} \left(\sqrt{\frac{\lambda_{\mathbf{B}_l,i}}{\mu_l \sigma_{O,i}}} - \frac{1}{\sigma_{O,i}} \right)^+ = P_{r,l}$. This solution is also known as the water-filling solution. As the most computationally intensive operation of optimizing $\mathbf{T}_l$ is calculating the EVD of $\mathbf{O}$, the complexity order of optimizing $\mathbf{T}_l$ is $\mathcal{O}(N_B^3)$.

2.3.4 Optimization of $\mathbf{T}_L$

Similar to the problem (2.39), the problem (2.41) can be converted to a convex SDP problem if $\mathbf{O} = \mathbf{I}_{N_B}$. But for $\mathbf{O} \neq \mathbf{I}_{N_B}$, the problem is unable to formulate into a convex

optimization problem. Considered a single-hop MIMO channel with

$$\tilde{\mathbf{y}}_{d,m} = \mathbf{H}_{L,m}\tilde{\mathbf{T}}_L\mathbf{s} + \mathbf{n}_{d,m}, \tag{2.57}$$

and by using (2.57), the function in (2.41a) can be reformulated as

$$\begin{aligned} &tr\{\mathbf{O}(\mathbf{I}_{N_B} + \tilde{\mathbf{T}}_L^H\widehat{\mathbf{H}}_{L,m}^H\boldsymbol{\Upsilon}_{L,m}^{-1}\widehat{\mathbf{H}}_{L,m}\tilde{\mathbf{T}}_L)^{-1}\} \\ &= \min_{\boldsymbol{\Theta}_m} E_H\{tr(\mathbf{O}E\{(\boldsymbol{\Theta}_m^H\tilde{\mathbf{y}}_{d,m} - \mathbf{s})(\boldsymbol{\Theta}_m^H\tilde{\mathbf{y}}_{d,m} - \mathbf{s})^H\})\} \end{aligned} \tag{2.58}$$

where $\boldsymbol{\Theta}_m, m = 1, \cdots, M$ is the weight matrix of the mth linear receiver for the MIMO system in (2.57), for $m = 1, \cdots, M$. Further, the proof of the left-hand side of (2.58) is presented in Appendix 2.6.3. By utilizing (2.58), the problem (2.41) can be solved through the following problem

$$\begin{aligned} \min_{\tilde{\mathbf{T}}_L,\{\boldsymbol{\Theta}_m\}} \max_m tr\Big\{&(\mathbf{O}^{\frac{H}{2}}\boldsymbol{\Theta}_m^H\widehat{\mathbf{H}}_{L,m}\tilde{\mathbf{T}}_L - \mathbf{O}^{\frac{H}{2}})(\mathbf{O}^{\frac{H}{2}}\boldsymbol{\Theta}_m^H\widehat{\mathbf{H}}_{L,m}\tilde{\mathbf{T}}_L - \mathbf{O}^{\frac{H}{2}})^H \\ &+\mathbf{O}^{\frac{H}{2}}\boldsymbol{\Theta}_m^H\boldsymbol{\Upsilon}_{L,m}\boldsymbol{\Theta}_m\mathbf{O}^{\frac{1}{2}}\Big\} \qquad (2.59a) \\ s.t.\ &tr\{\tilde{\mathbf{T}}_L\tilde{\mathbf{T}}_L^H\} \le P_{r,L} \qquad (2.59b) \end{aligned}$$

where $\{\boldsymbol{\Theta}_m\} \triangleq \{\boldsymbol{\Theta}_m, m = 1, \cdots, M\}$. Based on the technique used for optimizing $\{\mathbf{F}_k\}$ and $\{\mathbf{T}_l\}$, an upper-bound of $\boldsymbol{\Upsilon}_{L,m}, m = 1, \cdots, M$ is given by

$$\boldsymbol{\Upsilon}_{L,m} \le P_{r,L}\lambda_m(\boldsymbol{\Psi}_{L,m})\boldsymbol{\Sigma}_{L,m} + \mathbf{I}_{N_D} \triangleq \boldsymbol{\Phi}_{L,m}, m = 1, \cdots, M. \tag{2.60}$$

Using (2.60), the problem (2.59) can be written as

$$\begin{aligned} \min_{\tilde{\mathbf{T}}_L,\{\boldsymbol{\Theta}_m\}} \max_m tr\Big\{&(\mathbf{O}^{\frac{H}{2}}\boldsymbol{\Theta}_m^H\widehat{\mathbf{H}}_{L,m}\tilde{\mathbf{T}}_L - \mathbf{O}^{\frac{H}{2}})(\mathbf{O}^{\frac{H}{2}}\boldsymbol{\Theta}_m^H\widehat{\mathbf{H}}_{L,m}\tilde{\mathbf{T}}_L \\ &-\mathbf{O}^{\frac{H}{2}})^H + \mathbf{O}^{\frac{H}{2}}\boldsymbol{\Theta}_m^H\boldsymbol{\Phi}_{L,m}\boldsymbol{\Theta}_m\mathbf{O}^{\frac{1}{2}}\Big\} \qquad (2.61a) \\ s.t.\ &tr\{\tilde{\mathbf{T}}_L\tilde{\mathbf{T}}_L^H\} \le P_{r,L}. \qquad (2.61b) \end{aligned}$$

Because of high complexity objective function (2.61a), the min-max problem (2.61) is difficult to solve. Hence, an iterative algorithm is proposed to obtain the solution of the problem (2.61). In the proposed algorithm, $\boldsymbol{\Theta}_m$ is optimized by (2.68) based on $\tilde{\mathbf{T}}_L$ from the previous iteration. Then using $\{\boldsymbol{\Theta}_m\}$ obtained from the current iteration, $\tilde{\mathbf{T}}_L$ is obtained by optimizing the following problem

$$\begin{aligned} \min_{\tilde{\mathbf{T}}_L} \max_m &tr\Big\{(\mathbf{O}^{\frac{H}{2}}\boldsymbol{\Theta}_m^H\widehat{\mathbf{H}}_{L,m}\tilde{\mathbf{T}}_L - \mathbf{O}^{\frac{H}{2}})(\mathbf{O}^{\frac{H}{2}}\boldsymbol{\Theta}_m^H\widehat{\mathbf{H}}_{L,m}\tilde{\mathbf{T}}_L - \mathbf{O}^{\frac{H}{2}})^H\Big\} \qquad (2.62a) \\ s.t.\ &tr\{\tilde{\mathbf{T}}_L\tilde{\mathbf{T}}_L^H\} \le P_{r,L}. \qquad (2.62b) \end{aligned}$$

The $\{\mathbf{\Theta}_m\}$ and $\tilde{\mathbf{T}}_L$ are iteratively updated till convergence.

A real-valued slack variable γ and positive semidefinite (PSD) matrices $\mathbf{C}_m$, $m = 1, \cdots, M$, are introduced with

$$\mathbf{C}_m \geq (\mathbf{O}^{\frac{H}{2}}\mathbf{\Theta}_m^H\widehat{\mathbf{H}}_{L,m}\tilde{\mathbf{T}}_L - \mathbf{O}^{\frac{H}{2}})(\mathbf{O}^{\frac{H}{2}}\mathbf{\Theta}_m^H\widehat{\mathbf{H}}_{L,m}\tilde{\mathbf{T}}_L - \mathbf{O}^{\frac{H}{2}})^H$$

and $\mathbf{Q} \geq \tilde{\mathbf{T}}_L\tilde{\mathbf{T}}_L^H$. By applying the Schur complement, the optimization problem (2.62) can be expressed as

$$\min_{\gamma,\mathbf{Q},\{\mathbf{C}_m\},\tilde{\mathbf{T}}_L} \gamma \tag{2.63a}$$

$$s.t.\ tr\{\mathbf{C}_m\} \leq \gamma, \qquad m = 1, \cdots, M \tag{2.63b}$$

$$\begin{pmatrix} \mathbf{C}_m & \bar{\mathbf{K}}_m \\ \bar{\mathbf{K}}_m^H & \mathbf{I}_{N_B} \end{pmatrix} \geq 0,\ m = 1, \cdots, M \tag{2.63c}$$

$$tr\{\mathbf{Q}\} \leq P_{r,L}, \qquad \mathbf{Q} \geq 0 \tag{2.63d}$$

$$\begin{pmatrix} \mathbf{Q} & \tilde{\mathbf{T}}_L \\ \tilde{\mathbf{T}}_L^H & \mathbf{I}_{N_B} \end{pmatrix} \geq 0 \tag{2.63e}$$

where $\bar{\mathbf{K}}_m = \mathbf{O}^{\frac{H}{2}}\mathbf{\Theta}_m^H\widehat{\mathbf{H}}_{L,m}\tilde{\mathbf{T}}_L - \mathbf{O}^{\frac{H}{2}}$, $m = 1, \cdots, M$ and $\{\mathbf{C}_m\} = \{\mathbf{C}_m, m = 1, \cdots, M\}$. The problem (2.63) is a convex SDP problem which can be solved by the convex programming toolbox CVX [90]. The complexity of the optimization problem (2.63) will increase in the complexity order of $\mathcal{O}((N_{R,L-1}^2 + (M+1)N_B^2)^2(M+1)^{1.5}N_B^{2.5})$.

2.4 Numerical Example

In this section, the performance of the proposed transceiver design algorithm with robustness for multihop multicasting MIMO relay system is investigated through simulations. AF MIMO relay multicasting system with $L = 3$ hops and $K = 2$ source nodes where $N_{S,1} = N_{S,2} = N_S = 2$, $N_{R,1} = 8$, $N_{R,2} = 4$, and $N_D = 8$ is simulated. The information-carrying symbols are modulated by Quadrature Phase Shift Keying (QPSK) constellations. $P_{s,1} = P_{s,2} = P_s$ and the SNRs of the first hop and the other two hops are set as $\text{SNR}_1 = P_s/N_S$ and $\text{SNR}_2 = P_{r,1}/N_{R_1} = P_{r,2}/N_{R_2}$, respectively. In each channel realization, each source node sends 1000 randomly generated bits. The mean simulation result from 1000 independent channel realization is obtained.

In the simulations, the weight matrix, $\mathbf{O}$, is set as $\mathbf{O} = \mathbf{I}_{N_B}$. The correlation matrices of channel estimation errors are modeled as the following [91]

$$
\begin{aligned}
[\mathbf{\Psi}_{1,k}]_{p,q} &= \alpha^{|p-q|},\ p,q = 1,\cdots,N_{S,k},\ k = 1,\cdots,K \\
[\mathbf{\Psi}_{l}]_{p,q} &= \alpha^{|p-q|},\ p,q = 1,\cdots,N_{R,l-1},\ l = 2,\cdots,L-1 \\
[\mathbf{\Psi}_{L,m}]_{p,q} &= \alpha^{|p-q|},\ p,q = 1,\cdots,N_{L},\ m = 1,\cdots,M \\
[\mathbf{\Sigma}_{1,k}]_{p,q} &= \sigma_e^2\beta^{|p-q|},\ p,q = 1,\cdots,N_{R_1},\ k = 1,\cdots,K \\
[\mathbf{\Sigma}_{l}]_{p,q} &= \sigma_e^2\beta^{|p-q|},\ p,q = 1,\cdots,N_{R,l},\ l = 2,\cdots,L-1 \\
[\mathbf{\Sigma}_{L,m}]_{p,q} &= \sigma_e^2\beta^{|p-q|},\ p,q = 1,\cdots,N_{D},\ m = 1,\cdots,M
\end{aligned}
$$

where $\alpha \in [0,1]$ and $\beta \in [0,1]$ are correlation coefficients, and σ_e^2 represents the variance of the estimation error. $\alpha = 0.1$ and $\beta = 0.01$ are set in the simulations. The estimated channel matrices $\widehat{\mathbf{H}}_{1,k}$, $\widehat{\mathbf{H}}_{l}$, and $\widehat{\mathbf{H}}_{2,m}$ are modelled through the distributions given as [75]

$$
\begin{aligned}
\widehat{\mathbf{H}}_{1,k} &\sim \mathcal{CN}\Big(\mathbf{0}, \frac{1-\sigma_e^2}{\sigma_e^2}\mathbf{\Sigma}_{1,k}\otimes\mathbf{\Psi}_{1,k}^T\Big), \quad k = 1,\cdots,K \\
\widehat{\mathbf{H}}_{l} &\sim \mathcal{CN}\Big(\mathbf{0}, \frac{1-\sigma_e^2}{\sigma_e^2}\mathbf{\Sigma}_{l}\otimes\mathbf{\Psi}_{l}^T\Big), \quad l = 2,\cdots,L-1 \\
\widehat{\mathbf{H}}_{L,m} &\sim \mathcal{CN}\Big(\mathbf{0}, \frac{1-\sigma_e^2}{\sigma_e^2}\mathbf{\Sigma}_{L,m}\otimes\mathbf{\Psi}_{L,m}^T\Big),\ m = 1,\cdots,M.
\end{aligned}
$$

The system performance of the proposed robust algorithm (Robust) is compared against the algorithm given in [71] using only the estimated CSI $\widehat{\mathbf{H}}_{1,k}$, $k = 1,\cdots,K$, $\widehat{\mathbf{H}}_{l}$, $l = 2,\cdots,L-1$, and $\widehat{\mathbf{H}}_{L,m}$, $m = 1,\cdots,M$ (denoted the Non-Robust algorithm). The performance of the algorithm in [71] with full CSI, $\mathbf{H}_{1,k}$, $k = 1,\cdots,K$, $\mathbf{H}_{l}$, $l = 2,\cdots,L-1$, and $\mathbf{H}_{L,m}$, $m = 1,\cdots,M$ (denoted the FCSI algorithm) is also shown and included as a benchmark.

In the first numerical example, the convergence rate of the proposed transceiver algorithm is investigated with the predefined value set as $SNR_1 = 25$dB, $L = 3$, $M = 4$, $\sigma_e^2 = 0.0001$, $\alpha = 0.1$ and $\beta = 0.01$ for the simulation. The simulation is carried out at three different values of SNR_2, i.e $SNR_2 = 5$dB, $SNR_2 = 10$dB and $SNR_2 = 15$dB, while the proposed transceiver algorithm is initialised as a scaled identity matrix or a square matrix with randomized entries. Fig. 2.2 illustrates the number of iterations required for the proposed robust algorithm to achieve the convergence value of the normalized MSE (NMSE) for the system. It can be noted from the Fig. 2.2 that the NMSE decreases until it reaches the optimal value of the given system with an increment of the number of iterations. It is also observed that the convergence rate of the proposed transceiver algorithm increased with SNR_2. Based on the comparison between the

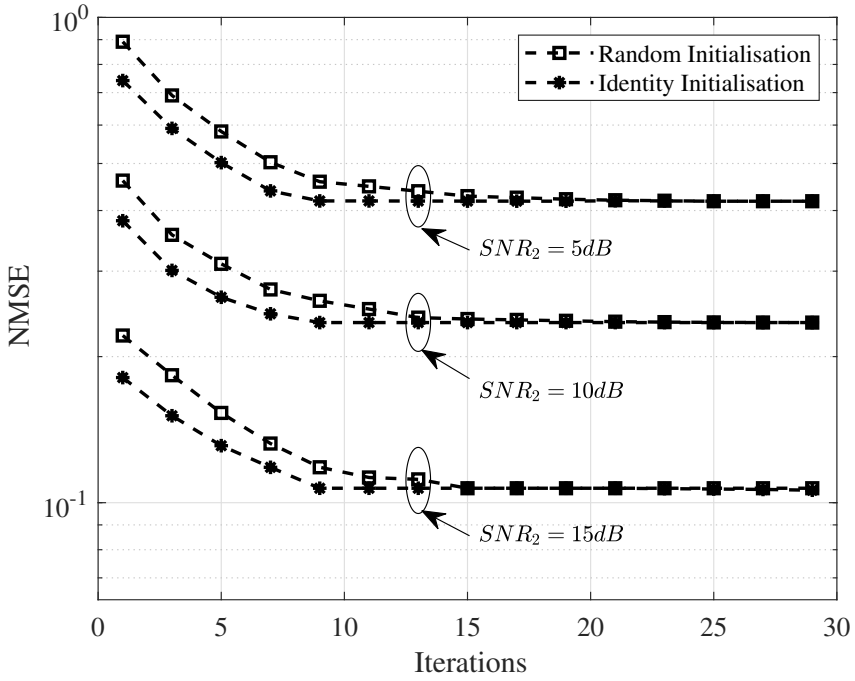

Figure 2.2: Example 1: NMSE versus number of iterations at different SNR_2. $\sigma_e^2 = 0.0001$ and $\text{SNR}_1 = 25$ dB.

randomized square matrix initialization and the scaled identity matrix initialization, it can be seen that the algorithm initialized with scaled identity matrix requires less number of iterations to achieve the convergence value of the system. Thus, the robust algorithm is initialized with a scaled identity matrix for a greater convergence rate in the remaining numerical examples.

In the second numerical example, the MI between the source and the destination nodes is investigated for the proposed robust transceiver design algorithm. Fig. 2.3 demonstrates the system MI versus SNR_2 at $K = 2$, $L = 3$, $M = 4$, $\sigma_e^2 = 0.0001$ and $SNR_1 = 25$dB. It can be noticed that the system MI with FCSI is the upper-bound for the simulated system, while the proposed robust algorithm outperforms the existing non-robust algorithm across SNR_2. It is important to note that the FCSI system is the ideal condition where the full CSI is known at the receiving nodes, which is unavailable in practice. Through this numerical example, it is shown that the maximal capacity of the system can be obtained via a WMMSE problem as proposed in the chapter, where the weight matrix $\mathbf{O}$ is updated iteratively, and usually, it is not an identity matrix after the first iteration. In the subsequent iteration, the weight matrix is equal to the inverse of the MSE matrix [82]. In the remaining numerical examples, the NMSE and

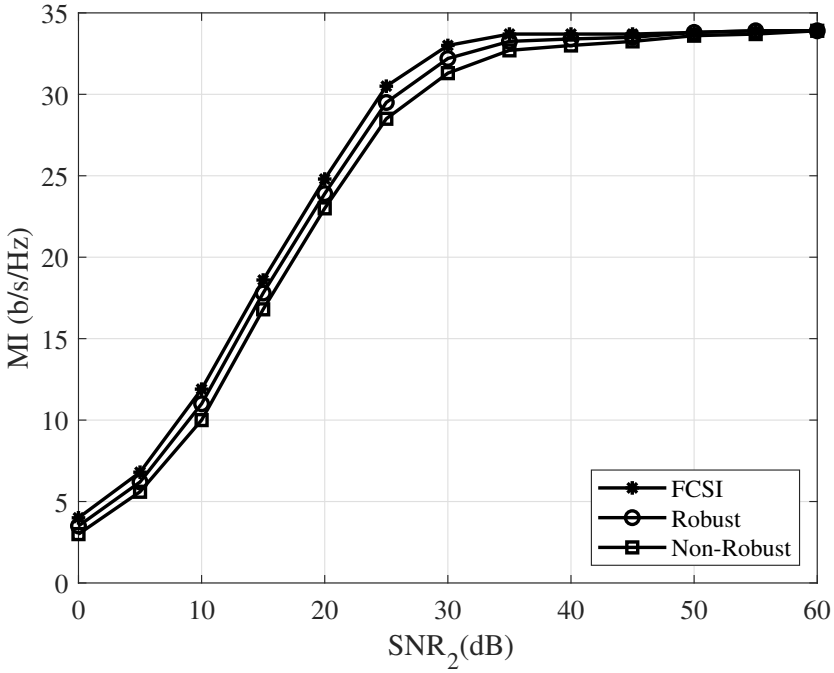

Figure 2.3: Example 2: MI versus SNR_2. $\sigma_e^2 = 0.0001$ and $\text{SNR}_1 = 25$ dB.

BER performance of the proposed robust system are investigated. In the simulation examples, initially, the weight matrix, $\mathbf{O}$ is set as an identity matrix.

In the third simulation results, the bit-error-rate (BER) performance of the proposed robust transceiver design algorithm is studied. Fig. 2.4 illustrates the BER performance of the three algorithms versus SNR_1 at $\text{SNR}_2 = 25$ dB with $\sigma_e^2 = 0.001$ and $\sigma_e^2 = 0.0001$. In this simulation, the $\text{SNR}_2 = 25$ dB is set. This is because the assumption where $\mathbf{Z}_l \approx \mathbf{O}$ is achieved at high SNR. Hence, for the sake of simplification, the SNR_2 is set as 25dB. This consideration ($\text{SNR}_1 = 25$dB and/or SNR_2) is remain the same in the followings simulation results. It is noted from Fig. 2.4 that the proposed robust algorithm consistently outperforms the non-robust algorithm over the entire SNR_1 region. Moreover, the results in Fig. 2.4 demonstrates that the FCSI algorithm provides a lower bound of the system BER. When CSI mismatch is small, the performance of the proposed robust optimization algorithm is close to that of the FCSI scheme.

In the fourth simulation results, the proposed algorithm system performance at $\text{SNR}_1 = 25$ dB with $\sigma_e^2 = 0.001$ and $\sigma_e^2 = 0.0001$ is studied. The NMSE performance is illustrated in Fig. 2.5 and the BER performance is illustrated in Fig. 2.6 for all the algorithms versus SNR_2. It is noticed from Figs. 2.5 and 2.6 that the system performances of the proposed robust algorithm in term of NMSE and BER are better

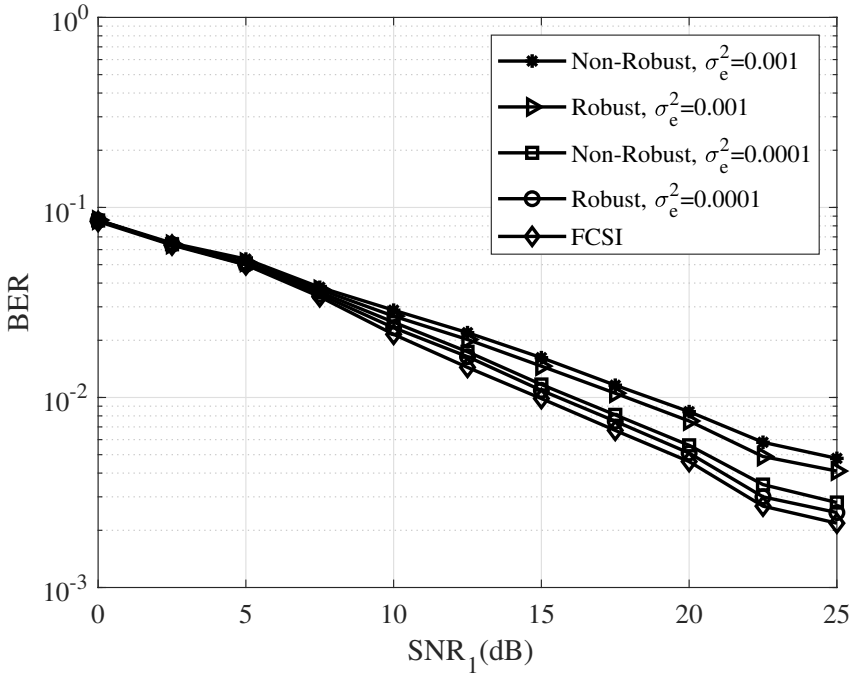

Figure 2.4: Example 3: BER versus SNR_1 at various σ_e^2. $M = 4$ and $\mathrm{SNR}_2 = 25$ dB.

than that of the non-robust algorithm over the entire SNR_2 range. When σ_e^2 is reduced, the system NMSE and BER decrease for both the proposed robust and non-robust algorithms. When $\sigma_e^2 = 0.0001$, the performance of the proposed algorithm is very close to that of the FCSI scheme.

In the fifth simulation results, the BER performance of the proposed robust algorithm with vary number of destination nodes is investigated. In this simulation, $\mathrm{SNR}_1 = 25$ dB and $\sigma_e^2 = 0.0001$ are set. Fig. 2.7 displays the BER performance of the proposed algorithm and the FCSI scheme versus SNR_2 for $M = 2$, $M = 4$, and $M = 8$. It can be seen from Fig. 2.7 that as the number of destination nodes increases, the BER keeps increasing, which is analogous to the results obtained in [72]. This is because it is more likely to find a worse relay-receiver channel among an increased number of users, and the worst-user MSE is selected as the objective function. For a various number of destination nodes, the average BER of the users are very similar up to $\mathrm{SNR}_2 = 15$ dB.

In the last simulation example, the NMSE performance of the proposed robust algorithm is studied with a different number of relay nodes of the MIMO relay communication system. $SNR_1 = 25$dB, $\sigma_e^2 = 0.0001$, $K = 2$ and $M = 4$ are set for the simulation. Fig. 2.8 illustrates the NMSE performance of the tested algorithms, i.e. proposed robust algorithm and FCSI algorithm, versus SNR_2 for $L = 3$, 4 and 5. It is noticeable that

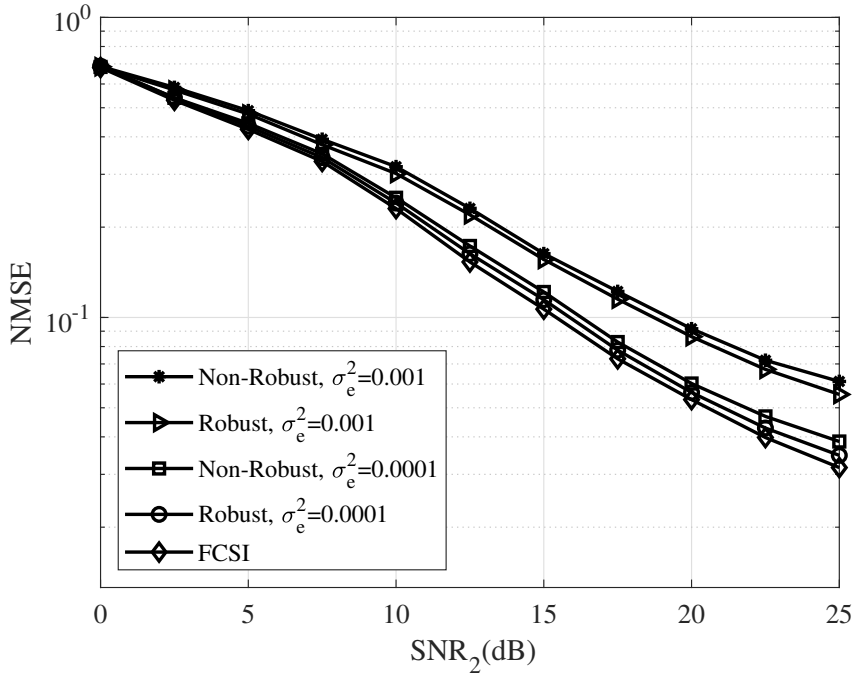

Figure 2.5: Example 4: NMSE versus SNR_2 at different σ_e^2. $M = 4$ and $\mathrm{SNR}_1 = 25$ dB.

the NMSE increased with the number of hops in the MIMO communication system. With a larger number of hops, the communication between the source nodes and the destination nodes is over a longer distance. With the mathematical representation as provided in (2.28), it can be noted that with an increasing number of hops, there are more subsequent terms in the WMMSE function. Hence, the NMSE of the system is increased by increasing the number of hops.

2.5 Chapter Summary

In Chapter 2, the problem of robust transceiver design for multihop multicasting AF MIMO relay systems from multiple sources is investigated with the consideration of channel mismatch between the exact and estimated signal waveform. Multiple source nodes broadcast their message to a group of destination nodes through multiple relay nodes in the investigated system. In the proposed transceiver design, the Gaussian-Kronecker model was adopted for the CSI mismatch. Furthermore, a robust transceiver design algorithm was developed to jointly optimize the source, relay, and destination matrices to minimize the maximal WMSE of the received signal at all destination nodes. It can be noticed that the WMSE is made statistically robust against the CSI mismatch

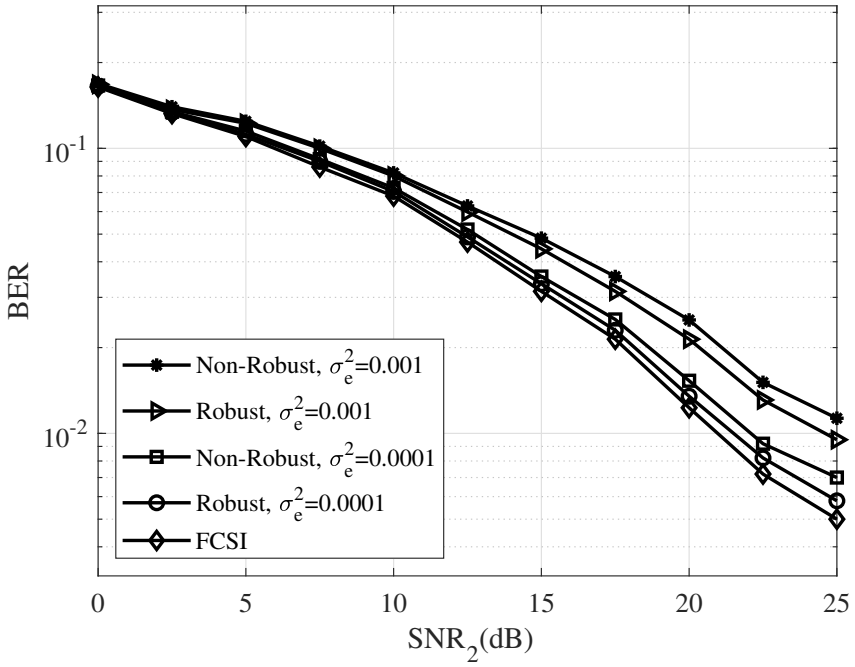

Figure 2.6: Example 4: BER versus SNR_2 at different σ_e^2. $M = 4$ and $\mathrm{SNR}_1 = 25$ dB.

by averaging through the distributions of the exact CSI. Moreover, the WMSE decomposition was exploited in the proposed transceiver design to reduce the computational complexity of the transceiver optimization problem. Numerical examples demonstrated improved performance of the proposed transceiver optimization algorithm against the channel mismatch between the exact and estimated signals waveform.

2.6 Appendices

2.6.1 Derivation of 2.22

In the appendix, the derivation of (2.22) is presented. By substituting (2.19) into the WMSE function (2.21), the following is obtained,

$$\begin{aligned} J_m \triangleq & tr\big\{\mathbf{O}(\mathbf{W}_m E_H\{E\{\mathbf{y}_{d,m}\mathbf{y}_{d,m}^H\}\}\mathbf{W}_m^H - \mathbf{W}_m E_H\{\bar{\mathbf{A}}_m\} - E_H\{\bar{\mathbf{A}}_m^H\}\mathbf{W}_m^H + \mathbf{I}_{N_B})\big\} \\ = & tr\{\mathbf{O}(\mathbf{I}_{N_B} + \mathbf{W}_m\mathbf{R}_{\mathbf{y}_{d,m}}\mathbf{W}_m^H - \mathbf{W}_m\widehat{\mathbf{A}}_m - \widehat{\mathbf{A}}_m^H\mathbf{W}_m^H)\}, \quad m = 1, \cdots, M \end{aligned} \tag{2.64}$$

where $\mathbf{R}_{\mathbf{y}_{d,m}}$ and $\widehat{\mathbf{A}}_m$ are derived as the following

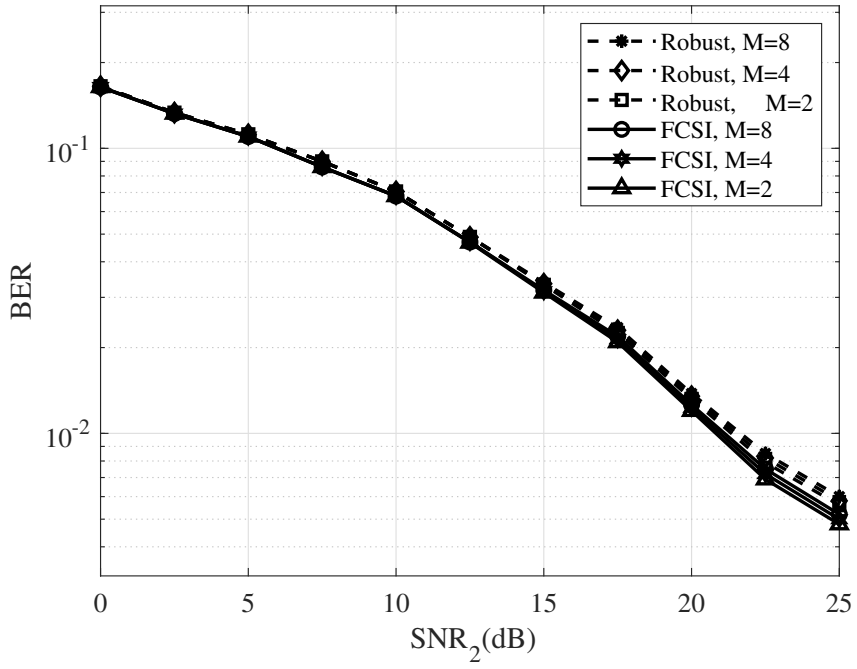

Figure 2.7: Example 5: BER versus SNR_2 at different M. $\sigma_e^2 = 0.0001$ and $\mathrm{SNR}_1 = 25$ dB.

$$
\begin{aligned}
\mathbf{R}_{\mathbf{y}_{d,m}} &= E_H\{E\{\mathbf{y}_{d,m}\mathbf{y}_{d,m}^H\}\} \\
&= E_H\{\mathbf{H}_{L,m}\mathbf{G}_L\mathbf{R}_{\mathbf{y}_{L-1}}\mathbf{G}_L^H\mathbf{H}_L^H\} + \mathbf{I}_{N_D} \\
&= \widehat{\mathbf{H}}_{L,m}\mathbf{G}_L\mathbf{R}_{\mathbf{y}_{L-1}}\mathbf{G}_L^H\widehat{\mathbf{H}}_L^H + tr\{\mathbf{G}_L\mathbf{R}_{\mathbf{y}_{L-1}}\mathbf{G}_L^H\mathbf{\Psi}_{L,m}\}\mathbf{\Sigma}_{L,m} + \mathbf{I}_{N_D} \\
\widehat{\mathbf{A}}_m &= E_H\{\bar{\mathbf{A}}_m\} \\
&= \widehat{\mathbf{H}}_{L,m}\mathbf{G}_L\prod_{l=L-1}^{1}\left(\widehat{\mathbf{H}}_l\mathbf{G}_l\right).
\end{aligned}
$$

By applying *Lemma 1*, third equation of $\mathbf{R}_{\mathbf{y}_{d,m}}$ is derived.

2.6.2 Proof of left-hand side of 2.42

In the appendix, the proof of the left-hand side of (2.42) is presented. By resolving the right-hand side statistically expectation of (2.42) and using *Lemma 1*, the following can be obtained,

$$
\begin{aligned}
&E_H\{tr(\mathbf{O}E\{(\mathbf{L}^H\mathbf{y}_1 - \mathbf{s})(\mathbf{L}^H\mathbf{y}_1 - \mathbf{s})^H\})\} \\
&= E_H\{tr\{\mathbf{O}[\mathbf{L}^H(\mathbf{H}_1\mathbf{G}_1\mathbf{G}_1^H\mathbf{H}_1^H + \mathbf{I}_{N_R})\mathbf{L} - \mathbf{L}^H\mathbf{H}_1\mathbf{G}_1 - \mathbf{G}_1^H\mathbf{H}_1^H\mathbf{L} + \mathbf{I}_{N_B}]\}\} \\
&= tr\{\mathbf{O}[\mathbf{L}^H(\widehat{\mathbf{H}}_1\mathbf{G}_1\mathbf{G}_1^H\widehat{\mathbf{H}}_1^H + \mathbf{\Xi}_1)\mathbf{L} - \mathbf{L}^H\widehat{\mathbf{H}}_1\mathbf{G}_1 - \mathbf{G}_1^H\widehat{\mathbf{H}}_1^H\mathbf{L} + \mathbf{I}_{N_B}]\}. \qquad (2.65)
\end{aligned}
$$

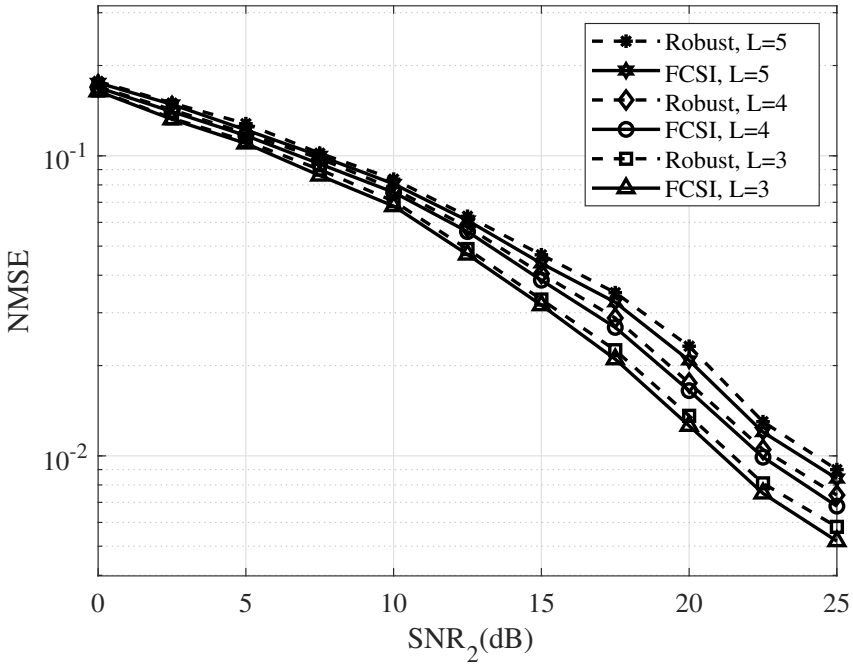

Figure 2.8: Example 6: NMSE versus SNR_2 at different L. $\sigma_e^2 = 0.0001$ and $\mathrm{SNR}_1 = 25$ dB.

It is obvious that the optimal $\mathbf{L}$ minimizing (2.65) is the Wiener filter [85] which is given by

$$\mathbf{L} = (\widehat{\mathbf{H}}_1\mathbf{G}_1\mathbf{G}_1^H\widehat{\mathbf{H}}_1^H + \mathbf{\Xi}_1)^{-1}\widehat{\mathbf{H}}_1\mathbf{G}_1. \tag{2.66}$$

After substituting (2.66) back into (2.65), the left-hand side of (2.42) is obtained.

2.6.3 Proof of left-hand side of 2.58

In the appendix, the proof of the left-hand side of (2.58) is presented. By resolving the right-hand side statistically expectation of (2.58) and using *Lemma 1*, the following can be obtained,

$$\begin{aligned} &E_H\{tr\{\mathbf{O}E\{(\mathbf{\Theta}_m^H\tilde{\mathbf{y}}_{d,m} - \mathbf{s})(\mathbf{\Theta}_m^H\tilde{\mathbf{y}}_{d,m} - \mathbf{s})^H\}\}\} \qquad (2.67)\\ &= E_H\{tr\{\mathbf{O}[\mathbf{\Theta}_m^H(\mathbf{H}_{L,m}\tilde{\mathbf{T}}_L\tilde{\mathbf{T}}_L^H\mathbf{H}_{L,m}^H + \mathbf{I}_{N_D})\mathbf{\Theta}_m - \mathbf{\Theta}_m^H\mathbf{H}_{L,m}\tilde{\mathbf{T}}_L - \tilde{\mathbf{T}}_L^H\mathbf{H}_{L,m}^H\mathbf{\Theta}_m + \mathbf{I}_{N_B}]\}\}\\ &= tr\{\mathbf{O}[\mathbf{\Theta}_m^H(\widehat{\mathbf{H}}_{L,m}\tilde{\mathbf{T}}_L\tilde{\mathbf{T}}_L^H\widehat{\mathbf{H}}_{L,m}^H + \mathbf{\Upsilon}_{L,m})\mathbf{\Theta}_m - \mathbf{\Theta}_m^H\widehat{\mathbf{H}}_{L,m}\tilde{\mathbf{T}}_L - \tilde{\mathbf{T}}_L^H\widehat{\mathbf{H}}_{L,m}^H\mathbf{\Theta}_m + \mathbf{I}_{N_B}]\}. \end{aligned}$$

It is clear that the optimal $\mathbf{\Theta}_m, m = 1, \cdots, M$ minimizing (2.67) is the Wiener filter [85] given by

$$\boldsymbol{\Theta}_m = \left(\widehat{\mathbf{H}}_{L,m}\tilde{\mathbf{T}}_L\tilde{\mathbf{T}}_L^H\widehat{\mathbf{H}}_{L,m}^H + \boldsymbol{\Upsilon}_{L,m}\right)^{-1}\widehat{\mathbf{H}}_{L,m}\tilde{\mathbf{T}}_L. \tag{2.68}$$

After substituting (2.68) back into (2.67), the left-hand side of (2.58) can be obtained.

Chapter 3

Transceiver Design for SWIPT MIMO Relay Systems with Hybridized Power-Time Splitting-Based Relaying Protocol

A dual-hop SWIPT based AF MIMO relay communication system with an energy-constraint relay node where the relay node harvests energy based on RF signals transmitted from the source node through the HPTSR protocol to forward information to the destination node is investigated in this chapter. The joint optimization of the TS factor, source, and relay precoding matrices, and the PS ratio vector is proposed to maximize the MI between the source and destination nodes. The optimal structure for the source and relay precoding matrices are derived to simplify the transceiver optimization problem. Two algorithms based on the upper bound and lower bound of the objective function are proposed to solve the optimization problem efficiently with low computational complexity. Numerical examples demonstrate that the proposed algorithms provide a better MI performance compared with TS based and PS based EH relay systems.

The rest of this chapter is organized as follows. In Section 3.1, an overview of existing techniques provided in literature is presented. In Section 3.2, the system model of a dual-hop AF SWIPT MIMO relay system with the HPTSR protocol is introduced. In

Section 3.3, the optimization problem for the proposed transceiver design is mathematically presented and simplified to a power allocation problem by adapting the proposed optimal structure for precoding matrices. To solve the power allocation problem, a lower bound based algorithm is derived in Section 3.4 and an upper bound based algorithm is developed in Section 3.5. In Section 3.6, numerical examples are displayed to illustrate the performance of the proposed algorithm compared with existing works. A summary regarding to this chapter is drawn in section 3.7.

3.1 Overview of Existing Techniques

The number of wireless devices around the world is having a skyrocketing increase for the past few years. However, the performance of these devices is highly limited due to their finite lifetime and tight energy constraint. Even though battery replacing is a solution to prolong the lifetime of those devices, physical and/or economic constraints often make it hard to perform battery replacing for the devices. For instance, some wireless devices are lodged inside building structures or human bodies to collect information [1]. Thus, EH is suggested as an alternative solution that can prolong the lifetime of wireless devices [92]. Conventional EH methods have limitations as they heavily rely on natural resources to harvest energy, which is unreliable as natural resources are difficult to manage. Thus conventional EH methods are not convenient to provide reliable energy sources to wireless devices. To overcome the limitation of conventional EH methods, a new EH method that can harvest energy from RF signals is proposed to provide stable and controllable wireless energy supply [3]. Moreover, the EH method based on RF signals has noticeable advantages for wireless networks as RF signals are not only used for transferring power but also for delivering information. The EH method which exploits the usage of RF signals in WPT and WIT simultaneously is known as SWIPT [4].

In [2], an ideal SWIPT receiver design is proposed to perform ID and EH simultaneously, and the tradeoff between the harvested energy and achievable MI rate is investigated using the capacity-energy function. However, the ideal SWIPT receiver has limitations in practical applications [5] as EH-circuits in practice are unable to perform ID for the information carried in the same signals directly. Two SWIPT receiver architectures, namely the TS protocol and the PS protocol, are presented in [5] to overcome the limitation through coordinated WIT and WPT at the receiver.

The PS and TS protocols for the SWIPT receiver are extended in [11] to relay communication systems by introducing TS-based and PS-based relaying protocols to perform EH and ID at the relay node. Relay technology is commonly used to extend the network coverage of wireless communication [8]. A relay node implemented in a SWIPT relay communication system with the EH relaying protocol introduced in [11] is capable of performing EH and ID from the received signals transmitted from the source node. The SWIPT relay node exploits the harvested energy to process and forwards the received signals to the destination node. Relay communication systems with SWIPT relay nodes have been investigated in [13–18]. In [13], a cooperative communication system is investigated where multiple pairs of transmitter-receiver interact with each other through an EH relay node; the focus is on the relay's strategies regarding user power allocation of the harvested energy and influences on the system performance. In [14], the authors designed a game-theoretical scheme to tackle the power distribution problem for SWIPT in interference relay communication networks. In [15], the harvest-use and harvest-use-store models are investigated with full-duplex EH relay communication systems using the PS-based relaying protocol. In [16], the impact of CCI towards a wireless communication system using a SWIPT full-duplex relay with the PS-based relaying protocol has been studied. In [17], the achievable rate of full-duplex relay communication systems is studied on both the AF relaying scheme as well as the DF relaying scheme under the TS-based EH relay protocol. In [18], the authors investigated the influence of decoding cost on the performance of the communication system with a DF relay using the PS-based protocol by deriving and optimizing the system achievable rate. The decoding cost is introduced at both the relay and destination nodes to perform ID.

By installing multiple antennas at nodes in wireless communication systems, the MIMO technique is famous for its capability in boosting the spectral and energy efficiency of communication systems [34]. With multiple antennas at nodes compared with single-antenna, RF energy transmission to wireless devices is more efficient. Studies regarding the application of SWIPT in MIMO relay communication systems have emerged rapidly in recent years [1, 36, 46–50, 54–56, 93]. In [1], an AF MIMO OFDM EH relay communication system adopted with TS-based and PS-based EH relaying protocols is investigated by jointly optimizing multiple system configuration parameters to achieve the maximum achievable rate. In [36], the R-E region which demonstrates the

energy-rate tradeoffs under several EH relaying schemes in a SWIPT MIMO relay communication system is investigated. Moreover, the challenges faced in this research field are introduced and discussed in [36]. In [46], the authors investigated the relay matrix optimization of a communication system with single-antenna source and destination nodes and a multi-antenna relay node. In [47], two approaches, known as the iterative algorithm and the channel diagonalization-based algorithm, are developed to solve the joint source and relay precoder optimization problem in wireless powered MIMO relay networks. In [48], a SWIPT MIMO relay communication system with PS-based relaying scheme is investigated with iterative algorithms for uniform and arbitrary source precoding scenarios. In [49], a SWIPT MIMO AF relay communication system is investigated by designing the optimal source matrix and relay matrix to characterize the R-E region defined by the achievable rate of the system and harvested energy at the relay node for the ideal EH scheme, the PS relaying scheme, and the TS relaying scheme. In [50], the work of [49] is extended to the DF relaying scheme with possibly imperfect channel knowledge. The optimization problem for SWIPT MIMO relay communication systems with TS-based relaying scheme is investigated in [54] for non-regenerative relays. In [55], the joint optimization problem of a source precoding matrix, relay matrix, and PS factor matrix is solved with the SQP approach, the SDP approach, and the primal-dual search approach. In [56], the works of [54] and [55] are extended to regenerative relaying scheme. In [93], the performance tradeoff of an orthogonal space-time block-code (OSTBC)-based non-regenerative MIMO OFDM relay communication system with two destination nodes performing EH and ID separately is investigated; the joint source and relay precoder optimization problem is proposed to achieve the R-E region which characterizes the system performance tradeoff.

In this chapter, a dual-hop MIMO relay communication system with an EH relay node using the AF relaying protocol is investigated. Relay nodes play an important role in communication systems where the direct link between the source and destination node is unavailable due to shadowing and pathloss effects [1, 48–50, 54–56, 93]. Unlike existing works using the PSR protocol [1, 48–50, 55] and the TSR protocol [1, 49, 50, 54, 56], a hybrid EH scheme, which is known as HPTSR protocol, is adopted at the relay node to increase the energy harvested at the relay node. The HPTSR protocol is expected to provide better performance for the proposed system. The HPTSR scheme works by transmitting energy-bearing RF signals to the relay node for EH in the first time slot while transmitting information-carrying RF signals to the relay node for ID in

the second time slot. In particular, in the second time slot, the received signals are split into two portions for EH and ID, respectively. Therefore, the existing knowledge with regard to EH relaying protocols is extended to the innovative HPTSR protocol. Introducing PS in the second time slot provides additional degrees of freedom to optimize the system performance. For instance, if the relay node requires additional power, instead of adjusting a single TS factor to allow additional time for energy harvesting as in the TS protocol, which affects *all sub-channels*, introducing PS in the second time slot allows adjusting the PS ratio in *each sub-channel* for an optimal energy harvesting and information transmission.

It is noted that several existing works have considered the HPTSR protocol [24–26, 94]. However, the system nodes in previous research are installed with one antenna, and as mentioned before, MIMO techniques provide better performance for SWIPT communication systems. In this chapter, the application of the HPTSR protocol is extended from the SISO relay communication systems to the MIMO relay communication systems. Moreover, compared with existing PS-based MIMO relay systems where a constant PS ratio is usually adopted for all antennas [46–50], a more general system with corresponding PS ratio for each antenna is considered, which enhances the system performance.

It is clear that the transceiver optimization problem is much more challenging in an HPTSR-based MIMO relay system. The optimal structure of the source and relay precoding matrices are derived to simplify the transceiver optimization problem to a low complexity power allocation problem with scalar variables. However, the non-convexity of the power allocation problem remains. Two approaches by exploiting the lower and upper bounds of the objective function are proposed to tackle the non-convexity. It is demonstrated that both the upper bound and lower bound based problems can be converted to convex optimization problems, which can be solved with low computational complexity. Simulation results show that the proposed HPTSR based MIMO relay system achieves better performance compared with existing approaches.

3.2 SWIPT Relay System Model with HPTSR Scheme

A dual-hop three-node MIMO relay communication system where the source node transmits information signals to the destination node with the help of a single relay node as displayed in Fig. 3.1 is considered. The source, relay, and destination nodes are installed

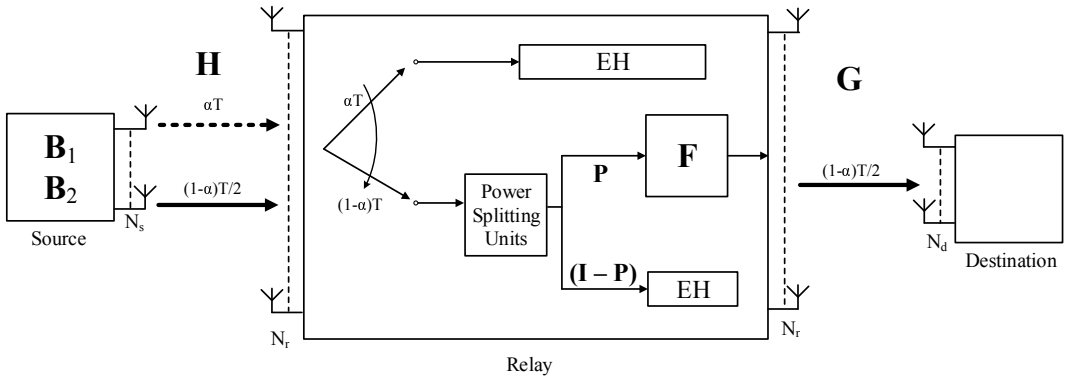

Figure 3.1: Block diagram of a dual-hop AF SWIPT MIMO relay system with the HPTSR protocol.

with N_s, N_r, and N_d antennas, respectively. The source node is considered as a self-powered node. Besides, the relay node requires to be powered by energy harvested from received RF signals. In a single communication cycle, there are two phases. The source node transmits energy-carrying and information-bearing signals to the relay node in the source phase. The energy-carrying signals are harvested by the relay node with the TS protocol, while the information-bearing signals are directed to the PS unit to undergo EH and ID with the PS protocol. Due to the simplicity of the AF relaying scheme, it is implemented at the relay node. Moreover, the AF scheme reduces the decoding cost required in a DF scheme to decode and re-encode the received signals, which helps in energy saving. Thus, with the AF scheme, the portion of information-bearing signals at the relay node for ID is linearly precoded and transmitted to the destination node at the relay phase. Due to severe pathloss and shadowing, the source node cannot communicate with the destination node directly without the help of the relay node. Besides, the source, relay, and destination nodes are perfectly synchronized.

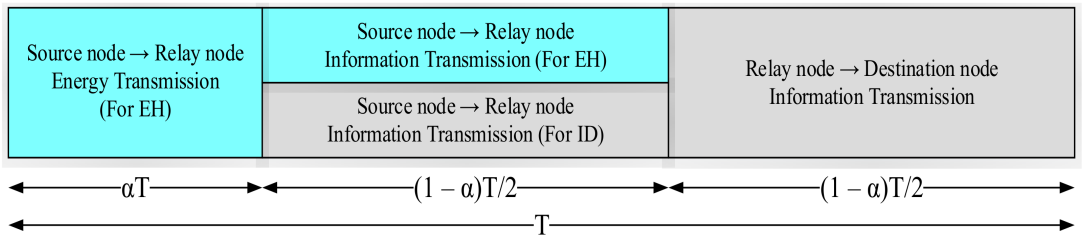

Figure 3.2: The diagram of the HPTSR protocol.

The diagram of the HPTSR protocol is shown in Fig. 3.2. It can be seen that the

total time of one communication cycle T is divided into three time-intervals. In the first time-interval, for a duration of αT, the energy-carrying signal is transferred from the source node to the relay node, where $\alpha \in [0, 1]$ represents the TS factor. In the second time-interval, for a duration of $(1-\alpha)T/2$, the source node transmits the information-bearing signal to the relay node. Then, the received signal at the ith antenna of the relay node is split into two independent signal streams with a PS ratio of p_i, where $p_i \in [0, 1]$ for $i = 1, \cdots, N_r$. One of the signal streams with a power ratio of p_i is sent towards the ID receiver, while the other signal stream with a power ratio of $(1-p_i)$ is sent towards the EH receiver. In the last time-interval, for the remaining duration of $(1-\alpha)T/2$, the relay node precodes the signal stream at the ID receiver and transmits the precoded signal to the destination node. Due to simplicity, $T = 1$.

During the first time-interval, the energy-carrying signal vector $\mathbf{s}_1 \in \mathbb{C}^{N_1 \times 1}$ with a covariance matrix given by $E\{\mathbf{s}_1\mathbf{s}_1^H\} = \mathbf{I}_{N_1}$ is transmitted from the source node with the source precoding matrix $\mathbf{B}_1 \in \mathbb{C}^{N_s \times N_1}$ to the relay node, where $\mathbf{I}_n$ is an identity matrix of size $n \times n$, $E\{\cdot\}$ denotes the statistical expectation, and $(\cdot)^H$ stands for the Hermitian transpose. Thus, the received signal at the first time-interval $\mathbf{y}_{r,1}$ at the relay node is given as

$$\mathbf{y}_{r,1} = \mathbf{H}\mathbf{B}_1\mathbf{s}_1 + \mathbf{n}_{r,1} \tag{3.1}$$

where $\mathbf{H} \in \mathbb{C}^{N_r \times N_s}$ is the MIMO channel matrix between the source and relay nodes, while $\mathbf{n}_{r,1} \in \mathbb{C}^{N_r \times 1}$ is the AWGN vector at the relay node during the first time-interval. From (3.1), the RF energy harvested during the first time-interval at the relay node without the noise component [6] is written as

$$E_{r,1} = \alpha\eta \, tr\big\{\mathbf{H}\mathbf{B}_1\mathbf{B}_1^H\mathbf{H}^H\big\} \tag{3.2}$$

where $\eta \in [0, 1]$ is the conversion efficiency at the relay node and $tr\{\cdot\}$ denotes the matrix trace[1].

During the second time-interval, the information-bearing signal vector $\mathbf{s}_2 \in \mathbb{C}^{N_2 \times 1}$ with a covariance matrix given as $E\{\mathbf{s}_2\mathbf{s}_2^H\} = \mathbf{I}_{N_2}$ is transmitted from the source node

[1]It is shown [95–98] that in practice the energy harvesting efficiency is a function of input power, and for input power below the harvesting circuit power sensitivity threshold, the harvested power can be zero. Similar to [1], [54], [99], a simplified linear energy harvesting model is considered with a constant η. It is important to highlight that the algorithms proposed in this chapter can be applied to any given η.

with the source precoding matrix $\mathbf{B}_2 \in \mathbb{C}^{N_s \times N_2}$ to the relay node. The received signal at second time-interval $\mathbf{y}_{r,2}$ at the relay node is given as

$$\mathbf{y}_{r,2} = \mathbf{H}\mathbf{B}_2\mathbf{s}_2 + \mathbf{n}_{r,2} \tag{3.3}$$

where $\mathbf{n}_{r,2} \in \mathbb{C}^{N_r \times 1}$ with a covariance matrix of $E\{\mathbf{n}_{r,2}\mathbf{n}_{r,2}^H\} = \sigma_r^2\mathbf{I}_{N_r}$ is the AWGN vector at the relay node during the second time-interval. At the relay node, the received signal (3.3) is split into two signal vectors with a diagonal PS matrix $\mathbf{P} = \text{diag}(p_1, \cdots, p_{N_r})$, where $\mathbf{P}^{\frac{1}{2}}\mathbf{y}_{r,2}$ is for information transmission and $(\mathbf{I}_{N_r} - \mathbf{P})^{\frac{1}{2}}\mathbf{y}_{r,2}$ is for energy harvesting. Here diag$(\cdot)$ denotes a diagonal matrix. The RF energy harvested during the second time-interval at the relay node without the noise component [6] is written as

$$E_{r,2} = \frac{1-\alpha}{2}\eta\, tr\big\{(\mathbf{I}_{N_r} - \mathbf{P})\mathbf{H}\mathbf{B}_2\mathbf{B}_2^H\mathbf{H}^H\big\}. \tag{3.4}$$

From (3.2) and (3.4), the total available transmission energy at the relay node obtained from the RF energy harvested during the first and second time intervals is given as

$$E_r = \alpha\eta\, tr\big\{\mathbf{H}\mathbf{B}_1\mathbf{B}_1^H\mathbf{H}^H\big\} + \frac{1-\alpha}{2}\eta\, tr\big\{(\mathbf{I}_{N_r} - \mathbf{P})\mathbf{H}\mathbf{B}_2\mathbf{B}_2^H\mathbf{H}^H\big\}. \tag{3.5}$$

During the last time-interval, the linearly precoded signal vector $\mathbf{x}_r$ given by

$$\mathbf{x}_r = \mathbf{F}\mathbf{P}^{\frac{1}{2}}\mathbf{y}_{r,2} \tag{3.6}$$

is transmitted to the destination node, where $\mathbf{F} \in \mathbb{C}^{N_r \times N_r}$ is the relay precoding matrix. The received signal at the destination node is given as

$$\begin{aligned}\mathbf{y}_d &= \mathbf{G}\mathbf{x}_r + \mathbf{n}_d \\ &= \mathbf{G}\mathbf{F}\mathbf{P}^{\frac{1}{2}}\mathbf{H}\mathbf{B}_2\mathbf{s}_2 + \mathbf{G}\mathbf{F}\mathbf{n}_{r,2} + \mathbf{n}_d\end{aligned} \tag{3.7}$$

where $\mathbf{G} \in \mathbb{C}^{N_d \times N_r}$ is the MIMO channel matrix between the relay and destination nodes and $\mathbf{n}_d \in \mathbb{C}^{N_d \times 1}$ is the AWGN vector at the destination node with a covariance matrix of $E\{\mathbf{n}_d\mathbf{n}_d^H\} = \sigma_d^2\mathbf{I}_{N_d}$. From (3.7), the mutual information between source and destination is written as

$$\begin{aligned}\text{MI}(\alpha, \mathbf{P}, \mathbf{B}_2, \mathbf{F}) = \frac{1-\alpha}{2}\ \log\Big|&\mathbf{I}_{N_2} + \mathbf{B}_2^H\mathbf{H}^H\mathbf{P}^{\frac{1}{2}}\mathbf{F}^H\mathbf{G}^H \\ &\big(\sigma_r^2\mathbf{G}\mathbf{F}\mathbf{F}^H\mathbf{G}^H + \sigma_d^2\mathbf{I}_{N_d}\big)^{-1}\mathbf{G}\mathbf{F}\mathbf{P}^{\frac{1}{2}}\mathbf{H}\mathbf{B}_2\Big|\end{aligned} \tag{3.8}$$

where $(\cdot)^{-1}$ denotes the matrix inverse and $|\cdot|$ stands for the matrix determinant. For simplicity, the MIMO channel matrices $\mathbf{H}$ and $\mathbf{G}$ are are assumed to be fully-known by

the relay and destination nodes, respectively. Moreover, the value of N_2 is set to satisfy $N_2 < \min(\text{rank}(\mathbf{H}), \text{rank}(\mathbf{G}))$ and $\text{rank}(\mathbf{B}_2) = \text{rank}(\mathbf{F}) = N_2$ in order not to waste the transmission power available at the source and relay nodes.

The required transmission energy at the source node to transmit signal vectors $\mathbf{s}_1$ and $\mathbf{s}_2$ is written as the following, respectively

$$E_{u,s,1} = \alpha \; tr\{\mathbf{B}_1\mathbf{B}_1^H\} \tag{3.9}$$

$$E_{u,s,2} = \frac{1-\alpha}{2} \; tr\{\mathbf{B}_2\mathbf{B}_2^H\} \tag{3.10}$$

where the total transmission energy required by the source node can be considered as $E_{u,s} = E_{u,s,1} + E_{u,s,2}$. Thus, the transmission energy constraint at the source node is considered as

$$E_{u,s} \leq \frac{1+\alpha}{2} P_s \tag{3.11}$$

where $P_s > 0$ is the power budget available at the source node. In [1], the authors assumed that a constant power is used for both energy-transferring and information-bearing signal transmission which is given by

$$tr\{\mathbf{B}_1\mathbf{B}_1^H\} \leq P_s \qquad tr\{\mathbf{B}_2\mathbf{B}_2^H\} \leq P_s. \tag{3.12}$$

It is noticeable that (3.12) is a special example of (3.11). In other words, (3.11) has a larger feasible region compared to (3.12). It can be observed the source precoding matrices $\mathbf{B}_1$ and $\mathbf{B}_2$ are connected through a single energy constraint in (3.11). This enables the source node to transmit at different power levels accommodated to the purpose of energy-transferring and information transmission. Thus, (3.11) is more general than (3.12) and the transceiver designs proposed under (3.11) are expected to provide a better performance compared to the transceiver designs proposed under (3.12).

From (3.6), the transmission energy required by the relay node is written as

$$E_{u,r} = \frac{1-\alpha}{2} \; tr\big\{\mathbf{F}\big(\mathbf{P}^{\frac{1}{2}}\mathbf{H}\mathbf{B}_2\mathbf{B}_2^H\mathbf{H}^H\mathbf{P}^{\frac{1}{2}} + \sigma_r^2\mathbf{I}_{N_r}\big)\mathbf{F}^H\big\}. \tag{3.13}$$

All energy harvested at the relay node given by (3.5) is used to transmit information signals received from the source node to the destination node. Thus, the transmission energy constraint for the relay node is considered as

$$E_{u,r} \leq E_r. \tag{3.14}$$

The objective in the proposed transceiver design is to maximize the mutual information (3.8) between the source and destination nodes subjecting to energy constraints

at the source and the relay nodes given by (3.11) and (3.14), respectively. From (3.8), (3.11), and (3.14), the transceiver optimization problem for dual-hop HPTSR-based AF MIMO relay systems can be written as

$$\max_{\alpha,\mathbf{P},\mathbf{B}_1,\mathbf{B}_2,\mathbf{F}} \ \mathrm{MI}\big(\alpha,\mathbf{P},\mathbf{B}_2,\mathbf{F}\big) \tag{3.15a}$$

$$s.t. \ \ \alpha tr\big\{\mathbf{B}_1\mathbf{B}_1^H\big\} + \frac{1-\alpha}{2} tr\big\{\mathbf{B}_2\mathbf{B}_2^H\big\} \le \frac{1+\alpha}{2} P_s \tag{3.15b}$$

$$\frac{1-\alpha}{2} tr\big\{\mathbf{F}\big(\mathbf{P}^{\frac{1}{2}}\mathbf{H}\mathbf{B}_2\mathbf{B}_2^H\mathbf{H}^H\mathbf{P}^{\frac{1}{2}} + \sigma_r^2\mathbf{I}_{N_r}\big)\mathbf{F}^H\big\}$$

$$\le \alpha\eta\, tr\big\{\mathbf{H}\mathbf{B}_1\mathbf{B}_1^H\mathbf{H}^H\big\} + \frac{1-\alpha}{2}\eta\, tr\big\{(\mathbf{I}_{N_r} - \mathbf{P})\mathbf{H}\mathbf{B}_2\mathbf{B}_2^H\mathbf{H}^H\big\} \tag{3.15c}$$

$$0 \le p_i \le 1, \quad i = 1, \cdots, N_r \tag{3.15d}$$

$$0 \le \alpha \le 1. \tag{3.15e}$$

3.3 Proposed Transceiver Design

It is noticeable that the problem (3.15) is nonconvex in nature with matrix variables, which is quite hard to solve. Moreover, compared with existing TS and PS based system designs, the transmission energy constraint (3.15c) from the HPTSR protocol further increases the technical difficulty in solving the problem (3.15). In this section, the optimal structure of $\mathbf{B}_1$, $\mathbf{B}_2$, and $\mathbf{F}$ are derived to solve the nonconvex optimization problem (3.15).

It can be observed that $\mathbf{B}_1$ is not in the objective function (3.15a), but it can influence (3.15a) by varying the feasible region of the problem (3.15) specified by constraints (3.15b) and (3.15c). Thus, in order to maximize the feasible region of the problem (3.15), for any $tr\{\mathbf{B}_1\mathbf{B}_1^H\}$ in the left-hand side of (3.15b), it is important to maximize $tr\{\mathbf{H}\mathbf{B}_1\mathbf{B}_1^H\mathbf{H}^H\}$ in the right-hand side of (3.15c). This constrained maximization problem can be formulated as the problem below [1], [54]

$$\max_{\mathbf{B}_1} \ tr\{\mathbf{H}\mathbf{B}_1\mathbf{B}_1^H\mathbf{H}^H\} \tag{3.16a}$$

$$s.t. \ tr\{\mathbf{B}_1\mathbf{B}_1^H\} = \lambda_1 \tag{3.16b}$$

where λ_1 is a positive scalar value. The SVD of $\mathbb{H}$ is introduced as $\mathbf{H} = \mathbf{U}_h\mathbf{\Lambda}_h^{\frac{1}{2}}\mathbf{V}_h^H$ with the diagonal elements of $\mathbf{\Lambda}_h$ are arranged in descending order. The EVD of $\mathbf{B}_1\mathbf{B}_1^H$ is introduced as $\mathbf{U}_b\mathbf{\Lambda}_b\mathbf{U}_b^H$, where the diagonal elements of $\mathbf{\Lambda}_b$ are arranged in descending

order, too. Based on [88], the following inequality is given as

$$tr\{\mathbf{UV}\} = \sum_i \lambda_i(\mathbf{UV}) \leq \sum_i \lambda_i(\mathbf{U})\lambda_i(\mathbf{V}) \tag{3.17}$$

where $\lambda_i(\mathbf{X})$ indicates the ith eigenvalue of $\mathbf{X}$ and $\lambda_i(\mathbf{U})$ and $\lambda_i(\mathbf{V})$ are arranged in the same order. By applying (3.17), the SVD of $\mathbf{H}$, and the EVD of $\mathbf{B}_1\mathbf{B}_1^H$, (3.16a) can be upper-bounded by

$$tr\{\mathbf{H}\mathbf{B}_1\mathbf{B}_1^H\mathbf{H}^H\} = tr\{\mathbf{\Lambda}_h\mathbf{\Lambda}_b\} \leq \sum_{i=1}^{N_s} \lambda_{h,i}\lambda_{b,i} \tag{3.18}$$

where $\lambda_{h,i}$ and $\lambda_{b,i}$ are the ith diagonal entry of $\mathbf{\Lambda}_h$ and $\mathbf{\Lambda}_b$, respectively. It is noticeable in (3.18) that the equality is achieved when $\mathbf{U}_b = \mathbf{V}_h\tilde{\mathbf{I}}$, where $\tilde{\mathbf{I}} \in \mathbb{C}^{N_s \times N_s}$ is a diagonal matrix with unit norm diagonal elements. For simplicity, $\tilde{\mathbf{I}}$ is set to be $\mathbf{I}_{N_s}$ and $\mathbf{U}_b = \mathbf{V}_h$. Thus, by exploiting the upper bound in (3.18), the optimization problem (3.16) is rewritten into

$$\max_{\{\lambda_{b,i}\}} \sum_{i=1}^{N_s} \lambda_{h,i}\lambda_{b,i} \tag{3.19a}$$

$$s.t. \sum_{i=1}^{N_s} \lambda_{b,i} = \lambda_1 \tag{3.19b}$$

where $\{\lambda_{b,i}\} = \{\lambda_{b,i}, i = 1, \cdots, N_s\}$. The solution to the problem (3.19) is $\lambda_{b,1} = \lambda_1$ which results in $\mathbf{B}_1\mathbf{B}_1^H = \lambda_1\mathbf{v}_{h,1}\mathbf{v}_{h,1}^H$ where $\mathbf{v}_{h,1}$ is the first column of $\mathbf{V}_h$. Therefore, the optimal structure for $\mathbf{B}_1$ is given by

$$\mathbf{B}_1 = \lambda_1^{\frac{1}{2}}\mathbf{v}_{h,1}\mathbf{v}^H \tag{3.20}$$

where $\mathbf{v}$ can be any $N_1 \times 1$ vector with $\mathbf{v}^H\mathbf{v} = 1$. It is interesting to note that the optimal $\mathbf{B}_1$ derived in (3.20) has a rank-1 structure matched to $\mathbf{v}_{h,1}$. Thus, to maximize the energy harvested at the relay node, all transmission power during the first time interval at the source node is allocated to the channel linked to the largest singular value of $\mathbf{H}$. In other words, only λ_1 need to be optimized in $\mathbf{B}_1$ and $tr\{\mathbf{B}_1\mathbf{B}_1^H\} = \lambda_1$. By applying (3.20), the optimization problem (3.15) is equivalently converted to

$$\max_{\alpha,\lambda_1,\mathbf{P},\mathbf{B}_2,\mathbf{F}} \quad \frac{1-\alpha}{2}\log\Big|\mathbf{I}_{N_2}+\mathbf{B}_2^H\mathbf{H}^H\mathbf{P}^{\frac{1}{2}}\mathbf{F}^H\mathbf{G}^H\big(\sigma_r^2\mathbf{G}\mathbf{F}\mathbf{F}^H\mathbf{G}^H+\sigma_d^2\mathbf{I}_{N_d}\big)^{-1}\mathbf{G}\mathbf{F}\mathbf{P}^{\frac{1}{2}}\mathbf{H}\mathbf{B}_2\Big| \tag{3.21a}$$

$$s.t. \quad \alpha\lambda_1+\frac{1-\alpha}{2}tr\{\mathbf{B}_2\mathbf{B}_2^H\}\le\frac{1+\alpha}{2}P_s \tag{3.21b}$$

$$tr\big\{\mathbf{F}(\mathbf{P}^{\frac{1}{2}}\mathbf{H}\mathbf{B}_2\mathbf{B}_2^H\mathbf{H}^H\mathbf{P}^{\frac{1}{2}}+\sigma_r^2\mathbf{I}_{N_r})\mathbf{F}^H\big\}\le \kappa\eta\lambda_1+\eta\, tr\big\{(\mathbf{I}_{N_r}-\mathbf{P})\mathbf{H}\mathbf{B}_2\mathbf{B}_2^H\mathbf{H}^H\big\} \tag{3.21c}$$

$$0\le p_i\le 1, \quad i=1,\cdots,N_r \tag{3.21d}$$

$$0\le\alpha\le 1 \tag{3.21e}$$

where $\kappa=2\alpha\lambda_{h,1}/(1-\alpha)$.

By applying the Weinstein-Aronszajn identity [100], the objective function (3.21a) can be rewritten as

$$\frac{1-\alpha}{2}\log\Big|\mathbf{I}_{N_d}+\mathbf{G}\mathbf{F}\mathbf{\Xi}\mathbf{F}^H\mathbf{G}^H\big(\sigma_r^2\mathbf{G}\mathbf{F}\mathbf{F}^H\mathbf{G}^H+\sigma_d^2\mathbf{I}_{N_d}\big)^{-1}\Big| \tag{3.22}$$

where $\mathbf{\Xi}=\mathbf{P}^{\frac{1}{2}}\mathbf{H}\mathbf{B}_2\mathbf{B}_2^H\mathbf{H}^H\mathbf{P}^{\frac{1}{2}}$ is considered and designed into a diagonal matrix as based on the Hadamard's inequality [101] on matrix determinant, the objective function (3.22) is maximized when $\mathbf{G}\mathbf{F}\mathbf{\Xi}\mathbf{F}^H\mathbf{G}^H\big(\sigma_r^2\mathbf{G}\mathbf{F}\mathbf{F}^H\mathbf{G}^H+\sigma_d^2\mathbf{I}_{N_d}\big)^{-1}$ is diagonal. For any given value of α, λ_1, $\mathbf{P}$, and $\mathbf{B}_2$, the optimization problem for $\mathbf{F}$ is viewed as

$$\max_{\mathbf{F}} \quad \frac{1-\alpha}{2}\log\Big|\mathbf{I}_{N_d}+\mathbf{G}\mathbf{F}\mathbf{\Xi}\mathbf{F}^H\mathbf{G}^H\big(\sigma_r^2\mathbf{G}\mathbf{F}\mathbf{F}^H\mathbf{G}^H+\sigma_d^2\mathbf{I}_{N_d}\big)^{-1}\Big| \tag{3.23a}$$

$$s.t. \quad tr\big\{\mathbf{F}(\mathbf{\Xi}+\sigma_r^2\mathbf{I}_{N_r})\mathbf{F}^H\big\}\le\kappa\eta\lambda_1+\eta\, tr\big\{(\mathbf{I}_{N_r}-\mathbf{P})\mathbf{H}\mathbf{B}_2\mathbf{B}_2^H\mathbf{H}^H\big\}. \tag{3.23b}$$

The SVD of $\mathbf{G}$ is introduced as $\mathbf{G}=\mathbf{U}_g\mathbf{\Lambda}_g^{\frac{1}{2}}\mathbf{V}_g^H$ with the diagonal elements of $\mathbf{\Lambda}_g$ sorted in descending order. From [102], it is noted that the optimal structure of $\mathbf{F}$ under the optimization problem (3.23) with a diagonal $\mathbf{\Xi}$ is given as

$$\mathbf{F}=\mathbf{V}_g\dot{\mathbf{\Lambda}}_f^{\frac{1}{2}} \tag{3.24}$$

where $\dot{\mathbf{\Lambda}}_f\in\mathbb{C}^{N_r\times N_r}$ is a diagonal matrix. As the maximal number of concurrent data streams for information transmission by the relay system is N_2, the optimal $\dot{\mathbf{\Lambda}}_f=\mathrm{bd}(\mathbf{\Lambda}_f,\mathbf{0}_{N_r-N_2})$ where $\mathbf{\Lambda}_f\in\mathbb{C}^{N_2\times N_2}$ is a diagonal matrix and $\mathrm{bd}(\cdot)$ represents a block diagonal matrix. Similarly, with the consideration of the maximal number of concurrent data streams, the optimal $\mathbf{P}$ is given as $\mathrm{bd}(\mathbf{P}_M,\mathbf{0}_{N_r-N_2})$, where $\mathbf{P}_M\in\mathbb{C}^{N_2\times N_2}$ is a diagonal matrix containing the PS ratios p_i for $i=1,\cdots,N_2$. In other words, the

remaining $N_r - N_2$ antennas are solely used for EH with the corresponding PS ratios set to 0.

To design $\boldsymbol{\Xi}$ into a diagonal matrix for maximizing the objective function (3.22), the following is introduced,

$$\mathbf{H}_M \mathbf{B}_2 \mathbf{B}_2^H \mathbf{H}_M^H = \boldsymbol{\Lambda}_2 \tag{3.25}$$

where $\mathbf{H}_M$ contains the first N_2 rows of $\mathbf{H}$ and $\boldsymbol{\Lambda}_2 \in \mathbb{C}^{N_2 \times N_2}$ is a diagonal matrix. By introducing the SVD of $\mathbf{H}_M$ as $\mathbf{H}_M = \mathbf{U}_{h,1} \boldsymbol{\Lambda}_{h,1}^{\frac{1}{2}} \mathbf{V}_{h,1}^H$ where the diagonal entries of $\boldsymbol{\Lambda}_{h,1}$ are arranged in descending order, the optimal structure of $\mathbf{B}_2$ is proposed to be written as

$$\mathbf{B}_2 = \mathbf{V}_{h,1} \boldsymbol{\Lambda}_{h,1}^{-\frac{1}{2}} \mathbf{U}_{h,1}^H \boldsymbol{\Lambda}_2^{\frac{1}{2}}. \tag{3.26}$$

By applying the optimal structure of the precoding matrices $\mathbf{F}$ and $\mathbf{B}_2$ given by (3.24) and (3.26), respectively, the optimization problem (3.21) is rewritten as

$$\max_{\alpha, \lambda_1, \mathbf{P}_M, \boldsymbol{\Lambda}_2, \boldsymbol{\Lambda}_f} \frac{1-\alpha}{2} \log \left| \mathbf{I}_{N_2} + \boldsymbol{\Lambda}_g \boldsymbol{\Lambda}_f \mathbf{P}_M \boldsymbol{\Lambda}_2 \big(\sigma_r^2 \boldsymbol{\Lambda}_g \boldsymbol{\Lambda}_f + \sigma_d^2 \mathbf{I}_{N_2}\big)^{-1} \right| \tag{3.27a}$$

$$s.t. \;\; \alpha\lambda_1 + \frac{1-\alpha}{2} tr\{\boldsymbol{\Lambda}_2 \boldsymbol{\Upsilon}\} \leq \frac{1+\alpha}{2} P_s \tag{3.27b}$$

$$tr\{\boldsymbol{\Lambda}_f (\mathbf{P}_M \boldsymbol{\Lambda}_2 + \sigma_r^2 \mathbf{I}_{N_r})\} \leq \kappa\eta\lambda_1 + \eta tr\big\{(\boldsymbol{\Psi} - \mathbf{P}_M)\boldsymbol{\Lambda}_2\big\} \tag{3.27c}$$

$$0 \leq p_i \leq 1, \quad i = 1, \cdots, N_2 \tag{3.27d}$$

$$0 \leq \alpha \leq 1 \tag{3.27e}$$

where $\boldsymbol{\Upsilon} = \mathbf{U}_{h,1} \boldsymbol{\Lambda}_{h,1}^{-1} \mathbf{U}_{h,1}^H$, $\boldsymbol{\Psi} = \mathbf{I}_{N_2} + \widehat{\mathbf{H}}^H \widehat{\mathbf{H}}$, $\widehat{\mathbf{H}} = \mathbf{H}_m \mathbf{V}_{h,1} \boldsymbol{\Lambda}_{h,1}^{-\frac{1}{2}} \mathbf{U}_{h,1}^H$, and $\mathbf{H}_m$ contains the last $N_r - N_2$ rows of $\mathbf{H}$. It is noticeable in (3.27a) that $\boldsymbol{\Lambda}_g$, $\boldsymbol{\Lambda}_f$, $\mathbf{P}_M$, and $\boldsymbol{\Lambda}_2$ are diagonal matrices, hence the problem (3.27) can be equivalently rewritten into the following power allocation problem with scalar variables

$$\max_{\alpha, \lambda_1, \mathbf{p}, \boldsymbol{\lambda}_2 \boldsymbol{\lambda}_f} \frac{1-\alpha}{2} \sum_{i=1}^{N_2} \log \left(1 + \frac{p_i \, \lambda_{2,i} \, \lambda_{f,i} \, \lambda_{g,i}}{\lambda_{f,i} \, \lambda_{g,i} + 1} \right) \tag{3.28a}$$

$$s.t. \;\; \alpha\lambda_1 + \frac{1-\alpha}{2} \sigma_r^2 \sum_{i=1}^{N_2} \delta_i \, \lambda_{2,i} \leq \frac{1+\alpha}{2} P_s \tag{3.28b}$$

$$\sum_{i=1}^{N_2} \lambda_{f,i} \big(p_i \, \lambda_{2,i} + 1\big) \leq \kappa\eta\lambda_1 + \eta\sigma_r^2 \sum_{i=1}^{N_2} \big(\varepsilon_i - p_i\big)\lambda_{2,i} \tag{3.28c}$$

$$\lambda_{2,i} \geq 0, \qquad \lambda_{f,i} \geq 0 \tag{3.28d}$$

$$0 \leq p_i \leq 1, \quad i = 1, \cdots, N_2 \tag{3.28e}$$

$$0 \leq \alpha \leq 1 \tag{3.28f}$$

where $\lambda_{2,i} = \widetilde{\lambda}_{2,i}/\sigma_r^2$, $\lambda_{f,i} = \sigma_r^2\widetilde{\lambda}_{f,i}$, $\lambda_{g,i} = \widetilde{\lambda}_{g,i}/\sigma_d^2$ for $i = 1, \cdots, N_2$, $\widetilde{\lambda}_{2,i}$, $\widetilde{\lambda}_{f,i}$, $\widetilde{\lambda}_{g,i}$, δ_i, and ε_i represent the ith diagonal elements of $\mathbf{\Lambda}_2$, $\mathbf{\Lambda}_f$, $\mathbf{\Lambda}_g$, $\mathbf{\Upsilon}$, and $\mathbf{\Psi}$ respectively, $\mathbf{p} = [p_1, \cdots, p_{N_2}]^T$, $\boldsymbol{\lambda}_2 = [\lambda_{2,1} \cdots, \lambda_{2,N_2}]^T$, $\boldsymbol{\lambda}_f = [\lambda_{f,1} \cdots, \lambda_{f,N_2}]^T$, and $(\cdot)^T$ denotes the matrix and vector transpose.

With the introduction of $z_i = \lambda_{f,i}(p_i\,\lambda_{2,i} + 1), i = 1, \cdots, N_2$, the optimization problem (3.28) can be written as

$$\max_{\alpha,\lambda_1,\mathbf{p},\mathbf{z},\boldsymbol{\lambda}_2} \frac{1-\alpha}{2}\sum_{i=1}^{N_2}\log\left(1 + \frac{p_i\,z_i\,\lambda_{2,i}\,\lambda_{g,i}}{p_i\,\lambda_{2,i} + z_i\,\lambda_{g,i} + 1}\right) \tag{3.29a}$$

$$s.t.\ \ \alpha\lambda_1 + \frac{1-\alpha}{2}\sigma_r^2\sum_{i=1}^{N_2}\delta_i\,\lambda_{2,i} \le \frac{1+\alpha}{2}P_s \tag{3.29b}$$

$$\sum_{i=1}^{N_2} z_i \le \kappa\eta\lambda_1 + \eta\sigma_r^2\sum_{i=1}^{N_2}\big(\varepsilon_i - p_i\big)\lambda_{2,i} \tag{3.29c}$$

$$\lambda_{2,i} \ge 0, \quad z_i \ge 0 \tag{3.29d}$$

$$0 \le p_i \le 1, \quad i = 1, \cdots, N_2 \tag{3.29e}$$

$$0 \le \alpha \le 1 \tag{3.29f}$$

where $\mathbf{z} = [z_1, \cdots, z_{N_2}]^T$.

Since (3.29a) is an increasing function of z_i, for any given α, λ_1, and $\mathbf{p}$, the optimal $\mathbf{z}$ must satisfy the equality in (3.29c) which is given as

$$\sum_{i=1}^{N_2} z_i = \kappa\eta\lambda_1 + \eta\sigma_r^2\sum_{i=1}^{N_2}(\varepsilon_i - p_i)\lambda_{2,i}. \tag{3.30}$$

By applying (3.30) to the optimization problem (3.29), the problem (3.29) is equivalently converted to

$$\max_{\alpha,\mathbf{p},\mathbf{z},\boldsymbol{\lambda}_2} \frac{1-\alpha}{2}\sum_{i=1}^{N_2}\log\left(1 + \frac{p_i\,z_i\,\lambda_{2,i}\,\lambda_{g,i}}{p_i\,\lambda_{2,i} + z_i\,\lambda_{g,i} + 1}\right) \tag{3.31a}$$

$$s.t.\ \ \sum_{i=1}^{N_2}\frac{z_i}{\sigma_r^2\eta\lambda_{h,1}} + \sum_{i=1}^{N_2}\left(\delta_i + \frac{p_i - \varepsilon_i}{\lambda_{h,1}}\right)\lambda_{2,i} \le \frac{1+\alpha}{1-\alpha}\sigma_r^{-2}P_s \tag{3.31b}$$

$$\lambda_{2,i} \ge 0, \quad z_i \ge 0 \tag{3.31c}$$

$$0 \le p_i \le 1, \quad i = 1, \cdots, N_2 \tag{3.31d}$$

$$0 \le \alpha \le 1. \tag{3.31e}$$

By introducing $a_i = \delta_i^{-1}$, $b_i = \sigma_r^2\eta\lambda_{h,1}\lambda_{g,i}$, $x_i = \delta_i\lambda_{2,i}$, $y_i = z_i/\sigma_r^2\eta\lambda_{h,1}$, and $w_i = p_i x_i$ for $i = 1, \cdots, N_2$, the optimization problem (3.31) is rewritten into

$$\max_{\alpha,\mathbf{w},\mathbf{x},\mathbf{y}} \frac{1-\alpha}{2}\sum_{i=1}^{N_2}\log\left(1+\frac{a_i\,w_i\,b_i\,y_i}{1+a_iw_i+b_iy_i}\right) \tag{3.32a}$$

$$s.t.\ \sum_{i=1}^{N_2} y_i+\sum_{i=1}^{N_2}\frac{a_iw_i}{\lambda_{h,1}}+\sum_{i=1}^{N_2}\left(1-\frac{a_i\,\varepsilon_i}{\lambda_{h,1}}\right)x_i \le \frac{1+\alpha}{1-\alpha}\sigma_r^{-2}P_s \tag{3.32b}$$

$$x_i \ge w_i \ge 0, \quad y_i \ge 0, \quad i=1,\cdots,N_2 \tag{3.32c}$$

$$0 \le \alpha \le 1 \tag{3.32d}$$

where $\mathbf{x}=[x_1,\cdots,x_{N_2}]^T$ and $\mathbf{y}=[y_1,\cdots,y_{N_2}]^T$. As the problem (3.32) is a non-convex optimization problem with multiple variables, its globally optimal solution is difficult to obtain with a tractable computational complexity. In order to solve the problem (3.32) with a polynomial computational complexity, in the following sections, the lower bound and the upper bound of the objective function (3.32a) are exploited to solve the optimization problem (3.32).

3.4 Lower Bound Based Algorithm

In this section, an algorithm is proposed to solve the optimization problem (3.32) based on a tight lower bound of (3.32a) given as

$$1+\frac{a_i\,w_i\,b_i\,y_i}{1+a_i\,w_i+b_i\,y_i}=\frac{(1+a_i\,w_i)(1+b_i\,y_i)}{1+a_i\,w_i+b_i\,y_i}\ge\frac{(1+a_i\,w_i)(1+b_i\,y_i)}{2+a_i\,w_i+b_i\,y_i}. \tag{3.33}$$

The optimization problem (3.32) is rewritten into the following

$$\min_{\alpha,\mathbf{w},\mathbf{x},\mathbf{y}} \frac{1-\alpha}{2}\sum_{i=1}^{N_2}\log\left(\frac{1}{1+a_i\,w_i}+\frac{1}{1+b_i\,y_i}\right) \tag{3.34a}$$

$$s.t.\ \sum_{i=1}^{N_2} y_i+\sum_{i=1}^{N_2}\frac{a_iw_i}{\lambda_{h,1}}+\sum_{i=1}^{N_2}\left(1-\frac{a_i\,\varepsilon_i}{\lambda_{h,1}}\right)x_i \le \frac{1+\alpha}{1-\alpha}\sigma_r^{-2}P_s \tag{3.34b}$$

$$x_i \ge w_i \ge 0, \quad y_i \ge 0, \quad i=1,\cdots,N_2 \tag{3.34c}$$

$$0 \le \alpha \le 1. \tag{3.34d}$$

By introducing $\widetilde{w}_i=\beta\,w_i$, $\widetilde{x}_i=\beta\,x_i$, and $\widetilde{y}_i=\beta\,y_i$ for $i=1,\cdots,N_2$, where $\beta=1-\alpha$, the optimization problem (3.34) is equivalently rewritten as

$$\min_{\beta,\widetilde{\mathbf{w}},\widetilde{\mathbf{x}},\widetilde{\mathbf{y}}} \ \frac{\beta}{2}\sum_{i=1}^{N_2}\log\left(\frac{1}{1+a_i\,\widetilde{w}_i/\beta}+\frac{1}{1+b_i\,\widetilde{y}_i/\beta}\right) \tag{3.35a}$$

$$s.t. \quad \sum_{i=1}^{N_2}\widetilde{y}_i+\sum_{i=1}^{N_2}\frac{a_i\widetilde{w}_i}{\lambda_{h,1}}+\sum_{i=1}^{N_2}\left(1-\frac{a_i\,\varepsilon_i}{\lambda_{h,1}}\right)\widetilde{x}_i\le(2-\beta)\sigma_r^{-2}P_s \tag{3.35b}$$

$$\widetilde{x}_i\ge\widetilde{w}_i\ge 0,\quad \widetilde{y}_i\ge 0,\quad i=1,\cdots,N_2 \tag{3.35c}$$

$$0\le\beta\le 1 \tag{3.35d}$$

where $\widetilde{\mathbf{w}}=[\widetilde{w}_1,\cdots,\widetilde{w}_{N_2}]^T$, $\widetilde{\mathbf{x}}=[\widetilde{x}_1,\cdots,\widetilde{x}_{N_2}]^T$, and $\widetilde{\mathbf{y}}=[\widetilde{y}_1,\cdots,\widetilde{y}_{N_2}]^T$. By introducing

$$\left(\frac{1}{\beta+a_i\,\widetilde{w}_i}+\frac{1}{\beta+b_i\,\widetilde{y}_i}\right)^{-1}\ge q_i \tag{3.36}$$

for $i=1,\cdots,N_2$, the optimization problem (3.35) can be rewritten into

$$\max_{\beta,\widetilde{\mathbf{w}},\widetilde{\mathbf{x}},\widetilde{\mathbf{y}},\mathbf{q}} \ \frac{\beta}{2}\sum_{i=1}^{N_2}\log\left(\frac{q_i}{\beta}\right) \tag{3.37a}$$

$$s.t. \quad \left(\frac{1}{\beta+a_i\,\widetilde{w}_i}+\frac{1}{\beta+b_i\,\widetilde{y}_i}\right)^{-1}\ge q_i$$

$$i=1,\cdots,N_2 \tag{3.37b}$$

$$\sum_{i=1}^{N_2}\widetilde{y}_i+\sum_{i=1}^{N_2}\frac{a_i\widetilde{w}_i}{\lambda_{h,1}}+\sum_{i=1}^{N_2}\left(1-\frac{a_i\,\varepsilon_i}{\lambda_{h,1}}\right)\widetilde{x}_i\le(2-\beta)\sigma_r^{-2}P_s \tag{3.37c}$$

$$\widetilde{x}_i\ge\widetilde{w}_i\ge 0,\quad \widetilde{y}_i\ge 0,\quad i=1,\cdots,N_2 \tag{3.37d}$$

$$0\le\beta\le 1 \tag{3.37e}$$

where $\mathbf{q}=[q_1,\cdots,q_{N_2}]^T$. Since the left-hand side of (3.37b) is a harmonic mean, the constraint (3.37b) is convex [89]. Moreover, the objective function (3.37a) is a perspective function [89], which is concave with respect to q_i and β. Thus, the problem (3.37) is a convex optimization problem. By using the convex programming toolbox CVX's [90] in-built primal-dual interior-point solver, the convex problem (3.37) can be solved with a computational complexity of $\mathcal{O}((6N_2+2)^3)$ per iteration.

3.5 Upper Bound Based Algorithm

In this section, an algorithm is proposed to solve the optimization problem (3.32) based on a tight upper bound of (3.32a) written as

$$\frac{a_i\,w_i\,b_i\,y_i}{1+a_i\,w_i+b_i\,y_i}\le\frac{a_i\,w_i\,b_i\,y_i}{a_i\,w_i+b_i\,y_i}. \tag{3.38}$$

By exploiting the upper bound given in (3.38), the optimization problem (3.32) is rewritten as

$$\max_{\alpha,\mathbf{w},\mathbf{x},\mathbf{y}} \frac{1-\alpha}{2}\sum_{i=1}^{N_2}\log\left(1+\frac{a_i\,w_i\,b_i\,y_i}{a_i\,w_i+b_i\,y_i}\right) \tag{3.39a}$$

$$s.t.\ \sum_{i=1}^{N_2} y_i+\sum_{i=1}^{N_2}\frac{a_i w_i}{\lambda_{h,1}}+\sum_{i=1}^{N_2}\left(1-\frac{a_i\,\varepsilon_i}{\lambda_{h,1}}\right)x_i \le \frac{1+\alpha}{1-\alpha}\sigma_r^{-2}P_s \tag{3.39b}$$

$$x_i \ge w_i \ge 0, \quad y_i \ge 0, \quad i=1,\cdots,N_2 \tag{3.39c}$$

$$0 \le \alpha \le 1. \tag{3.39d}$$

By applying variable substitutions of $\widetilde{w}_i$, $\widetilde{x}_i$, and $\widetilde{y}_i$ for $i=1,\cdots,N_2$, which lead to (3.35), the optimization problem (3.39) is equivalently converted to

$$\max_{\beta,\widetilde{\mathbf{w}},\widetilde{\mathbf{x}},\widetilde{\mathbf{y}}} \frac{\beta}{2}\sum_{i=1}^{N_2}\log\left(1+\frac{a_i\,(\widetilde{w}_i/\beta)\,b_i\,(\widetilde{y}_i/\beta)}{a_i\,(\widetilde{w}_i/\beta)+b_i\,(\widetilde{y}_i/\beta)}\right) \tag{3.40a}$$

$$s.t. \quad \sum_{i=1}^{N_2}\widetilde{y}_i+\sum_{i=1}^{N_2}\frac{a_i\widetilde{w}_i}{\lambda_{h,1}}+\sum_{i=1}^{N_2}\left(1-\frac{a_i\,\varepsilon_i}{\lambda_{h,1}}\right)\widetilde{x}_i \le (2-\beta)\sigma_r^{-2}P_s \tag{3.40b}$$

$$\widetilde{x}_i \ge \widetilde{w}_i \ge 0, \quad \widetilde{y}_i \ge 0, \quad i=1,\cdots,N_2 \tag{3.40c}$$

$$0 \le \beta \le 1. \tag{3.40d}$$

For $i=1,\cdots,N_2$, by introducing

$$\frac{a_i\,(\widetilde{w}_i/\beta)\,b_i\,(\widetilde{y}_i/\beta)}{a_i\,(\widetilde{w}_i/\beta)+b_i\,(\widetilde{y}_i/\beta)} \ge \frac{t_i}{\beta} \tag{3.41}$$

the optimization problem (3.40) can be rewritten as

$$\max_{\beta,\widetilde{\mathbf{w}},\widetilde{\mathbf{x}},\widetilde{\mathbf{y}},\mathbf{t}} \frac{\beta}{2}\sum_{i=1}^{N_2}\log\left(1+\frac{t_i}{\beta}\right) \tag{3.42a}$$

$$s.t. \quad \frac{a_i\,(\widetilde{w}_i/\beta)\,b_i\,(\widetilde{y}_i/\beta)}{a_i\,(\widetilde{w}_i/\beta)+b_i\,(\widetilde{y}_i/\beta)} \ge \frac{t_i}{\beta}, \quad i=1,\cdots,N_2 \tag{3.42b}$$

$$\sum_{i=1}^{N_2}\widetilde{y}_i+\sum_{i=1}^{N_2}\frac{a_i\widetilde{w}_i}{\lambda_{h,1}}+\sum_{i=1}^{N_2}\left(1-\frac{a_i\,\varepsilon_i}{\lambda_{h,1}}\right)\widetilde{x}_i \le (2-\beta)\sigma_r^{-2}P_s \tag{3.42c}$$

$$\widetilde{x}_i \ge \widetilde{w}_i \ge 0, \quad \widetilde{y}_i \ge 0, \quad i=1,\cdots,N_2 \tag{3.42d}$$

$$0 \le \beta \le 1. \tag{3.42e}$$

From (3.42b), the following can be derived

$$\frac{(a_i\,(\widetilde{w}_i/\beta)+b_i\,(\widetilde{y}_i/\beta))^2-(a_i\,(\widetilde{w}_i/\beta))^2-(b_i\,(\widetilde{y}_i/\beta))^2}{2(a_i\,(\widetilde{w}_i/\beta)+b_i\,(\widetilde{y}_i/\beta))}-\frac{t_i}{\beta}\ge 0 \tag{3.43}$$

for $i = 1, \cdots, N_2$. The inequality (3.43) can be equivalently expressed as

$$\begin{aligned} &a_i\left(\widetilde{w}_i/\beta\right) + b_i\left(\widetilde{y}_i/\beta\right) - a_i\left(\widetilde{w}_i/\beta\right)\left(a_i\left(\widetilde{w}_i/\beta\right) + b_i\left(\widetilde{y}_i/\beta\right)\right)^{-1} a_i\left(\widetilde{w}_i/\beta\right) \\ &-b_i\left(\widetilde{y}_i/\beta\right)\left(a_i\left(\widetilde{w}_i/\beta\right) + b_i\left(\widetilde{y}_i/\beta\right)\right)^{-1} b_i\left(\widetilde{y}_i/\beta\right) - 2(t_i/\beta) \geq 0 \end{aligned} \tag{3.44}$$

for $i = 1, \cdots, N_2$, which can be further written as a positive semidefinite (PSD) constraint given as

$$\begin{pmatrix} a_i\,\widetilde{w}_i + b_i\,\widetilde{y}_i - 2t_i & a_i\,\widetilde{w}_i & b_i\,\widetilde{y}_i \\ a_i\,\widetilde{w}_i & a_i\,\widetilde{w}_i + b_i\,\widetilde{y}_i & 0 \\ b_i\,\widetilde{y}_i & 0 & a_i\,\widetilde{w}_i + b_i\,\widetilde{y}_i \end{pmatrix} \geq 0. \tag{3.45}$$

The matrix written in (3.45) is a PSD matrix. By applying (3.45) to the optimization problem (3.42), the optimization problem can be expressed as

$$\max_{\beta, \widetilde{\mathbf{w}}, \widetilde{\mathbf{x}}, \widetilde{\mathbf{y}}, \mathbf{t}} \frac{\beta}{2} \sum_{i=1}^{N_2} \log\left(1 + \frac{t_i}{\beta}\right) \tag{3.46a}$$

$$s.t. \begin{pmatrix} a_i\widetilde{w}_i + b_i\widetilde{y}_i - 2t_i & a_i\widetilde{w}_i & b_i\widetilde{y}_i \\ a_i\widetilde{w}_i & a_i\widetilde{w}_i + b_i\widetilde{y}_i & 0 \\ b_i\widetilde{y}_i & 0 & a_i\widetilde{w}_i + b_i\widetilde{y}_i \end{pmatrix} \geq 0, \quad i = 1, \cdots, N_2 \tag{3.46b}$$

$$\sum_{i=1}^{N_2} \widetilde{y}_i + \sum_{i=1}^{N_2} \frac{a_i\widetilde{w}_i}{\lambda_{h,1}} + \sum_{i=1}^{N_2} \left(1 - \frac{a_i\,\varepsilon_i}{\lambda_{h,1}}\right) \widetilde{x}_i \leq (2-\beta)\sigma_r^{-2} P_s \tag{3.46c}$$

$$\widetilde{x}_i \geq \widetilde{w}_i \geq 0, \quad \widetilde{y}_i \geq 0, \quad i = 1, \cdots, N_2 \tag{3.46d}$$

$$0 \leq \beta \leq 1. \tag{3.46e}$$

The optimization problem (3.46) is an SDP problem which can be efficiently solved by the disciplined convex programming toolbox CVX [90]. Based on [103], the computational complexity of solving the problem (3.46) is $\mathcal{O}(c_2(4N_2)^2(12N_2+2))$, where c_2 is the number of iterations till convergence. It will be shown in Section VI that the upper bound and lower bound based algorithms have a similar performance. This indicates that the problem (3.32) can be solved via the upper bound and lower bound based algorithms with a high accuracy.

3.6 Numerical Example

In this section, the performance of the proposed lower bound algorithm (HPTSR-LB) and upper bound algorithm (HPTSR-UP) is investigated through numerical simulations. The source, relay, and destination nodes in the relay communication system are

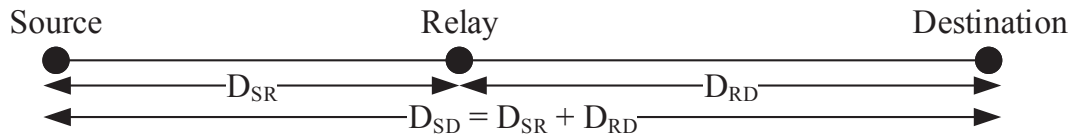

Figure 3.3: Position of source, relay, and destination nodes in the simulation.

positioned as demonstrated in Fig. 3.3 for the investigation of the system performance against the relay position. The source-destination distance is set to $D_{SD} = 20$ meters, where the source-relay distance is $D_{SR} = 10l$ meters and the relay-destination distance is $D_{RD} = 10(2 - l)$ meters. The value of l $(0 < l < 2)$ is normalized over a distance of 10 meters. This normalization provides easy identification of the position of the relay node. For $0 < l < 1$, the relay position is nearer to the source node, and for $1 < l < 2$, the relay position is nearer to the destination node. In the simulation, $0.2 \leq l \leq 1.8$ is selected such that $D_{SR} \geq 2$ m and $D_{RD} \geq 2$ m.

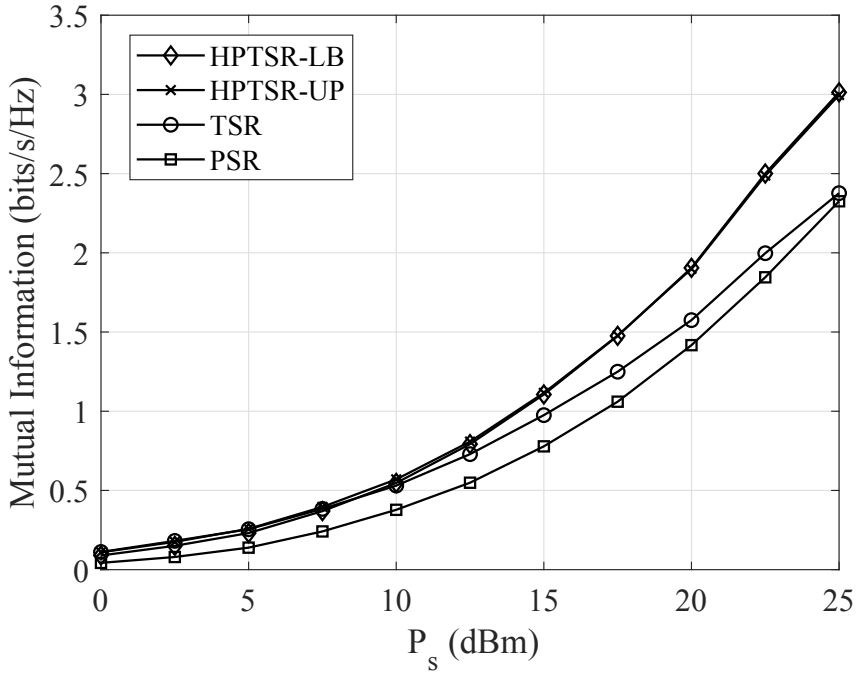

Figure 3.4: Example 1: MI versus P_s with $\eta = 0.8$, $N_s = N_r = N_d = 2$, and $l = 1$.

Similar to existing works [46, 47, 54, 55], the channel matrices are set as $\mathbf{H} = D_{SR}^{-\xi/2}\bar{\mathbf{H}}$ and $\mathbf{G} = D_{RD}^{-\xi/2}\bar{\mathbf{G}}$ where $D_{SR}^{-\xi}$ and $D_{RD}^{-\xi}$ represent the large-scale pathloss with ξ being the pathloss exponent. By considering the suburban communication scenario, $\xi = 3$

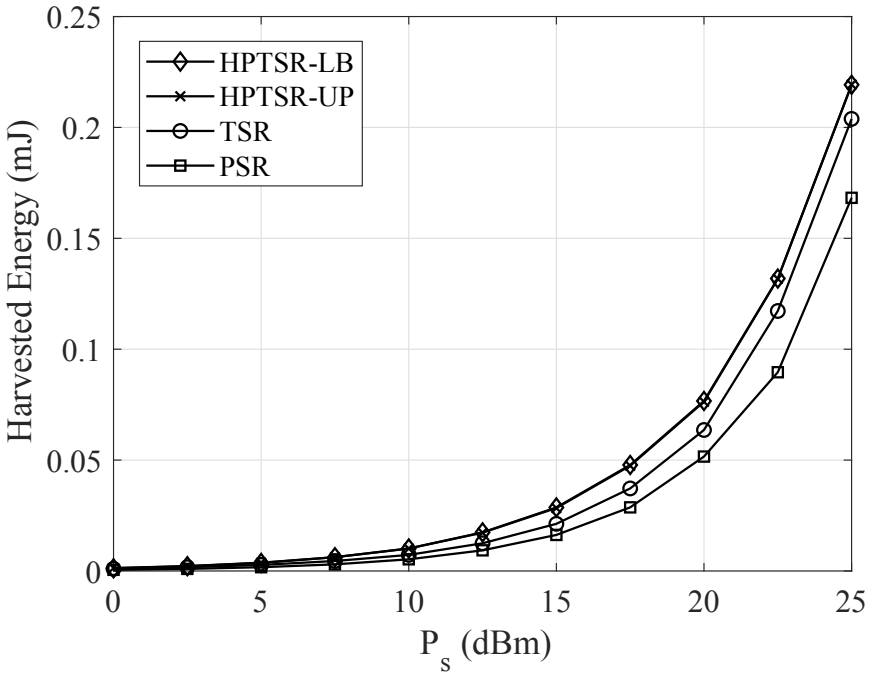

Figure 3.5: Example 1: Harvested energy at the relay node versus P_s with $\eta = 0.8$, $N_s = N_r = N_d = 2$, and $l = 1$.

[104]. $\bar{\mathbf{H}}$ and $\bar{\mathbf{G}}$ are constructed according to the Rayleigh fading model with their elements drawn from i.i.d. complex Gaussian distribution with zero mean and variances of $1/N_s$ and $1/N_r$, respectively. The noise variance at the relay and destination nodes as $\sigma_r^2 = \sigma_d^2 = -50$dBm. The performances of both proposed algorithms are compared with the TS-based relaying (TSR) protocol for the AF MIMO relay system given in [54] and the PS-based relaying (PSR) protocol for the AF MIMO relay system given in [55]. The upper bound based algorithm in [54] is used to demonstrate the performance of the system with the TSR protocol. While the proposed method 2 in [55] which exploits the upper bound of the MI in the given system is used to demonstrate the performance of the system using the PSR protocol. All the numerical example results are averaged over 1000 independent channel realizations.

In the first numerical example, $\eta = 0.8$, and $N_s = N_r = N_d = N_2 = 2$ are defined, and the system MI for the tested algorithms versus the source node power with the relay node located at $l = 1$ are studied. Fig. 3.4 demonstrates the MI performance versus the source node power P_s. Fig. 3.5 shows the harvested energy at the relay node using the tested systems versus P_s. It is observed that the MI performance of the HPTSR-

LB algorithm and the HPTSR-UP algorithm outperform the TSR algorithm given in [54] and the PSR algorithm in [55]. It is also noticed that the system performance of the HPTSR-LB algorithm is similar to that of the HPTSR-UP algorithm. With the increase of P_s, the MI gap between both the HPTSR-LB algorithm and the HPTSR-UP algorithm to the TSR algorithm as well as the PSR algorithm increases. This is because the harvested energy at the relay node using the HPTSR protocol is higher than that using the TSR protocol and the PSR protocol, which can be seen from Fig. 3.5. In other words, both the HPTSR-LB algorithm and the HPTSR-UP algorithm provide a higher power efficiency in terms of the MI per unit power available at the source node compared with the existing TSR algorithm and PSR algorithm, as the two proposed algorithms (HPTSR-LB and HPTSR-UP) yield a larger MI with the same transmission power budget at the source node. From the numerical results, it is clear that by hybridizing the TSR protocol and the PSR protocol, the system performance is greatly improved compared to the system with only the TSR protocol or the PSR protocol. This is because the HPTSR protocol provides more degrees of freedom for the optimization of system performance.

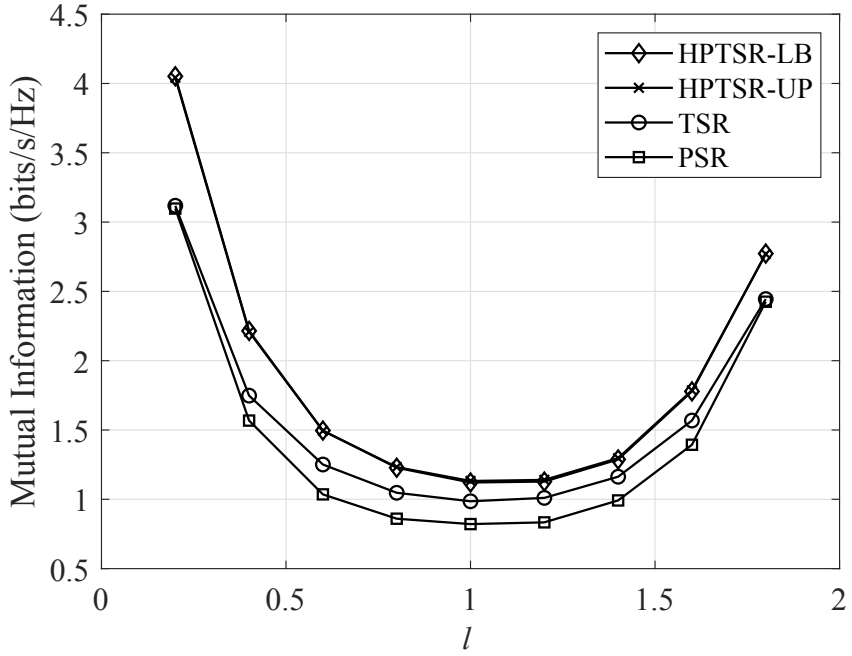

Figure 3.6: Example 2: MI versus l with $P_s = 15$dBm, $\eta = 0.8$, and $N_s = N_r = N_d = 2$.

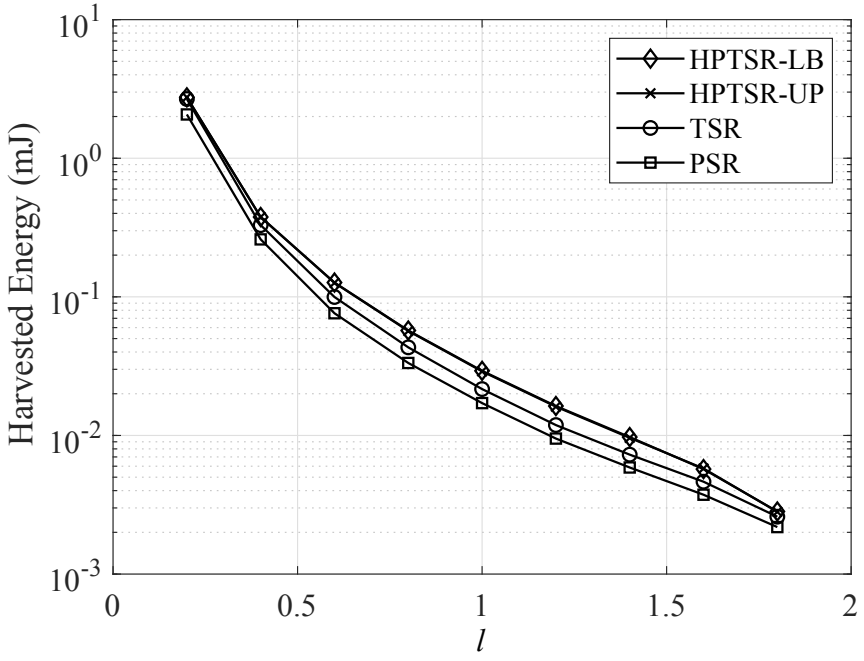

Figure 3.7: Example 2: Harvested energy at the relay node versus l with $P_s = 15$dBm, $\eta = 0.8$, and $N_s = N_r = N_d = 2$.

In the second numerical example, the system MI of the tested algorithms at various positions of the relay node is investigated. Fig. 3.6 and Fig. 3.7 correspondingly show the MI performance and the energy harvested at the relay node of the tested algorithms versus l at $P_s = 15$dBm, $\eta = 0.8$, and $N_s = N_r = N_d = 2$. From Fig. 3.6 it is observed that both the HPTSR-LB algorithm and the HPTSR-UP algorithm have the highest MI at all l compared to the TSR algorithm and the PSR algorithm. This indicates that the proposed HPTSR protocol outperforms the existing TSR protocol and PSR protocol regardless of the position of the relay node. This can be explained from Fig. 3.7, where it can be seen that the HPTSR-LB algorithm and the HPTSR-UP algorithm provide more harvested energy at the relay node compared to the TSR algorithm and the PSR algorithm. Besides, it is also noticeable from Fig. 3.7 that the harvested energy at the relay node for all the tested algorithms is reduced when the relay node is located further away from the source node. This results in the decrease of the system MI for all the tested algorithms as illustrated in Fig. 3.6 when $0.2 \leq l \leq 1$. However, when $1 \leq l \leq 1.9$, the system MI for all the tested algorithms as illustrated in Fig. 3.6 increases with l even though the available transmission energy at the relay node gained from the harvested

energy reduces with l. This is due to the shorter distance between the relay and the destination nodes, which leads to a better second-hop channel and thus improves the system MI.

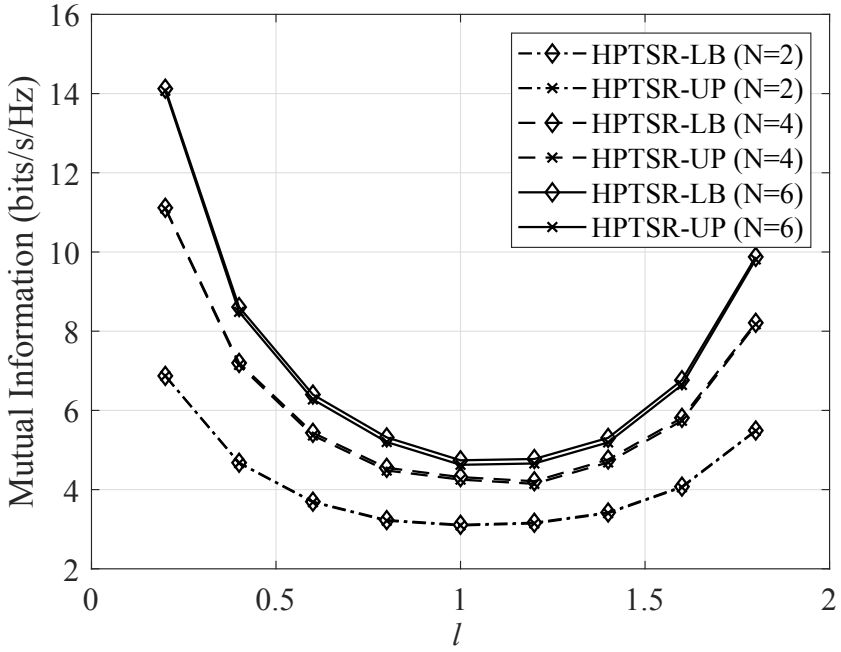

Figure 3.8: Example 3: MI versus l at various N with $P_s = 25$dBm and $\eta = 0.8$.

In the third numerical example, the MI performance of the HPTSR-LB algorithm and the HPTSR-UP algorithm at various positions of the relay node with different combinations of N_s, N_r, and N_d is studied. Fig. 3.8 illustrates the system MI of the HPTSR-LB algorithm and HPTSR-UP algorithm versus l with $P_s = 25$dBm and $\eta = 0.8$ at $N_s = N_r = N_d = N$ with $N = 2$, $N = 4$, and $N = 6$. It can be noticed that the system MI increases with N. This is because, with the increase of N, the number of concurrent data streams N_2 also increases, which results in a higher system MI. Fig. 3.9 illustrates the MI performance of the proposed algorithms versus the source node power P_s with the same largest number of concurrent data streams $N_2 = N_s = N_d = 2$ when $N_r = 2$, $N_r = 4$, and $N_r = 6$ at $\eta = 0.8$ and $l = 1$. It can notice that the system with a larger number of relay antennas provides a better MI performance. This is because the relay antennas which are unused for ID are solely used for EH, which also increases the energy harvested at the relay node. Thus, the MI performance of the system can be effectively improved by installing more antennas at the relay node.

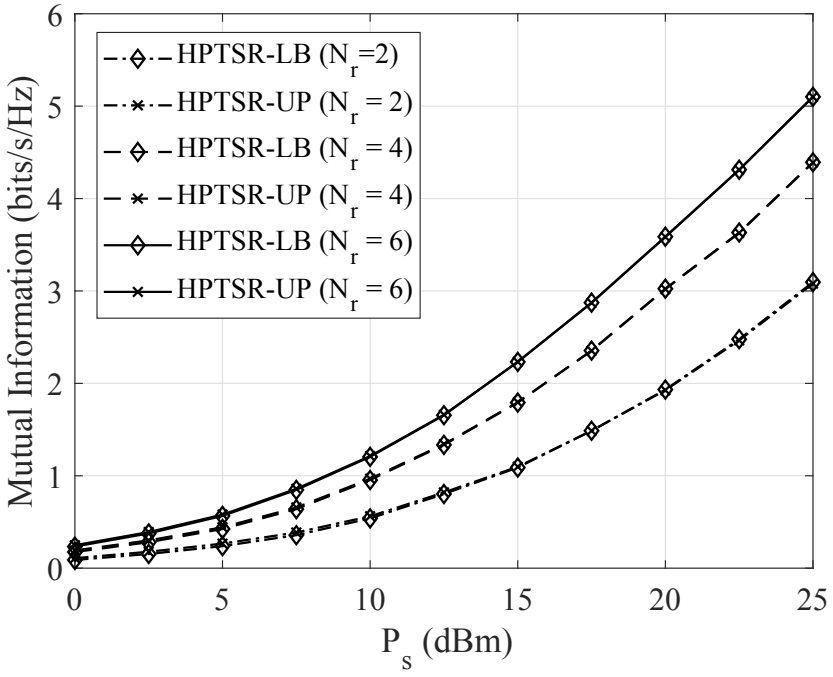

Figure 3.9: Example 3: MI versus P_s at various N_r with $l = 1$, $\eta = 0.8$, and $N_s = N_d = 2$.

3.7 Chapter Summary

The transceiver design for a dual-hop MIMO AF relay communication system with the HPTSR-based EH relaying protocol is investigated in this chapter. The architecture of the HPTSR-based protocol combines the TS-based and PS-based EH relaying protocols. The optimal structure of the source and relay precoding matrices is proposed to convert the highly challenging joint transceiver design problem to a joint transceiver power allocation problem with low complexity. Two algorithms are derived to solve the optimal power allocation problem. In general, the two proposed algorithms provide a better MI performance compared to existing TSR and PSR based algorithms. It is obvious to notice that the system MI performance is better when the relay node is located closer to the source or destination nodes. Moreover, the MI performance of the system can be improved by installing more antennas at the relay node.

Chapter 4

Robust Transceiver Design for SWIPT DF MIMO Relay System with Time Switching Relaying Protocol

A dual-hop SWIPT DF MIMO relay communication system in which the relay node harvests energy based on the RF signal transmitted from the source node through the TS protocol to decode and forward the re-encoded information to the destination node is investigated in this chapter. With consideration of the channel estimation error, the joint optimization of the TS factor, source and relay precoding matrices is proposed with robustness against the CSI mismatch to maximize the MI between the source and destination node. The optimal structure for the source and relay precoding matrices is derived to simplify the transceiver optimization problem under fixed and flexible power constraints. Numerical examples illustrate that the proposed algorithms with robustness provide better MI performance compared with the non-robust algorithm.

The remainder of this chapter is structured as follows. In Section 4.1, an overview of existing techniques provided in literature is presented. In Section 4.2, the system model of a dual-hop MIMO relay system with EH relay adopting TS protocol and consideration of the CSI mismatch is presented. In Section 4.3, the robust transceiver design algorithm is developed with a fixed transmission power scheme at the source node. In Section 4.4,

the robust transceiver design algorithm is developed with a flexible transmission power scheme at the source node. In Section 4.5, the peak power limits for the source node and relay node are considered in the optimization problem. Numerical results are presented in Section 4.6 and conclusions are drawn in Section 4.7.

4.1 Overview of Existing Techniques

Recently, the application of SWIPT technology in the energy-limited wireless system has attracted much attention from researchers around the world. This is due to the capability of the SWIPT technology to prolong the lifespan of a wireless system by harvesting energy from RF signals while receiving information date from the transmitter. There are two types of SWIPT receivers in practice, which are known as the TS and PS SWIPT receivers [6].

In a scenario where the source and destination nodes are located over a long distance, it is necessary to deploy relay nodes for the wireless system. By utilizing relay technology, the network coverage of wireless communication is extended [8]. There are mainly two types of relaying schemes commonly used in practice, namely the AF relaying scheme and the DF relaying scheme. The AF relaying scheme amplifies the received signal and forwards it to the next nodes, while the DF relaying scheme decodes the received information and then encodes it before forwarding the information signal to the next node. In [11], the TS and PS protocols for SWIPT receiver are adopted to wireless relay system by introducing TS-based and PS-based relaying protocols to perform EH and ID from the received signal at the relay node. The SWIPT relay node processes and forwards the received signals to the destination node by utilizing the energy harvested.

The MIMO technique, which is implemented by installing multiple antennas at the system nodes, can enhance the spectral efficiency of a relay system [105]. MIMO relay communication systems with application of SWIPT relay node have been investigated in [1, 45, 54–56]. In [1], the authors investigated the dual-hop SWIPT AF MIMO OFDM relay system and developed the TS and PS protocols for the relay system. In [45], SWIPT AF massive MIMO relay networks with PSR scheme and TSR scheme were investigated. The authors derived the asymptotic harvested energy and sum rate expression for a relay with infinite number of antennas. In [54], the joint optimization problem in maximizing the MI between the source and destination node for SWIPT AF MIMO relay communication system with TSR scheme was investigated. The joint

optimization problem was solved by using the primal decomposition based algorithm and upper bound based algorithm. In [55], the authors investigated a two-hop SWIPT AF MIMO relay communication system with PSR scheme. The source and relay precoding matrices with the PS factor matrices were jointly optimized by the SQP approach, the SDP approach, and the primal-dual search approach to achieve the maximal system MI. In [56], the authors extended the work in [54] and [55] to a dual-hop SWIPT DF MIMO relay communication systems.

In [1, 45, 54–56], the authors assumed that the exact CSI is available. However, the exact CSI is unobtainable in practice due to the CSI mismatch between the exact CSI and estimated CSI. The channel mismatch between the exact and estimated CSI deteriorates the performance of the proposed relay systems [72, 79]. Studies regarding the imperfect CSI in SWIPT MIMO relay systems have been carried out in [49, 50, 106–108]. In [49], the authors investigate a dual-hop SWIPT MIMO AF relay communication system for the ideal EH scheme, the PSR scheme and the TSR scheme. Furthermore, the authors consider the imperfect CSI when optimizing the SWIPT MIMO AF relay communication system with the TSR scheme. In [50], the work in [49] is extended to a DF relay communication system. Similarly, the impact of the imperfect CSI is considered for the TSR scheme. It is noted that the imperfect CSI considered in [49] and [50] is a special case, where the authors assumed scaled identity matrices as the row and column covariance matrices of the CSI mismatch matrices, and the CSI mismatch is treated as noise. However, in many practical applications, there is channel correlation. Hence, the correlation matrix is not an identity matrix. Thus, the assumption made in [49] and [50] is not valid. In [106], a dual-hop multirelay SWIPT wireless communication system with the TSR protocol was investigated with the consideration of CSI mismatch. The wireless communication between the multi-antenna source node and destination node is carried out with multiple single-antenna relay nodes arranged in parallel. In [107], a SWIPT MIMO AF relay communication system is investigated with imperfect CSI. The TSR protocol is used to perform EH and ID at the relay node. In the considered system, the transmit antenna selection strategy is used to reduce system complexity. The system nodes transmit information signal, e.g., the source node and relay node, are treated as single-antenna system nodes during the signal transmission. In [108], an energy-efficient optimization design for a two-way MIMO relay networks with PSR protocol is investigated with the consideration of the CSI mismatch. It is observed that the CSI mismatch considered in [108] is modelled based on the Euclidean-norm bounded

model. Unlike [49, 50, 106, 108], the well-known Gaussian Kronecker model is adopted in this chapter to model the CSI mismatch. The Gaussian-Kronecker model is used because, in the practical scenario, there is always correlation of the channel. Different to [106], the system node considered in this chapter are all equipped with multiple antennas. Moreover, different to [107], all the antennas installed at the system nodes will be used.

A transceiver design is proposed for a dual-hop MIMO relay communication system with a SWIPT relay using the DF relaying protocol. The transceiver is designed with the consideration of imperfect CSI. The implementation of the robust SWIPT DF MIO relay system can be performed in a similar way to those non-robust design. The focus of this chapter is on system optimization. There is no existing work has been carried out in SWIPT DF MIMO relay system with consideration of imperfect CSI, which modelled based on the Gaussian Kronecker model. Through numerical simulations, it is shown that the proposed scheme improves the robustness of SWIPT DF MIMO relay system against the channel estimation error.

The contributions/challenges of this chapter are summarized below:

- The impact of the CSI mismatch modelled based on the Gaussian Kronecker model towards the system performance of a dual-hop SWIPT AF MIMO relay systems with energy-limited relay is examined. There is no existing work carried out in a dual-hop SWIPT DF MIMO relay systems with consideration of practical imperfect CSI based on the Gaussian-Kronecker model.

- The works carried out in this chapter extend the existing work [50] from the special case where the channel correlation matrices are assumed as scaled identity matrices to scenarios with general channel correlation matrices.

- The algorithm proposed for the transceiver design in this chapter provides robustness to counter the inevitable channel mismatch between the exact and estimated CSI in practice. The proposed algorithm helps to improve the system performance of the existing transceiver design under a similar system mode [56].

- With the proposed optimal structure for the source and relay precoding matrices, the complex optimization problem with any given TS ratio is simplified into two simple power-allocation subproblems (for fixed power scheme) and/or one master problem with two associated simple power-allocation subproblems (for flexible

power scheme) which greatly reduce the computational complexity of the optimization problem.

4.2 SWIPT DF Relay System Model with TS Relaying Scheme

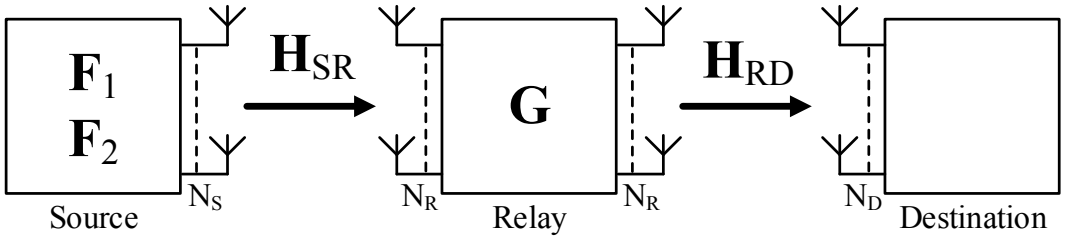

Figure 4.1: Block diagram of a dual-hop MIMO relay system with EH relay using TS protocol.

A dual-hop three-node MIMO relay communication system is considered in this chapter where information signals are transmitted from the source node to the destination node with the help of a relay node as displayed in Fig. 4.1. The number of antennas installed at the source, relay, and the destination node are denoted as N_S, N_R, and N_D respectively. The source node has an in-built power supply, while the relay node is required to be powered by energy harvested from the received RF signals. It is also assumed that the direct link between the source and destination node is negligible due to severe pathloss and shadowing. Compared with the AF relaying scheme, the DF relaying scheme is selected for the relay as it does not amplify and forward the noise introduced at the relay node.

For the EH scheme at the relay node, the TS protocol is adopted to the system. In one communication cycle, the total time T is divided into three time-frames. During the first time-frame of αT, the source node transmits the energy-bearing signal vector $\mathbf{s}_1 \in \mathbb{C}^{N_S \times 1}$ to the relay node for EH where $\alpha \in [0, 1]$ represents the TS ratio and the covariance matrix of $\mathbf{s}_1$ is given as $E\{\mathbf{s}_1\mathbf{s}_1^H\} = \mathbf{F}_1$, where $E\{\cdot\}$ and $(\cdot)^H$ denote the statistical expectation and Hermitian transpose, respectively. During the second time-frame of $(1-\alpha)T/2$, the source node transmits information-bearing signal vector $\mathbf{s}_2 \in \mathbb{C}^{N_S \times 1}$ with covariance matrix given as $E\{\mathbf{s}_2\mathbf{s}_2^H\} = \mathbf{F}_2$ to the relay node for ID where the relay decodes and re-encodes the received signal. During the final time-frame

of $(1-\alpha)T/2$, the relay forwards the encoded signal $\bar{\mathbf{s}} \in \mathbb{C}^{N_R \times 1}$ to the destination node, where $\bar{\mathbf{s}}$ has the covariance matrix given as $E\{\bar{\mathbf{s}}\bar{\mathbf{s}}^H\} = \mathbf{G}$. For simplicity, $T = 1$.

The received signal at the relay node for EH during the first time-frame is given as

$$\mathbf{y}_{r,1} = \mathbf{H}_{SR}\mathbf{s}_1 + \mathbf{n}_{r,1} \tag{4.1}$$

where $\mathbf{H}_{SR}$ is the MIMO channel matrix of the source-relay link and $\mathbf{n}_{r,1}$ is the AWGN at the relay node during the first time-frame. Thus, the RF energy E_r harvested at the relay node without noise component can be written as

$$E_r = \alpha\eta \; tr\{\mathbf{H}_{SR}\mathbf{F}_1\mathbf{H}_{SR}^H\} \tag{4.2}$$

where $\eta \in [0, 1]$ is the conversion efficiency at the relay node and $tr\{\cdot\}$ denotes the matrix trace.

During the second time-frame, the received signal at the relay node for ID is given as

$$\mathbf{y}_{r,2} = \mathbf{H}_{SR}\mathbf{s}_2 + \mathbf{n}_{r,2} \tag{4.3}$$

where $\mathbf{n}_{r,2}$ is the AWGN noise at the relay node with a covariance matrix of $\sigma_r^2\mathbf{I}_{N_R}$ and $\mathbf{I}_n$ denotes an $n \times n$ identity matrix. During the final time-frame, the relay node forwards the re-encoded information to the destination node. The received signal at the destination node is given as

$$\mathbf{y}_d = \mathbf{H}_{RD}\bar{\mathbf{s}} + \mathbf{n}_d \tag{4.4}$$

where $\mathbf{H}_{RD}$ is the MIMO channel matrix of the relay-destination link and $\mathbf{n}_d$ is the AWGN noise at the destination node with a covariance matrix of $\sigma_d^2\mathbf{I}_{N_D}$.

In existing work, the exact CSI is assumed to be known at the relay and destination nodes. However, the exact CSI is unavailable in the practical scenario due to the channel estimation error, which results in the CSI mismatch between the exact and estimated CSI. Thus, the true MIMO channel matrices with consideration of imperfect CSI are given as

$$\mathbf{H}_{SR} = \widehat{\mathbf{H}}_{SR} + \mathbf{\Delta}_{SR}, \qquad \mathbf{H}_{RD} = \widehat{\mathbf{H}}_{RD} + \mathbf{\Delta}_{RD} \tag{4.5}$$

where $\widehat{\mathbf{H}}_{SR}$ and $\widehat{\mathbf{H}}_{RD}$ are the estimated channel matrices for source-relay link and relay-destination link respectively, $\mathbf{\Delta}_{SR}$ and $\mathbf{\Delta}_{RD}$ are the corresponding CSI mismatch

matrices. Based on the Gaussian-Kronecker model, the CSI mismatch matrices are modelled as

$$\mathbf{\Delta}_{SR} \sim \mathcal{CN}(\mathbf{0}, \mathbf{\Sigma}_{SR} \otimes \mathbf{\Phi}_{SR}^{T}) \tag{4.6}$$
$$\mathbf{\Delta}_{RD} \sim \mathcal{CN}(\mathbf{0}, \mathbf{\Sigma}_{RD} \otimes \mathbf{\Phi}_{RD}^{T}) \tag{4.7}$$

where $\otimes$ denotes the matrix Kronecker product, $(\cdot)^T$ stands for the matrix transpose, $\mathbf{\Sigma}_{SR}$ and $\mathbf{\Sigma}_{RD}$ are the row covariance matrices while $\mathbf{\Phi}_{SR}$ and $\mathbf{\Phi}_{RD}$ are the column covariance matrices for $\mathbf{\Delta}_{SR}$ and $\mathbf{\Delta}_{RD}$ respectively.

The MI across the source-destination link [109], $\mathcal{I}_{SD}$ is the minimum of the MI across the source-relay link, $\mathcal{I}_{SR}$ and the MI across the relay-destination link, $\mathcal{I}_{RD}$, and can be expressed as

$$\mathcal{I}_{SD} = \min\left(\mathcal{I}_{SR}, \mathcal{I}_{RD}\right). \tag{4.8}$$

With the consideration of CSI mismatch, $\mathcal{I}_{SR}$ and $\mathcal{I}_{RD}$ can be written as [110]

$$\mathcal{I}_{SR} = \frac{1-\alpha}{2}\log_2\left|\mathbf{I}_{N_R} + \mathbf{T}_{SR}^{-\frac{1}{2}}\widehat{\mathbf{H}}_{SR}\mathbf{F}_2\widehat{\mathbf{H}}_{SR}^{H}\mathbf{T}_{SR}^{-\frac{H}{2}}\right| \tag{4.9}$$
$$\mathcal{I}_{RD} = \frac{1-\alpha}{2}\log_2\left|\mathbf{I}_{N_D} + \mathbf{T}_{RD}^{-\frac{1}{2}}\widehat{\mathbf{H}}_{RD}\mathbf{G}\widehat{\mathbf{H}}_{RD}^{H}\mathbf{T}_{RD}^{-\frac{H}{2}}\right| \tag{4.10}$$

where

$$\mathbf{T}_{SR} = \sigma_r^2\mathbf{I}_{N_R} + tr\{\mathbf{F}_2\mathbf{\Phi}_{SR}\}\mathbf{\Sigma}_{SR} \tag{4.11}$$
$$\mathbf{T}_{RD} = \sigma_d^2\mathbf{I}_{N_D} + tr\{\mathbf{G}\mathbf{\Phi}_{RD}\}\mathbf{\Sigma}_{RD}. \tag{4.12}$$

Moreover, with the consideration of the CSI mismatch, E_r from (4.2) is rewritten into

$$E_r = \alpha\eta\, tr\{\widehat{\mathbf{H}}_{SR}\mathbf{F}_1\widehat{\mathbf{H}}_{SR}^{H} + tr\{\mathbf{F}_1\mathbf{\Phi}_{SR}\}\mathbf{\Sigma}_{SR}\}. \tag{4.13}$$

In the TS protocol, there are two schemes of transmission power constraint [6] which are known as the fixed power scheme and the flexible power scheme. The transmission power constraint for the source and relay nodes in the case of the fixed power scheme is given as

$$tr\left\{\mathbf{F}_1\right\} \leq P_s,\ \ tr\left\{\mathbf{F}_2\right\} \leq P_s,\ \ \frac{1-\alpha}{2}tr\left\{\mathbf{G}\right\} \leq E_r \tag{4.14}$$

and in the case of the flexible power scheme is given as

$$\alpha tr\{\mathbf{F}_1\} + \frac{1-\alpha}{2}tr\{\mathbf{F}_2\} \leq \frac{1+\alpha}{2}P_s,\ \ \frac{1-\alpha}{2}tr\{\mathbf{G}\} \leq E_r \tag{4.15}$$

where $P_s > 0$ is the power budget available at the source node.

The main objective of the proposed transceiver design scheme is to maximize $\mathcal{I}_{SD}$ subjecting to each variation of transmission power constraints at the source and relay nodes as given in (4.14) and (4.15).

Different from [50], CSI mismatch covariance matrices, $\mathbf{\Phi}_{SR}$, $\mathbf{\Phi}_{RD}$, $\mathbf{\Sigma}_{SR}$ and $\mathbf{\Sigma}_{RD}$ in general cases are not scaled identity matrices which result in difficulties when solving the optimization problem. In general cases where $\mathbf{\Phi}_{SR} \neq \sigma_e^2 \mathbf{I}_{N_S}$ and $\mathbf{\Phi}_{RD} \neq \sigma_e^2 \mathbf{I}_{N_R}$, the inequality [75] as follows is introduced to overcome the challenge.

$$tr\{\mathbf{AB}\} \leq tr\{\mathbf{A}\}\lambda_M(\mathbf{B}) \tag{4.16}$$

where $\lambda_M(\cdot)$ denotes the maximal eigenvalue of a matrix. By applying (4.16) to (4.11) and (4.12), the upper bound of $\mathbf{T}_{SR}$ and $\mathbf{T}_{RD}$ are given as

$$\mathbf{T}_{SR} = \sigma_r^2 \mathbf{I}_{N_R} + tr\{\mathbf{F}_2\}\varphi_{SR}\mathbf{\Sigma}_{SR} \tag{4.17}$$
$$\mathbf{T}_{RD} = \sigma_d^2 \mathbf{I}_{N_D} + tr\{\mathbf{G}\}\varphi_{RD}\mathbf{\Sigma}_{RD} \tag{4.18}$$

where φ_{SR} and φ_{RD} denote the maximal eigenvalue of $\mathbf{\Phi}_{SR}$ and $\mathbf{\Phi}_{RD}$ respectively. By substituting (4.17) and (4.18) to (4.8), the objective function $\mathcal{I}_{SD}$ which exploited the lower bound of $\mathcal{I}_{SR}$ and $\mathcal{I}_{SD}$ is optimized. Notably, (4.17) and (4.18) are also applicable in the case where $\mathbf{\Phi}_{SR} = \sigma_e^2 \mathbf{I}_{N_S}$ and $\mathbf{\Phi}_{RD} = \sigma_e^2 \mathbf{I}_{N_R}$. By applying (4.16), the upper bound of E_r which is exploited is given as

$$E_r = \alpha\eta tr\{\widehat{\mathbf{H}}_{SR}\mathbf{F}_1\widehat{\mathbf{H}}_{SR}^H + tr\{\mathbf{F}_1\}\varphi_{SR}\mathbf{\Sigma}_{SR}\}. \tag{4.19}$$

In general cases where $\mathbf{\Sigma}_{SR} \neq \mathbf{I}_{N_R}$ and $\mathbf{\Sigma}_{RD} \neq \mathbf{I}_{N_D}$, the EVD of $\mathbf{\Sigma}_{SR}$ and $\mathbf{\Sigma}_{RD}$ are introduced as follows to reduce the complexity of the objective function

$$\mathbf{\Sigma}_{SR} = \mathbf{V}_{\Sigma_{SR}}\mathbf{\Lambda}_{\Sigma_{SR}}\mathbf{V}_{\Sigma_{SR}}^H, \quad \mathbf{\Sigma}_{RD} = \mathbf{V}_{\Sigma_{RD}}\mathbf{\Lambda}_{\Sigma_{RD}}\mathbf{V}_{\Sigma_{RD}}^H. \tag{4.20}$$

With the introduction of (4.20), $\mathcal{I}_{SR}$ and $\mathcal{I}_{RD}$ are equivalently rewritten into

$$\mathcal{I}_{SR} = \frac{1-\alpha}{2}\log_2\left|\mathbf{I}_{N_R} + \widetilde{\mathbf{H}}_{SR}[tr\{\mathbf{F}_2\}]\mathbf{F}_2\widetilde{\mathbf{H}}_{SR}[tr\{\mathbf{F}_2\}]^H\right| \tag{4.21}$$

$$\mathcal{I}_{RD} = \frac{1-\alpha}{2}\log_2\left|\mathbf{I}_{N_D} + \widetilde{\mathbf{H}}_{RD}[tr\{\mathbf{G}\}]\mathbf{G}\widetilde{\mathbf{H}}_{RD}[tr\{\mathbf{G}\}]^H\right| \tag{4.22}$$

where

$$\widetilde{\mathbf{H}}_{SR}[tr\{\mathbf{F}_2\}] = \left(\sigma_r^2\mathbf{I}_{N_R} + tr\{\mathbf{F}_2\}\varphi_{SR}\mathbf{\Lambda}_{\Sigma_{SR}}\right)^{-\frac{1}{2}}\mathbf{V}_{\Sigma_{SR}}^H\widehat{\mathbf{H}}_{SR}$$
$$\widetilde{\mathbf{H}}_{RD}[tr\{\mathbf{G}\}] = \left(\sigma_d^2\mathbf{I}_{N_D} + tr\{\mathbf{G}\}\varphi_{RD}\mathbf{\Lambda}_{\Sigma_{RD}}\right)^{-\frac{1}{2}}\mathbf{V}_{\Sigma_{RD}}^H\widehat{\mathbf{H}}_{RD}$$

can be viewed as the source-relay link channel matrix with dependence on $tr\{\mathbf{F}_2\}$ and the relay-destination link channel matrix with dependence on $tr\{\mathbf{G}\}$, respectively, with the corresponding compact SVD given as

$$\widetilde{\mathbf{H}}_{SR}[tr\{\mathbf{F}_2\}] = \widetilde{\mathbf{U}}_{SR}[tr\{\mathbf{F}_2\}]\widetilde{\mathbf{\Lambda}}_{SR}[tr\{\mathbf{F}_2\}]^{\frac{1}{2}}\widetilde{\mathbf{V}}_{SR}[tr\{\mathbf{F}_2\}]^H \tag{4.23}$$
$$\widetilde{\mathbf{H}}_{RD}[tr\{\mathbf{G}\}] = \widetilde{\mathbf{U}}_{RD}[tr\{\mathbf{G}\}]\widetilde{\mathbf{\Lambda}}_{RD}[tr\{\mathbf{G}\}]^{\frac{1}{2}}\widetilde{\mathbf{V}}_{RD}[tr\{\mathbf{G}\}]^H \tag{4.24}$$

where $\widetilde{\mathbf{\Lambda}}_{SR}[tr\{\mathbf{F}_2\}]$ and $\widetilde{\mathbf{\Lambda}}_{RD}[tr\{\mathbf{G}\}]$ are size $K_{SR} = \min(N_S, N_R)$ and $K_{RD} = \min(N_R, N_D)$ diagonal matrices, respectively, with the diagonal elements arranged in descending order. The energy harvested at the relay node E_r is also rewritten as

$$E_r = \alpha\eta\left(tr\{\widehat{\mathbf{H}}_{SR}\mathbf{F}_1\widehat{\mathbf{H}}_{SR}^H\} + tr\{\mathbf{F}_1\}\varphi_{SR}\sum_{i=1}^{N_R}\lambda_{\Sigma_{SR},i}\right) \tag{4.25}$$

where $\lambda_{\Sigma_{SR},i}$ denotes the ith diagonal element of $\mathbf{\Lambda}_{\Sigma_{SR}}$.

4.3 Optimization Problem under Fixed Power Scheme

In this section, the optimization problem which maximizes $\mathcal{I}_{SD}$ is investigated with $\mathcal{I}_{SR}$ and $\mathcal{I}_{RD}$ expressed in (4.21) and (4.22), respectively. Subjecting to the fixed transmission power constraint as given in (4.14), the optimization problem can be written as

$$\max_{\alpha,\mathbf{F}_1,\mathbf{F}_2,\mathbf{G}} \ \mathcal{I}_{SD} \tag{4.26a}$$
$$s.t.\ tr\{\mathbf{F}_1\} \le P_s \quad tr\{\mathbf{F}_2\} \le P_s \tag{4.26b}$$
$$\frac{1-\alpha}{2}tr\{\mathbf{G}\} \le E_r \tag{4.26c}$$
$$0 \le \alpha \le 1, \quad \mathbf{F}_1 \ge 0, \quad \mathbf{F}_2 \ge 0, \quad \mathbf{G} \ge 0. \tag{4.26d}$$

It is noticeable that $\mathbf{F}_1$ is not involved in the objective function, but it affects the transmission energy available at the relay node. Thus, the optimization problem for $\mathbf{F}_1$ can be viewed as

$$\max_{\mathbf{F}_1} \; tr\{\widehat{\mathbf{H}}_{SR}\mathbf{F}_1\widehat{\mathbf{H}}_{SR}^H\} + tr\{\mathbf{F}_1\}\varphi_{SR}\sum_{i=1}^{N_R}\lambda_{\Sigma_{SR},i} \tag{4.27a}$$

$$s.t. \; tr\{\mathbf{F}_1\} \le P_s, \quad \mathbf{F}_1 \ge 0. \tag{4.27b}$$

As the optimal $\mathbf{F}_1$ must achieve the equality of the transmission power constraint (4.27b), the second term of the objective function (4.27a) can equivalently be viewed as a constant, and the optimal structure [1] for $\mathbf{F}_1 = P_s\widehat{\mathbf{v}}_{SR,1}\widehat{\mathbf{v}}_{SR,1}^H$ where $\widehat{\mathbf{v}}_{SR,1}$ is the leftmost column of $\widehat{\mathbf{V}}_{SR}$ which can be obtained from the SVD of $\widehat{\mathbf{H}}_{SR} = \widehat{\mathbf{U}}_{SR}\widehat{\mathbf{\Lambda}}_{SR}^{\frac{1}{2}}\widehat{\mathbf{V}}_{SR}^H$ where the diagonal elements of $\widehat{\mathbf{\Lambda}}_{SR}$ are arranged in a decreasing order. By adopting the optimal structure of $\mathbf{F}_1$, the optimization problem (4.26) can be rewritten as

$$\max_{\alpha,\mathbf{F}_2,\mathbf{G}} \; \mathcal{I}_{SD} \tag{4.28a}$$

$$s.t. \; tr\{\mathbf{F}_2\} \le P_s \tag{4.28b}$$

$$tr\{\mathbf{G}\} \le E_\alpha \tag{4.28c}$$

$$0 \le \alpha \le 1 \quad \mathbf{F}_2 \ge 0, \quad \mathbf{G} \ge 0 \tag{4.28d}$$

where $E_\alpha = 2\alpha\eta\chi P_s/(1-\alpha)$,

$$\chi = \widehat{\lambda}_{SR,1} + \varphi_{SR}\sum_{i=1}^{N_R}\lambda_{\Sigma_{SR},i} \tag{4.29}$$

and $\widehat{\lambda}_{SR,1}$ is the largest diagonal element of $\widehat{\mathbf{\Lambda}}_{SR}$.

The optimization problem (4.28) is solved by an iterative method. $\mathcal{I}_{SD}\{\alpha\}$ is denoted as the optimal $\mathcal{I}_{SD}$ with any given α value. Firstly, the optimization problem is solved with fixed α. It is noted that E_α is a constant with any given α. It can be shown that $\mathcal{I}_{SR}$ in (4.9) is monotonically increasing with respect to $tr\{\mathbf{F}_2\}$ and $\mathcal{I}_{RD}$ in (4.10) increases monotonically with respect to $tr\{\mathbf{G}\}$. Thus, it is obvious that the optimal $\mathbf{F}_2$ and $\mathbf{G}$ must achieve the equality of corresponding power constraints, (4.28b) and (4.28c). Thus, under fixed transmission power constraint, $\widetilde{\mathbf{H}}_{SR}[tr\{\mathbf{F}_2\}] = \widetilde{\mathbf{H}}_{SR}[P_s]$ and $\widetilde{\mathbf{H}}_{RD}[tr\{\mathbf{G}\}] = \widetilde{\mathbf{H}}_{RD}[E_\alpha]$ can be rewritten as

$$\begin{aligned}\widetilde{\mathbf{H}}_{SR}[P_s] &= \left(\sigma_r^2\mathbf{I}_{N_R} + P_s\varphi_{SR}\mathbf{\Lambda}_{\Sigma_{SR}}\right)^{-\frac{1}{2}}\mathbf{V}_{\Sigma_{SR}}^H\widehat{\mathbf{H}}_{SR}\\ \widetilde{\mathbf{H}}_{RD}[E_\alpha] &= \left(\sigma_d^2\mathbf{I}_{N_D} + E_\alpha\varphi_{RD}\mathbf{\Lambda}_{\Sigma_{RD}}\right)^{-\frac{1}{2}}\mathbf{V}_{\Sigma_{RD}}^H\widehat{\mathbf{H}}_{RD}.\end{aligned}$$

with the corresponding compact SVD written as

$$\widetilde{\mathbf{H}}_{SR}[P_s] = \widetilde{\mathbf{U}}_{SR}\widetilde{\mathbf{\Lambda}}_{SR}[P_s]^{\frac{1}{2}}\widetilde{\mathbf{V}}_{SR}^{H} \tag{4.30}$$

$$\widetilde{\mathbf{H}}_{RD}[E_\alpha] = \widetilde{\mathbf{U}}_{RD}\widetilde{\mathbf{\Lambda}}_{RD}[E_\alpha]^{\frac{1}{2}}\widetilde{\mathbf{V}}_{RD}^{H} \tag{4.31}$$

The diagonal elements of $\widetilde{\mathbf{\Lambda}}_{SR}[P_s]$ and $\widetilde{\mathbf{\Lambda}}_{RD}[E_\alpha]$ are arranged in descending order and the ith diagonal element of the corresponding matrices are denoted as $\widetilde{\lambda}_{SR,i}[P_s]$ for $i = 1, \cdots, K_{SR}$ and $\widetilde{\lambda}_{RD,i}[E_\alpha]$ for $i = 1, \cdots, K_{RD}$. As mentioned in [79], when $tr\{\mathbf{F}_2\}$ and $tr\{\mathbf{G}\}$ are constants, $\widetilde{\mathbf{U}}_{SR}, \widetilde{\mathbf{U}}_{RD}, \widetilde{\mathbf{V}}_{SR}$ and $\widetilde{\mathbf{V}}_{RD}$ do not depends on $\mathbf{F}_2$ and $\mathbf{G}$. It can be shown that the optimal structures for $\mathbf{F}_2$ and $\mathbf{G}$ are given by

$$\mathbf{F}_2 = \widetilde{\mathbf{V}}_{SR}\mathbf{\Lambda}_2\widetilde{\mathbf{V}}_{SR}^{H}, \qquad \mathbf{G} = \widetilde{\mathbf{V}}_{RD}\mathbf{\Lambda}_g\widetilde{\mathbf{V}}_{RD}^{H} \tag{4.32}$$

where $\mathbf{\Lambda}_2$ and $\mathbf{\Lambda}_g$ are diagonal matrices of size K_{SR} and K_{RD}, respectively. The ith diagonal elements for $\mathbf{\Lambda}_2$ and $\mathbf{\Lambda}_g$ are correspondingly denoted as $\lambda_{2,i}$ for $i = 1, \cdots, K_{SR}$ and $\lambda_{g,i}$ for $i = 1, \cdots, K_{RD}$. By adopting the optimal structures of $\mathbf{F}_2$ and $\mathbf{G}$, the optimization problem (4.28) is simplified to a power allocation problem with scalar variables which can be further reduced to two sub-problems. In particular, the source-relay link optimization problem is given as

$$\max_{\boldsymbol{\lambda}_2} \frac{1-\alpha}{2} \sum_{i=1}^{K_{SR}} \log_2\left(1 + \widetilde{\lambda}_{SR,i}[P_s]\lambda_{2,i}\right) \tag{4.33a}$$

$$s.t. \sum_{i=1}^{K_{SR}} \lambda_{2,i} \leq P_s, \quad \lambda_{2,i} \geq 0, \quad i = 1, \cdots, K_{SR} \tag{4.33b}$$

where $\boldsymbol{\lambda}_2 = [\lambda_{2,1}, \cdots, \lambda_{2,K_{SR}}]^T$, while the relay-destination link optimization problem is given as

$$\max_{\boldsymbol{\lambda}_g} \frac{1-\alpha}{2} \sum_{i=1}^{K_{RD}} \log_2\left(1 + \widetilde{\lambda}_{RD,i}[E_\alpha]\lambda_{g,i}\right) \tag{4.34a}$$

$$s.t. \sum_{i=1}^{K_{RD}} \lambda_{g,i} \leq E_\alpha, \quad \lambda_{g,i} \geq 0, \quad i = 1, \cdots, K_{RD} \tag{4.34b}$$

where $\boldsymbol{\lambda}_g = [\lambda_{g,1}, \cdots, \lambda_{g,K_{RD}}]^T$. By using the KKT conditions, the optimal $\lambda_{2,i}$ for $i = 1, \cdots, K_{SR}$ is given as

$$\lambda_{2,i}^{*} = \frac{1}{\widetilde{\lambda}_{SR,i}[P_s]}\left[\frac{1-\alpha}{2}\frac{\widetilde{\lambda}_{SR,i}[P_s]}{\mu_1 \ln 2} - 1\right]^{+} \quad i = 1, \cdots, K_{SR} \tag{4.35}$$

and the optimal $\lambda_{g,i}$ for $i = 1, \cdots, K_{RD}$ is written as

$$\lambda_{g,i}^{*} = \frac{1}{\widetilde{\lambda}_{RD,i}[E_\alpha]} \left[\frac{1-\alpha}{2} \frac{\widetilde{\lambda}_{RD,i}[E_\alpha]}{\mu_2 \ln 2} - 1 \right]^{+} \quad i = 1, \cdots, K_{RD} \tag{4.36}$$

where $(\cdot)^*$ represents the optimal value, ln denotes natural logarithm, $[x]^+ = \max(x, 0)$, $\mu_1 > 0$ and $\mu_2 > 0$ are the Lagrange multipliers to (4.33b) and (4.34b) respectively.

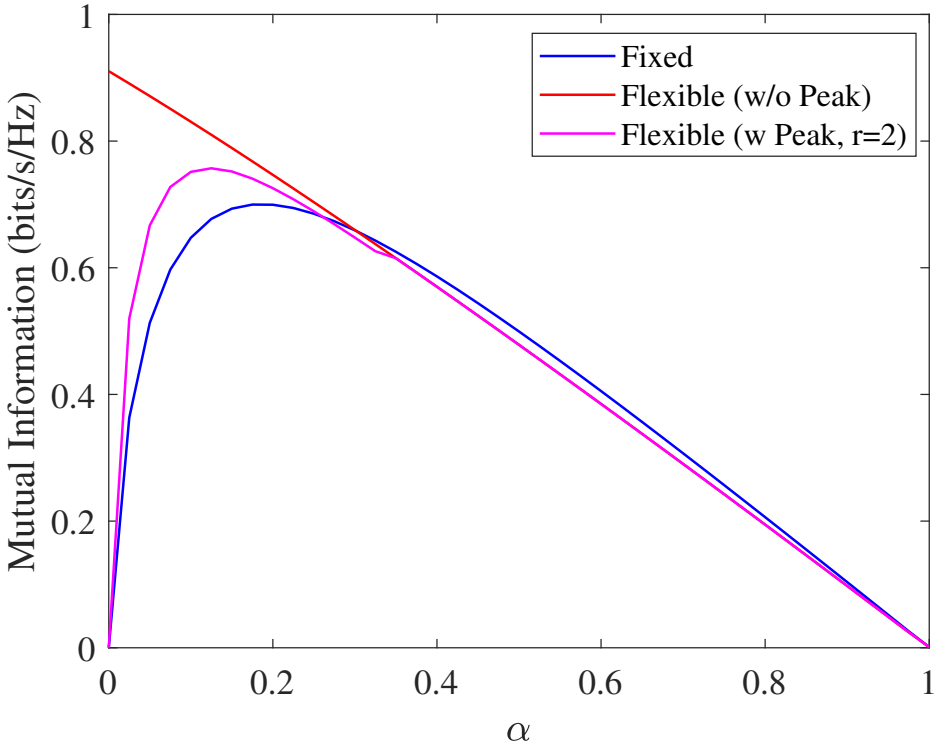

Figure 4.2: Unimodality of $\mathcal{I}_{SD}$ at $P_s = 20$dBm and $N_S = N_R = N_D = 2$.

It can be seen that the objective function, $\mathcal{I}_{SD}$ for fixed transmission power constraint is an unimodal function of α as illustrated in Fig. 4.2 and the feasibility region of (4.28c) is monotonically increasing with α. Thus, the optimal α can be obtained through the golden section search method with the golden number ratio $\delta = 1.618$ [111]. The procedure of the golden section search method is presented in Algorithm 1, where $\varepsilon > 0$ is a small number controlling the convergence of the algorithm.

Algorithm 1 Golden Section Search Method to Find the Optimal α

Initialization: $\alpha_U = 1$ and $\alpha_L = 0$

while $|\alpha_U - \alpha_L| \geq \varepsilon$ **do**
  Set $\rho_1 = (\delta - 1)\alpha_L + (2 - \delta)\alpha_U$.
  Set $\rho_2 = (2 - \delta)\alpha_L + (\delta - 1)\alpha_U$.
  Compute $\mathcal{I}_{SD}\{\rho_1\}$ and $\mathcal{I}_{SD}\{\rho_2\}$.
  if $\mathcal{I}_{SD}\{\rho_1\} - \mathcal{I}_{SD}\{\rho_2\} \geq 0$ **then**
    $\alpha_U = \rho_2$
  else
    $\alpha_L = \rho_1$
  end if
end while
$\alpha^* = (\alpha_L + \alpha_U)/2$

4.4 Optimization Problem under Flexible Power Scheme

In this section, the optimization problem which maximizes $\mathcal{I}_{SD}$ is investigated with $\mathcal{I}_{SR}$ and $\mathcal{I}_{RD}$ expressed in (4.21) and (4.22) respectively. With the assumption of the ideal scenario, i.e. the source node is equipped with infinite transmission energy, it is noted that subjecting to the flexible power constraint as given in (4.15), the optimization problem can be expressed as

$$\max_{\alpha, \mathbf{F}_1, \mathbf{F}_2, \mathbf{G}} \ \mathcal{I}_{SD} \tag{4.37a}$$

$$s.t.\ \alpha tr\{\mathbf{F}_1\} + \frac{1-\alpha}{2} tr\{\mathbf{F}_2\} \leq \frac{1+\alpha}{2} P_s \tag{4.37b}$$

$$\frac{1-\alpha}{2} tr\{\mathbf{G}\} \leq E_r \tag{4.37c}$$

$$0 \leq \alpha \leq 1, \quad \mathbf{F}_1 \geq 0, \quad \mathbf{F}_2 \geq 0, \quad \mathbf{G} \geq 0. \tag{4.37d}$$

It is noticeable that the optimal $\mathbf{F}_1$ is not involved in the objective function (4.37a), but it will affect the objective function by varying the feasible region of the problem. To maximize the energy harvested at the relay node, the source node transmission power for energy-carrying signal should be located to the strongest sub-channel of $\mathbf{H}_{SR}$. By assuming that $tr\{\mathbf{F}_1\} = \lambda_1$, the optimization of $\mathbf{F}_1$ can be reduced to λ_1 with the

optimal structure for $\mathbf{F}_1 = \lambda_1 \widehat{\mathbf{v}}_{SR,1} \widehat{\mathbf{v}}_{SR,1}^H$. By adopting the optimal structure of $\mathbf{F}_1$, the optimization problem is rewritten as

$$\max_{\alpha,\lambda_1,\mathbf{F}_2,\mathbf{G}} \ \mathcal{I}_{SD} \tag{4.38a}$$

$$s.t.\ \alpha\lambda_1 + \frac{1-\alpha}{2} tr\{\mathbf{F}_2\} \leq \frac{1+\alpha}{2} P_s \tag{4.38b}$$

$$\frac{1-\alpha}{2} tr\{\mathbf{G}\} \leq \alpha\eta\lambda_1\chi \tag{4.38c}$$

$$0 \leq \alpha \leq 1 \quad \lambda_1 \geq 0, \quad \mathbf{F}_2 \geq 0, \quad \mathbf{G} \geq 0. \tag{4.38d}$$

With any given α and λ_1, the transmission power constraint (4.38c) must satisfy the equality with the optimal $\mathbf{G}$, i.e.

$$tr\{\mathbf{G}\} = \frac{2\eta\chi}{1-\alpha}\alpha\lambda_1. \tag{4.39}$$

By applying (4.39), the optimization problem (4.38) is rewritten as

$$\max_{\alpha,\mathbf{F}_2,\mathbf{G}} \ \mathcal{I}_{SD} \tag{4.40a}$$

$$s.t.\ tr\{\mathbf{F}_2\} + \frac{1}{\eta\chi} tr\{\mathbf{G}\} \leq P_\alpha \tag{4.40b}$$

$$0 \leq \alpha \leq 1 \quad \mathbf{F}_2 \geq 0, \quad \mathbf{G} \geq 0 \tag{4.40c}$$

where $P_\alpha = \frac{1+\alpha}{1-\alpha} P_s$.

Similar to Section 4.3, an iterative method is developed to solve the problem (4.40). It is noticed that the optimal $\mathbf{F}_2$ and $\mathbf{G}$ are coupled in the transmission power constraint (4.40b) with any given α. By applying the primal decomposition method [112] with introduction of $k \geq tr\{\mathbf{F}_2\}$ where $k \in [0, P_\alpha]$, the optimization problem (4.40) is equivalently decomposed into

$$\max_{\mathbf{F}_2} \ \mathcal{I}_{SR}(k) = \frac{1-\alpha}{2} \log_2 \left| \mathbf{I}_{N_R} + \widetilde{\mathbf{H}}_{SR}[tr\{\mathbf{F}_2\}] \mathbf{F}_2 \widetilde{\mathbf{H}}_{SR}[tr\{\mathbf{F}_2\}]^H \right| \tag{4.41a}$$

$$s.t. \ \ tr\{\mathbf{F}_2\} \leq k, \quad \mathbf{F}_2 \geq 0 \tag{4.41b}$$

and

$$\max_{\mathbf{G}} \ \mathcal{I}_{RD}(k) = \frac{1-\alpha}{2} \log_2 \left| \mathbf{I}_{N_D} + \widetilde{\mathbf{H}}_{RD}[tr\{\mathbf{G}\}] \mathbf{G} \widetilde{\mathbf{H}}_{RD}[tr\{\mathbf{G}\}]^H \right| \tag{4.42a}$$

$$s.t. \ \ tr\{\mathbf{G}\} \leq (P_\alpha - k)\eta\chi, \quad \mathbf{G} \geq 0 \tag{4.42b}$$

where $\mathcal{I}_{SR}(k)$ and $\mathcal{I}_{RD}(k)$ are the optimal $\mathcal{I}_{SR}$ and $\mathcal{I}_{RD}$ with a given k. Moreover, the master problem of optimizing $\mathbf{F}_2$ and $\mathbf{G}$ is given as

$$\max_{k} \min(\mathcal{I}_{SR}(k), \mathcal{I}_{RD}(k)) \tag{4.43a}$$

$$s.t.\ 0 \leq k \leq P_\alpha. \tag{4.43b}$$

It can be easily seen that the equality of (4.41b) and (4.42b) must be achieved with the optimal $\mathbf{F}_2$ for the problem (4.41) and $\mathbf{G}$ for the problem (4.42). Thus, $\widetilde{\mathbf{H}}_{SR}[tr\{\mathbf{F}_2\}] = \widetilde{\mathbf{H}}_{SR}[k]$ and $\widetilde{\mathbf{H}}_{RD}[tr\{\mathbf{G}\}] = \widetilde{\mathbf{H}}_{RD}[(P_\alpha - k)\eta\chi]$ can be rewritten as

$$\widetilde{\mathbf{H}}_{SR}[k] = \left(\sigma_r^2 \mathbf{I}_{N_R} + k\varphi_{SR}\mathbf{\Lambda}_{\Sigma_{SR}}\right)^{-\frac{1}{2}} \mathbf{V}_{\Sigma_{SR}}^H \widehat{\mathbf{H}}_{SR}$$
$$\widetilde{\mathbf{H}}_{RD}[(P_\alpha - k)\eta\chi] = \left(\sigma_d^2 \mathbf{I}_{N_D} + (P_\alpha - k)\eta\chi\varphi_{RD}\mathbf{\Lambda}_{\Sigma_{RD}}\right)^{-\frac{1}{2}} \mathbf{V}_{\Sigma_{RD}}^H \widehat{\mathbf{H}}_{RD}$$

where the corresponding singular value matrices 4.23 and 4.24 are given as $\widetilde{\mathbf{\Lambda}}_{SR}[k]$ and $\widetilde{\mathbf{\Lambda}}_{RD}[(P_\alpha - k)\eta\chi]$ with its diagonal elements arranged in descending order. The ith diagonal element of $\widetilde{\mathbf{\Lambda}}_{SR}[k]$ and $\widetilde{\mathbf{\Lambda}}_{RD}[(P_\alpha - k)\eta\chi]$ are correspondingly denoted as $\widetilde{\lambda}_{SR,i}[k]$ for $i = 1, \cdots, K_{SR}$ and $\widetilde{\lambda}_{RD,i}[(P_\alpha - k)\eta\chi]$ for $i = 1, \cdots, K_{RD}$. Using the optimal structure of $\mathbf{F}_2$ and $\mathbf{G}$ given in (4.32) and the corresponding SVDs of $\widetilde{\mathbf{H}}_{SR}[k]$ and $\widetilde{\mathbf{H}}_{RD}[(P_\alpha - k)\eta\chi]$ for the flexible power scheme, the optimization sub-problem (4.41) can be equivalently expressed as

$$\max_{\mathbf{x}} \ \frac{1-\alpha}{2} \sum_{i=1}^{K_{SR}} \log_2(1 + a_i x_i) \tag{4.44a}$$

$$s.t. \ \sum_{i=1}^{K_{SR}} x_i \leq k, \quad x_i \geq 0, \quad i = 1, \cdots, K_{SR} \tag{4.44b}$$

where $\mathbf{x} = [x_1, \cdots, x_{K_{SR}}]^T$, and for $i = 1, \cdots, K_{SR}$, $a_i = \widetilde{\lambda}_{SR,i}[k]$ and $x_i = \lambda_{2,i}$, while the optimization sub-problem (4.42) is rewritten as

$$\max_{\mathbf{y}} \ \frac{1-\alpha}{2} \sum_{i=1}^{K_{RD}} \log_2(1 + b_i y_i) \tag{4.45a}$$

$$s.t. \ \sum_{i=1}^{K_{RD}} y_i \leq P_\alpha - k, \quad y_i \geq 0, \quad i = 1, \cdots, K_{RD} \tag{4.45b}$$

where $\mathbf{y} = [y_1, \cdots, y_{K_{RD}}]^T$, and for $i = 1, \cdots, K_{RD}$, $b_i = \widetilde{\lambda}_{RD,i}[(P_\alpha - k)\eta\chi]\eta\chi$ and $y_i = \lambda_{g,i}/\eta\chi$. It is obvious to note that the problem (4.44) and (4.45) are convex and can be easily solved by the water-filling algorithm.

To obtain the optimal k, the bisection method is used to solve the master problem (4.43). For $i = 1, \cdots, n$, where n is the number of iterations needed to obtain the

optimal k, the search region in the ith iteration is denoted as $[L_i, R_i]$ with $L_1 = 0$ and $R_1 = P_\alpha$, while the k for the ith iteration is $k_i = (L_i + R_i)/2$. For each iteration, the value of $\mathcal{I}_{SR}(k_i)$ and $\mathcal{I}_{RD}(k_i)$ is obtained by solving the problem (4.44) and (4.45), respectively. In the case of $\mathcal{I}_{SR}(k_i) < \mathcal{I}_{RD}(k_i)$, $L_{i+1} = k_i$, and if $\mathcal{I}_{SR}(k_i) > \mathcal{I}_{RD}(k_i)$, then $R_{i+1} = k_i$. The steps of bisection are repeated until the difference between the value of $\mathcal{I}_{SR}(k_n)$ and $\mathcal{I}_{RD}(k_n)$ is less than ϑ where ϑ is a positive constant close to 0. The process of solving the primal decomposition optimization problem by using the bisection method is summarized in Algorithm 2.

Algorithm 2 Solving the Problem (4.40) by the Primal Decomposition Method

Initialization: $n = 1$, $L_1 = 0$, and $R_1 = P_\alpha$.

1: **do**
2: Obtain $k_n = (L_n + R_n)/2$.
3: Obtain SVD of $\widetilde{\mathbf{H}}_{SR}$ and $\widetilde{\mathbf{H}}_{RD}$ with k_n.
4: Compute a_i, $i = 1, \cdots, K_{SR}$ and b_j, $j = 1, \cdots, K_{RD}$ and solve (4.44) and (4.45).
5: Compute $\mathcal{I}_{SR}(k_n)$ as (4.44a) and $\mathcal{I}_{RD}(k_n)$ as (4.45a).
6: **if** $\mathcal{I}_{SR}(k_n) - \mathcal{I}_{RD}(k_n) < 0$ **then**
7: $L_{n+1} = k_n$.
8: **else if** $\mathcal{I}_{SR}(k_n) - \mathcal{I}_{RD}(k_n) > 0$ **then**
9: $R_{n+1} = k_n$.
10: **end if**
11: $n \leftarrow n + 1$
12: **while** $|\mathcal{I}_{SR}(k_{n-1}) - \mathcal{I}_{RD}(k_{n-1})| \geq \vartheta$
13: Find $\mathbf{x}^*$ and $\mathbf{y}^*$ with $k^* = k_{n-1}$ by solving (4.44) and (4.45)

Next, as illustrated in Fig. 4.2, the objective function, $\mathcal{I}_{SD}$ with flexible power constraint is monotically decreasing with regards to α while the feasible region of (4.38c) is monotonically increasing with α. Hence, the optimal α can be obtained by using the golden section search method as presented in Algorithm 1.

4.5 Optimization Problem with Peak Power Constraints

In Section 4.4, it is worth mentioning that in the problem (4.37), the transmission power $tr\{\mathbf{F}_1\}$ may approach infinity when α approaches 0, and the $tr\{\mathbf{F}_2\}$ and $tr\{\mathbf{G}\}$

may become infinite when α is close to 1. However, infinite transmission power is not achievable in practice. Thus, $\widehat{P}_s$ and $\widehat{P}_r$ are introduced to represent the peak power limits at the source and relay nodes, respectively, to impose practical peak transmission power constraints which are given as $tr\{\mathbf{F}_1\} \leq \widehat{P}_s$, $tr\{\mathbf{F}_2\} \leq \widehat{P}_s$ and $tr\{\mathbf{G}\} \leq \widehat{P}_r$ to the optimization problem (4.38) with the optimal structure of $\mathbf{F}_1 = \lambda_1 \widehat{\mathbf{v}}_{SR,1} \widehat{\mathbf{v}}_{SR,1}^H$ and $0 \leq \lambda_1 \leq \widehat{P}_s$. Hence, the optimization problem with the consideration of peak power limits at the source and relay nodes is written as

$$\max_{\alpha, \mathbf{F}_2, \mathbf{G}} \ \mathcal{I}_{SD} \tag{4.46a}$$

$$s.t. \ tr\{\mathbf{F}_2\} + \frac{1}{\eta\chi} tr\{\mathbf{G}\} \leq P_\alpha \tag{4.46b}$$

$$tr\{\mathbf{F}_2\} \leq \widehat{P}_s \tag{4.46c}$$

$$tr\{\mathbf{G}\} \leq \min\left(\widehat{E}_\alpha, \widehat{P}_r\right) \tag{4.46d}$$

$$0 \leq \alpha \leq 1, \quad \mathbf{F}_2 \geq 0, \quad \mathbf{G} \geq 0 \tag{4.46e}$$

where $\widehat{E}_\alpha = 2\eta\chi\alpha\widehat{P}_s/(1-\alpha)$.

It is noticed that the optimization problem (4.46) can be viewed as a problem extended from the problem (4.40) with the introduction of peak power constraints given as (4.46c) and (4.46d). Hence, the solution of (4.40) with fixed α can be exploited and denote it as $\mathbf{F}_2'$ and $\mathbf{G}'$ when solving the optimization problem (4.46) with fixed α. In the case where the peak power constraint (4.46c) and (4.46d) are satisfied with $\mathbf{F}_2'$ and $\mathbf{G}'$, then the optimal $\mathbf{F}_2$ and $\mathbf{G}$ for the optimization problem (4.46) are $\mathbf{F}_2'$ and $\mathbf{G}'$. In the case where the peak power constraint (4.46c) is violated with $\mathbf{F}_2'$, but $\mathbf{G}'$ satisfies (4.46d), the optimal $\mathbf{F}_2$ is obtained by solving the following optimization problem

$$\max_{\mathbf{F}_2} \ \mathcal{I}_{SR} \tag{4.47a}$$

$$s.t. \ tr\{\mathbf{F}_2\} \leq \widehat{P}_s, \mathbf{F} \geq 0. \tag{4.47b}$$

As the equality of (4.47b) holds with the optimal $\mathbf{F}_2$, $\widetilde{\mathbf{H}}_{SR}[tr\{\mathbf{F}_2\}] = \widetilde{\mathbf{H}}_{SR}[\widehat{P}_s]$ which can be rewritten as

$$\widetilde{\mathbf{H}}_{SR}[\widehat{P}_s] = \left(\sigma_r^2 \mathbf{I}_{N_R} + \widehat{P}_s \varphi_{SR} \mathbf{\Lambda}_{\Sigma_{SR}}\right)^{-\frac{1}{2}} \mathbf{V}_{\Sigma_{SR}}^H \widehat{\mathbf{H}}_{SR} \tag{4.48}$$

and its singular value matrix (4.23) is given by $\widetilde{\mathbf{\Lambda}}_{SR}[\widehat{P}_s]$ with the diagonal elements arranged in descending order. The ith diagonal element of $\widetilde{\mathbf{\Lambda}}_{SR}[\widehat{P}_s]$ is denoted as $\widetilde{\lambda}_{SR,i}[\widehat{P}_s]$

for $i = 1, \cdots, K_{SR}$. By using the optimal structure of $\mathbf{F}_2$ proposed in (4.32) with the corresponding SVD of $\widetilde{\mathbf{\Lambda}}_{SR}[\widehat{P}_s]$, the problem (4.47) can be rewritten as

$$\max_{\widehat{\mathbf{x}}} \ \frac{1-\alpha}{2} \sum_{i=1}^{K_{SR}} \log_2(1 + \widehat{a}_i \widehat{x}_i) \tag{4.49a}$$

$$s.t. \ \sum_{i=1}^{K_{SR}} \widehat{x}_i \leq \widehat{P}_s, \quad \widehat{x}_i \geq 0, \quad i = 1, \cdots, K_{SR} \tag{4.49b}$$

where $\widehat{\mathbf{x}} = [\widehat{x}_1, \cdots, \widehat{x}_{K_{SR}}]^T$ and for $i = 1, \cdots, K_{SR}$, $\widehat{a}_i = \widetilde{\lambda}_{SR,i}[\widehat{P}_s]$ and $\widehat{x}_i = \lambda_{2,i}$. The problem (4.49) can be easily solved by the water-filling algorithm.

In the case where the peak power constraint (4.46d) is violated with $\mathbf{G}'$, but $\mathbf{F}_2'$ satisfies (4.46c), the optimal $\mathbb{G}$ is obtained by solving the following optimization problem

$$\max_{\mathbf{G}} \ \mathcal{I}_{RD} \tag{4.50a}$$

$$s.t. \ tr\{\mathbf{G}\} \leq \tau, \quad \mathbf{G} \geq 0 \tag{4.50b}$$

where $\tau = \min(\widehat{E}_\alpha, \widehat{P}_r)$. As the equality (4.50b) holds with the optimal $\mathbf{G}$ for the problem (4.50), there is $\widetilde{\mathbf{H}}_{RD}[tr\{\mathbf{G}\}] = \widetilde{\mathbf{H}}_{RD}[\tau]$, which can be rewritten as

$$\widetilde{\mathbf{H}}_{RD}[\tau] = \left(\sigma_d^2 \mathbf{I}_{N_D} + \tau \varphi_{RD} \mathbf{\Lambda}_{\Sigma_{RD}}\right)^{-\frac{1}{2}} \mathbf{V}_{\Sigma_{RD}}^H \widehat{\mathbf{H}}_{RD}$$

and its singular value matrix (4.24) is given by $\widetilde{\mathbf{\Lambda}}_{RD}[\tau]$ with its diagonal elements arranged in descending order. The ith diagonal element of $\widetilde{\mathbf{\Lambda}}_{RD}[\tau]$ is denoted as $\widetilde{\lambda}_{RD,i}[\tau]$ for $i = 1, \cdots, K_{RD}$. By using the optimal structure of $\mathbf{G}$ in (4.32) with the corresponding SVD of $\widetilde{\mathbf{\Lambda}}_{RD}[\tau]$, the problem (4.50) can be rewritten as

$$\max_{\widehat{\mathbf{y}}} \ \frac{1-\alpha}{2} \sum_{i=1}^{K_{RD}} \log_2(1 + \widehat{b}_i \widehat{y}_i) \tag{4.51a}$$

$$s.t. \ \sum_{i=1}^{K_{RD}} \widehat{y}_i \leq \tau, \quad \widehat{y}_i \geq 0, \quad i = 1, \cdots, K_{RD} \tag{4.51b}$$

where $\widehat{\mathbf{y}} = [\widehat{y}_1, \cdots, \widehat{y}_{K_{RD}}]^T$ and for $i = 1, \cdots, K_{RD}$, $\widehat{b}_i = \widetilde{\lambda}_{RD,i}[\tau]$ and $\widehat{y}_i = \lambda_{g,i}$. The problem (4.51) is convex which can be easily solved by the water-filling algorithm.

Finally, if both (4.46c) and (4.46d) are violated, the problem (4.49) and (4.51) are solved for the optimal $\mathbf{F}_2$ and $\mathbf{G}$, respectively. The process of solving the problem (4.46) is summarized in Algorithm 3. It is important to mention that the optimal $\mathcal{I}_{SD}\{\alpha\} = \min(\mathcal{I}_{SR}, \mathcal{I}_{RD})$ with the optimal $\mathbf{F}_2$ and $\mathbf{G}$ obtained. The optimal α is obtained through golden section search method which follows the Algorithm 1.

Algorithm 3 Solving (4.46) with given α

1: Solve (4.40) with Algorithm 2 to obtain $\mathbf{F}_2'$ and $\mathbf{G}'$.
2: **if** $tr\{\mathbf{F}_2'\} \leq \widehat{P}_s$ **then**
3: $\quad \mathbf{F}_2^* = \mathbf{F}_2'$.
4: **else**
5: $\quad$ Find $\widehat{\mathbf{x}}^*$ by solving (4.49).
6: $\quad$ Compute $\boldsymbol{\lambda}_2^*$ with $\widehat{\mathbf{x}}^*$ then find $\mathbf{F}_2^*$ with (4.32).
7: **end if**
8: **if** $tr\{\mathbf{G}'\} \leq \tau$ **then**
9: $\quad \mathbf{G}^* = \mathbf{G}'$.
10: **else**
11: $\quad$ Find $\widehat{\mathbf{y}}^*$ by solving (4.51).
12: $\quad$ Compute $\boldsymbol{\lambda}_g^*$ with $\widehat{\mathbf{y}}^*$ then find $\mathbf{G}^*$ with (4.32).
13: **end if**

4.6 Numerical Example

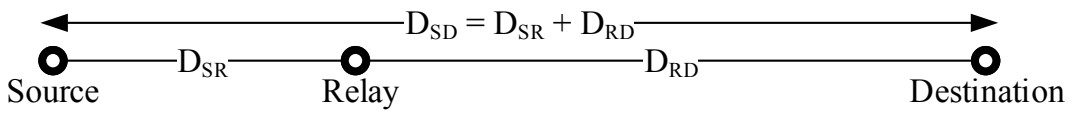

Figure 4.3: Placement of the source, relay and destination nodes in relay communication system.

In this section, the performance of the proposed robust transceiver designs under fixed power scheme (Fixed), flexible power scheme without peak power limit (Flexible (w/o Peak)) and flexible power scheme with peak power limit (Flexible (w Peak)) are investigated. In the numerical examples, $\eta = 0.8$. The peak power limits are assumed as $\widehat{P}_s = \widehat{P}_r = rP_s$, $(r \geq 1)$ in the numerical examples. The nodes in the relay communication system are considered to be placed as illustrated in Fig. 4.3. The source-relay distance and the relay-destination distance are set as $D_{SR} = 10\nu$ meters and $D_{RD} = 10(2-\nu)$ meters respectively with the total distance between the source and destination nodes given as $D_{SD} = 20$ meters. To determine the relay position with ease, the value of ν $(0 < \nu < 2)$ is normalized over a distance of 10 meters. When $0 < \nu < 1$,

the relay is located closer to the source node as indicated by $D_{SR} < D_{RD}$, whereas $D_{SR} > D_{RD}$ when $1 < \nu < 2$ indicating the relay is located closer to the destination node. $D_{SR} \geq 2$m and $D_{RD} \geq 2$m is set with $0.2 \leq \nu \leq 1.8$.

With the consideration of channel pathloss, the channel matrices $\mathbf{H}_{SR}$ and $\mathbf{H}_{RD}$ are constructed as $\mathbf{H}_{SR} = D_{SR}^{-\xi/2}\left(\widehat{\mathbf{H}}_{SR} + \mathbf{\Delta}_{SR}\right)$ and $\mathbf{H}_{RD} = D_{RD}^{-\xi/2}\left(\widehat{\mathbf{H}}_{RD} + \mathbf{\Delta}_{RD}\right)$ where $D_{SR}^{-\xi}$ and $D_{RD}^{-\xi}$ denote the largescale pathloss between the source-relay link and the relay-destination link, respectively, with ξ being the pathloss exponent. $\xi = 3$ for suburban communication scenario [104]. The estimated channel matrices, $\widehat{\mathbf{H}}_{SR}$ and $\widehat{\mathbf{H}}_{RD}$ are modelled as [110]

$$\widehat{\mathbf{H}}_{SR} \sim \mathcal{CN}\left(\mathbf{0}, \frac{1-\sigma_e^2}{\sigma_e^2}\mathbf{\Sigma}_{SR} \otimes \mathbf{\Psi}_{SR}^T\right)$$
$$\widehat{\mathbf{H}}_{RD} \sim \mathcal{CN}\left(\mathbf{0}, \frac{1-\sigma_e^2}{\sigma_e^2}\mathbf{\Sigma}_{RD} \otimes \mathbf{\Psi}_{RD}^T\right)$$

where σ_e^2 represents the variance of estimation error. Note that $\widehat{\mathbf{H}}_{SR}$, $\mathbf{\Delta}_{SR}$, $\widehat{\mathbf{H}}_{RD}$ and $\mathbf{\Delta}_{RD}$ can be equivalently expressed as

$$\widehat{\mathbf{H}}_{SR} = \sqrt{\frac{1-\sigma_e^2}{\sigma_e^2}}\mathbf{\Sigma}_{SR}^{\frac{1}{2}}\widehat{\mathbf{H}}_{\omega_{SR}}\mathbf{\Psi}_{SR}^{\frac{1}{2}}, \qquad \mathbf{\Delta}_{SR} = \mathbf{\Sigma}_{SR}^{\frac{1}{2}}\mathbf{\Delta}_{\omega_{SR}}\mathbf{\Psi}_{SR}^{\frac{1}{2}},$$
$$\widehat{\mathbf{H}}_{RD} = \sqrt{\frac{1-\sigma_e^2}{\sigma_e^2}}\mathbf{\Sigma}_{RD}^{\frac{1}{2}}\widehat{\mathbf{H}}_{\omega_{RD}}\mathbf{\Psi}_{RD}^{\frac{1}{2}}, \qquad \mathbf{\Delta}_{RD} = \mathbf{\Sigma}_{RD}^{\frac{1}{2}}\mathbf{\Delta}_{\omega_{RD}}\mathbf{\Psi}_{RD}^{\frac{1}{2}}$$

where $\widehat{\mathbf{H}}_{\omega_{SR}}$, $\widehat{\mathbf{H}}_{\omega_{RD}}$, $\mathbf{\Delta}_{\omega_{SR}}$ and $\mathbf{\Delta}_{\omega_{RD}}$ are complex Gaussian matrices whose entries are i.i.d. with zero mean and variance of $1/N_S$ (for $\widehat{\mathbf{H}}_{\omega_{SR}}$ and $\mathbf{\Delta}_{\omega_{SR}}$) and $1/N_R$ (for $\widehat{\mathbf{H}}_{\omega_{RD}}$ and $\mathbf{\Delta}_{\omega_{RD}}$). In the simulations, $\mathbf{\Phi}_{SR}$, $\mathbf{\Phi}_{RD}$, $\mathbf{\Sigma}_{SR}$ and $\mathbf{\Sigma}_{RD}$ are simulated as

$$[\mathbf{\Phi}_{SR}]_{ij} = \sigma_e^2\rho_t^{|i-j|} \quad i,j = 1,\cdots,N_S$$
$$[\mathbf{\Phi}_{RD}]_{ij} = \sigma_e^2\rho_t^{|i-j|} \quad i,j = 1,\cdots,N_R$$
$$[\mathbf{\Sigma}_{SR}]_{ij} = \rho_r^{|i-j|} \quad i,j = 1,\cdots,N_R$$
$$[\mathbf{\Sigma}_{RD}]_{ij} = \rho_r^{|i-j|} \quad i,j = 1,\cdots,N_D$$

where $[\cdot]_{ij}$ stand for the ith row and the jth column matrix entry, $\rho_t \in [0,1]$ and $\rho_r \in [0,1]$ represent the correlation coefficients of the channel correlation matrices. In the numerical examples, $\rho_t = 0.1$ and $\rho_r = 0.01$ are set. The noise variance at the relay and destination nodes are set as $\sigma_r^2 = \sigma_d^2 = -50$dBm. The number of antennas at the source, relay and destination nodes are considered as $N_S = N_R = N_D = 2$. These predefined

values remain the same for all numerical examples unless specifically mentioned. The results, which are averaged through 1000 independent channel realizations, are obtained from the numerical simulation. The proposed transceiver design with robustness is compared with the transceiver design in [56] using the estimated CSI which is denoted as (Non-Rob Flexible) and the transceiver design with the full CSI which is denoted as (FCSI) in the numerical examples.

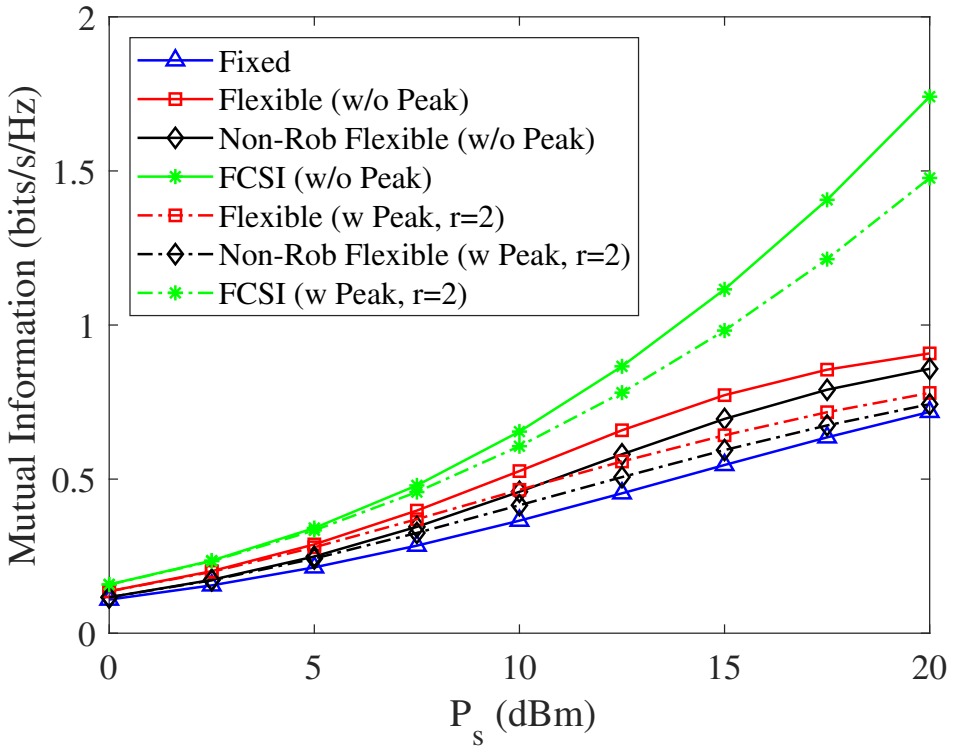

Figure 4.4: Example 1: MI versus P_s with $\nu = 1$, $\sigma_e^2 = 0.15$.

For numerical example 1, the MI performance versus P_s is investigated for the proposed transceiver designs with robustness and non-robust transceiver design given in [56] using only the estimated CSI. The transceiver design in [56] using the full CSI is set as the benchmark in the simulation. It is important to note that the transceiver design with full CSI is unavailable in practice due to the inevitable CSI mismatch. In this numerical simulation, $\nu = 1$ and $\sigma_e^2 = 0.15$. Fig. 4.4 and 4.5 display the system MI and the amount of harvested energy at the relay node versus P_s for the tested systems respectively. For the systems with and without peak power limits ($r = 2$), it is noticed that the FCSI transceiver design provides an upper bound of the system

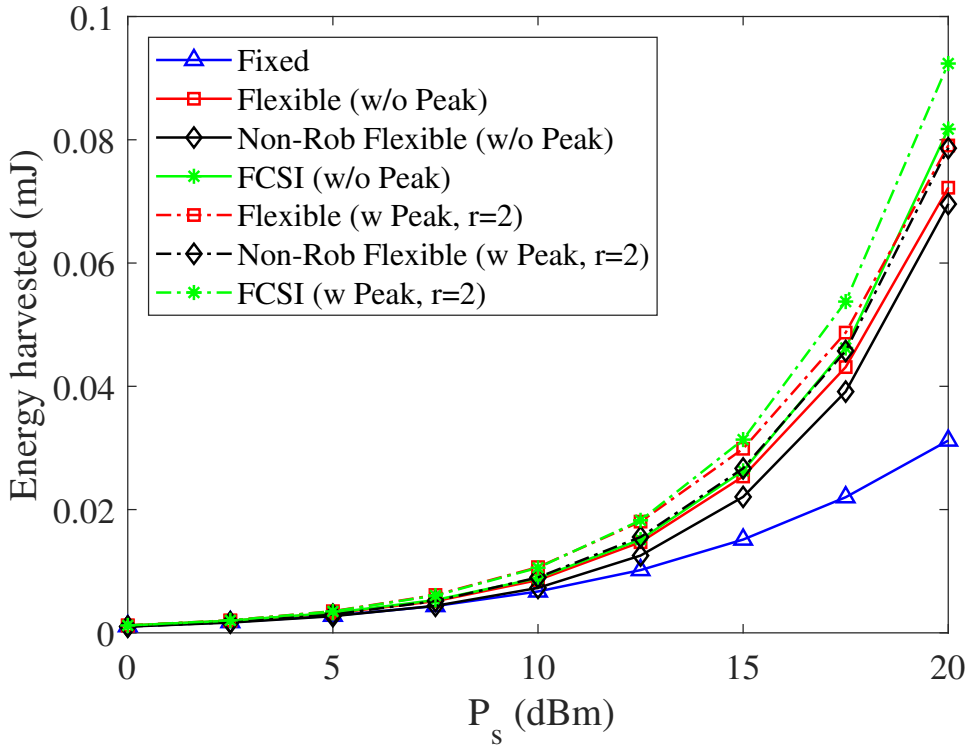

Figure 4.5: Example 1: Harvested energy at the relay node versus P_s with $\nu = 1$ and $\sigma_e^2 = 0.15$.

MI, and the CSI mismatch heavily degrades the MI performance of the system when P_s is high. It is noticeable that the MI performance of the system with the robust transceiver design is higher than the system using the non-robust transceiver design. In other words, the robust transceiver design has a better performance compared with the non-robust transceiver design. Besides, the energy harvested at the relay node is also influence by the CSI mismatch. The proposed transceiver design with robustness harvest more energy at the relay node as compared with the existing transceiver design without robustness. Moreover, the system with fixed power scheme has the lowest MI performance. This is because the feasible region of the system with fixed power constraint is smaller than the system with flexible power constraint as illustrated in Fig. 4.5. It is observed that the energy harvested with fixed power constraint is smaller than the system with flexible power constraint. In the following numerical examples, the non-robust transceiver design and FCSI transceiver design will be carried out without the consideration of the peak power limits. For a fair comparison, the proposed robust

transceiver design under the flexible power scheme will be used.

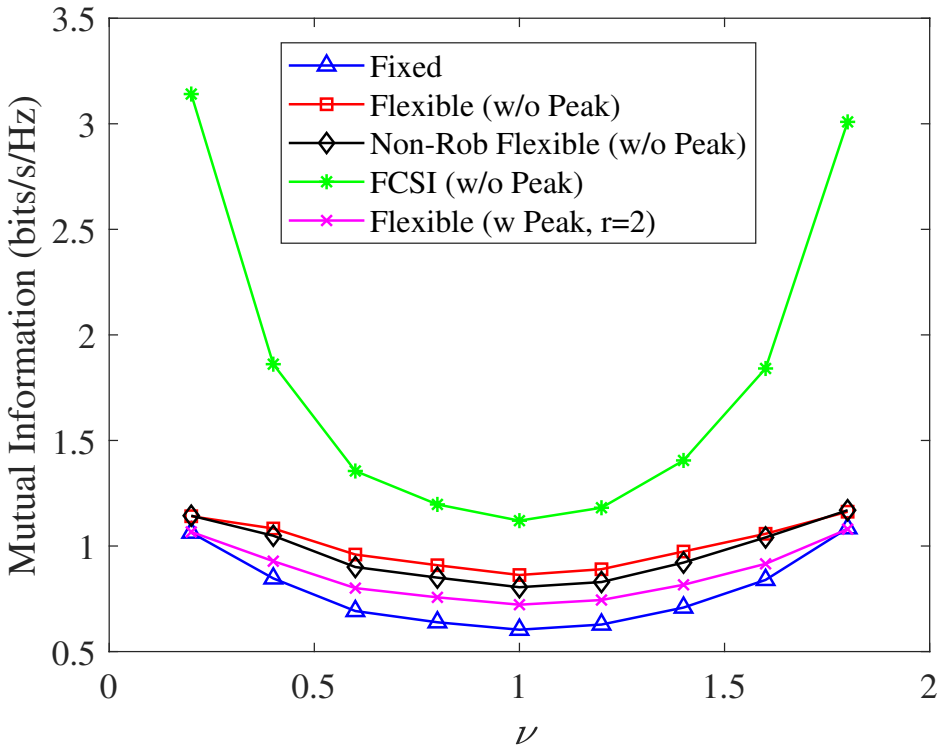

Figure 4.6: Example 2: MI versus ν at $P_s = 10$dBm and $\sigma_e^2 = 0.1$.

For numerical example 2, the MI performance of the transceiver designs is investigated at various relay positions. Fig. 4.6 displays the MI performance of the simulated transceiver designs and Fig. 4.7 displays the harvested energy at the relay node for the tested system across various ν with $P_s = 10$dBm and $\sigma_e^2 = 0.1$. It is observed that the MI performance is higher when the relay node is located closer to the source node or the destination node. This can be explained as below, when the relay node is located closer to the source node ($0 < \nu < 1$), more RF energy can be harvested at the relay node, which can be observed in Fig. 4.7, as the RF energy transmission loss at the source-relay link is reduced. This enhances the MI performance of the system. Even though the RF energy harvested at the relay node is smaller when the relay node is located closer to the destination node ($1 < \nu < 2$), however, the relay-destination distance is shorter, which helps in improving the MI performance of the system. Even though it is observed that the energy harvested at the relay node by the proposed transceiver design and the existing non-robust transceiver design across various ν are approximately similar,

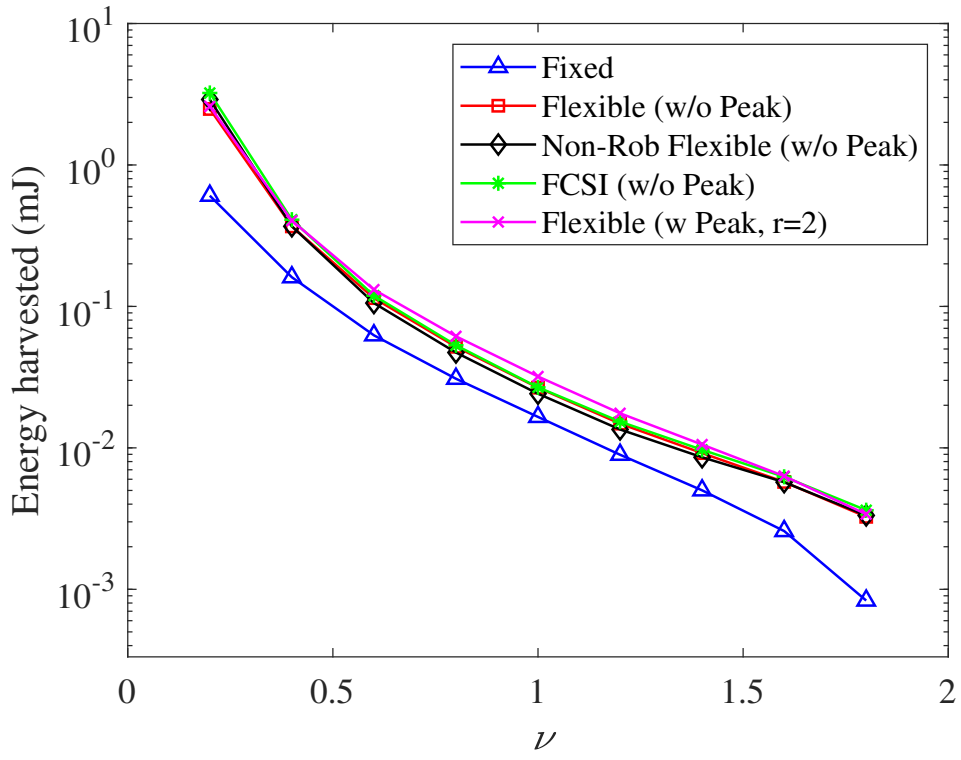

Figure 4.7: Example 2: Harvested energy at the relay node versus ν at $P_s = 10$ dBm and $\sigma_e^2 = 0.1$.

the proposed transceiver design with robustness performs better than the non-robust transceiver design at any relay node position. This indicated that the CSI mismatch cause greater degradation to the system MI compare to the harvested energy at the relay node.

For numerical example 3, the impact of σ_e^2 on the MI performance is investigated for the tested systems. The MI performance versus P_s for the tested systems are displayed in Fig. 4.8 with $\nu = 1$ and $r = 2$ at $\sigma_e^2 = 0.01$ and $\sigma_e^2 = 0.3$. It is observed that when σ_e^2 is smaller, the MI performance for the tested systems are approaching the system MI with FCSI. This observation indicates that the CSI mismatch with greater channel estimation error will cause a significant loss in the system MI. Moreover, the gap between the MI performance of the robust transceiver design and non-robust transceiver design is larger with higher σ_e^2. This is because when the CSI mismatch is greater with a higher σ_e^2, it causes more degradation to the system using the non-robust transceiver design.

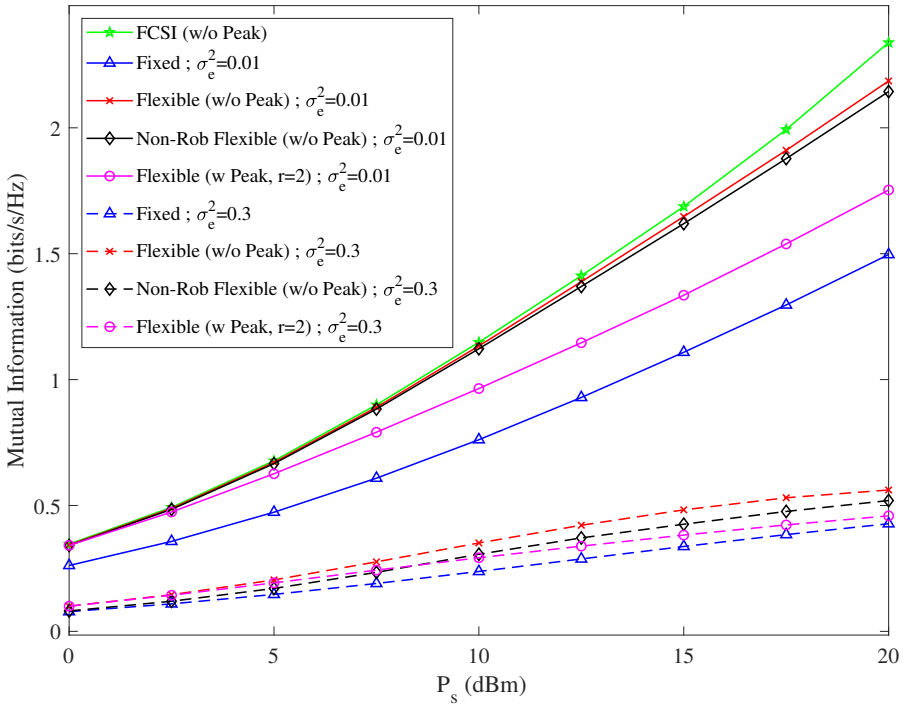

Figure 4.8: Example 3: MI versus P_s with $\nu = 1$.

For numerical example 4, the impact of peak power limits on the system MI is investigated. Fig. 4.9 displays the MI performance versus P_s with various peak power limits at $r = 1$, $r = 2$, $r = 5$ and $r = 100$ for the robust transceiver design at $\nu = 1$ and $\sigma_e^2 = 0.15$. It can be noticed that the MI performance increases with an increase of r. It is noticed that when r is sufficiently large, the MI performance of the system with peak power constraint is similar to the system without peak power constraint. This is because the peak power constraint is easier to be satisfied when the power limit is large. It is also noticed when $r = 1$, the system MI for flexible power constraint with peak power limits is approximately identical to the system MI for fixed power constraint at low P_s. At high P_s, the proposed robust transceiver design with fixed power constraint is greater than the proposed robust transceiver design with flexible power constraint with peak power limits.

For numerical example 5, the influence of the number of antennas at the system nodes towards the system MI is investigated. Fig. 4.10 displays the MI performance versus P_s at various combination of $[N_S, N_R, N_D]$ for the robust transceiver design under the flexible power scheme with peak power constraint with $r = 2$, $\nu = 1$ and $\sigma_e^2 = 0.15$.

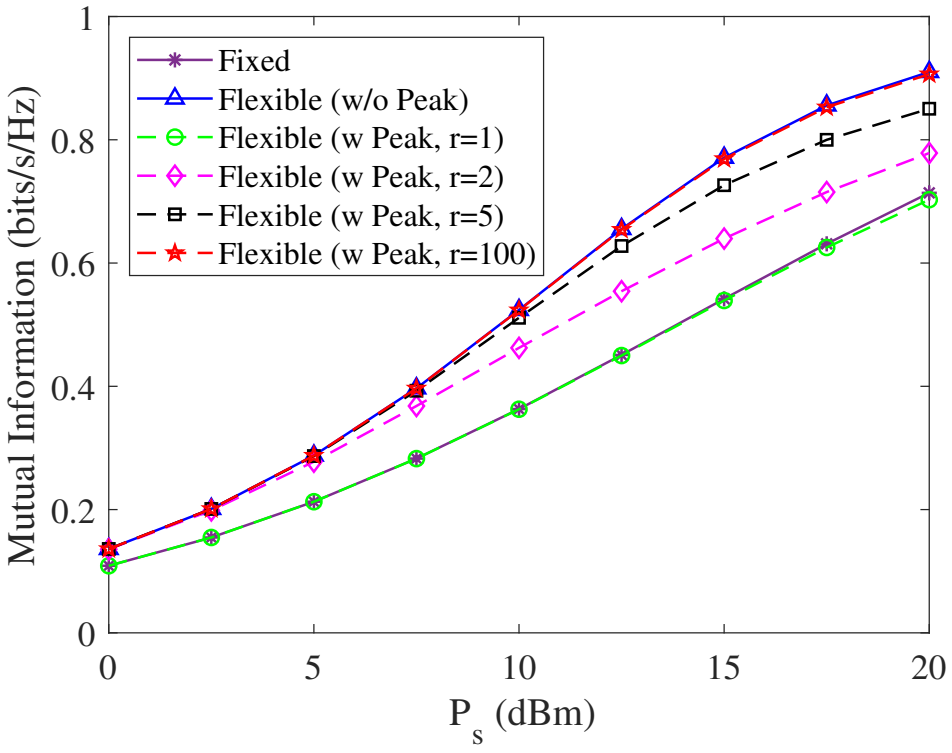

Figure 4.9: Example 4: MI versus P_s with $\sigma_e^2 = 0.15$ and $\nu = 1$.

It can be noticed when the number of the antenna at all system nodes increases from 3 to 5, and the system MI has a significant increase. It is noticed when only the number of the antenna at the source node increase, i.e., from $[3, 3, 3]$ distribution to $[5, 3, 3]$ distribution, the system MI is almost identical. This indicates that the increment of the number of antennas at the source node does not heavily influence the system MI. However, when increasing the number of antennas at the relay and/or destination node, the system MI for $[3, 5, 3]$ and $[3, 3, 5]$ distributions is higher than the system MI for $[5, 3, 3,]$ distribution. This is because the system MI is limited by the MI of the relay-destination link, which is due to the transmission energy available at the relay node is smaller than the transmission power available at the source node. Thus, increasing the number of antennas at the relay and destination node will enhance the MI performance of the given system.

In the last numerical example, the performance of the proposed algorithms is investigated for the scenario where the CSI mismatch matrices is different to the presumed one. Follows [50], the CSI mismatch matrices are modelled as Gaussian random matrices

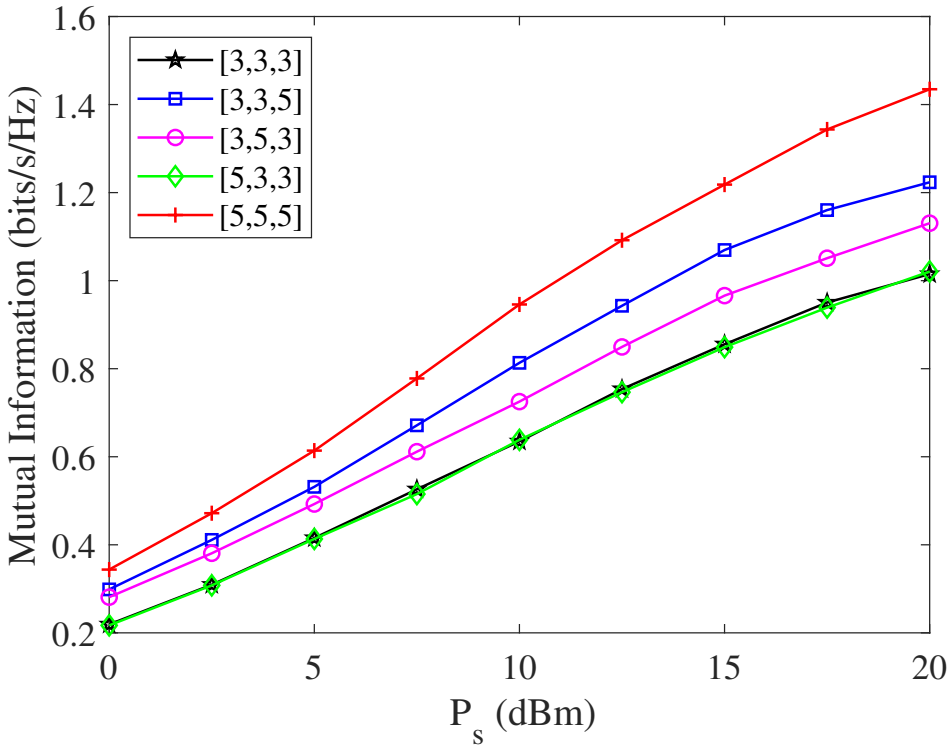

Figure 4.10: Example 5: MI versus P_s for robust transceiver design with peak power constraint at various $[N_S,N_R,N_D]$, $r = 2$, $\nu = 1$ and $\sigma_e^2 = 0.15$.

with zero mean and variances equal to σ_e^2. In this numerical example, the CSI mismatch matrices are uncorrelated with $\mathbf{H}_{SR}$ and $\mathbf{H}_{RD}$. It is noticeable that the proposed algorithms are providing better performance as compared to the non-robust algorithm. Besides, it is observed that even though the CSI mismatch model is different to the presumed one, the proposed algorithms achieves a good performance. This observation indicated that the changes in the applied CSI mismatch model will not heavily influence the performance of the proposed algorithms.

4.7 Chapter Summary

In this chapter, the robust transceiver design for dual-hop DF MIMO relay communication system with TS-based EH protocol is investigated. The transceiver design with robustness helps reduce the degradation caused by the CSI mismatch between the exact and estimated CSI available in the system. With the consideration of CSI mismatch, the

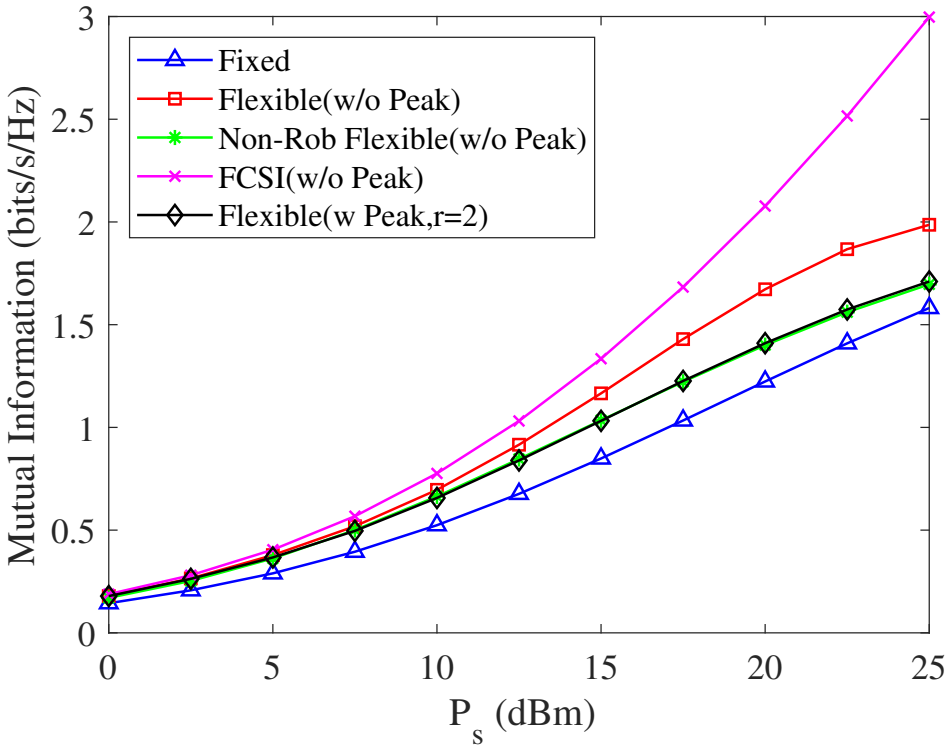

Figure 4.11: Example 6: MI versus P_s with $\nu = 1$, $\sigma_e^2 = 0.05$.

optimization problem is more challenging to solve. KKT conditions are applied to solve the source and relay precoding matrices optimization problem under the fixed power scheme, and the primal decomposition method is applied to solve the source and relay precoding matrices optimization problem under flexible power constraint. The golden section search method is adopted to obtain the optimized TS factor. The proposed transceiver design with robustness provides better performance than the non-robust transceiver design, as shown through numerical examples.

Chapter 5

Robust Transceiver Design for AF MIMO Relay System with Time-Switching Relaying Protocol

In this chapter, a dual-hop SWIPT AF MIMO relay communication system with an energy-limited relay node is investigated. The relay node harvests energy based on the RF signal transmitted from the source node through the TS protocol and fully uses the harvested energy to precode and forward the information to the destination node. With the consideration of the channel estimation error, the joint optimization of the TS factor, source and relay precoding matrices is proposed with robustness against the CSI mismatch to maximize the MI between the source and destination nodes. The optimal structure for the source and relay precoding matrices is derived to simplify the transceiver optimization problem. The numerical simulations show that the system performance provided by the proposed algorithms with robustness is better than the non-robust algorithm.

The rest of this chapter is constructed as follows. In Section 5.1, an overview of existing techniques provided in literature is presented. In Section 5.2, the system model of a dual-hop MIMO relay system with EH relay adopting TS protocol and consideration of the CSI mismatch is presented. In Section 5.3, the optimization problem for the

proposed robust transceiver design are mathematically presented. The source and relay precoding matrices and the TS ratio are jointly optimized to maximize the system MI. Numerical results are presented in Section 5.4 and conclusions are drawn in Section 5.5.

5.1 Overview of Existing Techniques

In the fifth-generation (5G) networks, the research trends is shifting to a greener communication system [58]. Besides being eco-friendly wireless networks, the 5G network is also expected to provide an improved system capacity, data rate, and better quality of services. Hence, SWIPT technology plays a vital role in developing the 5G networks. The RF signals are utilized in the SWIPT technology by transferring information and power at the same time. In the early studies of the SWIPT technology [2], an ideal receiver structure is proposed to perform ID and EH from the same received RF signals simultaneously. However, the ideal receiver is challenging to implement in practice [5]. This is because the practical EH circuits are unable to perform ID, and the practical ID circuits are unable to perform EH from the same received RF signals. Besides, wireless information transfer and wireless power transfer function in different sensitivity. In [6], two practical SWIPT receiver architectures are proposed, namely the TS receiver and PS receiver. In the TS receiver, a time-switch is installed at the receiving antenna to rhythmically switch between EH and ID circuit according to the designed TS-sequences. In the PS receiver, a PS unit is implemented at the receiving antenna to divide the receiving RF signals into two portions of signals, where one portion is used for ID while the remaining portion is used for EH.

In the scenario where the source and destination node are located very far apart, a relay node is needed to improve the system performance as it helps in extending the network coverage of wireless communication [8]. In [11], the author extended the SWIPT receiver architectures by implementing them in the energy-constricted relay node, such EH relaying protocols are known as the TSR protocol and the PSR protocol [11]. The energy harvested by the SWIPT relay node is used to process and forward the received information signals to the destination node. Generally, to improve the spectral and energy efficiency of a communication system, the MIMO technology is usually adopted. MIMO technology can be easily implemented by providing multiple antennas at the system nodes. Moreover, the MIMO technology also improves the efficiency for the RF energy transmission to wireless devices [105]. Recently, the application of SWIPT

in MIMO relay system with EH relay node has been studied in [1, 54–56]. In [1], the source and relay precoding matrices are jointly optimized to achieve the maximal achievable rate for the AF MIMO relay system with the relay node adopting either the TSR protocol or the PSR protocol. In [54], the optimization problem for SWIPT MIMO relay communication system with TSR protocol is investigated for AF relay. In [55], the authors study the AF MIMO relay system with the relay node adopting the PSR protocol and tackle the joint optimization problem for the source and relay precoding matrices with the PS factor matrix by using several optimization techniques, such as the sequential quadratic programming approach and the semi-definite programming approach. In [56], the authors extend the investigation carried out in [54] and [55] to regenerative relay.

It can be noticed that in the existing studies [1, 54–56], the CSI is assumed to be fully known at the receiving nodes. However, it is impossible to have the exact CSI in practice due to the channel estimation error. The mismatch between the estimated CSI and the exact CSI results in degradation of the proposed system performance [72, 79]. In [49, 50, 106–108], the influence of the imperfect CSI in SWIPT MIMO relay systems has been investigated. It is observed that the imperfect CSI considered in [49] and [50] is a special case, where the authors assumed the transmit and receive antennas correlation matrices are scaled identity matrices, and the CSI mismatch is treated as noise. However, in practical scenario, the assumption considered in [49] and [50] concerning the identity correlation matrix is not valid. This is because there is always correlation of the channel. Thus, in contrast to [49] and [50], no specific forms is assumed for the transmit and receive antennas correlation matrices, and the CSI mismatch is modeled based on the Gaussian-Kronecker model. In [106], a SWIPT relay wireless communication system where multi-antenna source and destination node communicate with each other via the help of multiple single antenna relay node using the TSR protocol which arranged in parallel is investigated with the consideration of CSI mismatch. Different to [106], instead of using multiple single-antenna relay node, a multi-antenna relay node is used to forward the information signal received from the source node to the destination node by using energy harvested through the TSR protocol. Transmit antenna selection strategy is used in [107] to reduce the system complexity for a dual-hop SWIPT MIMO AF relay communication system with consideration of the imperfect CSI. It is observed that the system nodes which transmit information, e.g., source node and the relay node, are treated as single-antenna system nodes in [107]. In contrast to [107], all the antennas

considered in this chapter will be used to transmit/receive RF signal. In [108], an energy-efficient optimization design for a two-way MIMO relay networks with PSR protocol is investigated with the consideration of the CSI mismatch. As compared to [108], a one-way MIMO relay is used due to its simplicity. Moreover, the PSR protocol require high complexity hardware implementation, thus instead of the PSR protocol, the TSR protocol is used in the relay node to harvest energy from the RF signal transmitted by the source node. With the consideration of imperfect CSI, a transceiver design is proposed for a two-hop AF MIMO relay communication system where the relay is adopting the TSR protocol to harvest energy. Different to [49], the algorithms proposed in this chapter do not assume the transmit and receive antennas correlation matrices as scaled identity matrices. To the best of our knowledge, there is no existing work carried out for the SWIPT AF MIMO relay system with the consideration of practical imperfect CSI. Hence, to fill in the gap, this research is performed. It is demonstrated through numerical simulations that the proposed scheme enhances the robustness of the SWIPT AF MIMO relay system against the CSI mismatch.

The main contributions of the investigation carried out in this chapter are listed as follows:

- The proposed algorithm in this chapter for a two-hop AF MIMO relay system with the relay node adopting the TSR protocol provides better robustness compared to the existing non-robust algorithms.

- Compared to [49], a more general CSI mismatch based on the Gaussian-Kronecker model is considered in optimizing the system performance for a two-hop AF MIMO relay system. When the transmit and receive antennas correlation matrices are not identity matrices, the optimization problem is more complicated to solve, which is tackled in this chapter.

- The structure of the source and relay precoding matrices is exploited to simplify the complex joint transceiver design problem to optimal power allocation problem.

- The proposed algorithm provides a better system MI compared to the existing algorithm proposed in [54] in practical channel matrices.

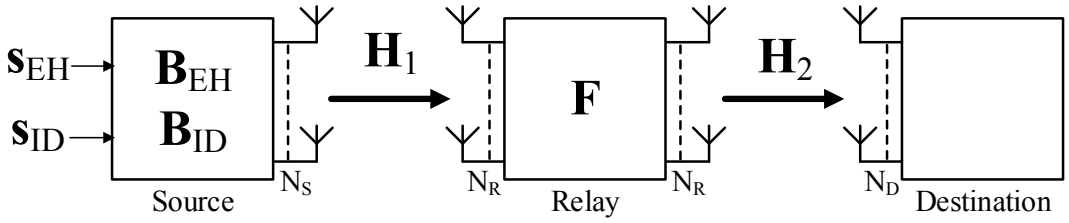

Figure 5.1: Block diagram of a two-hop MIMO relay system with EH relay using TS protocol.

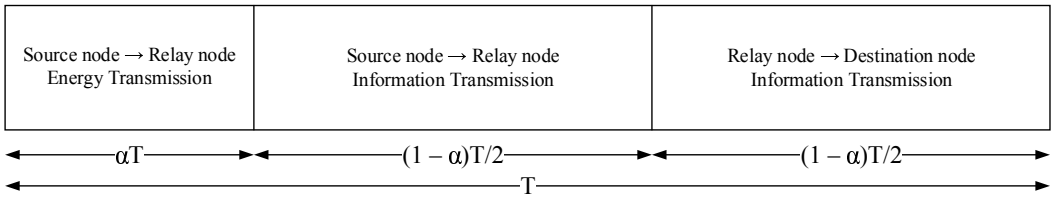

Figure 5.2: Framework of TS protocol.

5.2 SWIPT AF Relay System Model with TSR Scheme

In this chapter, the system model as illustrated in Fig. 5.1 is considered, where it is a two-hop three-nodes relay communication system, and the information signal is transmitted from the source node to the destination node through a relay node. The source, relay and destination node are respectively installed with N_S, N_R and N_D antennas. For the relay node, AF relaying scheme is used due to its simplicity, where the received information-carrying signal is linearly precoded and forwarded to the destination node. The impact of the direct link between the source node and the destination node is assumed to negligible due to severe shadowing and pathloss. The source node is provided with an individual power supply where a given power budget of P_s is allocated for the source node to transmit information signal. The relay node is considered as an energy-limited wireless-powered device where it is required to be powered by the energy harvested from the received RF signals through the TS protocol.

With the TS protocol implemented for EH at the relay node, a full communication cycle with the duration of T is separated into three sections as illustrated in Fig. 5.2. In the first time frame with a duration of αT, where $\alpha \in [0, 1]$ is the TS ratio, the source node precodes and transmits the signal vector, $\mathbf{s}_{EH}$, to the relay node with the source node precoding matrix at the first time section denoted as $\mathbf{B}_{EH}$, where $\mathbf{s}_{EH}$ is the energy-bearing signal with covariance matrix given as $\mathrm{E}\{\mathbf{s}_{EH}\mathbf{s}_{EH}^H\} = \mathbf{I}_{N_{EH}}$ while

$\mathrm{E}\{\cdot\}$ denotes the statistical expectation, $(\cdot)^H$ denotes the Hermitian matrix transpose and $\mathbf{I}_m$ denotes a size m identity matrix. Hence, the received signal vector at the relay node for EH during the first time frame is given as

$$\mathbf{y}_{r,EH} = \mathbf{H}_1\mathbf{B}_{EH}\mathbf{s}_{EH} + \mathbf{n}_{r,EH} \tag{5.1}$$

where $\mathbf{H}_1$ is the first hop MIMO channel matrix in the communication system, $\mathbf{n}_{r,EH}$ is the AWGN introduced at the relay node during the first time frame. Without considering the noise component, the harvested energy at the relay node, E_r is given as

$$E_r = \alpha\eta\, tr\left\{\mathbf{H}_1\mathbf{B}_{EH}\mathbf{B}_{EH}^H\mathbf{H}_1^H\right\} \tag{5.2}$$

where $\eta \in [0,1]$ is the energy harvesting efficiency and $tr\{\cdot\}$ denotes the matrix trace. In the second time frame with a duration of $(1-\alpha)T/2$, the source node precodes and transmits the signal vector, $\mathbf{s}_{ID}$, to the relay node with the source node precoding matrix at second time frame denoted as $\mathbf{B}_{ID}$, where $\mathbf{s}_{ID}$ is the information-carrying signal with covariance matrix given as $\mathrm{E}\{\mathbf{s}_{ID}\mathbf{s}_{ID}^H\} = \mathbf{I}_{N_{ID}}$ and $N_{ID} = \min(N_S, N_R, N_D)$. The received signal vector at the relay node for ID during the second time frame is given as

$$\mathbf{y}_{r,ID} = \mathbf{H}_1\mathbf{B}_{ID}\mathbf{s}_{ID} + \mathbf{n}_{r,ID} \tag{5.3}$$

where $\mathbf{n}_{r,ID}$ is the AWGN introduced at the relay node during the second time frame with the noise covariance matrix given as $\mathrm{E}\{\mathbf{n}_{r,ID}\mathbf{n}_{r,ID}^H\} = \sigma_r^2\mathbf{I}_{N_R}$. During the third time frame, the relay node precodes and transmits the received signal vector, $\mathbf{y}_{r,ID}$ to the destination node with the relay node precoding matrix denoted as $\mathbf{F}$. The received signal at the destination node is given as

$$\mathbf{y}_d = \mathbf{H}_2\mathbf{F}\mathbf{H}_1\mathbf{B}_{ID}\mathbf{s}_{ID} + \mathbf{H}_2\mathbf{F}\mathbf{n}_{r,ID} + \mathbf{n}_d \tag{5.4}$$

where $\mathbf{H}_2$ is the second hop MIMO channel matrix in the communication system and $\mathbf{n}_d$ is the AWGN introduced at the destination node with the noise covariance matrix given as $\mathrm{E}\{\mathbf{n}_d\mathbf{n}_d^H\} = \sigma_d^2\mathbf{I}_{N_D}$. Without wasting the available transmission power at the source and relay node, $\mathrm{r}(\mathbf{B}_{ID}) = \mathrm{r}(\mathbf{F}) = N_{ID}$, where $\mathrm{r}(\cdot)$ denotes the rank of a matrix.

Different from the ideal situation, only partial CSI is available at the relay and destination node in practice. This is because of the channel estimation error which

results in the mismatch between the exact CSI and the estimated CSI. Hence, the true MIMO channel matrices with consideration of the CSI mismatch are given as

$$\mathbf{H}_1 = \widehat{\mathbf{H}}_1 + \boldsymbol{\Delta}_1 \quad \mathbf{H}_2 = \widehat{\mathbf{H}}_2 + \boldsymbol{\Delta}_2 \tag{5.5}$$

where $\widehat{\mathbf{H}}_1$ and $\widehat{\mathbf{H}}_2$ are the estimated channel matrices for the first and the second hop of the communication system, while $\boldsymbol{\Delta}_1$ and $\boldsymbol{\Delta}_2$ are the respective CSI mismatch matrices. The CSI mismatch matrices are modeled based on the Gaussian-Kronecker model [79], which are written as

$$\boldsymbol{\Delta}_1 \sim CN(\mathbf{0}, \boldsymbol{\Sigma}_1 \otimes \boldsymbol{\Phi}_1^T) \quad \boldsymbol{\Delta}_2 \sim CN(\mathbf{0}, \boldsymbol{\Sigma}_2 \otimes \boldsymbol{\Phi}_2^T) \tag{5.6}$$

where $\otimes$ denotes the matrix Kronecker product, $\boldsymbol{\Phi}_1$ and $\boldsymbol{\Sigma}_1$ are the transmit and receive antennas correlation matrices for $\mathbf{H}_1$ while $\boldsymbol{\Phi}_2$ and $\boldsymbol{\Sigma}_2$ are the transmit and receive antennas correlation matrices for $\mathbf{H}_2$. From (5.6), the true MIMO channel matrices can be written as

$$\mathbf{H}_1 = \widehat{\mathbf{H}}_1 + \boldsymbol{\Sigma}_1^{\frac{1}{2}} \boldsymbol{\Delta}_{\omega,1} \boldsymbol{\Phi}_1^{\frac{1}{2}} \quad \mathbf{H}_2 = \widehat{\mathbf{H}}_2 + \boldsymbol{\Sigma}_2^{\frac{1}{2}} \boldsymbol{\Delta}_{\omega,2} \boldsymbol{\Phi}_2^{\frac{1}{2}} \tag{5.7}$$

where $\boldsymbol{\Delta}_{\omega,1}$ and $\boldsymbol{\Delta}_{\omega,2}$ are the zero-mean unit-variance complex Gaussian matrix with independent and identically distribution (i.i.d.) entries. By substituting (5.5) into 5.4 , the received signal at the destination node with the consideration of CSI mismatch can be equivalently rewritten as

$$\begin{aligned} \mathbf{y}_d &= \widehat{\mathbf{H}}_2 \mathbf{F} \widehat{\mathbf{H}}_1 \mathbf{B}_{ID} \mathbf{s}_{ID} + \widehat{\mathbf{H}}_2 \mathbf{F} \left(\boldsymbol{\Delta}_1 \mathbf{B}_{ID} \mathbf{s}_{ID} + \mathbf{n}_{r,ID} \right) \\ &\quad + \boldsymbol{\Delta}_2 \mathbf{F} \left(\widehat{\mathbf{H}}_1 \mathbf{B}_{ID} \mathbf{s}_{ID} + \boldsymbol{\Delta}_1 \mathbf{B}_{ID} \mathbf{s}_{ID} + \mathbf{n}_{r,ID} \right) + \mathbf{n}_d \\ &\triangleq \widehat{\mathbf{H}} \mathbf{s}_{ID} + \mathbf{n} \end{aligned} \tag{5.8}$$

where

$$\widehat{\mathbf{H}} \triangleq \widehat{\mathbf{H}}_2 \mathbf{F} \widehat{\mathbf{H}}_1 \mathbf{B}_{ID} \tag{5.9}$$

$$\begin{aligned} \mathbf{n} \triangleq\ & \widehat{\mathbf{H}}_2 \mathbf{F} \left(\boldsymbol{\Delta}_1 \mathbf{B}_{ID} \mathbf{s}_{ID} + \mathbf{n}_{r,ID} \right) + \boldsymbol{\Delta}_2 \mathbf{F} \left(\widehat{\mathbf{H}}_1 \mathbf{B}_{ID} \mathbf{s}_{ID} + \boldsymbol{\Delta}_1 \mathbf{B}_{ID} \mathbf{s}_{ID} + \mathbf{n}_{r,ID} \right) \\ & + \mathbf{n}_d \end{aligned} \tag{5.10}$$

in which $\widehat{\mathbf{H}}$ can be viewed as the estimated MIMO channel matrix between the source node and the destination node, while $\mathbf{n}$ is the total noise introduced throughout the

system due to noise at the receiving antennas and channel estimation error. Meanwhile, the covariance matrix for $\mathbf{n}$ is expressed as

$$\mathbf{R}_n = \widehat{\mathbf{H}}_2\mathbf{F}\left(\gamma_1\mathbf{\Sigma}_1 + \sigma_r^2\mathbf{I}_{N_R}\right)\mathbf{F}^H\widehat{\mathbf{H}}_2^H + \gamma_2\mathbf{\Sigma}_2 + \sigma_d^2\mathbf{I}_{N_D} \tag{5.11}$$

where

$$\gamma_1 = tr\left\{\mathbf{B}_{ID}\mathbf{B}_{ID}^H\mathbf{\Phi}_1\right\}$$
$$\gamma_2 = tr\left\{\mathbf{F}\left(\widehat{\mathbf{H}}_1\mathbf{B}_{ID}\mathbf{B}_{ID}^H\widehat{\mathbf{H}}_1^H + \gamma_1\mathbf{\Sigma}_1 + \sigma_r^2\mathbf{I}_{N_R}\right)\mathbf{F}^H\mathbf{\Phi}_2\right\}.$$

Based on [110], the mutual information between the source node and the destination node is given as

$$\mathfrak{I}_{SD} = \frac{1-\alpha}{2}\log\left|\mathbf{I}_{N_{ID}} + \widehat{\mathbf{H}}^H\mathbf{R}_n^{-1}\widehat{\mathbf{H}}\right|. \tag{5.12}$$

With the consideration of channel mismatch, the harvested energy at the relay node, E_r is written as

$$E_r = \alpha\eta\, tr\left\{\widehat{\mathbf{H}}_1\mathbf{B}_{EH}\mathbf{B}_{EH}^H\widehat{\mathbf{H}}_1^H + tr\{\mathbf{B}_{EH}\mathbf{B}_{EH}^H\mathbf{\Phi}_1\}\mathbf{\Sigma}_1\right\}. \tag{5.13}$$

By using matrix trace properties, E_r can be equivalently expressed as

$$E_r = \alpha\eta\, tr\left\{\mathbf{B}_{EH}\mathbf{B}_{EH}^H\left(\widehat{\mathbf{H}}_1^H\widehat{\mathbf{H}}_1 + tr\{\mathbf{\Sigma}_1\}\mathbf{\Phi}_1\right)\right\}. \tag{5.14}$$

As the transmission energy required at the source node for the first time section and the second time section are respectively given as $\alpha tr\{\mathbf{B}_{EH}\mathbf{B}_{EH}^H\}$ and $\frac{1-\alpha}{2}tr\{\mathbf{B}_{ID}\mathbf{B}_{ID}^H\}$, hence the transmission energy constraint at the source node is written as

$$\alpha tr\{\mathbf{B}_{EH}\mathbf{B}_{EH}^H\} + \frac{1-\alpha}{2}tr\{\mathbf{B}_{ID}\mathbf{B}_{ID}^H\} \leq \frac{1+\alpha}{2}P_s. \tag{5.15}$$

Moreover, the necessary transmission energy needed at the relay node, E_u is given as

$$E_u = \frac{1-\alpha}{2}tr\left\{\mathbf{F}\left(\widehat{\mathbf{H}}_1\mathbf{B}_{ID}\mathbf{B}_{ID}^H\widehat{\mathbf{H}}_1^H + \gamma_1\mathbf{\Sigma}_1 + \sigma_r^2\mathbf{I}_{N_R}\right)\mathbf{F}^H\right\} \tag{5.16}$$

and the available transmission energy at the relay node is solely rely on E_r. Hence, the transmission energy constraint at the relay node is given as

$$E_u \leq E_r. \tag{5.17}$$

The objective of this chapter is to obtain the optimal source and relay precoding matrices to maximize the system MI given as (5.12), subjecting to the transmission

energy constraint at the source node and the relay node which are respectively given as (5.15) and (5.17). Hence, the optimization problem can be expressed as

$$\max_{\alpha,\mathbf{B}_{EH},\mathbf{B}_{ID},\mathbf{F}} \frac{1-\alpha}{2}\log\left|\mathbf{I}_{N_{ID}}+\widehat{\mathbf{H}}^H\mathbf{R}_n^{-1}\widehat{\mathbf{H}}\right| \tag{5.18a}$$

$$s.t.\ \alpha tr\{\mathbf{B}_{EH}\mathbf{B}_{EH}^H\}+\frac{1-\alpha}{2}tr\{\mathbf{B}_{ID}\mathbf{B}_{ID}^H\}\leq\frac{1+\alpha}{2}P_s \tag{5.18b}$$

$$E_u \leq E_r \tag{5.18c}$$

$$0\leq\alpha\leq 1. \tag{5.18d}$$

5.3 Proposed Transceiver Algorithm with Robustness

It can be observed that the source precoding matrix $\mathbf{B}_{EH}$ does not appear in the objective function (5.18a). However, it plays an important role in varying the feasible region of the optimization problem, as it affects the transmission energy available at the relay node [54]. Thus, to maximize the energy harvested at the relay node, the optimization problem for $\mathbf{B}_{EH}$ can be viewed as

$$\max_{\mathbf{B}_{EH}} tr\left\{\mathbf{B}_{EH}\mathbf{B}_{EH}^H\left(\widehat{\mathbf{H}}_1^H\widehat{\mathbf{H}}_1+tr\{\mathbf{\Sigma}_1\}\mathbf{\Phi}_1\right)\right\} \tag{5.19a}$$

$$s.t.\ tr\{\mathbf{B}_{EH}\mathbf{B}_{EH}^H\}\leq\lambda_e \tag{5.19b}$$

where λ_e is a positive scalar variable. $\mathbf{Q}$ is introduced as

$$\mathbf{Q}=\widehat{\mathbf{H}}_1^H\widehat{\mathbf{H}}_1+tr\{\mathbf{\Sigma}_1\}\mathbf{\Phi}_1 \tag{5.20}$$

with the corresponding eigenvalue decomposition (EVD) given as $\mathbf{V}_q\mathbf{\Lambda}_q\mathbf{V}_q^H$ where $\mathbf{\Lambda}_q$ is a diagonal matrix with its diagonal elements arranged in descending order. To diagonalize the objective function (5.19a), the optimal structure of $\mathbf{B}_{EH}$ is given as

$$\mathbf{B}_{EH}=\mathbf{V}_{q,1}\mathbf{\Lambda}_{EH}^{\frac{1}{2}}\mathbf{U}^H \tag{5.21}$$

where $\mathbf{V}_{q,1}$ contains the leftmost N_{EH} columns of $\mathbf{V}_q$ and $\mathbf{\Lambda}_{EH}$ is a diagonal matrix of size N_{EH} and $\mathbf{U}$ is a unitary matrix. The optimization problem (5.19) can be expressed as

$$\max_{\boldsymbol{\lambda}_{EH}} \sum_{i=1}^{N_{EH}}\lambda_{q,i}\lambda_{EH,i} \quad s.t.\ \sum_{i=1}^{N_{EH}}\lambda_{EH,i}=\lambda_e \tag{5.22}$$

where $\boldsymbol{\lambda}_{EH} = [\lambda_{EH,1}, \cdots, \lambda_{EH,N_{EH}}]^T$, $\lambda_{q,i}$ and $\lambda_{EH,i}$ denote the ith diagonal elements of $\boldsymbol{\Lambda}_q$ and $\boldsymbol{\Lambda}_{EH}$, respectively. Clearly, the optimal solution to the optimization problem (5.22) is $\boldsymbol{\lambda}^*_{EH} = [\lambda_e, 0, \cdots, 0]^T$, where $(\cdot)^*$ denotes the optimal value. Hence, the optimal structure of $\mathbf{B}_{EH}$ can be written as

$$\mathbf{B}^*_{EH} = \lambda_e^{\frac{1}{2}} \mathbf{v}_{q,1} \mathbf{u}_1^H \tag{5.23}$$

where $\mathbf{v}_{q,1}$ and $\mathbf{u}_1$ are the first column of $\mathbf{V}_q$ and $\mathbf{U}$, respectively. By using (5.23), the optimization problem (5.18) is rewritten as

$$\max_{\alpha,\lambda_e,\mathbf{B}_{ID},\mathbf{F}} \frac{1-\alpha}{2} \log \left| \mathbf{I}_{N_{ID}} + \widehat{\mathbf{H}}^H \mathbf{R}_n^{-1} \widehat{\mathbf{H}} \right| \tag{5.24a}$$

$$s.t.\ \alpha\lambda_e + \frac{1-\alpha}{2} tr\{\mathbf{B}_{ID}\mathbf{B}_{ID}^H\} \leq \frac{1+\alpha}{2} P_s \tag{5.24b}$$

$$tr\{\mathbf{F}(\widehat{\mathbf{H}}_1 \mathbf{B}_{ID} \mathbf{B}_{ID}^H \widehat{\mathbf{H}}_1^H + \gamma_1 \boldsymbol{\Sigma}_1 + \sigma_r^2 \mathbf{I}_{N_R})\mathbf{F}^H\} \leq \frac{2\alpha\eta\lambda_{q,1}}{1-\alpha}\lambda_e \tag{5.24c}$$

$$\lambda_e \geq 0 \quad 0 \leq \alpha \leq 1. \tag{5.24d}$$

For the optimal value of $\mathbf{F}$ and $\mathbf{B}_{ID}$, it is obvious that for any fixed α and λ_e, the equality of (5.24c) must holds, i.e.

$$tr\{\mathbf{F}(\widehat{\mathbf{H}}_1 \mathbf{B}_{ID} \mathbf{B}_{ID}^H \widehat{\mathbf{H}}_1^H + \gamma_1 \boldsymbol{\Sigma}_1 + \sigma_r^2 \mathbf{I}_{N_R})\mathbf{F}^H\} = \frac{2\alpha\eta\lambda_{q,1}}{1-\alpha}\lambda_e. \tag{5.25}$$

By using (5.25), the optimization problem (5.24) can be rewritten as

$$\max_{\alpha,\mathbf{B}_{ID},\mathbf{F}} \frac{1-\alpha}{2} \log \left| \mathbf{I}_{N_{ID}} + \widehat{\mathbf{H}}^H \mathbf{R}_n^{-1} \widehat{\mathbf{H}} \right| \tag{5.26a}$$

$$s.t.\ \frac{tr\{\mathbf{F}(\widehat{\mathbf{H}}_1 \mathbf{B}_{ID} \mathbf{B}_{ID}^H \widehat{\mathbf{H}}_1^H + \gamma_1 \boldsymbol{\Sigma}_1 + \sigma_r^2 \mathbf{I}_{N_R})\mathbf{F}^H\}}{\eta\lambda_{q,1}} + tr\{\mathbf{B}_{ID}\mathbf{B}_{ID}^H\} \leq \frac{1+\alpha}{1-\alpha} P_s \tag{5.26b}$$

$$0 \leq \alpha \leq 1. \tag{5.26c}$$

To solve (5.26), a dual-loop iterative method is proposed. First, in the inner loop, the optimization problem given below is solved with fixed α.

$$\max_{\mathbf{B}_{ID},\mathbf{F}} \frac{1-\alpha}{2} \log \left| \mathbf{I}_{N_{ID}} + \widehat{\mathbf{H}}^H \mathbf{R}_n^{-1} \widehat{\mathbf{H}} \right| \tag{5.27a}$$

$$s.t.\ \frac{tr\{\mathbf{F}(\widehat{\mathbf{H}}_1 \mathbf{B}_{ID} \mathbf{B}_{ID}^H \widehat{\mathbf{H}}_1^H + \gamma_1 \boldsymbol{\Sigma}_1 + \sigma_r^2 \mathbf{I}_{N_R})\mathbf{F}^H\}}{\eta\lambda_{q,1}} + tr\{\mathbf{B}_{ID}\mathbf{B}_{ID}^H\} \leq P_\alpha \tag{5.27b}$$

$$\tag{5.27c}$$

where $P_\alpha = \frac{1+\alpha}{1-\alpha}P_s$ is a constant when α is a fixed value. The $\mathcal{I}_{SD}\{\alpha\}$ is denoted as the optimal value of (5.27a) with any given α. To solve (5.27), the optimal structure for $\mathbf{F}$ is introduced as

$$\mathbf{F}^* = \mathbf{TD} \tag{5.28}$$

where $\mathbf{D} = \mathbf{B}_{ID}^H \widehat{\mathbf{H}}_1^H \left(\widehat{\mathbf{H}}_1 \mathbf{B}_{ID} \mathbf{B}_{ID}^H \widehat{\mathbf{H}}_1^H + \gamma_1 \mathbf{\Sigma}_1 + \sigma_r^2 \mathbf{I}_{N_R}\right)^{-1}$ which can be treated as a weight matrix of a Wiener filter at the relay node, while $\mathbf{T}$ can be treated as the relay transmitting precoder matrix. By using matrix inversion lemma and (5.28), (5.27a) can be equivalently expressed as

$$\begin{aligned}\mathcal{I}_{SD}\{\alpha\} = \frac{1-\alpha}{2} \log \Bigg| \Bigg(\left(\mathbf{I}_{N_{ID}} + \mathbf{B}_{ID}^H \widehat{\mathbf{H}}_1^H \mathbf{\Xi}_1^{-1} \widehat{\mathbf{H}}_1 \mathbf{B}_{ID}\right)^{-1} \\ + \left(\mathbf{Z}^{-1} + \mathbf{T}^H \widehat{\mathbf{H}}_2^H \mathbf{\Xi}_2^{-1} \widehat{\mathbf{H}}_2 \mathbf{T}\right)^{-1} \Bigg)^{-1} \Bigg|\end{aligned} \tag{5.29}$$

where

$$\mathbf{\Xi}_1 = tr\left\{\mathbf{B}_{ID}\mathbf{B}_{ID}^H \mathbf{\Phi}_1\right\} \mathbf{\Sigma}_1 + \sigma_r^2 \mathbf{I}_{N_R} \tag{5.30}$$

$$\mathbf{\Xi}_2 = tr\left\{\mathbf{T}\mathbf{Z}\mathbf{T}^H \mathbf{\Phi}_2\right\} \mathbf{\Sigma}_2 + \sigma_d^2 \mathbf{I}_{N_D} \tag{5.31}$$

and

$$\mathbf{Z} = \mathbf{B}_{ID}^H \widehat{\mathbf{H}}_1^H \left(\widehat{\mathbf{H}}_1 \mathbf{B}_{ID} \mathbf{B}_{ID}^H \widehat{\mathbf{H}}_1^H + \mathbf{\Xi}_1\right)^{-1} \widehat{\mathbf{H}}_1 \mathbf{B}_{ID}. \tag{5.32}$$

By using matrix inversion lemma, it can equivalently expressed as

$$\mathbf{Z} = \mathbf{B}_{ID}^H \widehat{\mathbf{H}}_1^H \mathbf{\Xi}_1^{-1} \widehat{\mathbf{H}}_1 \mathbf{B}_{ID} \left(\mathbf{B}_{ID}^H \widehat{\mathbf{H}}_1^H \mathbf{\Xi}_1^{-1} \widehat{\mathbf{H}}_1 \mathbf{B}_{ID} + \mathbf{I}_{N_{ID}}\right)^{-1} \tag{5.33}$$

which can be noticed that $\mathbf{Z}$ can be approximated as $\mathbf{I}_{N_{ID}}$ with moderately high SNRs, i.e. $\mathbf{B}_{ID}^H \widehat{\mathbf{H}}_1^H \mathbf{\Xi}^{-1} \widehat{\mathbf{H}}_1 \mathbf{B}_{ID} \gg \mathbf{I}_{N_{ID}}$. Hence, (5.29) is rewritten as

$$\begin{aligned}\mathcal{I}_{SD}\{\alpha\} = \frac{1-\alpha}{2} \log \Bigg| \Bigg(\left(\mathbf{I}_{N_{ID}} + \mathbf{B}_{ID}^H \widehat{\mathbf{H}}_1^H \mathbf{\Xi}_1^{-1} \widehat{\mathbf{H}}_1 \mathbf{B}_{ID}\right)^{-1} \\ + \left(\mathbf{I}_{N_{ID}} + \mathbf{T}^H \widehat{\mathbf{H}}_2^H \mathbf{\Xi}_2^{-1} \widehat{\mathbf{H}}_2 \mathbf{T}\right)^{-1} \Bigg)^{-1} \Bigg|\end{aligned} \tag{5.34}$$

with $\mathbf{\Xi}_2 = tr\left\{\mathbf{T}\mathbf{T}^H \mathbf{\Phi}_2\right\} \mathbf{\Sigma}_2 + \sigma_d^2 \mathbf{I}_{N_D}$. By using (5.28), the transmission energy constraint (5.27b) is rewritten into

$$\frac{tr\{\mathbf{T}\mathbf{T}^H\}}{\eta \lambda_{q,1}} + tr\{\mathbf{B}_{ID}\mathbf{B}_{ID}^H\} \leq P_\alpha. \tag{5.35}$$

Different to [49], the case when the transmit and receive antennas correlation matrices, i.e. $\mathbf{\Phi}_1$, $\mathbf{\Phi}_2$, $\mathbf{\Sigma}_1$ and $\mathbf{\Sigma}_2$ are not scaled identity matrices is considered, in which it will result in difficulties in solving the optimization problem. Thus, the following inequality [75] is used to reduce the difficulties in solving the optimization problem.

$$tr\left\{\mathbf{XY}\right\} \leq tr\left\{\mathbf{X}\right\}\lambda_M(\mathbf{Y}) \tag{5.36}$$

where $\lambda_M(\cdot)$ denotes the largest eigenvalue of a matrix with equality holds when $\mathbf{Y}$ is a scaled identity matrix. By using (5.36), the upper-bound of $\mathbf{\Xi}_1$ and $\mathbf{\Xi}_2$ are respectively written as

$$\hat{\mathbf{\Xi}}_1[tr\left\{\mathbf{B}_{ID}\mathbf{B}_{ID}^H\right\}] = \phi_{1,1}tr\left\{\mathbf{B}_{ID}\mathbf{B}_{ID}^H\right\}\mathbf{\Sigma}_1 + \sigma_r^2\mathbf{I}_{N_R} \tag{5.37}$$

$$\hat{\mathbf{\Xi}}_2[tr\left\{\mathbf{B}_{ID}\mathbf{B}_{ID}^H\right\}] = \phi_{2,1}tr\left\{\mathbf{T}\mathbf{T}^H\right\}\mathbf{\Sigma}_2 + \sigma_d^2\mathbf{I}_{N_D} \tag{5.38}$$

with dependence on $tr\{\mathbf{B}_{ID}\mathbf{B}_{ID}^H\}$ and $tr\{\mathbf{T}\mathbf{T}^H\}$ where $\phi_{1,1}$ and $\phi_{2,1}$ denote the largest eigenvalue of $\mathbf{\Phi}_1$ and $\mathbf{\Phi}_2$ respectively. Then, $\mathbf{\Xi}_1$ and $\mathbf{\Xi}_2$ is replaced with the corresponding upper-bounds when solving (5.27). By exploiting the lower-bound of the objective function (5.27a), the optimization problem is changed to

$$\begin{aligned}
\min_{\mathbf{B}_{ID},\mathbf{T}} \ & \frac{1-\alpha}{2}\log\Big|\left(\mathbf{I}_{N_{ID}} + \mathbf{B}_{ID}^H\mathbf{M}_1[tr\left\{\mathbf{B}_{ID}\mathbf{B}_{ID}^H\right\}]\mathbf{B}_{ID}\right)^{-1} \\
& + \left(\mathbf{I}_{N_{ID}} + \mathbf{T}^H\mathbf{M}_2[tr\left\{\mathbf{B}_{ID}\mathbf{B}_{ID}^H\right\}]\mathbf{T}\right)^{-1}\Big| && \text{(5.39a)} \\
s.t. \ & \frac{tr\{\mathbf{T}\mathbf{T}^H\}}{\eta\lambda_{q,1}} + tr\{\mathbf{B}_{ID}\mathbf{B}_{ID}^H\} \leq P_\alpha && \text{(5.39b)} \\
& && \text{(5.39c)}
\end{aligned}$$

where

$$\mathbf{M}_1[tr\left\{\mathbf{B}_{ID}\mathbf{B}_{ID}^H\right\}] = \widehat{\mathbf{H}}_1^H\hat{\mathbf{\Xi}}_1[tr\left\{\mathbf{B}_{ID}\mathbf{B}_{ID}^H\right\}]^{-1}\widehat{\mathbf{H}}_1 \tag{5.40}$$

$$\mathbf{M}_2[tr\left\{\mathbf{T}\mathbf{T}^H\right\}] = \widehat{\mathbf{H}}_2^H\hat{\mathbf{\Xi}}_2[tr\left\{\mathbf{T}\mathbf{T}^H\right\}]^{-1}\widehat{\mathbf{H}}_2 \tag{5.41}$$

with the corresponding EVD given as

$$\begin{gathered}
\mathbf{V}_1[tr\left\{\mathbf{B}_{ID}\mathbf{B}_{ID}^H\right\}]\mathbf{\Lambda}_1[tr\left\{\mathbf{B}_{ID}\mathbf{B}_{ID}^H\right\}]\mathbf{V}_1[tr\left\{\mathbf{B}_{ID}\mathbf{B}_{ID}^H\right\}]^H \\
\mathbf{V}_2[tr\left\{\mathbf{T}\mathbf{T}^H\right\}]\mathbf{\Lambda}_2[tr\left\{\mathbf{T}\mathbf{T}^H\right\}]\mathbf{V}_2[tr\left\{\mathbf{T}\mathbf{T}^H\right\}]^H
\end{gathered}$$

where $\mathbf{\Lambda}[tr\left\{\mathbf{B}_{ID}\mathbf{B}_{ID}^H\right\}]$ and $\mathbf{\Lambda}[tr\left\{\mathbf{T}\mathbf{T}^H\right\}]$ are diagonal matrices of size N_{ID} with its diagonal elements arranged in descending order.

It is observed that the optimal $\mathbf{B}_{ID}$ and $\mathbf{T}$ are coupled in the transmission power constraint (5.39b). Hence, the optimization problem (5.39) can be solved by using the primal decomposition method [112] with the introduction of $\kappa \leq tr\left\{\mathbf{B}_{ID}\mathbf{B}_{ID}^H\right\}$ where $\kappa \in [0, P_\alpha]$. The subproblem is given as

$$\begin{aligned}
\min_{\mathbf{B}_{ID},\mathbf{T}} \ & \frac{1-\alpha}{2}\log\Big|\left(\mathbf{I}_{N_{ID}} + \mathbf{B}_{ID}^H\mathbf{M}_1[tr\left\{\mathbf{B}_{ID}\mathbf{B}_{ID}^H\right\}]\mathbf{B}_{ID}\right)^{-1} \\
& + \left(\mathbf{I}_{N_{ID}} + \mathbf{T}^H\mathbf{M}_2[tr\left\{\mathbf{T}\mathbf{T}^H\right\}]\mathbf{T}\right)^{-1}\Big| && (5.42a)\\
s.t. \ & tr\left\{\mathbf{B}_{ID}\mathbf{B}_{ID}^H\right\} \leq \kappa && (5.42b)\\
& tr\left\{\mathbf{T}\mathbf{T}^H\right\} \leq E_\kappa && (5.42c)\\
& && (5.42d)
\end{aligned}$$

where $E_\kappa = (P_\alpha - \kappa)\eta\lambda_{q,1}$, while the corresponding master problem is given as

$$\begin{aligned}
\min_{\kappa} \ & \mathfrak{I}_{SD}\{\alpha\}(\kappa) && (5.43a)\\
s.t. \ & 0 \leq \kappa \leq P_\alpha && (5.43b)
\end{aligned}$$

where $\mathfrak{I}_{SD}\{\alpha\}(\kappa)$ denotes the optimal value of the objective function (5.42a) with any given κ. It is obvious that the equality of (5.42b) and (5.42c) must be achieved with the optimal $\mathbf{B}_{ID}$ and $\mathbf{T}$. This is because (5.42a) is a monotonically decreasing function with respect to $tr\{\mathbf{B}_{ID}\mathbf{B}_{ID}^H\}$ and $tr\{\mathbf{T}\mathbf{T}^H\}$. Hence, $\mathbf{M}_1[tr\left\{\mathbf{B}_{ID}\mathbf{B}_{ID}^H\right\}] = \mathbf{M}_1[\kappa]$ and $\mathbf{M}_2[tr\left\{\mathbf{T}\mathbf{T}^H\right\}] = \mathbf{M}_2[E_\kappa]$ where

$$\mathbf{M}_1[\kappa] = \widehat{\mathbf{H}}_1^H\left(\phi_{1,1}\kappa\mathbf{\Sigma}_1 + \sigma_r^2\mathbf{I}_{N_R}\right)^{-1}\widehat{\mathbf{H}}_1 \tag{5.44}$$

$$\mathbf{M}_2[E_\kappa] = \widehat{\mathbf{H}}_2^H\left(\phi_{2,1}E_\kappa\mathbf{\Sigma}_2 + \sigma_d^2\mathbf{I}_{N_D}\right)^{-1}\widehat{\mathbf{H}}_2 \tag{5.45}$$

with the corresponding EVD given as

$$\mathbf{M}_1[\kappa] = \mathbf{V}_1\mathbf{\Lambda}_1[\kappa]\mathbf{V}_1^H \tag{5.46}$$

$$\mathbf{M}_2[E_\kappa] = \mathbf{V}_2\mathbf{\Lambda}_2[E_\kappa]\mathbf{V}_2^H \tag{5.47}$$

where the diagonal elements of $\mathbf{\Lambda}_1[\kappa]$ and $\mathbf{\Lambda}_2[E_\kappa]$ are sorted in descending order. Based on [79], the $\mathbf{V}_1$ and $\mathbf{V}_2$ do not depend on $\mathbf{B}_{ID}$ and $\mathbf{T}$ when $tr\{\mathbf{B}_{ID}\mathbf{B}_{ID}^H\}$ and $tr\{\mathbf{T}\mathbf{T}^H\}$ are constants. Based on Hadamard's inequality [101], for a positive semidefinite (PSD) matrix $\mathbf{X}$ of order N, the determinant of $\mathbf{X}$ follows the inequalities introduced as

$$|\mathbf{X}| \leq \prod_{i=1}^{N} x_i \tag{5.48}$$

where x_i denotes the ith diagonal element of $\mathbf{X}$. The equality of (5.48) is achieved when $\mathbf{X}$ is a diagonal matrix. Based on (5.48), the objective function (5.42a) is optimized when $\mathbf{B}_{ID}^H \mathbf{M}_1[\kappa]\mathbf{B}_{ID}$ and $\mathbf{T}^H \mathbf{M}_2[E_\kappa]\mathbf{T}$ are diagonal matrices. Hence, to diagonalize the objective function (5.42a), the optimal structure for $\mathbf{B}_{ID}$ and $\mathbf{T}$ are introduced as

$$\mathbf{B}_{ID}^* = \bar{\mathbf{V}}_1 \mathbf{\Lambda}_B^{\frac{1}{2}} \qquad \mathbf{T}^* = \bar{\mathbf{V}}_2 \mathbf{\Lambda}_T^{\frac{1}{2}} \tag{5.49}$$

where $\bar{\mathbf{V}}_1$ and $\bar{\mathbf{V}}_2$ contained the leftmost N_{ID} columns of $\mathbf{V}_1$ and $\mathbf{V}_2$ respectively while $\mathbf{\Lambda}_B$ and $\mathbf{\Lambda}_T$ are diagonal matrices of size N_{ID} with the corresponding ith diagonal element denoted as $\lambda_{b,i}$ and $\lambda_{t,i}$ for $i = 1, \cdots, N_{ID}$. By using (5.49), the optimization problem (5.42) is equivalently converted to a power allocation problem with scalar variables which is given as

$$\min_{\boldsymbol{\lambda}_b, \boldsymbol{\lambda}_t} \frac{1-\alpha}{2} \sum_{i=1}^{N_{ID}} \log\left(\frac{1}{1+\lambda_{1,i}\lambda_{b,i}} + \frac{1}{1+\lambda_{2,i}\lambda_{t,i}}\right) \tag{5.50a}$$

$$s.t. \sum_{i=1}^{N_{ID}} \lambda_{b,i} \leq \kappa \tag{5.50b}$$

$$\sum_{i=1}^{N_{ID}} \lambda_{t,i} \leq E_\kappa \tag{5.50c}$$

$$\lambda_{b,i} \geq 0 \quad \lambda_{t,i} \geq 0 \quad i = 1, \cdots, N_{ID} \tag{5.50d}$$

where $\boldsymbol{\lambda}_b = [\lambda_{b,1}, \cdots, \lambda_{b,N_{ID}}]^T$, $\boldsymbol{\lambda}_t = [\lambda_{t,1}, \cdots, \lambda_{t,N_{ID}}]^T$ and $\lambda_{1,i}$ and $\lambda_{2,i}$ denote the ith diagonal elements of $\mathbf{\Lambda}_1[\kappa]$ and $\mathbf{\Lambda}_2[E_\kappa]$ respectively. It is observed that the objective function (5.50a) is symmetric in $\boldsymbol{\lambda}_b$ and $\boldsymbol{\lambda}_t$. Moreover, the optimal $\boldsymbol{\lambda}_b$ and $\boldsymbol{\lambda}_t$ are having different transmission power constraint. Hence, the optimization problem (5.50) can be efficiently solved by using an iterative method [102, 113, 114], where the optimal $\boldsymbol{\lambda}_b$ and $\boldsymbol{\lambda}_t$ are iteratively updated until convergence.

With any fixed $\boldsymbol{\lambda}_t$, the optimal $\boldsymbol{\lambda}_b$ can be obtained by solving the power allocation problem given as

$$\min_{\boldsymbol{\lambda}_b} \frac{1-\alpha}{2} \sum_{i=1}^{N_{ID}} \log\left(\frac{1}{1+\lambda_{1,i}\lambda_{b,i}} + \frac{1}{z_i}\right) \tag{5.51a}$$

$$s.t. \sum_{i=1}^{N_{ID}} \lambda_{b,i} \leq \kappa \tag{5.51b}$$

$$\lambda_{b,i} \geq 0 \quad i = 1, \cdots, N_{ID} \tag{5.51c}$$

where $z_i = 1+\lambda_{2,i}\lambda_{t,i}$ for $i = 1, \cdots, N_{ID}$. By applying the KKT conditions, the optimal $\lambda_{b,i}$ for $i = 1, \cdots, N_{ID}$ is given as

$$\lambda_{b,i}^{*} = \frac{1}{2\lambda_{1,i}} \left(\sqrt{z_i^2 + \frac{4\lambda_{1,i} z_i}{\mu_1}} - z_i - 2 \right)^{+} \tag{5.52}$$

where $(x)^{+} = \max(0, x)$ and $\mu_1 > 0$ is the Lagrangian multiplier to (5.51b). μ_1 can be calculated by solving the equality of (5.51b) with $\lambda_{b,i}^{*}$ given in (5.52) using the bisection method.

Similarly, with any fixed $\boldsymbol{\lambda}_b$, the optimal $\boldsymbol{\lambda}_t$ can be obtained by solving the power allocation problem given as

$$\min_{\boldsymbol{\lambda}_t} \frac{1-\alpha}{2} \sum_{i=1}^{N_{ID}} \log \left(\frac{1}{y_i} + \frac{1}{1+\lambda_{2,i}\lambda_{t,i}} \right) \tag{5.53a}$$

$$s.t. \sum_{i=1}^{N_{ID}} \lambda_{t,i} \leq E_{\kappa} \tag{5.53b}$$

$$\lambda_{t,i} \geq 0 \quad i = 1, \cdots, N_{ID} \tag{5.53c}$$

where $y_i = 1+\lambda_{1,i}\lambda_{b,i}$ for $i = 1, \cdots, N_{ID}$. By applying the KKT conditions, the optimal $\lambda_{t,i}$ for $i = 1, \cdots, N_{ID}$ is given as

$$\lambda_{t,i}^{*} = \frac{1}{2\lambda_{2,i}} \left(\sqrt{y_i^2 + \frac{4\lambda_{2,i} y_i}{\mu_2}} - y_i - 2 \right)^{+} \tag{5.54}$$

where $\mu_2 > 0$ is the Lagrangian multiplier to (5.53b). μ_2 can be calculated by solving the equality of (5.53b) with $\lambda_{t,i}^{*}$ given in (5.54) using the bisection method. The proposed algorithm in solving the power allocation problem (5.50) is summarized in Algorithm 4, where ε_1 is a small positive number controlling the convergence of the algorithm.

With the optimal $\mathbf{B}_{ID}^{*}$ and $\mathbf{T}^{*}$ obtained via Algorithm 4, the master optimization problem (5.43) can be solved by using a one-dimensional search method to obtain the optimal κ. For the one-dimensional search method, the well-known golden section search method is used to obtain the optimal κ. The algorithm in solving the problem (5.43) is summarized in Algorithm 5 where $\delta = (1+\sqrt{5})/2$ is the golden number ratio and ε_2 is a small positive number controlling the convergence of the algorithm.

In the outer loop, the golden section search method [111] is used to find the optimal α. This is because the objective function (5.27a) is a unimodal function of α with its

Algorithm 4 Solving the problem (5.50) by an iterative method

Initialization: $\lambda_{b,i}^{\{0\}} = \frac{\kappa}{N_{ID}}$ and $\lambda_{t,i}^{\{0\}} = \frac{E_\kappa}{N_{ID}}$, $\forall i$

$n = 0$, flag $= 1$.
while flag $= 1$ **do**
  $n \leftarrow n + 1$.
  Find $\boldsymbol{\lambda}_b^{\{n\}}$ by solving (5.51) with fixed $\boldsymbol{\lambda}_t^{\{n-1\}}$.
  Find $\boldsymbol{\lambda}_t^{\{n\}}$ by solving (5.53) with fixed $\boldsymbol{\lambda}_b^{\{n\}}$.
  if $\max|\boldsymbol{\lambda}_b^{\{n\}} - \boldsymbol{\lambda}_b^{\{n-1\}}| \leq \varepsilon_1$ **then**
    if $\max|\boldsymbol{\lambda}_t^{\{n\}} - \boldsymbol{\lambda}_t^{\{n-1\}}| \leq \varepsilon_1$ **then**
      flag $= 0$, $m = n$.
    end if
  end if
end while
$\boldsymbol{\lambda}_b^* = \boldsymbol{\lambda}_b^{\{m\}}$ and $\boldsymbol{\lambda}_t^* = \boldsymbol{\lambda}_t^{\{m\}}$.
Compute $\mathbf{B}_{ID}^*$ and $\mathbf{T}^*$ as (5.49) with $\boldsymbol{\lambda}_b^*$ and $\boldsymbol{\lambda}_t^*$.

Algorithm 5 Solving the problem (5.43) by an one-dimensional search method

Initialization: $\delta = (1 + \sqrt{5})/2$, $\kappa_{lo} = 0$ and $\kappa_{up} = P_\alpha$

while $|\kappa_{up} - \kappa_{lo}| \geq \varepsilon_2$ **do**
  Set $k_1 = (\delta - 1)\kappa_{lo} + (2 - \delta)\kappa_{up}$.
  Set $k_2 = (2 - \delta)\kappa_{lo} + (\delta - 1)\kappa_{up}$.
  Compute $\mathcal{I}_{SD}\{\alpha\}(k_1)$ and $\mathcal{I}_{SD}\{\alpha\}(k_2)$.
  if $\mathcal{I}_{SD}\{\alpha\}(k_1) \geq \mathcal{I}_{SD}\{\alpha\}(k_2)$ **then**
    $\kappa_{lo} = k_1$.
  else
    $\kappa_{up} = k_2$.
  end if
end while
$\kappa^* = (\kappa_{lo} + \kappa_{up})/2$.

feasibility region of (5.27b) monotonically increasing with α. Hence, the optimal α can be obtained through the golden section search method with the golden number ratio. The procedure of the golden section search method is presented in Algorithm 6 where ε_3 is a small positive value which is used to control the convergence of the loop.

Algorithm 6 Golden Section Search Method to Find the Optimal α

Initialization: $\alpha_U = 1$ and $\alpha_L = 0$

while $|\alpha_U - \alpha_L| \geq \varepsilon_3$ **do**
  Set $a_1 = (\delta - 1)\alpha_L + (2 - \delta)\alpha_U$.
  Set $a_2 = (2 - \delta)\alpha_L + (\delta - 1)\alpha_U$.
  Compute $\mathcal{I}_{SD}\{a_1\}$ and $\mathcal{I}_{SD}\{a_2\}$.
  if $\mathcal{I}_{SD}\{a_1\} - \mathcal{I}_{SD}\{a_2\} \geq 0$ **then**
    $\alpha_U = a_2$.
  else
    $\alpha_L = a_1$.
  end if
end while
$\alpha^* = (\alpha_L + \alpha_U)/2$.
Compute $\mathcal{I}_{SD}\{\alpha^*\}$.

5.3.1 Peak Power Constraints

It is important to highlight the fact that when α approaches its boundary [6], i.e. $\alpha \to 0$ and $\alpha \to 1$, the transmission powers for the source node, i.e. $tr\{\mathbf{B}_{EH}\mathbf{B}_{EH}^H\}$ and $tr\{\mathbf{B}_{ID}\mathbf{B}_{ID}^H\}$ may approach infinity, while infinite transmission power is not achievable in practical scenario. Thus, to impose the practical peak power constraints to the optimization problem (5.39), $\hat{P}_s$ and $\hat{P}_r$ are introduced as the peak power limits at the source node and the relay node respectively, with the corresponding peak power transmission constraints given as $\lambda_e \leq \hat{P}_s$, $tr\{\mathbf{B}_{ID}\mathbf{B}_{ID}^H\} \leq \hat{P}_s$ and $tr\{\mathbf{T}\mathbf{T}^H\} \leq \widehat{P}_r$ and the optimization problem (5.39) with consideration of peak power limits is expressed as

$$\min_{\mathbf{B}_{ID},\mathbf{T}} \frac{1-\alpha}{2}\log\left|\left(\mathbf{I}_{N_{ID}}+\mathbf{B}_{ID}^H\mathbf{M}_1[tr\left\{\mathbf{B}_{ID}\mathbf{B}_{ID}^H\right\}]\mathbf{B}_{ID}\right)^{-1}\right.$$
$$\left.+\left(\mathbf{I}_{N_{ID}}+\mathbf{T}^H\mathbf{M}_2[tr\left\{\mathbf{B}_{ID}\mathbf{B}_{ID}^H\right\}]\mathbf{T}\right)^{-1}\right| \tag{5.55a}$$
$$s.t.\ \frac{tr\{\mathbf{T}\mathbf{T}^H\}}{\eta\lambda_{q,1}}+tr\{\mathbf{B}_{ID}\mathbf{B}_{ID}^H\}\le P_\alpha \tag{5.55b}$$
$$tr\{\mathbf{B}_{ID}\mathbf{B}_{ID}^H\}\le \widehat{P}_s \tag{5.55c}$$
$$tr\{\mathbf{T}\mathbf{T}^H\}\le \min\left(\hat{P}_r,\frac{2\alpha\eta\lambda_{q,1}}{1-\alpha}\hat{P}_s\right) \tag{5.55d}$$
$$\tag{5.55e}$$

Similar to the algorithm proposed to solve (5.39), when solving (5.55), the coupled transmission power constraint (5.55b) is decomposed by using the primal decomposition method with κ introduced as previous section. Thus, the subproblem (5.42) is extended to a subproblem with consideration of peak power limits which is given as

$$\min_{\mathbf{B}_{ID},\mathbf{T}} \frac{1-\alpha}{2}\log\left|\left(\mathbf{I}_{N_{ID}}+\mathbf{B}_{ID}^H\mathbf{M}_1[\vartheta_s]\mathbf{B}_{ID}\right)^{-1}+\left(\mathbf{I}_{N_{ID}}+\mathbf{T}^H\mathbf{M}_2[\vartheta_r]\mathbf{T}\right)^{-1}\right| \tag{5.56a}$$
$$s.t.\ tr\left\{\mathbf{B}_{ID}\mathbf{B}_{ID}^H\right\}\le\vartheta_s \tag{5.56b}$$
$$tr\left\{\mathbf{T}\mathbf{T}^H\right\}\le\vartheta_r \tag{5.56c}$$
$$\tag{5.56d}$$

where $\vartheta_s=\min(\kappa,\hat{P}_s)$, $\vartheta_r=\min(E_\kappa,\hat{P}_r,\frac{2\alpha\eta\lambda_{q,1}}{1-\alpha}\hat{P}_s)$ and

$$\mathbf{M}_1[\vartheta_s]=\widehat{\mathbf{H}}_1^H\left(\phi_{1,1}\vartheta_s\mathbf{\Sigma}_1+\sigma_r^2\mathbf{I}_{N_R}\right)^{-1}\widehat{\mathbf{H}}_1 \tag{5.57}$$
$$\mathbf{M}_2[\vartheta_r]=\widehat{\mathbf{H}}_2^H\left(\phi_{2,1}\vartheta_r\mathbf{\Sigma}_2+\sigma_d^2\mathbf{I}_{N_D}\right)^{-1}\widehat{\mathbf{H}}_2 \tag{5.58}$$

with the corresponding EVD given as

$$\mathbf{M}_1[\kappa]=\mathbf{V}_1\mathbf{\Lambda}_1[\vartheta_s]\mathbf{V}_1^H \tag{5.59}$$
$$\mathbf{M}_2[E_\kappa]=\mathbf{V}_2\mathbf{\Lambda}_2[\vartheta_r]\mathbf{V}_2^H \tag{5.60}$$

where the diagonal elements of $\mathbf{\Lambda}_1[\vartheta_s]$ and $\mathbf{\Lambda}_2[\vartheta_r]$ are sorted in descending order. The ith diagonal element of $\mathbf{\Lambda}_1[\vartheta_s]$ and $\mathbf{\Lambda}_2[\vartheta_r]$ are correspondingly denoted as $\widetilde{\lambda}_{1,i}$ and $\widetilde{\lambda}_{2,i}$ for $i=1,\cdots,N_{ID}$. By using (5.49), the optimization problem (5.56) is simplified to a power allocation problem given as

$$\min_{\boldsymbol{\lambda}_b,\boldsymbol{\lambda}_t} \frac{1-\alpha}{2}\sum_{i=1}^{N_{ID}} \log\left(\frac{1}{1+\widetilde{\lambda}_{1,i}\lambda_{b,i}}+\frac{1}{1+\widetilde{\lambda}_{2,i}\lambda_{t,i}}\right) \tag{5.61a}$$

$$s.t. \sum_{i=1}^{N_{ID}} \lambda_{b,i} \le \vartheta_s \tag{5.61b}$$

$$\sum_{i=1}^{N_{ID}} \lambda_{t,i} \le \vartheta_r \tag{5.61c}$$

$$\lambda_{b,i} \ge 0 \quad \lambda_{t,i} \ge 0 \quad i = 1, \cdots, N_{ID}. \tag{5.61d}$$

It can be noticed that the problem (5.61) has an identical form as the problem (5.50). Similarly, the optimal $\lambda_{b,i}$ and $\lambda_{t,i}$ with peak power limits can be efficiently obtained by using an iterative method. For $i = 1, \cdots, N_{ID}$, the optimal $\lambda_{b,i}$ with peak power limits at fixed $\boldsymbol{\lambda}_t$ is given as

$$\lambda_{b,i}^* = \frac{1}{2\widetilde{\lambda}_{1,i}}\left(\sqrt{\widetilde{z}_i^2 + \frac{4\widetilde{\lambda}_{1,i}\widetilde{z}_i}{\mu_a}} - \widetilde{z}_i - 2\right)^+ \tag{5.62}$$

where $\widetilde{z}_i = 1 + \widetilde{\lambda}_{2,i}\lambda_{t,i}$ for $i = 1, \cdots, N_{ID}$ and $\mu_a > 0$ is the Lagrangian multiplier to (5.61b). For $i = 1, \cdots, N_{ID}$, the optimal $\lambda_{t,i}$ with peak power limits at fixed $\boldsymbol{\lambda}_b$ is given as

$$\lambda_{t,i}^* = \frac{1}{2\widetilde{\lambda}_{2,i}}\left(\sqrt{\widetilde{y}_i^2 + \frac{4\widetilde{\lambda}_{2,i}\widetilde{y}_i}{\mu_b}} - \widetilde{y}_i - 2\right)^+ \tag{5.63}$$

where $\widetilde{y}_i = 1 + \widetilde{\lambda}_{1,i}\lambda_{b,i}$ for $i = 1, \cdots, N_{ID}$ and $\mu_b > 0$ is the Lagrangian multiplier to (5.61c). Moreover, μ_a and μ_b are the corresponding solution to

$$\sum_{i=1}^{N_{ID}} \frac{1}{2\widetilde{\lambda}_{1,i}}\left(\sqrt{\widetilde{z}_i^2 + \frac{4\widetilde{\lambda}_{1,i}\widetilde{z}_i}{\mu_a}} - \widetilde{z}_i - 2\right) = \vartheta_s \tag{5.64}$$

$$\sum_{i=1}^{N_{ID}} \frac{1}{2\widetilde{\lambda}_{2,i}}\left(\sqrt{\widetilde{y}_i^2 + \frac{4\widetilde{\lambda}_{2,i}\widetilde{y}_i}{\mu_b}} - \widetilde{y}_i - 2\right) = \vartheta_r. \tag{5.65}$$

In summary, the algorithm to solve the power allocation problem (5.61) with consideration of peak power limits is similar to the algorithm used to solve the problem (5.50) which is summarized in Algorithm 7, where ε_4 is a small positive number controlling the convergence of the algorithm.

Algorithm 7 Solving the problem (5.50) with Peak Power Limits

Initialization: $\lambda_{b,i}^{\{0\}} = \frac{\kappa}{N_{ID}}$ and $\lambda_{t,i}^{\{0\}} = \frac{E_\kappa}{N_{ID}}$, $\forall i$

$n = 0$, flag $= 1$.
while flag $= 1$ **do**
  $n \leftarrow n + 1$.
  Update $\boldsymbol{\lambda}_b^{\{n\}}$ with fixed $\boldsymbol{\lambda}_t^{\{n-1\}}$ by using (5.62).
  Update $\boldsymbol{\lambda}_t^{\{n\}}$ with fixed $\boldsymbol{\lambda}_b^{\{n\}}$ by using (5.63).
  if $\max|\boldsymbol{\lambda}_b^{\{n\}} - \boldsymbol{\lambda}_b^{\{n-1\}}| \leq \varepsilon_4$ **then**
    if $\max|\boldsymbol{\lambda}_t^{\{n\}} - \boldsymbol{\lambda}_t^{\{n-1\}}| \leq \varepsilon_4$ **then**
      flag $= 0$, $m = n$.
    end if
  end if
end while
$\boldsymbol{\lambda}_b^* = \boldsymbol{\lambda}_b^{\{m\}}$ and $\boldsymbol{\lambda}_t^* = \boldsymbol{\lambda}_t^{\{m\}}$.
Compute $\mathbf{B}_{ID}^*$ and $\mathbf{T}^*$ as (5.49) with $\boldsymbol{\lambda}_b^*$ and $\boldsymbol{\lambda}_t^*$.

5.4 Numerical Example

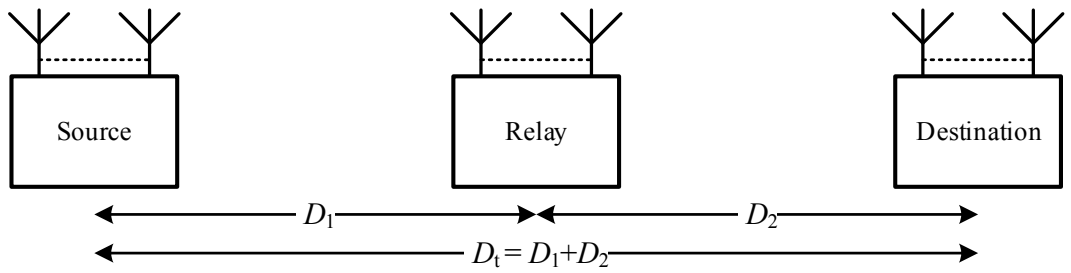

Figure 5.3: Location of the source, relay, and destination nodes in the relay communication system.

In this section, the system performance of the proposed robust transceiver designs is investigated without peak power limits (Robust w/o Peak Limits) and with peak power limits (Robust w Peak Limits). The peak power limits are given as $\widehat{P}_s = \widehat{P}_r = gP_s$, $(g \geq 1)$. The nodes in the relay communication system is placed as illustrated in Fig. 5.3, where the distance between the source and relay node, D_1 is set as $D_1 = 10d$ meters and

the distance between the relay and destination node, D_2 is set as $D_2 = 10(2-d)$ meters. The distance between the source and the destination node, i.e., the total distance, is set as $D_t = 20$ meters. The value of d, $(0 < d < 2)$, is normalized over a distance of 10 meters, so the relay position can be easily determined, i.e., when $D_1 < D_2$, the relay is placed closer to the source node, while $D_2 < D_1$ indicates the relay node is placed closer to the destination node. With $0.2 \leq d \leq 1.8$, $D_1 \geq 2$meters and $D_2 \geq 2$ meters.

With the consideration of channel pathloss, the channel matrices $\mathbf{H}_1$ and $\mathbf{H}_2$ are correspondingly modelled as $\mathbf{H}_1 = D_1^{-\xi/2}\left(\widehat{\mathbf{H}}_1 + \mathbf{\Delta}_1\right)$ and $\mathbf{H}_2 = D_2^{-\xi/2}\left(\widehat{\mathbf{H}}_2 + \mathbf{\Delta}_2\right)$, where $D_1^{-\xi/2}$ and $D_2^{-\xi/2}$ denote the large scale pathloss of the source-relay link and the relay-destination link, respectively, ξ denotes the pathloss exponent which $\xi = 3$ (suburban communication case) [104]. Based on the Gaussian-Kronecker model, the estimated channel matrices $\widehat{\mathbf{H}}_1$ and $\widehat{\mathbf{H}}_2$ are constructed as

$$\widehat{\mathbf{H}}_1 = \sqrt{\frac{1-\sigma_e^2}{\sigma_e^2}}\mathbf{\Sigma}_1^{\frac{1}{2}}\widehat{\mathbf{H}}_{\omega,1}\mathbf{\Phi}_1^{\frac{1}{2}} \qquad \widehat{\mathbf{H}}_2 = \sqrt{\frac{1-\sigma_e^2}{\sigma_e^2}}\mathbf{\Sigma}_2^{\frac{1}{2}}\widehat{\mathbf{H}}_{\omega,2}\mathbf{\Phi}_2^{\frac{1}{2}} \tag{5.66}$$

where σ_e^2 stands for the variance of estimation error, while $\widehat{\mathbf{H}}_{\omega,1}$ and $\widehat{\mathbf{H}}_{\omega,2}$ are complex Gaussian matrices whose entries are i.i.d. with zero mean and variance of $1/N_S$ and $1/N_R$ respectively. The transmit and receive antennas correlation matrices for $\mathbf{H}_1$ and $\mathbf{H}_2$ [110] are simulated as

$$\begin{aligned}
[\mathbf{\Phi}_1]_{ij} &= \sigma_e^2\beta_t^{|i-j|} \quad i,j = 1,\cdots,N_S \\
[\mathbf{\Sigma}_1]_{ij} &= \beta_r^{|i-j|} \quad i,j = 1,\cdots,N_R \\
[\mathbf{\Phi}_2]_{ij} &= \sigma_e^2\beta_t^{|i-j|} \quad i,j = 1,\cdots,N_R \\
[\mathbf{\Sigma}_2]_{ij} &= \beta_r^{|i-j|} \quad i,j = 1,\cdots,N_D
\end{aligned}$$

where $[\cdot]_{ij}$ stands for the ith row jth column matrix entry, $\beta_t \in [0,1]$ and $\beta_r \in [0,1]$ denote the correlation coefficients of the transmit and receive antenna correlation matrices. The noise variance at the relay and destination nodes are set as $\sigma_r^2 = \sigma_d^2 = -50$dBm. For numerical examples, $\beta_t = 0.1$, $\beta_r = 0.2$, $\eta = 0.8$, and $\varepsilon_1 = \varepsilon_2 = \varepsilon_3 = \varepsilon_4 = \varepsilon = 10^{-8}$. For the numerical examples, the obtained results are averaged through 1000 independent channel realizations. The proposed algorithms with robustness are compared to the upper-bound based algorithm developed in [54] using the estimated CSI which is denoted as (Non-Robust w/o Peak Limits). The upper-bound based algorithm developed in [54] using the full CSI which is denoted as (FCSI w/o Peak Limits) is set as the benchmark in the simulations. It is important to noted that the performance of the

algorithm using FCSI is not achievable in practice due to the absence of perfect CSI in the practical scenario.

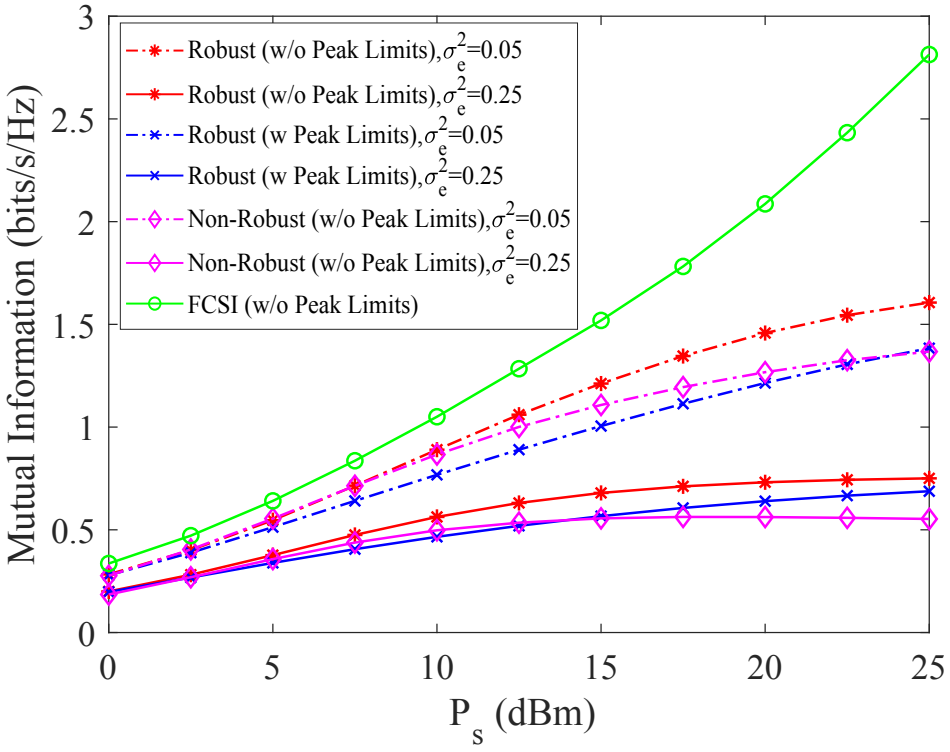

Figure 5.4: Example 1: MI versus P_s with $g = 2$, $d = 1$ and $N_S = N_R = N_D = 3$ at $\sigma_e^2 = 0.05$ and $\sigma_e^2 = 0.25$.

In numerical example 1, the system MI for the tested algorithms versus P_s at different σ_e^2 is investigated. Fig. 5.4 illustrates the MI performance versus P_s at $g = 2$, $d = 1$ and $N_S = N_R = N_D = 3$ with $\sigma_e^2 = 0.05$ and $\sigma_e^2 = 0.25$. It is noticeable that the FCSI algorithm provides an upper-bound of the system MI for the tested system. When σ_e^2 is sufficiently small, it is observed that the system MI for tested algorithms is approaching the MI performance of the FCSI algorithm. The observation indicates that the CSI with large channel estimation error would significantly degrade the system performance. It can also be observed that system MI provided by the proposed robust algorithm without peak power limits is better than the existing algorithm in both cases where $\sigma_e^2 = 0.05$ and $\sigma_e^2 = 0.25$. It is also noted that the MI performance of the non-robust algorithm without peak power limits is worse than the robust algorithm with peak power limits ($g = 2$) at relatively large P_s. The proposed algorithm provides robustness for the

system to combat the channel estimation error. Compared to the existing algorithms, the proposed algorithm provides better system MI in the practical scenario where the CSI mismatch is unavoidable. Moreover, when the channel mismatch is sufficiently small, the proposed algorithm is capable of providing equivalent performance as the FCSI algorithm.

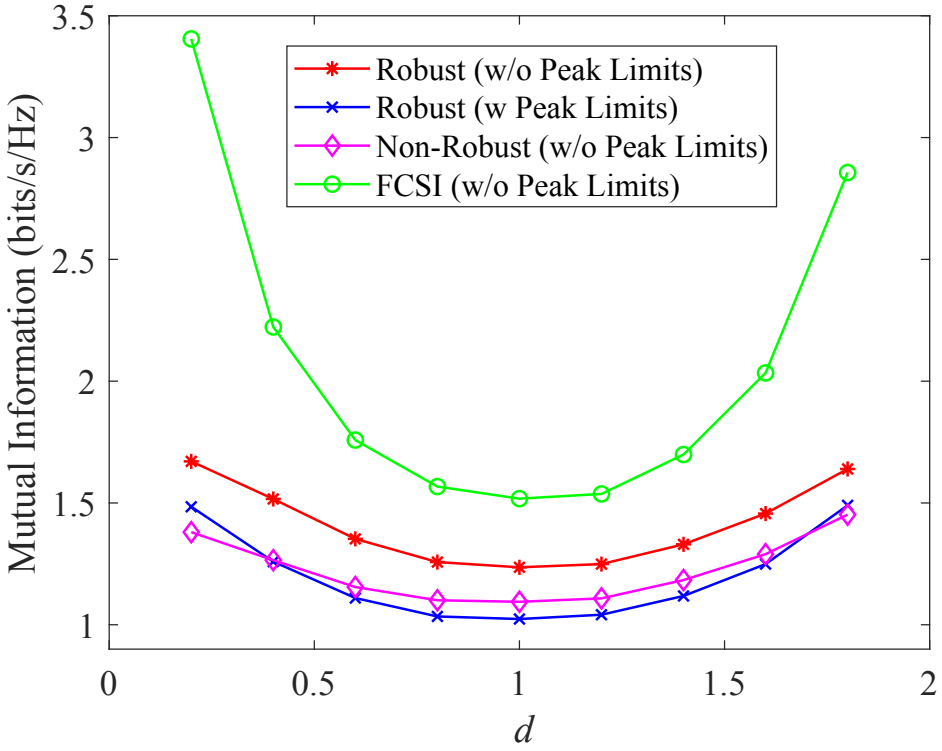

Figure 5.5: Example 2: MI versus d with $g = 2$, $P_s = 15$dBm, $\sigma_e^2 = 0.05$ and $N_S = N_R = N_D = 3$.

In numerical example 2, the system MI of the tested algorithms is investigated at various relay positions. Fig. 5.5 demonstrates the MI performance of the tested algorithms across various d with $P_s = 15$dBm, $\sigma_e^2 = 0.05$ and $N_S = N_R = N_D = 3$. It is noticeable the system MI is higher when the relay node is placed closer to the source node or the destination node. This is because when the relay node is placed closer to the source node, the RF energy transmission loss at the source-relay link is reduced, which increases the amount of energy harvested at the relay node. Hence, the MI performance is enhanced. When the relay node is placed further from the source node, i.e., located closer to the destination node, the harvested energy is greatly reduced. However, due to

the shorter relay-destination distance, the MI performance of the system is improved. It can be noticed that the FCSI algorithm provides an upper-bound for the system MI at various d. Moreover, the proposed robust algorithm without peak power limits provides better system MI compared to the non-robust algorithm without peak power limits developed in [54] at any relay node position. It is also interesting to note that the proposed robust algorithm with peak power limits have better performance compared to the non-robust algorithm without peak power limits when the relay is located relatively close to the source node and the destination node.

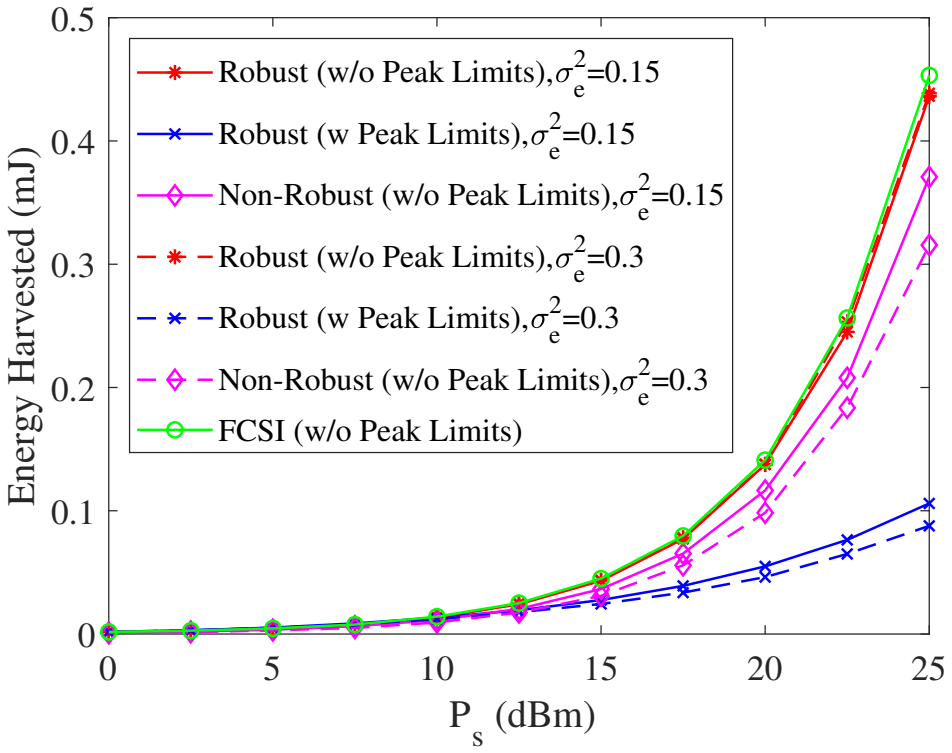

Figure 5.6: Example 3: Harvested energy at the relay node versus P_s with $g = 2$, $d = 1$, and $N_S = N_R = N_D = 3$ at $\sigma_e^2 = 0.15$ and $\sigma_e^2 = 0.3$.

In numerical example 3, the amount of energy harvested at the relay node is investigated for the tested algorithms. Fig. 5.6 illustrates the harvested at the relay node versus P_s at $g = 2$, $d = 1$, $\sigma_e^2 = 0.05$, and $N_S = N_R = N_D = 3$. With the increase of σ_e^2, the energy harvested at the relay node for the existing non-robust algorithm is reduced. This is because of the CSI mismatch is ignored in the existing non-robust algorithm. Hence, a portion of the channel is neglected when optimizing the $\mathbf{B}_{EH}$ to maximize the

energy harvested at the relay node. Moreover, it is noticed that the energy harvested at the relay node for the proposed algorithm at any σ_e^2 is almost identical to the FCSI algorithm. This observation indicated that the proposed algorithm are capable to tackle the CSI mismatch and provide almost equivalent harvested energy at the relay node as if the full CSI is available. Besides, it is also noted that the CSI mismatch does not only impact the system MI but also significantly reduce the energy harvested at the relay node.

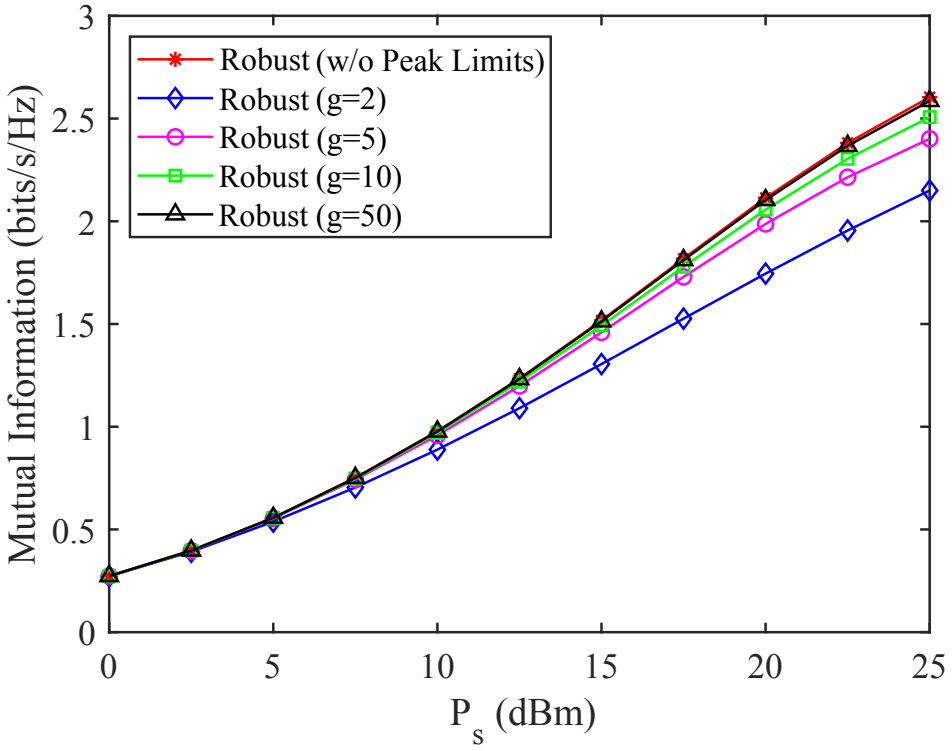

Figure 5.7: Example 4: MI versus P_s with different g at $d = 1$, $\sigma_e^2 = 0.01$, and $N_S = N_R = N_D = 3$.

In numerical example 4, the influence of the peak power limits on the system MI is investigated. Fig. 5.7 shows the system MI versus P_s with various peak power limits at $g = 2$. $g = 5$, $g = 10$ and $g = 50$ for the proposed algorithm with robustness at $d = 1$, $\sigma_e^2 = 0.01$ and $N_S = N_R = N_D = 3$. The MI performance of the algorithm without peak power limits served as an upper-bound for the MI performance of the algorithm with peak power limits. It is noted that the system MI increases with the increment of g. When g is sufficiently large, the system MI for the algorithm with peak power limits

is almost identical to the algorithm without peak power limits. This is because the peak power constraints are easier to be satisfied when the peak power limits are larger. It also indicated that the optimization problem (5.55) is an extension to the optimization problem (5.39) with the introduction of peak power limits.

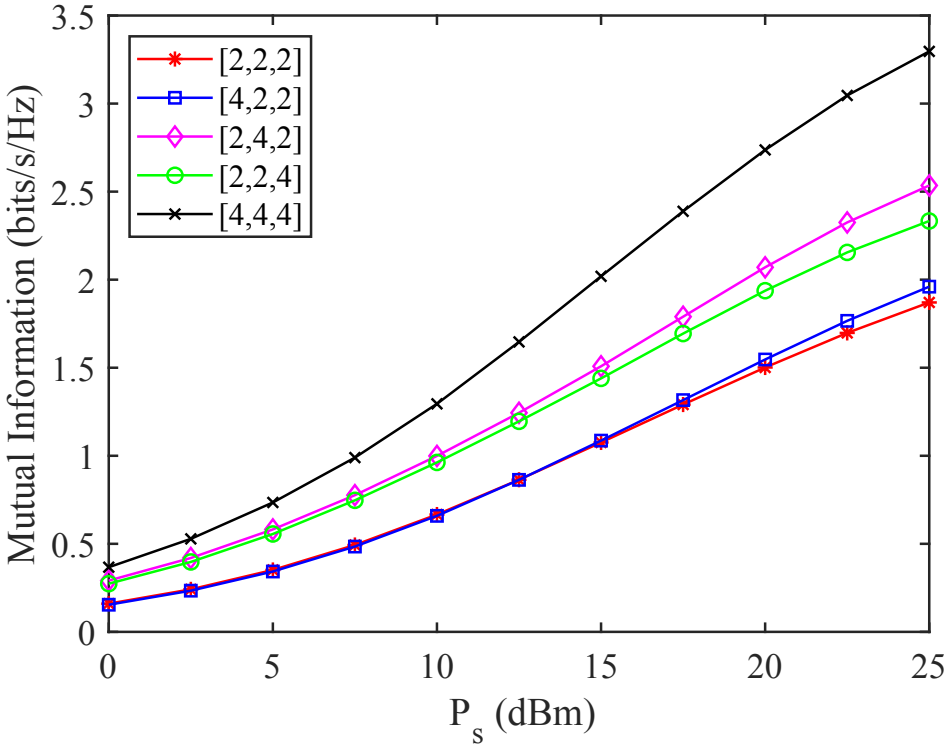

Figure 5.8: Example 5: MI versus P_s for robust transceiver design without peak power limits at different $[N_S,N_R,N_D]$ at $g = 2$, $d = 1$ and $\sigma_e^2 = 0.01$.

In numerical example 5, the study concerning the influence of the number of antennas at the system nodes towards the system MI is carried out. Fig. 5.8 displays the MI performance versus P_s at different combination of $[N_S,N_R,N_D]$ for the robust algorithm without peak power constraint at $d = 1$ and $\sigma_e^2 = 0.01$. When the number of antennas at all system nodes increases from 2 to 4, it can be noticed that the system MI increases significantly. This is because, with the increase of the number of antennas at all system nodes, N_{ID} of the given system is also increased. The system MI improved with a higher number of concurrent data streams. It can be noticed that when only the number of the antenna at the source node increase, i.e., from the $[2, 2, 2]$ combination to the $[4, 2, 2]$ combination, the system MI increases slightly. This shows that the number of antennas

at the source node does not heavily influence the MI performance of the system. On the other hand, when the number of antennas at the relay node or destination node increases, the system MI greatly increases. This is because the transmission energy available at the relay node is smaller than the transmission power available at the source node. Thus, increasing the number of antennas at the relay node or destination node helps in improving the system MI. Compared between the $[2, 4, 2]$ combination and the $[2, 2, 4]$ combination, it is more beneficial to increase the number of antennas at the relay node.

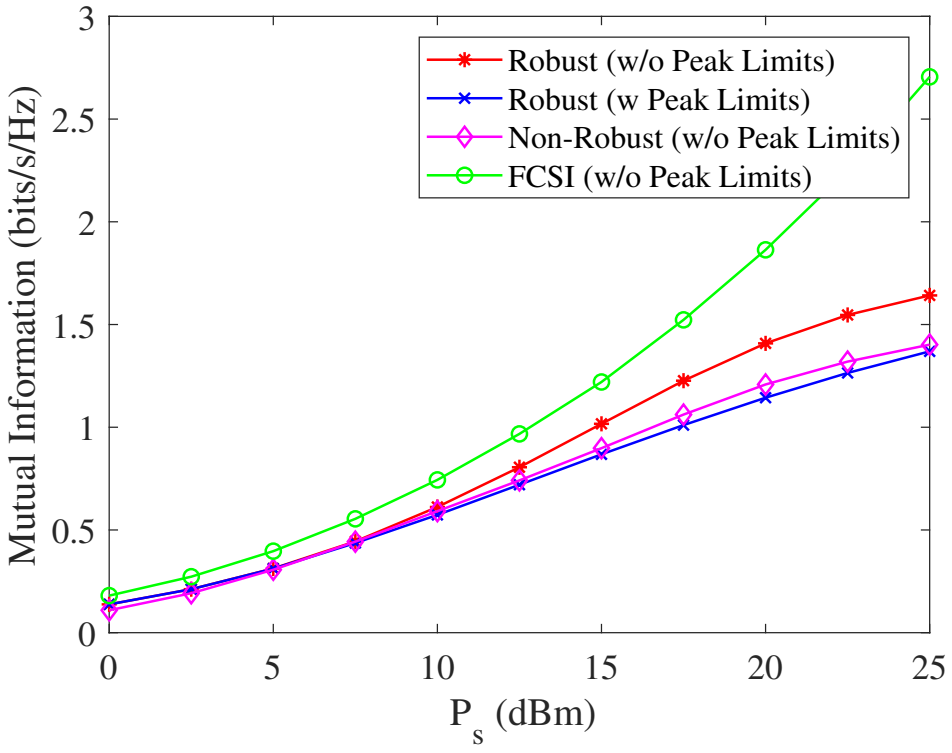

Figure 5.9: Example 6: MI versus P_s with $g = 2$, $d = 1$ and $N_S = N_R = N_D = 3$ at $\sigma_e^2 = 0.05$.

In the last numerical example, the performance of the proposed algorithms is investigated for the scenario where the CSI mismatch matrices is different to the presumed one. Follows [49], the CSI mismatch matrices are modelled as Gaussian random matrices with zero mean and variances equal to σ_e^2. In this numerical example, the CSI mismatch matrices are uncorrelated with $\mathbf{H}_{SR}$ and $\mathbf{H}_{RD}$. It is noticeable that the proposed algorithm are providing better performance as compared to the non-robust

algorithm. Besides, it is observed that even though the CSI mismatch model is different to the presumed one, the proposed algorithms achieves a good performance. Compared to Fig. 5.4, it can be observed that the MI performance are almost identical. This indicated that the proposed algorithms are robust against the difference in the applied CSI mismatch model.

5.5 Chapter Summary

In this chapter, the robust transceiver design for two hop AF MIMO relay communication systems with the TSR protocol is investigated. The transceiver design with robustness assists in reducing the degradation caused by the CSI mismatch between the exact and estimated CSI available in the system. With the consideration of CSI mismatch, it can be seen that the optimization problem is more difficult to solve. The KKT conditions with the primal decomposition method are used in solving the source and relay precoding matrices optimization problem. By using the golden section search method, the optimal TS factor can be obtained. It is demonstrated through numerical simulations that the proposed transceiver design with robustness provides better performance compared to the non-robust transceiver design.

Chapter 6

Conclusions and Future Works

Firstly, the impact of the channel estimation error is investigated for a general MIMO relay communication system. In the system considered in Chapter 2, multiple transmitters communicated with multiple receivers while the information signals are transmitted over multiple relay nodes arranged in series. Next, the general SWIPT relaying protocol with the combination of TSR and PSR protocol is investigated in Chapter 3. The studies show that the HPTSR protocol can provide a higher degree of freedom in optimizing the system performance while providing better performance compared to the existing EH relaying scheme. Then, the influence of the channel estimation error is investigated for the DF MIMO relay communication system with the TSR protocol. The CSI mismatch heavily degraded the system performance provided by the existing algorithm. Hence, the proposed algorithm provides robustness to counter the CSI mismatch. The AF MIMO relay communication system is also investigated with the consideration of CSI mismatch with the relay node adapting the TSR protocol. It is noticed that the proposed algorithms provided in Chapter 4 and Chapter 5 are better than the existing algorithms.

6.1 Concluding Remarks

In Chapter 2, the problem of robust transceiver design for multi-hop multicasting AF MIMO relay systems from multiple sources is investigated with the consideration of channel mismatch between the exact and estimated signal waveform. Multiple source nodes broadcast their message to a group of destination nodes through multiple relay

nodes in the investigated system. In the proposed transceiver design, the Gaussian-Kronecker model was adopted for the CSI mismatch. Furthermore, a robust transceiver design algorithm was developed to jointly optimize the source, relay, and destination matrices to minimize the maximal WMSE of the received signal at all destination nodes. It can be noticed that the WMSE is made statistically robust against the CSI mismatch by averaging through the distributions of the exact CSI. Moreover, the WMSE decomposition was exploited in the proposed transceiver design to reduce the computational complexity of the transceiver optimization problem. Numerical examples demonstrated improved performance of the proposed transceiver optimization algorithm against the channel mismatch between the exact and estimated signals waveform.

In Chapter 3, the transceiver design for a dual-hop MIMO AF relay communication system with the HPTSR-based EH relaying protocol is investigated. The architecture of the HPTSR-based protocol combines the TS-based and PS-based EH relaying protocols. The optimal structure of the source and relay precoding matrices is proposed to convert the highly challenging joint transceiver design problem to a joint transceiver power allocation problem with low complexity. Two algorithms are derived to solve the optimal power allocation problem. In general, the two proposed algorithms provide a better MI performance compared to existing TSR and PSR based algorithms. It is noticed that the system MI performance is better when the relay node is located closer to the source or destination nodes. Moreover, the MI performance of the system can be improved by installing more antennas at the relay node.

In Chapter 4, the transceiver design with robustness for dual-hop DF MIMO relay communication system with the relay node adapting the TS-based EH protocol is investigated. The transceiver design with robustness helps mitigate the degradation caused by the CSI mismatch between the exact and estimated CSI available in the system. With the consideration of CSI mismatch, the optimization problem is more challenging to solve. Under a fixed power scheme, the KKT conditions are applied to solve the source and relay precoding matrices optimization problem. The primal decomposition method is applied to solve the source and relay precoding matrices optimization problem under flexible power schemes. For the fixed power scheme and/or flexible power scheme, the optimal TS factor is obtained using the golden section search method. The proposed transceiver design with robustness provides better performance than the non-robust transceiver design, as shown through numerical examples.

In Chapter 5, the transceiver design for two hops AF MIMO relay communication system with TSR protocol is investigated under the consideration of channel estimation error. The transceiver design with robustness helps reduce the degradation caused by the CSI mismatch between the exact and estimated CSI available in the system. With the consideration of CSI mismatch, the optimization problem is more challenging to solve. The source and relay precoding matrices optimization problem is solved by using the KKT conditions and the primal decomposition method. The optimized TS factor is obtained by using the golden section search method. The proposed transceiver design with robustness provides better performance than the non-robust transceiver design, as shown through numerical examples.

6.2 Future Works

In this thesis, several advanced signal processing algorithms have been developed. For example, in Chapter 2, a robust transceiver design is developed for a multi-hop MIMO relay multicasting system with multiple sources for AF relaying scheme, while in Chapter 3, an innovative EH relaying scheme is proposed with the source and relay precoding matrices, the TS factor and the PS ratio matrix jointly optimized. In Chapter 4, the existing TSR protocol is investigated for MIMO DF relaying scheme with the consideration of CSI mismatch, and algorithms with robustness are proposed to combat against the channel estimation error. Lastly, in Chapter 5, the existing TSR protocol is investigated for MIMO AF relaying scheme with the consideration of CSI mismatch, and algorithms with robustness are proposed to improve the existing algorithm where the channel estimation error heavily degrades the performance of the existing algorithm. However, there are still many possibilities for extending this dissertation work.

The research works which can be considered in the future prior to the innovative knowledge provided in the Chapter 2 are

- Application of SWIPT in multi-hop MIMO relay system with the relay nodes considered as energy-limited wireless devices can be investigated. The TSR and/or PSR protocol can be adapted by the relay node to harvest the RF signals transmitted by the previous node. It has been shown in [19] that EH relays capable of providing equivalent diversity gain as self-powered relays. Hence, this is a promising way to improve the multi-hop MIMO relay system to be more eco-friendly.

- The relaying scheme used in Chapter 2 is the AF relaying scheme. Compared to AF relaying scheme, DF relaying scheme provide better system performance as the DF relaying scheme did not amplified the noise induced at the relay node. Thus, the investigation for DF multi-hop MIMO relay multicasting system with multiple source node can be carried out.

- Linear precoding technique is adapted at the source and relay node. Thus, the work performend in Chapter 2 can be extended to the non-linear precoding technique. There are two well-known non-linear precoding techniques known as the Tomlinson-Harashima precoding method and the Decision-Feedback Equalizer precoding method. It will be interesting to investigate the performance of the multi-hop MIMO relay multicasting system with non-linear precoding technique.

The research works which can be considered in the future prior to the innovative knowledge provided in the Chapter 3 are

- The MIMO relay system with the HPTSR protocol introduced in Fig.1.6 can be investigated. With the framework illustrated in Fig. 1.6, the source node can have optimized time-sequence allocated for the information transmission. Moreover, the HPTSR protocol can provide a higher degree of freedom to the system in optimizing the system performance.

- The system performance for MIMO relay multicasting system with the relay node adapting the HPTSR protocol introduced in Chapter 3 can be investigated. As the relay node can harvest more energy by using the HPTSR protocol, it would be interesting to test the limit of the system by letting the relay node multicast the information signals to multiple destination nodes. It is important for the next-generation wireless communication system to multicast a similar signal to a group of receivers. For instance, the students who participate in the e-classroom are needed to receive the information signal transmitted from the teacher simultaneously.

- The system performance for MIMO regenerative relay system with the DF relay node adapting the HPTSR protocol introduced in Chapter 3 can be investigated. The DF relaying scheme provides better performance than the AF relaying scheme as it does not amplify and transmit the noise introduced at the relay node. However, the decoding cost introduced to decode the received signal might be a burden

to energy-constrained relay. Thus, with the HPTSR protocol introduced to the relay node, the additional energy can support the decoding cost and improve the system MI.

The research works which can be considered in the future prior to the innovative knowledge provided in the Chapter 4 are

- The system performance for the DF MIMO relay system with the PSR protocol under the consideration of channel estimation error can be investigated and optimized. Compared to the TSR protocol, the PSR protocol does not require perfect time synchronisation and information and/or energy arrangement. However, it is more mathematically challenging to solve the MIMO relay system with the relay node adopting the PSR protocol under the consideration of CSI mismatch. Hence, it is an interesting topic to be tackled to improve the SWIPT MIMO relay communication system.

- The system performance for the application of TSR protocol in DF MIMO relay system with multiple source nodes can be investigated. It is clear that the energy harvested at the relay node is significantly increased when multiple source nodes transmit individual energy-bearing signals to the relay node. Thus, it would be interesting to investigate the system performance of the DF MIMO relay system when the relay node is receiving information from multiple transmitter.

- Linear precoding technique is adapted at the source and relay node. Thus, the work performed in Chapter 4 can be extended to the non-linear precoding technique. The investigation for the performance of the SWIPT DF MIMO relay system with a non-linear precoding technique can be carried out.

The research works which can be considered in the future prior to the innovative knowledge provided in the Chapter 5 are

- The system performance for the AF MIMO relay system with the PSR protocol under the consideration of channel estimation error can be investigated and optimized. Compared to the TSR protocol, the PSR protocol does not require perfect time synchronisation and information and/or energy arrangement. However, it is more mathematically challenging to solve the MIMO relay system with the relay node adopting the PSR protocol under the consideration of CSI mismatch.

Hence, it is an interesting topic to be tackled to improve the SWIPT MIMO relay communication system.

- The system performance for the application of TSR protocol in AF MIMO relay multicasting system can be investigated. With multiple destination node considered in the system, it is interesting to investigate the system performance. The behavior of the energy-constricted relay node in single destination node system might be different to the energy-constricted relay node in multiple destination nodes system. Thus, an investigation regarding AF MIMO relay multicasting system with the TSR protocol can be carried out in the future.

- Linear precoding technique is adapted at the source and relay node. Thus, the work performed in Chapter 5 can be extended to the non-linear precoding technique. The investigation for the system performance of the SWIPT AF MIMO relay system with either using the Tomlinson-Harashima precoding method and/or the Decision-Feedback Equalizer precoding method can be carried out.

Bibliography

[1] K. Xiong, P. Fan, C. Zhang, and K. B. Letaief, "Wireless information and energy transfer for two-hop non-regenerative MIMO-OFDM relay networks," *IEEE Journal on Selected Areas in Communications*, vol. 33, no. 8, pp. 1595–1611, Aug 2015.

[2] L. R. Varshney, "Transporting information and energy simultaneously," in *2008 IEEE International Symposium on Information Theory*, July 2008, pp. 1612–1616.

[3] J. Huang, Y. Zhou, Z. Ning, and H. Gharavi, "Wireless power transfer and energy harvesting: Current status and future prospects," *IEEE Wireless Communications*, vol. 26, no. 4, pp. 163–169, 2019.

[4] P. Grover and A. Sahai, "Shannon meets tesla: Wireless information and power transfer," in *2010 IEEE International Symposium on Information Theory*, June 2010, pp. 2363–2367.

[5] X. Zhou, R. Zhang, and C. K. Ho, "Wireless information and power transfer: Architecture design and rate-energy tradeoff," *IEEE Transactions on Communications*, vol. 61, no. 11, pp. 4754–4767, November 2013.

[6] R. Zhang and C. K. Ho, "MIMO broadcasting for simultaneous wireless information and power transfer," *IEEE Transactions on Wireless Communications*, vol. 12, no. 5, pp. 1989–2001, May 2013.

[7] D. W. K. Ng, E. S. Lo, and R. Schober, "Robust beamforming for secure communication in systems with wireless information and power transfer," *IEEE Transactions on Wireless Communications*, vol. 13, no. 8, pp. 4599–4615, Aug 2014.

[8] Y. Rong, *MIMO Relay*. Cham: Springer International Publishing, 2018, pp. 1–4.

[9] A. C. Cirik, Y. Rong, and Y. Hua, "Achievable rates of full-duplex MIMO radios in fast fading channels with imperfect channel estimation," *IEEE Transactions on Signal Processing*, vol. 62, no. 15, pp. 3874–3886, 2014.

[10] Y. Fan and J. Thompson, "MIMO configurations for relay channels: Theory and practice," *IEEE Transactions on Wireless Communications*, vol. 6, no. 5, pp. 1774–1786, 2007.

[11] A. A. Nasir, X. Zhou, S. Durrani, and R. A. Kennedy, "Relaying protocols for wireless energy harvesting and information processing," *IEEE Transactions on Wireless Communications*, vol. 12, no. 7, pp. 3622–3636, July 2013.

[12] Z. Ding, S. M. Perlaza, I. Esnaola, and H. V. Poor, "Simultaneous information and power transfer in wireless cooperative networks," in *2013 8th International Conference on Communications and Networking in China (CHINACOM)*, Aug 2013, pp. 252–255.

[13] Z. Ding, S. M. Perlaza, I. Esnaola, and H. V. Poor, "Power allocation strategies in energy harvesting wireless cooperative networks," *IEEE Transactions on Wireless Communications*, vol. 13, no. 2, pp. 846–860, 2014.

[14] H. Chen, Y. Li, Y. Jiang, Y. Ma, and B. Vucetic, "Distributed power splitting for SWIPT in relay interference channels using game theory," *IEEE Transactions on Wireless Communications*, vol. 14, no. 1, pp. 410–420, 2015.

[15] H. Liu, K. J. Kim, K. S. Kwak, and H. Vincent Poor, "Power splitting-based SWIPT with decode-and-forward full-duplex relaying," *IEEE Transactions on Wireless Communications*, vol. 15, no. 11, pp. 7561–7577, 2016.

[16] J. Guo, S. Zhang, N. Zhao, and X. Wang, "Performance of SWIPT for full-duplex relay system with co-channel interference," *IEEE Transactions on Vehicular Technology*, vol. 69, no. 2, pp. 2311–2315, 2020.

[17] C. Zhong, H. A. Suraweera, G. Zheng, I. Krikidis, and Z. Zhang, "Wireless information and power transfer with full duplex relaying," *IEEE Transactions on Communications*, vol. 62, no. 10, pp. 3447–3461, Oct 2014.

[18] M. Abedi, H. Masoumi, and M. J. Emadi, "Power splitting-based SWIPT systems with decoding cost," *IEEE Wireless Communications Letters*, vol. 8, no. 2, pp. 432–435, 2019.

[19] Z. Ding, I. Krikidis, B. Sharif, and H. V. Poor, "Wireless information and power transfer in cooperative networks with spatially random relays," *IEEE Transactions on Wireless Communications*, vol. 13, no. 8, pp. 4440–4453, 2014.

[20] R. Tao, A. Salem, and K. A. Hamdi, "Adaptive relaying protocol for wireless power transfer and information processing," *IEEE Communications Letters*, vol. 20, no. 10, pp. 2027–2030, 2016.

[21] S. Atapattu and J. Evans, "Optimal energy harvesting protocols for wireless relay networks," *IEEE Transactions on Wireless Communications*, vol. 15, no. 8, pp. 5789–5803, 2016.

[22] Y. Ye, Y. Li, L. Shi, R. Q. Hu, and H. Zhang, "Improved hybrid relaying protocol for DF relaying in the presence of a direct link," *IEEE Wireless Communications Letters*, vol. 8, no. 1, pp. 173–176, 2019.

[23] G. Li, D. Mishra, Y. Hu, and S. Atapattu, "Optimal designs for relay-assisted NOMA networks with hybrid SWIPT scheme," *IEEE Transactions on Communications*, vol. 68, no. 6, pp. 3588–3601, 2020.

[24] F. K. Ojo and M. F. Mohd Salleh, "Secrecy analysis of SWIPT-enabled cooperative networks with DF HPTSR protocol," *IEEE Access*, vol. 6, pp. 65 996–66 006, 2018.

[25] Y. Liu, R. Xiao, J. Shen, H. Yang, and C. Yan, "Performance analysis for hybrid AF relaying protocol in SWIPT systems with direct link," in *2019 IEEE/CIC International Conference on Communications Workshops in China (ICCC Workshops)*, 2019, pp. 109–113.

[26] F. K. Ojo and M. F. Mohd Salleh, "Throughput analysis of a hybridized power-time splitting based relaying protocol for wireless information and power transfer in cooperative networks," *IEEE Access*, vol. 6, pp. 24 137–24 147, 2018.

[27] A. J. Paulraj, D. A. Gore, R. U. Nabar, and H. Bolcskei, "An overview of MIMO communications - a key to gigabit wireless," *Proceedings of the IEEE*, vol. 92, no. 2, pp. 198–218, 2004.

[28] T. Jiang, D. Chen, C. Ni, and D. Qu, "Chapter 9 - MIMO OQAM/ FBMC," in *OQAM/FBMC for Future Wireless Communications*, T. Jiang, D. Chen, C. Ni, and D. Qu, Eds. Academic Press, 2018, pp. 213 – 245.

[29] S. M. Alamouti, "A simple transmit diversity technique for wireless communications," *IEEE Journal on Selected Areas in Communications*, vol. 16, no. 8, pp. 1451–1458, 1998.

[30] V. Tarokh, N. Seshadri, and A. R. Calderbank, "Space-time codes for high data rate wireless communication: performance criterion and code construction," *IEEE Transactions on Information Theory*, vol. 44, no. 2, pp. 744–765, 1998.

[31] M. A. Reşat, M. C. Karakoç, and S. Özyurt, "Improving physical layer security in alamouti OFDM systems with subcarrier coordinate interleaving," *IET Communications*, vol. 14, no. 16, pp. 2687–2693, 2020.

[32] S. X. Wu, W. Ma, and A. M. So, "Physical-layer multicasting by stochastic transmit beamforming and alamouti space-time coding," *IEEE Transactions on Signal Processing*, vol. 61, no. 17, pp. 4230–4245, 2013.

[33] H. Bolcskei, D. Gesbert, and A. J. Paulraj, "On the capacity of OFDM-based spatial multiplexing systems," *IEEE Transactions on Communications*, vol. 50, no. 2, pp. 225–234, 2002.

[34] X.Fang, Y. Zhang, Haiyan Cao, and Na Ying, "Spectral and energy efficiency analysis with massive MIMO systems," in *2015 IEEE 16th International Conference on Communication Technology (ICCT)*, 2015, pp. 837–843.

[35] B. Li, Y. Rong, J. Sun, and K. L. Teo, "A distributionally robust linear receiver design for multi-access space-time block coded MIMO systems," *IEEE Transactions on Wireless Communications*, vol. 16, no. 1, pp. 464–474, 2017.

[36] Z. Ding, C. Zhong, D. W. K. Ng, M. Peng, H. A. Suraweera, R. Schober, and H. V. Poor, "Application of smart antenna technologies in simultaneous wireless information and power transfer," *IEEE Communications Magazine*, vol. 53, no. 4, pp. 86–93, 4 2015.

[37] Z. Chen, Q. Shi, Q. Wu, and W. Xu, "Joint transceiver optimization of MIMO SWIPT systems for harvested power maximization," *IEEE Signal Processing Letters*, vol. 24, no. 10, pp. 1557–1561, 2017.

[38] K. Xiong, B. Wang, and K. J. R. Liu, "Rate-energy region of SWIPT for MIMO broadcasting under nonlinear energy harvesting model," *IEEE Transactions on Wireless Communications*, vol. 16, no. 8, pp. 5147–5161, 2017.

[39] H. Zhang, A. Dong, S. Jin, and D. Yuan, "Joint transceiver and power splitting optimization for multiuser MIMO SWIPT under MSE QoS constraints," *IEEE Transactions on Vehicular Technology*, vol. 66, no. 8, pp. 7123–7135, 2017.

[40] J. Tang, D. K. C. So, N. Zhao, A. Shojaeifard, and K. Wong, "Energy efficiency optimization with SWIPT in MIMO broadcast channels for internet of things," *IEEE Internet of Things Journal*, vol. 5, no. 4, pp. 2605–2619, 2018.

[41] D. Mishra and G. C. Alexandropoulos, "Transmit precoding and receive power splitting for harvested power maximization in MIMO SWIPT systems," *IEEE Transactions on Green Communications and Networking*, vol. 2, no. 3, pp. 774–786, 2018.

[42] X. Zhou and Q. Li, "Energy efficiency for SWIPT in MIMO two-way amplify-and-forward relay networks," *IEEE Transactions on Vehicular Technology*, vol. 67, no. 6, pp. 4910–4924, 2018.

[43] Y. Chen, Z. Wen, N. C. Beaulieu, S. Wang, and J. Sun, "Joint source-relay design in a MIMO two-hop power-splitting-based relaying network," *IEEE Communications Letters*, vol. 19, no. 10, pp. 1746–1749, 2015.

[44] B. Chen, X. Zhu, and X. Tu, "Joint precoder design for SWIPT-enabled MIMO relay networks with finite-alphabet inputs," *IEEE Access*, vol. 8, pp. 179 105–179 117, 2020.

[45] G. Amarasuriya, E. G. Larsson, and H. V. Poor, "Wireless information and power transfer in multiway massive MIMO relay networks," *IEEE Transactions on Wireless Communications*, vol. 15, no. 6, pp. 3837–3855, 2016.

[46] Y. Huang and B. Clerckx, "Joint wireless information and power transfer for an autonomous multiple antenna relay system," *IEEE Communications Letters*, vol. 19, no. 7, pp. 1113–1116, 2015.

[47] ——, "Relaying strategies for wireless-powered MIMO relay networks," *IEEE Transactions on Wireless Communications*, vol. 15, no. 9, pp. 6033–6047, 2016.

[48] Jialing Liao, M. R. A. Khandaker, and K. Wong, "Energy harvesting enabled MIMO relaying through power splitting," in *2016 IEEE 17th International Workshop on Signal Processing Advances in Wireless Communications (SPAWC)*, 2016, pp. 1–5.

[49] F. Benkhelifa and M. Alouini, "Precoding design of MIMO amplify-and-forward communication system with an energy harvesting relay and possibly imperfect CSI," *IEEE Access*, vol. 5, pp. 578–594, 2017.

[50] F. Benkhelifa, A. S. Salem, and M. Alouini, "Rate maximization in MIMO decode-and-forward communications with an EH relay and possibly imperfect CSI," *IEEE Transactions on Communications*, vol. 64, no. 11, pp. 4534–4549, 2016.

[51] R. Malik and M. Vu, "Optimizing throughput in a MIMO system with a self-sustained relay and non-uniform power splitting," *IEEE Wireless Communications Letters*, vol. 8, no. 1, pp. 205–208, 2019.

[52] ——, "Optimal transmission using a self-sustained relay in a full-duplex MIMO system," *IEEE Journal on Selected Areas in Communications*, vol. 37, no. 2, pp. 374–390, 2019.

[53] B. Li and Y. Rong, "AF MIMO relay systems with wireless powered relay node and direct link," *IEEE Transactions on Communications*, vol. 66, no. 4, pp. 1508–1519, 2018.

[54] ——, "Joint transceiver optimization for wireless information and energy transfer in nonregenerative MIMO relay systems," *IEEE Transactions on Vehicular Technology*, vol. 67, no. 9, pp. 8348–8362, 2018.

[55] B. Li, M. Zhang, H. Cao, Y. Rong, and Z. Han, "Transceiver design for AF MIMO relay systems with a power splitting based energy harvesting relay node," *IEEE Transactions on Vehicular Technology*, vol. 69, no. 3, pp. 2376–2388, 2020.

[56] B. Li, H. Cao, Y. Rong, T. Su, G. Yang, and Z. He, "Transceiver optimization for DF MIMO relay systems with a wireless powered relay node," *IEEE Access*, vol. 7, pp. 56 904–56 919, 2019.

[57] J. P. Kermoal, L. Schumacher, K. I. Pedersen, P. E. Mogensen, and F. Frederiksen, "A stochastic MIMO radio channel model with experimental validation," *IEEE Journal on Selected Areas in Communications*, vol. 20, no. 6, pp. 1211–1226, 2002.

[58] A. Abrol and R. K. Jha, "Power optimization in 5G networks: A step towards GrEEn communication," *IEEE Access*, vol. 4, pp. 1355–1374, 2016.

[59] R. O. Afolabi, A. Dadlani, and K. Kim, "Multicast scheduling and resource allocation algorithms for OFDMA-based systems: A survey," *IEEE Communications Surveys Tutorials*, vol. 15, no. 1, pp. 240–254, 2013.

[60] D. Lecompte and F. Gabin, "Evolved multimedia broadcast/multicast service (eMBMS) in LTE-advanced: overview and rel-11 enhancements," *IEEE Communications Magazine*, vol. 50, no. 11, pp. 68–74, 2012.

[61] N. D. Sidiropoulos, T. N. Davidson, and Zhi-Quan Luo, "Transmit beamforming for physical-layer multicasting," *IEEE Transactions on Signal Processing*, vol. 54, no. 6, pp. 2239–2251, 2006.

[62] N. Jindal and Z. Luo, "Capacity limits of multiple antenna multicast," in *2006 IEEE International Symposium on Information Theory*, 2006, pp. 1841–1845.

[63] S. Y. Park, D. J. Love, and D. H. Kim, "Capacity limits of multi-antenna multicasting under correlated fading channels," *IEEE Transactions on Communications*, vol. 58, no. 7, pp. 2002–2013, 2010.

[64] A. Z. Yalcin and M. Yuksel, "Precoder design for multi-group multicasting with a common message," *IEEE Transactions on Communications*, vol. 67, no. 10, pp. 7302–7315, 2019.

[65] D. Senaratne and C. Tellambura, "Beamforming for physical layer multicasting," in *2011 IEEE Wireless Communications and Networking Conference*, 2011, pp. 176–1781.

[66] H. Zhu, N. Prasad, and S. Rangarajan, "Precoder design for physical layer multicasting," *IEEE Transactions on Signal Processing*, vol. 60, no. 11, pp. 5932–5947, 2012.

[67] R. Duan, J. Wang, H. Zhang, Y. Ren, and L. Hanzo, "Joint multicast beamforming and relay design for maritime communication systems," *IEEE Transactions on Green Communications and Networking*, vol. 4, no. 1, pp. 139–151, 2020.

[68] N. Bornhorst, M. Pesavento, and A. B. Gershman, "Distributed beamforming for multi-group multicasting relay networks," *IEEE Transactions on Signal Processing*, vol. 60, no. 1, pp. 221–232, 2012.

[69] M. R. A. Khandaker and Y. Rong, "Precoding design for MIMO relay multicasting," *IEEE Transactions on Wireless Communications*, vol. 12, no. 7, pp. 3544–3555, 2013.

[70] ——, "Simplified MIMO relay design for multicasting from multiple-sources," in *2014 IEEE International Conference on Acoustics, Speech and Signal Processing (ICASSP)*, 2014, pp. 2739–2743.

[71] ——, "Transceiver optimization for multi-hop MIMO relay multicasting from multiple sources," *IEEE Transactions on Wireless Communications*, vol. 13, no. 9, pp. 5162–5172, 2014.

[72] L. Gopal, Y. Rong, and Z. Zang, "Robust MMSE transceiver design for nonregenerative multicasting MIMO relay systems," *IEEE Transactions on Vehicular Technology*, vol. 66, no. 10, pp. 8979–8989, 2017.

[73] L. Gopal, Y. Rong, and Z. Zang, "Simplified robust design for nonregenerativemm multicasting MIMO relay systems," in *2015 22nd International Conference on Telecommunications (ICT)*, April 2015, pp. 289–293.

[74] J. Liu, F. Gao, and Z. Qiu, "Robust transceiver design for multi-user multiple-input multiple-output amplify-and-forward relay systems," *IET Communications*, vol. 8, no. 12, pp. 2162–2170, 2014.

[75] C. Xing, S. Ma, and Y. C. Wu, "Robust joint design of linear relay precoder and destination equalizer for dual-hop amplify-and-forward MIMO relay systems," *IEEE Transactions on Signal Processing*, vol. 58, no. 4, pp. 2273–2283, April 2010.

[76] C. Xing, S. Ma, Z. Fei, Y. Wu, and H. V. Poor, "A general robust linear transceiver design for multi-hop amplify-and-forward MIMO relaying systems," *IEEE Transactions on Signal Processing*, vol. 61, no. 5, pp. 1196–1209, 2013.

[77] C. Xing, F. Gao, and Y. Zhou, "A framework for transceiver designs for multi-hop communications with covariance shaping constraints," *IEEE Transactions on Signal Processing*, vol. 63, no. 15, pp. 3930–3945, 2015.

[78] C. Xing, Y. Ma, Y. Zhou, and F. Gao, "Transceiver optimization for multi-hop communications with per-antenna power constraints," *IEEE Transactions on Signal Processing*, vol. 64, no. 6, pp. 1519–1534, 2016.

[79] Y. Rong, "Robust design for linear non-regenerative MIMO relays with imperfect channel state information," *IEEE Transactions on Signal Processing*, vol. 59, no. 5, pp. 2455–2460, 2011.

[80] B. Chalise and L. Vandendorpe, "Joint linear processing for an amplify-and-forward MIMO relay channel with imperfect channel state information," *EURASIP Journal on Advances in Signal Processing*, vol. 2010, 01 2010.

[81] A. Gupta and D. Nagar, *Matrix Variate Distributions*. Taylor & Francis, 1999.

[82] Z. He, S. Guo, Y. Ou, and Y. Rong, "Multiuser multihop MIMO relay system design based on mutual information maximization," *IEEE Transactions on Signal Processing*, vol. 62, no. 21, pp. 5725–5733, 2014.

[83] Q. Shi, M. Razaviyayn, Z. Luo, and C. He, "An iteratively weighted MMSE approach to distributed sum-utility maximization for a MIMO interfering broadcast channel," *IEEE Transactions on Signal Processing*, vol. 59, no. 9, pp. 4331–4340, 2011.

[84] C. Xing, S. Li, Z. Fei, and J. Kuang, "How to understand linear minimum mean-square-error transceiver design for multiple-input-multiple-output systems from quadratic matrix programming," *IET Communications*, vol. 7, no. 12, pp. 1231–1242, 2013.

[85] S. M. Kay, *Fundamentals of Statistical Signal Processing: Estimation Theory*. Prentice Hall, 1997.

[86] Y. Rong, "Robust design for linear non-regenerative MIMO relays," in *2010 Australian Communications Theory Workshop (AusCTW)*, Feb 2010, pp. 87–92.

[87] D. Bernstein, *Matrix Mathematics: Theory, Facts, and Formulas (Second Edition)*, ser. Princeton reference. Princeton University Press, 2009.

[88] A. W. Marshall, I. Olkin, and B. C. Arnold, *Inequalities: Theory of Majorization and its Applications*, 2nd ed. Springer, 2011, vol. 143.

[89] S. Boyd and L. Vandenberghe, *Convex Optimization*. Cambridge University Press, March 2004.

[90] M. Grant and S. Boyd, "CVX: Matlab software for disciplined convex programming, version 2.1," http://cvxr.com/cvx, Mar. 2014.

[91] C. Xing, Z. Fei, S. Ma, J. Kuang, and Y. Wu, "Robust linear transceiver design for multi-hop non-regenerative MIMO relaying systems," in *2011 International Conference on Wireless Communications and Signal Processing (WCSP)*, 2011, pp. 1–5.

[92] P. Kamalinejad, C. Mahapatra, Z. Sheng, S. Mirabbasi, V. C. M. Leung, and Y. L. Guan, "Wireless energy harvesting for the internet of things," *IEEE Communications Magazine*, vol. 53, no. 6, pp. 102–108, 2015.

[93] B. K. Chalise, Y. D. Zhang, and M. G. Amin, "Simultaneous transfer of energy and information for MIMO-OFDM relay system," in *2012 1st IEEE International Conference on Communications in China (ICCC)*, 2012, pp. 481–486.

[94] R. Xiao, Y. Liu, H. Yang, J. Shen, and C. Yan, "Performance analysis of hybrid protocol based two-way decode-and-forward relay networks," in *2018 IEEE 4th International Conference on Computer and Communications (ICCC)*, 2018, pp. 146–151.

[95] Z. Popović, E. A. Falkenstein, D. Costinett, and R. Zane, "Low-power far-field wireless powering for wireless sensors," *Proceedings of the IEEE*, vol. 101, no. 6, pp. 1397–1409, 2013.

[96] H. J. Visser and R. J. M. Vullers, "RF energy harvesting and transport for wireless sensor network applications: Principles and requirements," *Proceedings of the IEEE*, vol. 101, no. 6, pp. 1410–1423, 2013.

[97] S. D. Assimonis, S. Daskalakis, and A. Bletsas, "Sensitive and efficient RF harvesting supply for batteryless backscatter sensor networks," *IEEE Transactions on Microwave Theory and Techniques*, vol. 64, no. 4, pp. 1327–1338, 2016.

[98] C. R. Valenta and G. D. Durgin, "Harvesting wireless power: Survey of energy-harvester conversion efficiency in far-field, wireless power transfer systems," *IEEE Microwave Magazine*, vol. 15, no. 4, pp. 108–120, 2014.

[99] D. Darsena, "Noncoherent detection for ambient backscatter communications over OFDM signals," *IEEE Access*, vol. 7, pp. 159 415–159 425, 2019.

[100] A. Chervov, G. Falqui, and V. Rubtsov, "Algebraic properties of Manin matrices 1," *Advances in Applied Mathematics*, vol. 43, no. 3, pp. 239 – 315, 2009.

[101] J. Hadamard, "Resolution d'une question relative aux determinants," *Bull. des Sciences Math.*, vol. 2, pp. 240–246, 1893.

[102] Y. Rong, X. Tang, and Y. Hua, "A unified framework for optimizing linear nonregenerative multicarrier MIMO relay communication systems," *IEEE Transactions on Signal Processing*, vol. 57, no. 12, pp. 4837–4851, Dec 2009.

[103] Y. Nesterov and A. Nemirovskii, *Interior-Point Polynomial Algorithms in Convex Programming*. Society for Industrial and Applied Mathematics, 1994.

[104] C. Song, J. Park, B. Clerckx, I. Lee, and K. Lee, "Generalized precoder designs based on weighted MMSE criterion for energy harvesting constrained MIMO and multi-user MIMO channels," *IEEE Transactions on Wireless Communications*, vol. 15, no. 12, pp. 7941–7954, 2016.

[105] P. Arapoglou, P. Burzigotti, M. Bertinelli, A. Bolea Alamanac, and R. De Gaudenzi, "To MIMO or not to MIMO in mobile satellite broadcasting systems," *IEEE Transactions on Wireless Communications*, vol. 10, no. 9, pp. 2807–2811, 2011.

[106] R. Jiang, K. Xiong, P. Fan, L. Zhou, and Z. Zhong, "Outage probability and throughput of multirelay SWIPT-WPCN networks with nonlinear EH model and imperfect CSI," *IEEE Systems Journal*, vol. 14, no. 1, pp. 1206–1217, 2020.

[107] P. Shaik, P. K. Singya, N. Kumar, K. K. Garg, and V. Bhatia, "On impact of imperfect CSI over SWIPT device-to-device (D2D) MIMO relay systems," in *2020 International Conference on Signal Processing and Communications (SPCOM)*, 2020, pp. 1–5.

[108] Q. Li and L. Yang, "Robust optimization for energy efficiency in MIMO two-way relay networks with SWIPT," *IEEE Systems Journal*, vol. 14, no. 1, pp. 196–207, 2020.

[109] S. Simoens, O. Munoz-Medina, J. Vidal, and A. del Coso, "On the gaussian MIMO relay channel with full channel state information," *IEEE Transactions on Signal Processing*, vol. 57, no. 9, pp. 3588–3599, 2009.

[110] M. Ding and S. D. Blostein, "Maximum mutual information design for MIMO systems with imperfect channel knowledge," *IEEE Transactions on Information Theory*, vol. 56, no. 10, pp. 4793–4801, 2010.

[111] A. Antoniou and W. S. Lu, *Practical Optimization: Algorithms and Engineering Applications*, 1st ed. Springer Publishing Company, Incorporated, 2007.

[112] D. P. Palomar and Mung Chiang, "A tutorial on decomposition methods for network utility maximization," *IEEE Journal on Selected Areas in Communications*, vol. 24, no. 8, pp. 1439–1451, 2006.

[113] Z. Fang, Y. Hua, and J. C. Koshy, "Joint source and relay optimization for a non-regenerative MIMO relay," in *Fourth IEEE Workshop on Sensor Array and Multichannel Processing, 2006.*, July 2006, pp. 239–243.

[114] I. Hammerstrom and A. Wittneben, "Power allocation schemes for amplify-and-forward MIMO-OFDM relay links," *IEEE Transactions on Wireless Communications*, vol. 6, no. 8, pp. 2798–2802, 2007.